RTO-EN-028
AC/323(SET-058)TP/42

RTO-EN-028

NORTH ATLANTIC TREATY ORGANISATION

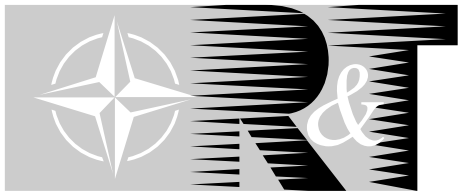

RESEARCH AND TECHNOLOGY ORGANISATION

BP 25, 7 RUE ANCELLE, F-92201 NEUILLY-SUR-SEINE CEDEX, FRANCE

RTO LECTURE SERIES 229

Optics Microwave Interactions

(Interactions entre optique et micro-ondes)

The material in this publication was assembled to support a Lecture Series under the sponsorship of the Sensors and Electronics Technology Panel (SET) and the Consultant and Exchange Programme of RTO presented on 2-3 September 2002 in Jouy en Josas, France, on 5-6 September 2002 in Duisburg, Germany and on 9-10 September 2002 in Budapest, Hungary.

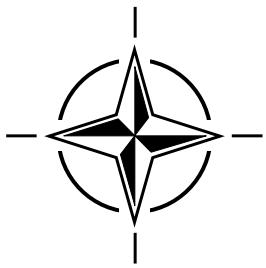

Published April 2003

Distribution and Availability on Back Cover

This page has been deliberately left blank

Page intentionnellement blanche

RTO-EN-028
AC/323(SET-058)TP/42

NORTH ATLANTIC TREATY ORGANISATION

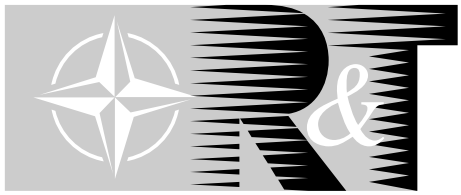

RESEARCH AND TECHNOLOGY ORGANISATION

BP 25, 7 RUE ANCELLE, F-92201 NEUILLY-SUR-SEINE CEDEX, FRANCE

RTO LECTURE SERIES 229

Optics Microwave Interactions

(Interactions entre optique et micro-ondes)

The material in this publication was assembled to support a Lecture Series under the sponsorship of the Sensors and Electronics Technology Panel (SET) and the Consultant and Exchange Programme of RTO presented on 2-3 September 2002 in Jouy en Josas, France, on 5-6 September 2002 in Duisburg, Germany and on 9-10 September 2002 in Budapest, Hungary.

The Research and Technology Organisation (RTO) of NATO

RTO is the single focus in NATO for Defence Research and Technology activities. Its mission is to conduct and promote cooperative research and information exchange. The objective is to support the development and effective use of national defence research and technology and to meet the military needs of the Alliance, to maintain a technological lead, and to provide advice to NATO and national decision makers. The RTO performs its mission with the support of an extensive network of national experts. It also ensures effective coordination with other NATO bodies involved in R&T activities.

RTO reports both to the Military Committee of NATO and to the Conference of National Armament Directors. It comprises a Research and Technology Board (RTB) as the highest level of national representation and the Research and Technology Agency (RTA), a dedicated staff with its headquarters in Neuilly, near Paris, France. In order to facilitate contacts with the military users and other NATO activities, a small part of the RTA staff is located in NATO Headquarters in Brussels. The Brussels staff also coordinates RTO's cooperation with nations in Middle and Eastern Europe, to which RTO attaches particular importance especially as working together in the field of research is one of the more promising areas of initial cooperation.

The total spectrum of R&T activities is covered by the following 7 bodies:

- AVT Applied Vehicle Technology Panel
- HFM Human Factors and Medicine Panel
- IST Information Systems Technology Panel
- NMSG NATO Modelling and Simulation Group
- SAS Studies, Analysis and Simulation Panel
- SCI Systems Concepts and Integration Panel
- SET Sensors and Electronics Technology Panel

These bodies are made up of national representatives as well as generally recognised 'world class' scientists. They also provide a communication link to military users and other NATO bodies. RTO's scientific and technological work is carried out by Technical Teams, created for specific activities and with a specific duration. Such Technical Teams can organise workshops, symposia, field trials, lecture series and training courses. An important function of these Technical Teams is to ensure the continuity of the expert networks.

RTO builds upon earlier cooperation in defence research and technology as set-up under the Advisory Group for Aerospace Research and Development (AGARD) and the Defence Research Group (DRG). AGARD and the DRG share common roots in that they were both established at the initiative of Dr Theodore von Kármán, a leading aerospace scientist, who early on recognised the importance of scientific support for the Allied Armed Forces. RTO is capitalising on these common roots in order to provide the Alliance and the NATO nations with a strong scientific and technological basis that will guarantee a solid base for the future.

Published April 2003

ISBN 92-837-1094-0

Printed by St. Joseph Print Group Inc.
(A St. Joseph Corporation Company)
1165 Kenaston Street, Ottawa, Ontario, Canada K1G 6S1

Optics Microwave Interactions

(RTO EN-028 / SET-058)

Executive Summary

The field of optics-microwave covered by this 2 day lecture series can generally be defined as the study of high speed devices and systems operating at microwave, millimeter wave and even THz frequencies. The benefits drawn by the introduction of optics in microwave techniques are illustrated through numerous examples.

This two-day lecture series covers the main applications of opto-microwaves to the defence area with a broad approach stretching from devices to systems.

The first day starts with a general overview and state of the art of the field. Then, the hybrid integration of opto-electronic components and associated technology are reviewed. The optoelectronic transducers from electronics to optics and optics to electronics are presented in detail. Then, a wide variety of applications is presented: recent developments in fiber-fed radio systems, optical distribution of broadband RF and MMW signals for mobile and wireless systems of RF signals to phased array antennas, beamforming, beam control and antenna remoting.

The second day presents the applications to optical processing of microwave signals and to optical control of microwave devices as well. Optical networks for radar and electronics warefare systems, for broadband applications (1-20 GHz) are also discussed. Finally, novel techniques of microwave photonics applied to optical Analogue to Digital Converters (ADC) and for medical imaging are also presented.

The material in this publication was assembled to support a Lecture Series under the sponsorship of the Sensors and Electronics Technology Panel (SET) and the Consultant and Exchange Programme of RTO presented on 2-3 September 2002 in Jouy en Josas, France, on 5-6 September 2002 in Duisburg, Germany and on 9-10 September 2002 in Budapest, Hungary.

Interactions entre optique et micro-ondes

(RTO EN-028 / SET-058)

Synthèse

Ce cours concerne toutes les interactions entre l'optique et les micro-ondes et vice-versa et les bénéfices liés à l'introduction de l'optique dans les techniques micro-ondes par rapport à une approche conventionnelle purement électrique sont illustrés par de nombreux exemples. Le domaine de fréquence exploré va des micro-ondes (GHz) au THz en passant par la gamme millimétrique.

Le cours est réparti sur deux journées, et les principales applications de l'optomicro-onde dans le domaine de la défense sont traitées, du dispositif au système applicatif.

La première journée est consacrée en partie à une introduction générale sur les domaines avec un rappel de l'état de l'art. Ensuite, l'intégration hybride de composants optique et micro-ondes, et la technologie associée seront présentées. Les composants optoélectroniques servant d'interface électrique/optique et optique/électrique seront revus en détail. La journée s'ouvre ensuite sur un vaste champ d'applications : les récentes avancées sur les systèmes radio sur fibre, la distribution optique de signaux RF large bande ou millimétrique pour les antennes à balayage de phase, les mobiles et les réseaux sans fils, la distribution radar, la formation et le contrôle de faisceaux, les antennes déportées.

La deuxième journée présente les applications au traitement optique du signal micro-ondes, le contrôle optique de dispositifs micro-ondes, la conversion analogique/numérique, la distribution optique dans les systèmes radars très large bande (1-20 GHz). Des récentes applications en plein essor telles que l'imagerie médicale sont aussi présentées.

Cette publication a été rédigée pour servir de support de cours pour le Cycle de conférences 229, organisé par la Commission de la technologie des capteurs et des dispositifs électroniques (SET) dans le cadre du programme des consultants et des échanges de la RTO du 2-3 septembre 2002 à Jouy en Josas, France, du 5-6 septembre 2002 à Duisburg, Allemagne et du 9-10 septembre 2002 à Budapest, Hongrie.

Click inside the blue boxes or on the titles to view the corresponding section

Contents

List of Authors/Lecturers

Lecture Series Directors:

Dr. Béatrice CABON
IMP/ENSERG
23 Avenue des Martyrs
BP 257
38016 Grenoble Cedex
FRANCE

Dr Jean CHAZELAS
THALES Airborne Systems
2 Avenue Gay Lussac
78851 Elancourt Cedex
FRANCE

Course Lecturers:

Prof Didier DECOSTER
IEMN-Cité Scientifique
BP 59
59652 Villeneuve d'Ascq Cedex
FRANCE

Mr. Afshin S. DARYOUSH
Drexel University
3141 Chestnut Street
Philadelphia
PA, 19104
UNITED STATES

Mr. Dieter JÄGER
Gerhard-Mercator University
Faculty of Electrical Engineering
ZHO Dept. of Optoelectronics
47048 Duisburg
GERMANY

Dr. J.J. LEE
Raytheon Co.
R2-V518, PO Box 902
El Segundo
CA 90245-0902
UNITED STATES

Pr Tibor BERCELI
Budapest University of
Technology and Economics
1111 Budapest
Goldmann György tér 3
HUNGARY

Co-Authors:

Dr. Samuel DUPONT
IEMN-Cité Scientifique
BP 59
59652 Villeneuve d'Ascq Cedex
FRANCE

Mr. A. STÖRH
Gerhard-Mercator-Universität Duisburg
ZHO – Optoelektronik
Lotharstrasse 55
D-47057 Duisburg
GERMANY

Dr. Vincent MAGNIN
IEMN-Cité Scientifique
BP 59
59652 Villeneuve d'Asq Cedex
FRANCE

M. CSÖRNYEI
Budapest University of
Technology and Economics
1111 Budapest
Goldmann György tér 3
HUNGARY

Microwave Photonics in Dual-Use Military Systems - A Personal Perspective

Afshin S. Daryoush
Department of Electrical and Computer Engineering
Drexel University, Philadelphia, PA 19104, USA

Daryoush@ece.drexel.edu

Abstract

Microwave photonics has come of age and there are a number of military applications that could directly benefit from. Optically controlled phased array antenna is one of the most widely pursued applications. The fiberoptic links are employed for distribution of a variety of communication, intelligence, tracking, radar signals. There are a number of issues that dictate the type of architecture that is employed for effective and reliable control of phased array. However, the most important benefit is in the optical signal processing of microwave signals. Fiber delay lines are an important element of an signal processing solutions.

1. Introduction

The last two decades of 20th century with significant advances of IC technologies and proliferation of commercial fiberoptic communication technologies, a gradual acceptance of microwave photonics is being experienced in the most conservative military circles. However, the question still remains whether microwave photonic techniques could fulfill its claim to deliver all the benefits, which were touted in many circles in late 1970's. Figure 1 depicts a conceptual representation of my personal view of future combat systems, where special operation units and low flying air vehicles are linked to the global information network using low profile wireless local area networks. The challenges that military system planners encounter are somewhat similar to the commercial needs that are being driven by consumers. In essence, except for a much higher reliability requirements imposed for the military operations in hostile environments, both civilian and military systems overlap in many technical aspects.

Among many aerospace and military applications of fiberoptic technology, none have received the same level of attention and support from technical and government as the concept of optically controlled phased array antenna systems. A historical perspective of phased array antenna evolution is depicted in Fig. 2, where a significant amount of electronics is distributed in the entire aperture. In fact, MMIC based active phased antennas are designed for radar, tracking, communication, and electronic warfare (EW) applications and still it appears that the role that photonics could play in this arena is not quite clear. It was recognized then and still considered that future demands for multibeam shared aperture phased array antennas could not be achieved without incorporation of significant amount of processing, control, and communication capability at each active array element. It is clear as the information throughput significantly increases, there is need for ultra high-speed fiberoptic links to transfer data, where standard electrical interconnect fails due to poor EMI, dispersion, loss, and large size. Both analog and digital fiberoptic links are crucial part of interconnects in any distributed system.

Paper presented at the RTO SET Lecture Series on "Optics Microwave Interactions", held in Jouy en Josas, France, 2-3 September 2002; Duisburg, Germany, 5-6 September 2002; Budapest, Hungary, 9-10 September 2002, and published in RTO-EN-028.

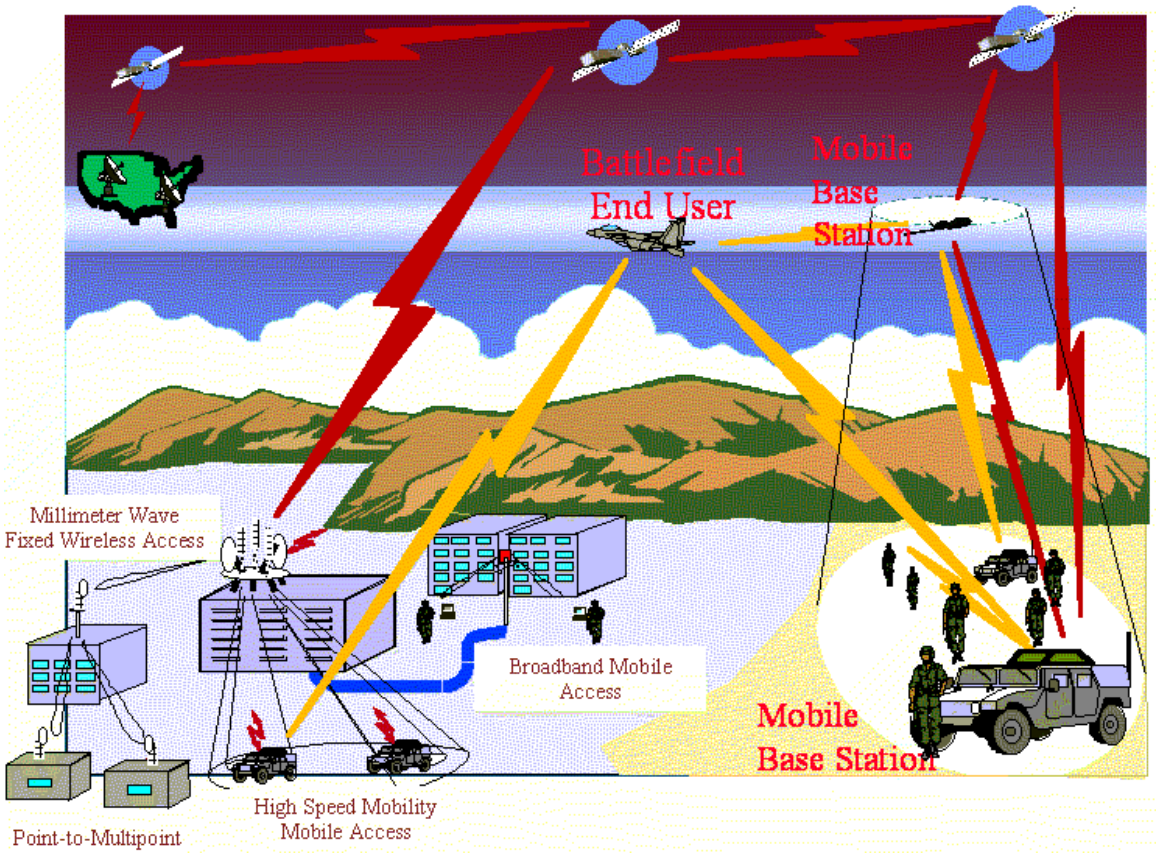

Fig. 1. Conceptual representation of a number of wireless networking used for Comm-on-the-Move for Future Combat Systems.

Conceptual representation of a shared aperture antenna for surface Navy vessels is depicted in Fig. 3, where the antennas and electronics for a variety functions are co located. In this figure, other conventional antenna structures are also depicted for comparison, where linear arrays (for L-band radar) and reflector antennas (for S-, C-, X- band radar, and C-band communication) are employed. One of challenges is efficient distribution of the modulated carrier, particularly at Ka-band frequencies and above. Performance of optical components in harsh military environment is discussed first followed with packaging issues that could reduce cost of optical alignment. Furthermore, phase and amplitude of the radiating element should be controlled in real-time to scan and shape the radiated beam in a particular direction. In multibeam phased array systems, beams are shaped for different directions in space at various operation frequencies. Both analog and digital beamforming networks has been demonstrated, however with advent of high-speed DSP it becomes more attractive to pursue the latter. Furthermore, it is predicted that future threats will employ EW measures to defeat the effectiveness of electronic support attained from multi-sensors. Therefore, electronic counter measures (ECM) based on radar warning receivers (RWR) are required to engage simultaneously a number of active threats. In my opinion the optical signal processing is where clearly advantages of photonic system become evident. Fiber optic delay lines are employed to generate memory devices, interference cancellation, and narrow bandpass filters.

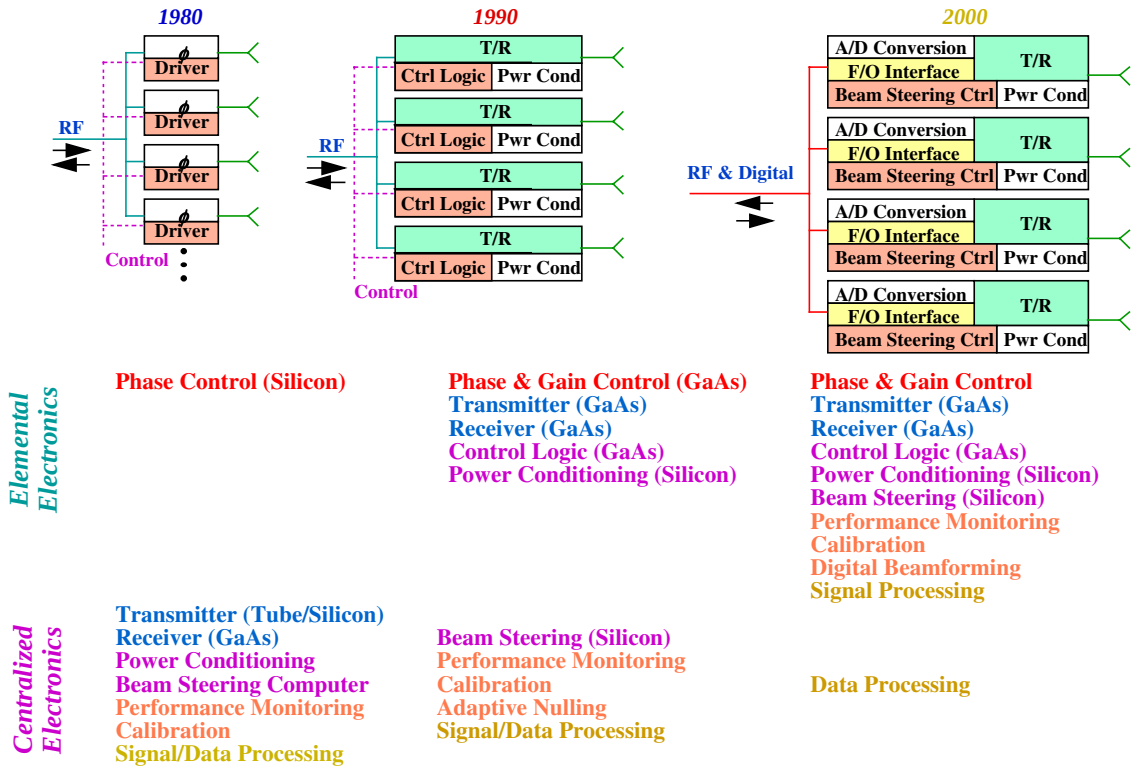

Fig. 2. A historical timeline presented evolution of phased array antennas in the last three decades. Note in this vision both MMIC and FO technologies are an integral part of future phased arrays.

Table I shows a composite of frequency bands allocated for radar, communication and EW systems. For a viable multifunction electronic systems to be used in the future shared aperture antennas, a distribution network are required to provide coherent signals to the T/R modules. Note that the desired RF signals could be obtained using mixing of the data signal with a stabilized local oscillator, as indicated in the column dealing with the *"FO link realization"*. Therefore, to realize a coherent front-end receiver and transmitter in phased arrays, each optically fed antenna should have its own antenna mounted front end electronics, which is composed of opto-electronic interface circuits, stabilized local oscillators up to the MMW frequencies, and efficient mixers. Various techniques that enable optical generation of MMW signals and opto-electronic mixing have been developed and a few are being presented as part of this lecture series by Professors Berceli, Cabon, and Jaeger. Author will also present phase noise coherency and opt-electronic mixing capability of fiberoptic links in an accompanying paper in this proceedings. Moreover different methods of building active phased array antennas are discussed by other presenters Chazelas and Lee.

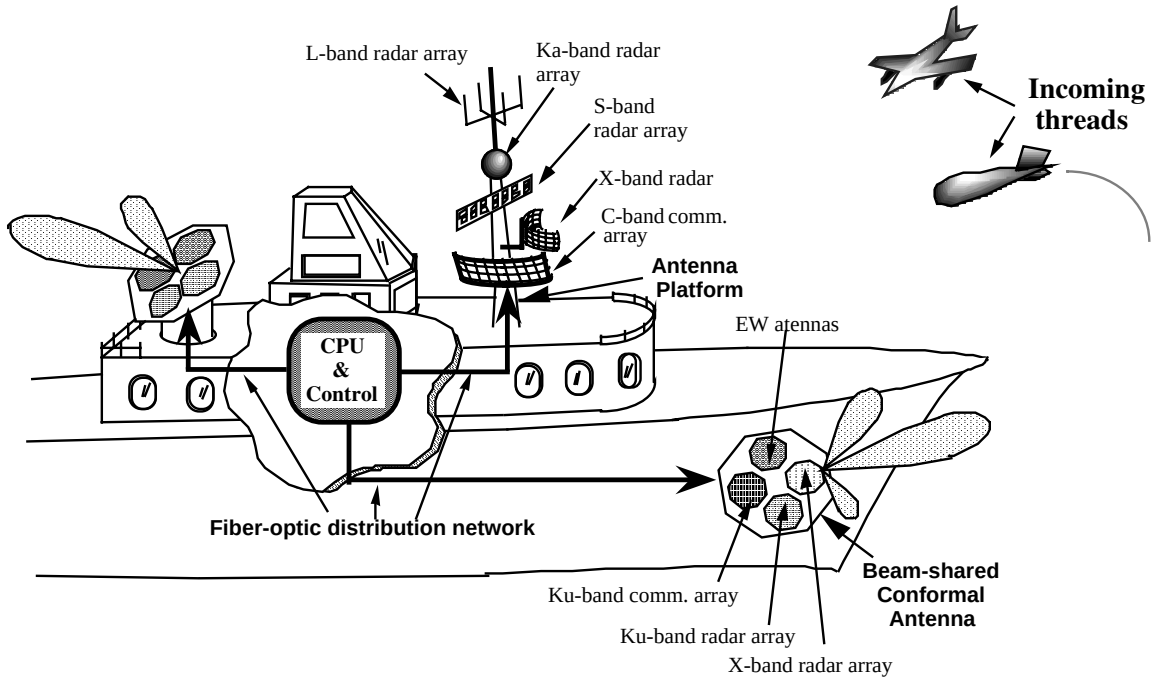

Fig. 3. Conceptual block diagram representation of a future generation of AEGIS cruiser with shared aperture concept, capable of radar, tracking, communication, and EW functions such as direction finding up to MMW.

Frequency band	Radar	Communication	EW	FO links Realization
L-band	2 - 3 GHz		≥ 2 GHz	**Radar**: 2-3 GHz FO link **EW**: 200MHz - 18 GHz FO link
C-band	5.2 - 5.8 GHz	4.2 -5.2 GHz	Entire band 4-8 GHz	**Radar** LO: 6GHz; IF: 200-800MHz **Comm.**LO: 6GHz;IF: 800-1300 MHz **EW:** 200MHz - 18 GHz FO link
X-band	9 - 10 GHz		Entire band 8- 12 GHz	**Radar** LO: 12 GHz; IF: 2-3 GHz (Lower sideband) **EW:** 200MHz - 18 GHz FO link
Ku-band		14 - 15 GHz	Entire band 12 -18 GHz	**Comm.** LO: 12 GHz ; IF: 2 - 3 GHz (Upper sideband) **EW:** DC - 18 GHz FO link
K-band			Entire band 18 - 30 GHz	**EW** LO: 12 GHz; IF: 6 - 18 GHz
Ka-band	33 - 34 GHz	21 - 22 GHz	Entire band 30 -42 GHz	**Radar** LO: 36 GHz; IF: 2 - 3 GHz; **Comm.** LO: 24 GHz; IF: 2 -3 GHz; **EW** LO: 24 GHz; IF 6-18 GHz

Table I. Composite of frequency band allocations for radar, communication, and EW for shared aperture systems.

3.0 Fiberoptic Distribution for Phased Array Antennas

One of the simplest methods of providing FO links for antenna remoting is based on the concept of direct replacement of the electrical interconnects. However, there are challenges associated with reliability of optical components, cost of system integration, and the architecture employed for achieving the best attributes possible.

Device Innovations and Reliability: A vast number of research work reported in literature have focused on the device improvements to meet the performance requirement of commercial fiber optic communication. Performance of sampled directly and externally modulated fiber optic links operating at S-band is rendered in Table II, where the best performance is achieved. For DFB laser monolithically integrated with EA modulator. The performance of mode-locked laser is quite acceptable (The results of MZ modulator may appear worse than what is reported in literature, but in this case a semiconductor laser with optical power of only a few mW is used as a source. Monolithically integrated EA modulator with sampled grating DBR laser (SGDBR) [1] has been developed where SFDR of 120 dB.Hz$^{2/3}$ is achieved over a large tuning bandwidth. However, the harsh military environment impose additional burden on the performance of lightwave technology components.

	Directly Modulated FO Links		Externally Modulated FO Links	
	Mode-Loked Laser	Ortel DFB Laser	DFB/EA Modulator	Sumitomo MZ Modulator
Frequency	2.2GHz	2.5GHz	2.2GHz	2.5GHz
Gain (dB)	-8	-44	-12	-40
IP3 (dBm)	+17	+27	+14	+23
Noise Floor (dBm/Hz)	-142	-151	-151	-151
SFDR (dB.Hz$^{2/3}$)	101	86	103	90

Table II. Comparison of various COT fiberoptic links at S-band. Note the MZ modulator is based on DFB laser as optical source.

Table III compares performance of passive optical components under harsh radiation and temperature environment of space. As result of extreme temperature variation, micobending losses will impact performance of fiber based products, whereas on insulated waveguide pyroelectric effect introduces change in coupling factor. Moreover radiation impacts losses due to absorption (i.e., generation of coloring centers) in optical fibers and coupling losses due to change in index of refraction as result of photorefractive effect in insulated waveguides. On the other hand, semiconductor based optical sources and amplifiers suffer from change in bandgap due to temperature variation, whereas the Er: doped fiber amplifiers (EDFA) suffer from the similar characteristics as optical fibers. There have not been any siginifcant studies on the impact of temperature variation on EA modulator and photodetectors, but one can predict that there will changes in bandgap and hence resulting in

shift in absorption edge. The impact of radiation on semiconductors is increase in shot noise and change in absorption bandedge in photodiodes and EA modulators. Optical sources and amplifiers suffer from change in gain, hence modifying its dynamic performance. Naturally, there are proposed solutions associated with each problem. Due to impact of radiation and temperature on insulated based waveguides, I will not focus on the MZ based system in the remaining discussions.

		Silica Fiber				Insulator WG	
		SM	PM	Cables	Couplers	Couplers	Modulators
Radiation	Damage	Coloring Center			Absorption	Photorefractive	
	Impact	Optical Loss			Coupling	Coupling	
	Solution	Rad Hard Fiber			Shielding	Shielding	
Temperature	Damage	Stiffness			N/A	Pyro-electric	
	Impact	Microbending Loss			N/A	Coupling Factor	
	Solution	Material/Internal			N/A	Temeprature Control	

Table III. Reliability of passive optical components in harsh environment of space.

		LED	LD	SOA	Er:Doped	Photodiode	EA Modulators
Radiation	Damage	Recombination Center			Absorption	Electron-Hole	
	Impact	Loss		Gain	Gain	Shot Noise	Band Edge
	Solution	Higher Bias Current			Rad Hard	Shielding	
Temperature	Damage	Bandgap			Stiffness	N/A	
	Impact	Gain			Microbending Loss	N/A	
	Solution	Internal/Temperature Controller			Internal	N/A	

Table IV. Reliability of active optical components in harsh environment of space.

Packaging Requirements: As indicated in the accompanying paper on fiberoptic link, a dB improvement in the optical coupling improves insertion gain by a 2dB. However, mechanical tolerances of optical fibers and sources are in sub-micron range, hence making the low cost integration of optical components with optical fibers challenging the least. More over this process has to be done in a cost effective manner. Another important aspect of the light coupling is that reflection has to be minimized since any optical feedback introduces modulation of the dynamic response which resembles the transmission characteristics of FP resonators. Therefore, optical isolators combined with angle polished fibers are required to reduce the light feedback level below 50 dB in certain applications. Another important aspect is temperature control of semiconductor devices to avoid any sensitivity to temperature in

harsh environments of space. Finally, directly modulated fiber optic links or externally modulated systems using EA modulators, experience input impedance that corresponds to high reflection coefficients (i.e., approximately short for laser diode and open for EA modulator). To avoid high reflection loss, impedance matching circuits are needed to be developed, which is not easy to accomplish over a large fractional bandwidth. Fig. 4 depicts a designed structure of monolithically integrated optical source with EA modulator [2], which is used for distribution of both LO signal and data signal.(The details of this source performance is presented in an accompanying paper dealing with FO links.) This structure is also based on cascading a number laser with monolithically long FP cavity in series, hence increasing the forward P-N junction resistance, while maintaining the same RF current modulating all the gain sections. In essence, since the input impedance of laser diodes is of forward biased P-N diode is about 4Ω, by series combination of the impedance a level closer to 50 Ω is achieved. Moreover a lower Q_{ex} factor is obtained, which simplify the matching circuit design. Finally, the fiber coupling is achieved cost effectively by combining a number of lensed fibers mounted on a silicon V-groove. This process will enable packaging a large number of laser diode sources.

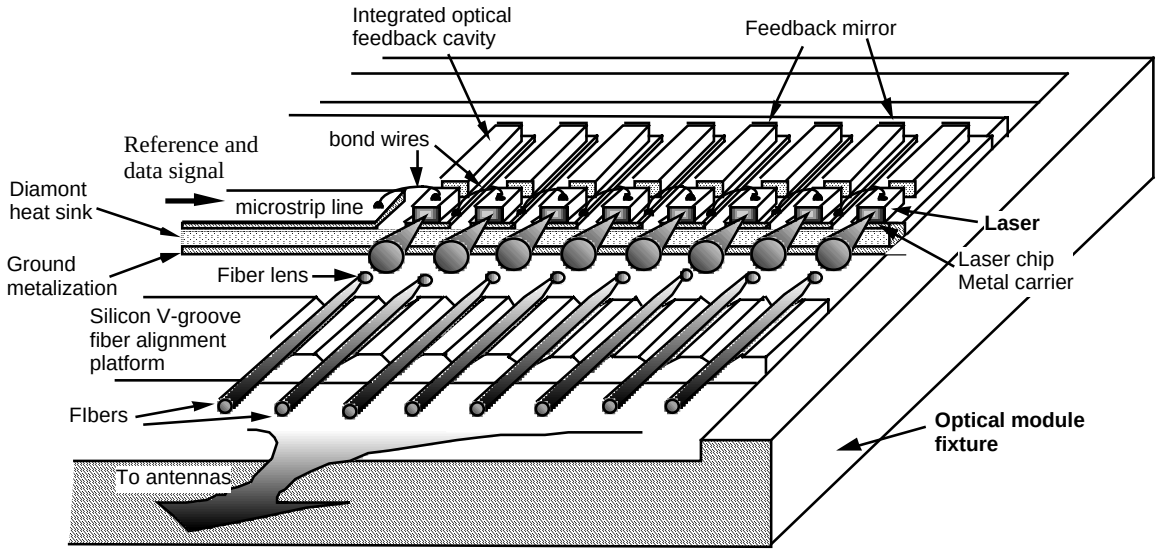

Fig. 4. Conceptual representation of an optimized optical transmitter using eight series mounted laser diodes with monolithically integrated external optical cavity coupled to the lensed fibers using a Si V-groove fiber alignment system.

Architecture Innovations: In large aperture phased array antennas, RF signal could be down converted to the IF signals for further processing at the centralized receiver. This architecture, shown in Fig. 5, is the conventional one. The challenges for implementation of optically controlled phased array using this architecture are: i) a high dynamic range fiber optic links are required at ultra-high frequencies, ii) phase and frequency control needs to be maintained in the distribution network all the way to the central processor, 3) as will be shown a higher resolution for true time delay device are required. On the other hand, the T/R Level Data Mixing architecture, shown in Fig. 6, provides a great opportunity to perform down conversion of the RF signals to IF and avoid the limitations that are encountered in the CPU level data mixing. The additional cost are: i) the need for stabilized LO at each element to coherently down- or up-convert the received RF or IF signals; ii) increase in the number of optical links; iii) the requirement of phase control in addition to TTD to obtain squint free

radiated beam. Nonetheless, experimental comparison of a 2x4 MMIC based C-band phase array antenna was conducted, where a superior dynamic range was measured for T/R level data mixing architecture over the CPU level one [3]. These apparent limitations were avoided using cascaded ILPLL oscillator [4], self-oscillating mixer [5], opto-electronic mixer using MLL [6]. The most important advantage of T/R level data mixing is its reduction of the number of resolution bit required to generate a squint free beams. This issue is highlighted next.

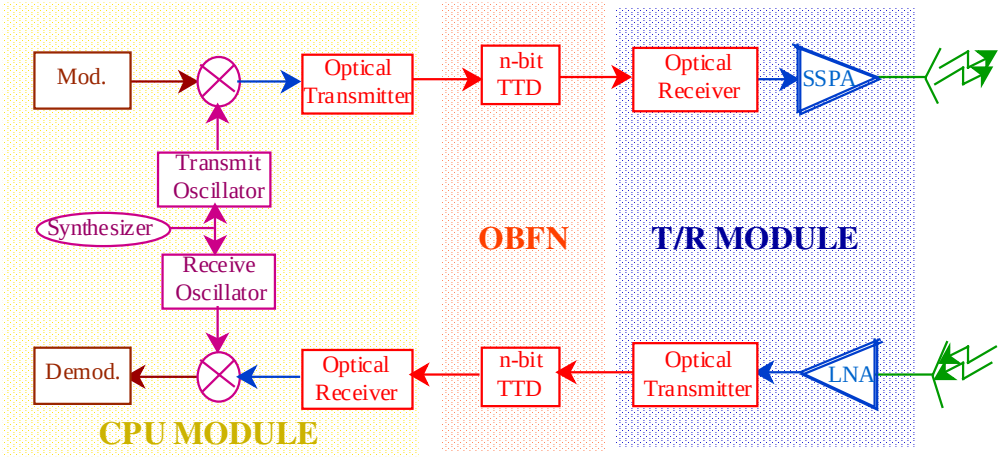

Fig. 5. CPU Level Data Mixing architecture for transmit and receive mode operation. Note true time delay devices are required for broadband operation without beam squint.

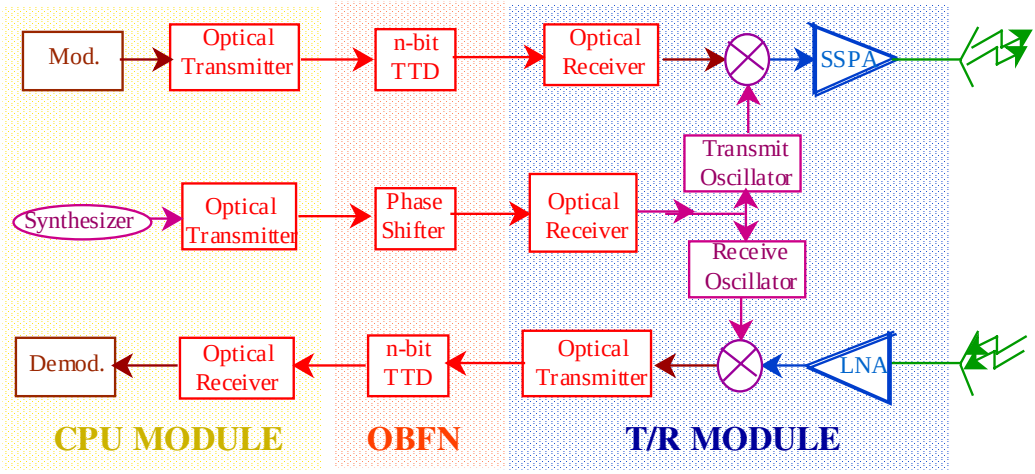

Fig.6. T/R Level Data Mixing architecture for transmit and receive mode operation, where distributed local oscillators need to be synchronized to a frequency reference. Note both true time delay and phase shifter devices are required for beam squint free operation in broadband systems.

Fig. 7 depicts radiation pattern of a 25 element linear phased array (with $\lambda/2$ separation) designed for operation at center frequency of 33 GHz with bandwidth of 3 GHz (i.e., each graph is composite of three simulated graphs at frequencies of 31.5, 33, and 34.5 GHz). The simulation results are for a CPU level data mixing. The required time delay is

achieved using a switched delay line TTD (true time delay device) with minimum time resolution of 10 ps. As this simulation result indicates as the beam is pointed away from broadside, sidelobe levels increase to only -6dBc and the main beam decreases by 2dB. On the other hand, Fig. 8 depicts the simulated performance of the same phased array when it is constructed based on T/R level data mixing. This structure employs a 2π analog phase shifter based on the concept of cascaded oscillators [4] along with a TTD with a time resolution of 30 ps (i.e., decreasing the time delay number of bits by about factor of 4). As this figure clearly represents no reduction in main beam peak level or the increase in side-lobe levels is observed for any scan angles. In fact, the sidelobe levels are compatible with the expected theoretical level of 13.6 dB for uniform array.

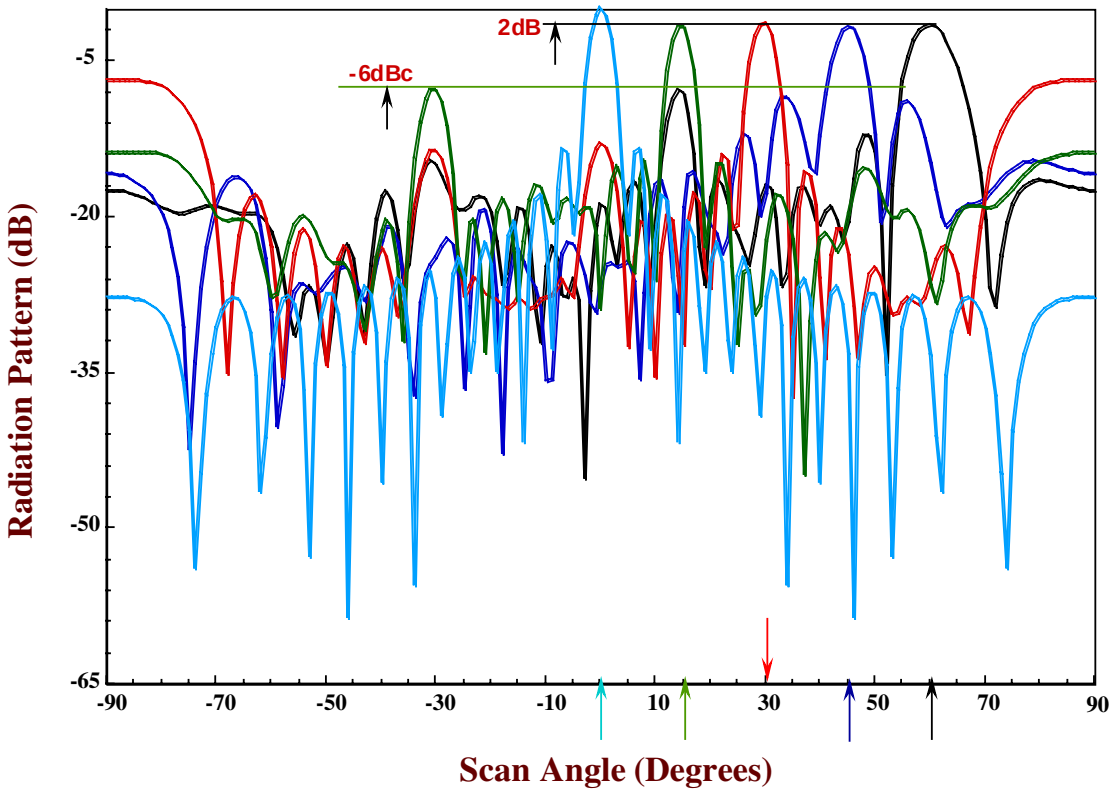

Fig.7. Simulated radiation pattern of 25 radiating element linear multibeam phased array antenna based on a CPU Level Data Mixing architecture where a true-time delay line with10 ps resolution is employed to generate beams at different angles (f_{LO}=24 GHz, f_{data}=7.5 – 10.5 GHz, f_{RF}=31.5 – 34.5 GHz).

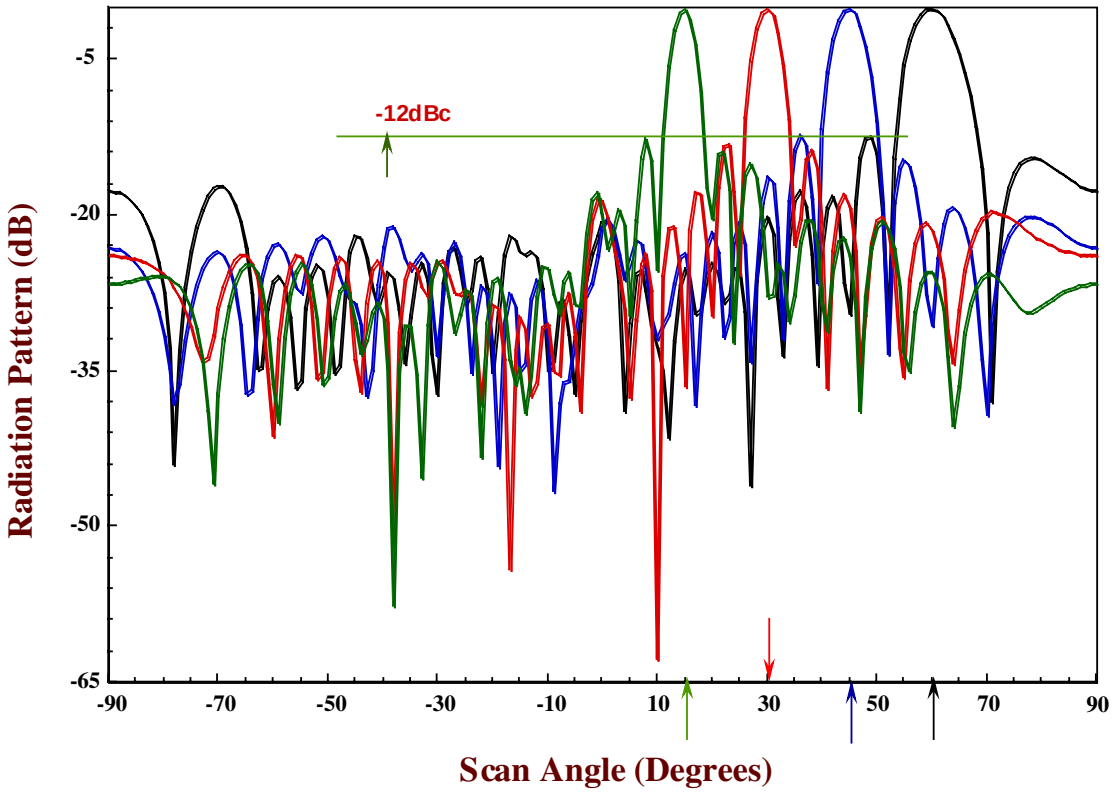

Fig. 8. Simulated radiation pattern of 25 radiating element linear multibeam phased array antenna based on a T/R Level Data Mixing architecture where a true-time delay line with 30 ps resolution along with analog phase shifter for LO is employed to generate beams at different angles (f_{LO}=24 GHz, f_{data}=7.5 – 10.5 GHz, f_{RF}=31.5 – 34.5 GHz).

4.0 Microwave Photonic Signal Processors

One of the most significant advantages of microwave photonics is not the antenna remoting concepts, rather the opportunity to perform signal processing in optical domain. The primary figure of merit is the time bandwidth product that could exceed 10^4, hence leading to significant rejection and filtering using various delay lines. A few realizations of signal processors using microwave photonic techniques are discussed next.

Memory Loop: Fiber optic based memory loops are used for recirculation of the incoming RF pulses. The simplified schematic diagram of a fiber optic based recirculating memory loop is conceptually shown in Fig. 9. This system consists of four basic elements: a switch, an electrical amplifier, a fiberoptic time delay element, and a gain equalizer. The gain equalizer in our system is composed of a YIG tunable filter and an attenuator. The RF input pulse is routed through the switch to the time delay device. The switch closes the loop and thus controls the recirculation. As the signal reenters the microwave circuit, it is amplified and rerouted through the fiber. As a result, a pulse train is obtained that has a pulse repetition interval corresponding to one recirculation time through the loop.

The number of recirculations is not limited by dispersion and for higher recirculation the following steps are devised: i) reducing the insertion loss and noise figure of the fiber optic link, and ii) flattening the frequency response of the closed loop system. Therefore, our

approach involves optimizing the performance of the fiberoptic delay element over the bandwidth of 2-4 GHz. A fiberoptic link is established over 2-4 GHz with a measured frequency response of the fiberoptic link has insertion loss of –11dB with flatness of 4dB was. The fiberoptic link has a compression dynamic range of 134 dB.Hz and spurious free dynamic range of 87 dB.$Hz^{2/3}$. A low noise figure fiber optic delay element is capable of recirculating a short electrical pulse as long as a millisecond, using 1 km optical delay line. The spectral purity of the recirculated signal is evaluated using the phase coherency measurement criteria. A plot of the phase noise degradation of the microwave carrier at three different recirculation times and offset carrier is shown in Fig. 10, where the spectral purity of the output pulses are shown after 10, 20, and 35 recirculations. The phase noise degradation is measured for offset carrier frequencies of 10, 50 and 100 Hz.

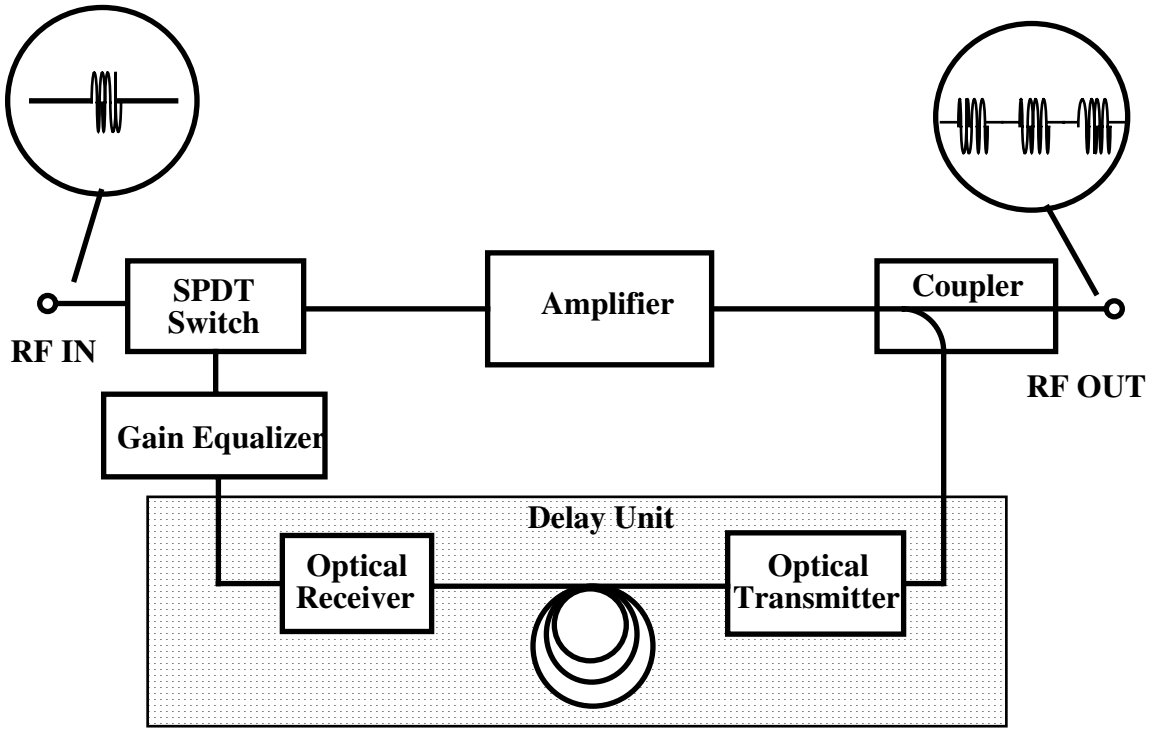

Fig. 9. Conceptual drawing of a fiberoptic based recirculating delay line. It is composed of a SPDT switch, electronic amplifier, coupler, optical delay element, and gain equalizer.

Since the frequency response of the open loop is not, in practice, flat over the bandwidth, for enhancing the performance of the memory loop, a gain equalizer is required. The amplification of the recirculating signal can be realized in either the electrical [7] or the optical domain. For broadband microwave signal processing, however, where the incoming signals in the frequency range of 2-18 GHz are analyzed, pulse recirculation in the optical domain is preferable to the electrical domain.

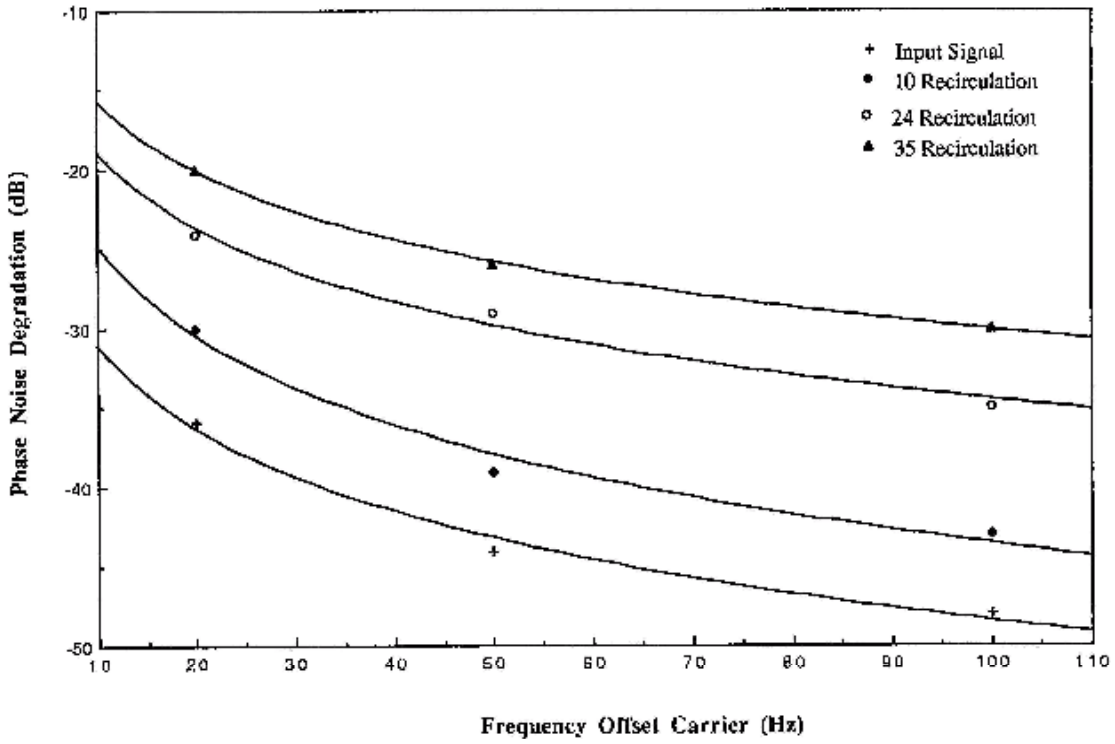

Fig. 10. Spectral purity and phase noise degradation compared to the input electrical pulse at various offset carrier as a function of number of recirulations.

The most limiting factor that degrades the output signal of the optical delay element is the noise build-up in the loop, whenever open loop gain is above unity. In particular, flatness and the noise figure are the limiting factors of Fiber Optic Memory Loop (FOML). The implication of non-flat frequency response of the delay unit is that the noise will increase faster at frequencies where the loop gain is high. Therefore, the nonflat frequency and high noise figure of the delay element will restrict the maximum number of recirculation attainable by the memory loop. The maximum number of recirculations in the loop in terms of the characteristics of the system components can then be numerically evaluated as a function of gain flatness, C. Particularly, the maximum number of recirculations, n_{max}, is limited to maximum number allowable by NF_{Tmax}, and the open loop noise figure NF_B as [7]:

$$NF_{Tmax} \approx \frac{1}{2}(NF_B\text{-}1)\left[\frac{1}{C^n}\frac{1\text{-}C^n}{1\text{-}C}+n\right]$$

The implication of non-flat frequency response of the delay unit is that the noise will increase at a faster rate at frequencies where open loop gain is greater than unity. Therefore, the non-flat frequency response and high noise figure of the delay element will restrict the maximum time delay attainable by the memory loop. Naturally, to overcome the n_{max} limitation, while achieving long total time delays, $n\tau$, one could increase the unit time delay, τ, but the long unit delay will produce a void in the time domain for the short input pulses. As an example, for the specified $(S/N)_{out}$=10 dB in a fiberoptic based memory loop using a

commercial FO link (Ortel link depicted in Table II), the maximum number of recirculation reduces from 954 for a flat frequency response to only 26 for a gain flatness of 1 dB. Whereas in case of reactively matched optical transmitter, the maximum numbers are 3070 and 37, respectively, because of the lower loss and noise figure of the fiberoptic link. Using a high gain reactively matched transmitter and an actively matched receiver leads to an unprecedented number of recirculation. Once again as, the link flatness reduces to 1dB of ripple, the maximum number of recirculation achieved would reduce to only 46 times. An adaptive gain equalization technique can be used to suppress the effect of noise build up in the system, which is enhanced by non flatness of the frequency response of the loop.

The maximum number of recirculation in the optical domain can be analyzed based on the noise performance of the commercially available optical amplifiers. The noise build-up in the optical system depends on many parameters such as optical power level, laser modulation index, light coupling factors, and quantum efficiencies of electro-optic transducers. Noise contribution of the spontaneous-spontaneous beat noise of the optical amplifier to the overall noise can be minimized by a reduction of the enormous gain bandwidth (>6000GHz) of the optical amplifier (to <100GHz).

For the memory loop system with narrow optical bandwidth, the major noise source of the system is signal-spontaneous beat noise. In this case, the maximum number of recirculations in the optical memory loop is dependent on the signal level and modulation index of the optical transmitter. As an example, a commercially available optical amplifier with the following characteristics is considered. The optical amplifier has internal gain of 15dB, saturation output power of 5 mW, noise enhancement factor of 2, and input and output coupling efficiencies of 33%. The signal-to-noise ratio was calculated as a function of number of recirculations with modulation index as a parameter. A plot showing the output signal-to-noise ratio for the internal gain of 15 dB is depicted in Fig. 11. In this figure modulation indexes of 0.1, 0.2, 0.3, 0.5, 0.75 and 1 are selected. Also shown here is the output signal-to-noise ratio of 6 dB, which corresponds to the minimum signal-to-noise ratio requirement for efficient detection. From this figure, based on a modulation index of 0.3, and for signal-to-noise ratio to be degradated to 6 dB, the maximum number of recirculations, as high as $n_{optical}$= 750, is obtained. This number shows that when the optical loop is operated at the proper bias and signal level for unit delay element of 1km, time delay in the range of millisecond can easily be achieved. However, as the optical gain increases, the number of optical recirculation diminishes precipitously.

Advanced Optical Signal Processing Techniques: The use of passive optical components such as optical isolators, array wave guide grating, superposed array grating, and spatial light modulators enable us now to perform a number of signal processing techniques to mitigate interference [8- 10], and adaptive waveform generation [11]. The basic principle of these techniques are based on translating spectrum to time using dispersive fibers or delay lines. As the number of taps increases, increased resolution in frequency domain could be observed. On the other hand, using mode-locke dpulses with short sampling period will increase the time resolution. As the tap weights and unit time delay are adjusted, aribtary waveform in time domain are generated that corresponds to the desired transfer function. Fig. 12 depicts structure of a tunable filter and a tunable filter Q as high as 800 has been demonstrated by Prof. Minasian. Even though discrete grating arrays are simpler in design and implementation, but for sampling bandwidth in the range of THz, superposed arrays are quite practical [12].

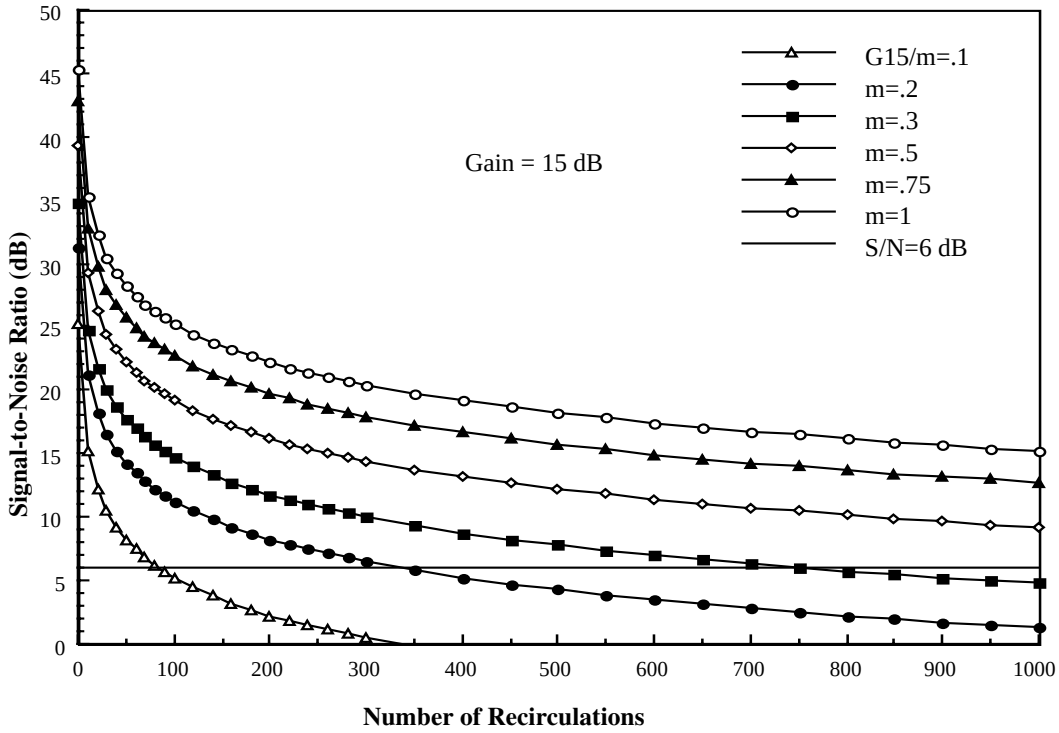

Fig. 11. Signal-to-noise ratio in an optical loop as a function of number of recirculations with modulation index as parameter. Amplifier gain is 15 dB and modulation indexes are 0.1, 0.2, 0.3, 0.5, 0.75 and 1.

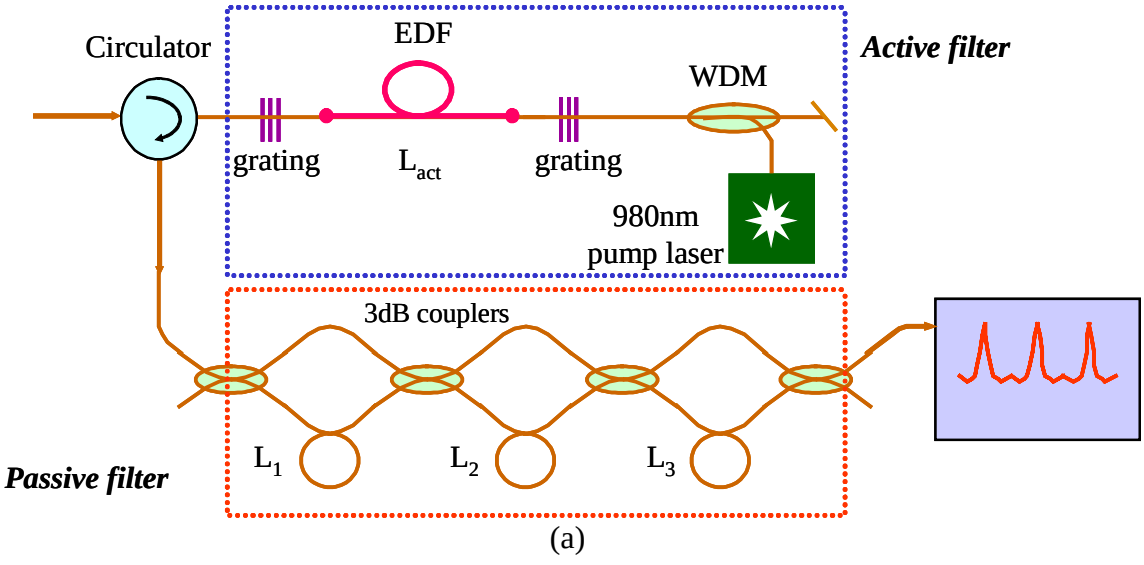

(a)

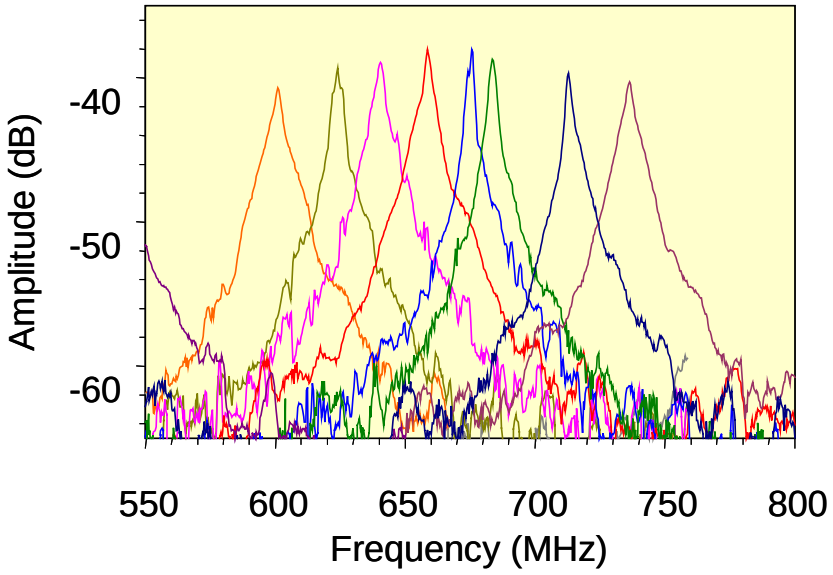

(b)

Fig. 12. Optical signal processing using a tunable filter. a) Experimental set-up, b) transfer function in terms of modulated frequency. (Courtesy of Prof. Robert Minasian of University of Sydney.)

Moreover, tapped delay line are employed in combination with positive and negative optical amplitude to adjust transfer function and shape of the transversal filter. High birefringence material combined with polarizer to create all optical transversal filters. Fig. 13 renders the shape of filter impulse response. The desired impulse response is converted to the desired bandpass filter. Moreover, notch filters could be developed using RF interference in the optical fiber while the other frequencies are transmitted through without much attenuation. Interference mitigation of 50dB at 75 MHz is experimentally demonstrated by Prof. Minasian.

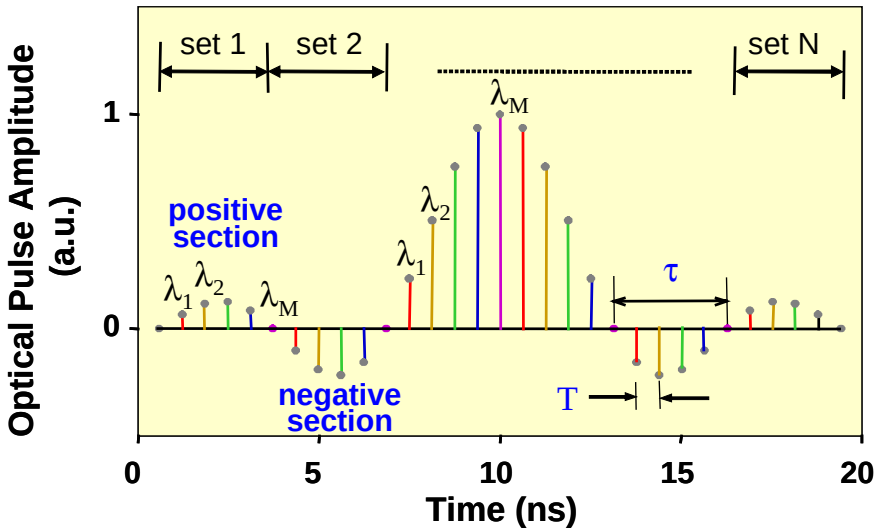

(a)

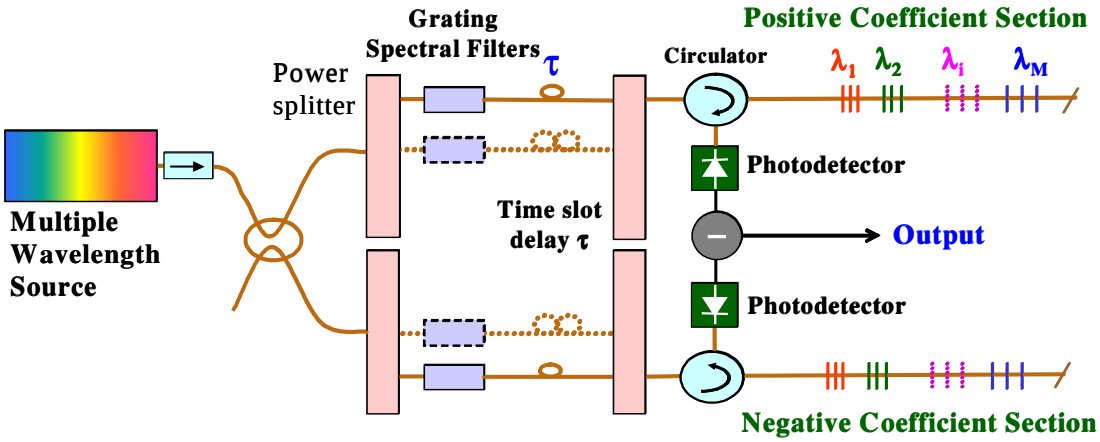

Fig. Filter Impulse Response (FIR) using spectral time mapping. a) Desired signal in time domain, and b) experimental set-up. (Courtesy of Prof. Robert Minasian of University of Sydney.)

5.0. CONCLUSIONS

This paper provides a personal perspective of microwave photonics and its direction of maturity. The direction of research is to develop novel devices that could meet high performance and low cost expectation. The harsh military environment also impacts the architecture of fiberoptic distribution networks. Among technologies that are unique to microwave photonics is the issue of optical signal processing which could lead to very large time-bandwidth products, hence resulting in high frequency selectivity. Memory loop devices, transversal filters, tapped delay lines are attractive solution that commands nitch market over the electrical signal processing techniques.

ACKNOWLEDGMENT

The author wishes to acknowledge the contribution of many of my students, partciularly Dr. Reza Saedi, Dr. Xiangdong Zhang, Dr. Manocher Ghanevati. Author also wishes to acknowledge contribution of Prof. Robert Minasian to the topics of transversal filter and tapped delay line.

REFERENCES

[1] H.X. Shi, D.A. Cohen, J. Barton, M. Majewski, L.A. Coldren, M.C. Larson, G.A. Fish, “Dynamics range of widely tunable sampled grating DBR lasers,” *Electron Lett.*, Vol 38, pp. 180-181, Feb. 2002.

[2] A. S. Daryoush, K. Sato, K. Horikawa, and H. Ogawa, "Dynamic Response of Long Optical Cavity Laser Diode for Ka-band Communication Satellites," *IEEE Trans. Microwave Theory and Techniques*, Vol. 45, no. 8, pp. 1288-1295, August 1997.

[3] R. Saedi, W. Jen, N. Samant, A.S. Daryoush, D. Sturzebecher, P. Herczfeld, "Comparison of CPU Level data Mixing to T/R Level Data Mixing Architectures in Optically Controlled Phased Arrays," *The 1993 International Microwave Symposium,* Atlanta, GA, June 1993.

[4] X. Zhang and A.S. Daryoush, "Full 360º Phase Shifting of Injection Locked Oscillators," *IEEE Microwave and Guided Wave Letters*, vol. 3, no. 1, pp. 14-16, 1993.

[5] X. Zhou and A. S. Daryoush, "An Efficient Self-Oscillating Mixer for Communications" *IEEE Trans. Microwave Theory and Techniques*, vol. 42, no.10, pp.1858-1862, Oct. 1994.
[6] A. S. Daryoush, K. Sato, K. Horikawa, and H. Ogawa, "Efficient Optoelectronic Mixing at Ka-Band Using a Mode-Locked Laser," *IEEE Microwave and Guided Wave Letters*, Vol. 9, no. 8, pp. 317-319, August 1999.
[7] R. Saedi, A.S. Daryoush, and P. Herczfeld, "Fiberoptic Based Recirculating Memory Loop" The 1992 *IEEE International Microwave Symposium Digest, 1992 IEEE MTT-S Microwave Symposium Digest*, vol. II, pp. 677-680, Albuquerque, NM, June 1992.
[8] D.B. Hunter, R.A. Minasian, P.A. Krug, "Tunable Optical Transversal Filter Based on Chirped Gratings," *Electron Lett*., vol. 31, pp.2205-2207, 1995.
[9] J. Campany, D. Pastor, B. Ortega, "New and Flexible Fiberoptic Delay Line Filters using Chirped Bragg Gratings and Laser Arrays," *IEEE Trans Microwave Theory Techn.*, Vol. 47, pp. 1321-1326, 1999.
[10] X. Wang and K.T. Chan, "Tunable All-Optical Incoherent Bipolar delay-Line Filter using Injection-locked FP laser and Fiber Bragg Gratings," *Electron Lett*., vol. 36, no.24, 2000.
[11] A.M. Weiner et al, IEEE J. Quantum Electron, vol. 28, p. 908, 1992.
[12] R.A. Minasian, K.E. Alameh, and E.H.W. Cahan, "Photonics-based Interference Mitigation Filters", *IEEE Trans on Microwave Theory & Techn.*, Special Issue on Microwave and Millimeter-wave Photonics, Vol. 49, No. 10, pp. 1894-1899, 2001.

This page has been deliberately left blank

Page intentionnellement blanche

Optoelectronic Components and Integrated Circuits including Up and Down Conversion Technique and Hybrid Integration Technology

D. Decoster, S. Dupont and V. Magnin
IEMN, UMR CNRS 8520
Université des Sciences et Technologies de Lille
BP 69, avenue Poincaré, 59652 Villeneuve d'Ascq Cedex, France
Tel : 33 3 20 19 79 70 - Fax : 33 3 20 19 79 66
e-mail : didier.decoster@iemn.univ-lille1.fr

Summary

Microwave optical links can be considered as basic bricks for some emerging system applications such as optically supplied microwave antennas... Emitters, optical switching matrices, high speed photodetectors and specific components for up or down conversion, are generic devices or functions for microwave optical links. We will describe main ways to generate microwave or millimetre wave signals through an optical fibre: direct and external modulation, optical control of microwave oscillators, generation of harmonics with laser non-linearities, dual mode emitters, with emphasis on new explored ways. Optical switching matrixes, which are basic photonic integrated circuits for optical processing are also examined, with recent cross-talk and phase noise results. The problem related to high speed photodetectors are also detailed with emphasis on waveguide photodetectors. The problem of up and down conversion is developed through specific optoelectronic devices. At last, we discuss the monolithic integration of optoelectronic or photonic devices, recalling that the industrial way is based on hybrid technology on silicon mother board, and we suggest new ways for the future.

1. Introduction

Microwave optical links can be considered as basic bricks for some emerging system applications such as optically supplied microwave antennas. Here we will focus our attention on emitters, switching matrices, and high speed photodetectors which can be considered as generic devices or functions for microwave optical links. The last section will be devoted to the crucial problem of the integration (hybrid versus monolithic) of components and circuits.

2. Emitters

There is a lot of techniques to generate a microwave or millimetre wave signal through an optical fibre. We present and discuss here several of them with examples of specific devices developed for the purpose.

2.1 Direct modulation of laser diode

This is the most simple and popular method. This approach is based on the modulation of the current injected into a laser diode. The frequency response is characterized by a resonance effect which frequency increases with the injected current. Bandwidth above 20 GHz have been achieved with InP DFB lasers using this technique, but the bias current is generally high (over 100 mA). These operation conditions degrade the performance of the microvave optical link, particularly in terms of dynamic.

Other modulation approaches are explored in order to overcome this limitation. A new concept proposed a few years ago is based on the parametric modulation. The principle is the modulation of the absorption in a

Paper presented at the RTO SET Lecture Series on "Optics Microwave Interactions", held in Jouy en Josas, France, 2-3 September 2002; Duisburg, Germany, 5-6 September 2002; Budapest, Hungary, 9-10 September 2002, and published in RTO-EN-028.

small part of the cavity, instead of modulation via the injected current, as usually made. To achieve such a goal, the cavity of the semiconductor laser is separated into two parts: one is devoted to the laser gain, and the second to the modulation (figure 1). It means that the p+ upper electrode of the laser is separated into these two parts: a long one for gain purpose on which a current is injected, a short one for modulation on which the microwave signal is applied. These two electrodes must be electrically isolated. Compared to dynamic response of classical semiconductor laser, theoretical results [1] predicted a strong enhancement of the resonance effects at the same frequency, with a lower decrease of the dynamic response at high frequencies, 20 dB instead of 40 dB per decade (figure 2).

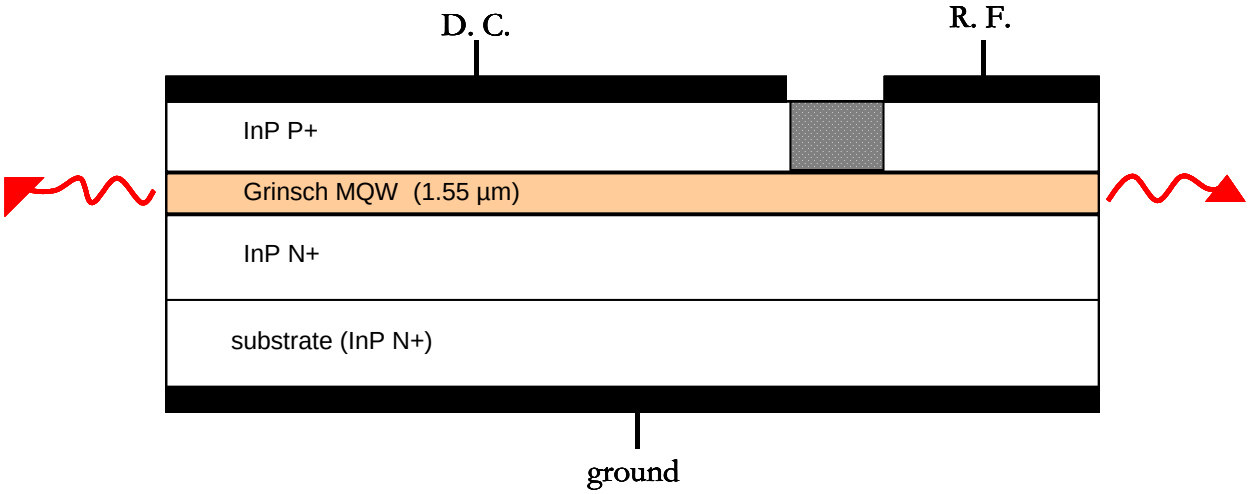

Figure 1 : Two electrode laser diode for parametric modulation.

This device was fabricated at Thales TRT. It was an InP MQW DFB laser with two electrodes (same axis) electrically isolated. Much attention was given to the isolation obtained by etching, and also to get low parasitic contact resistance and capacitance of the short length modulation zone. Experimental results confirmed theoretical predictions with the demonstration of a cut-off frequency over 30 GHz [2].

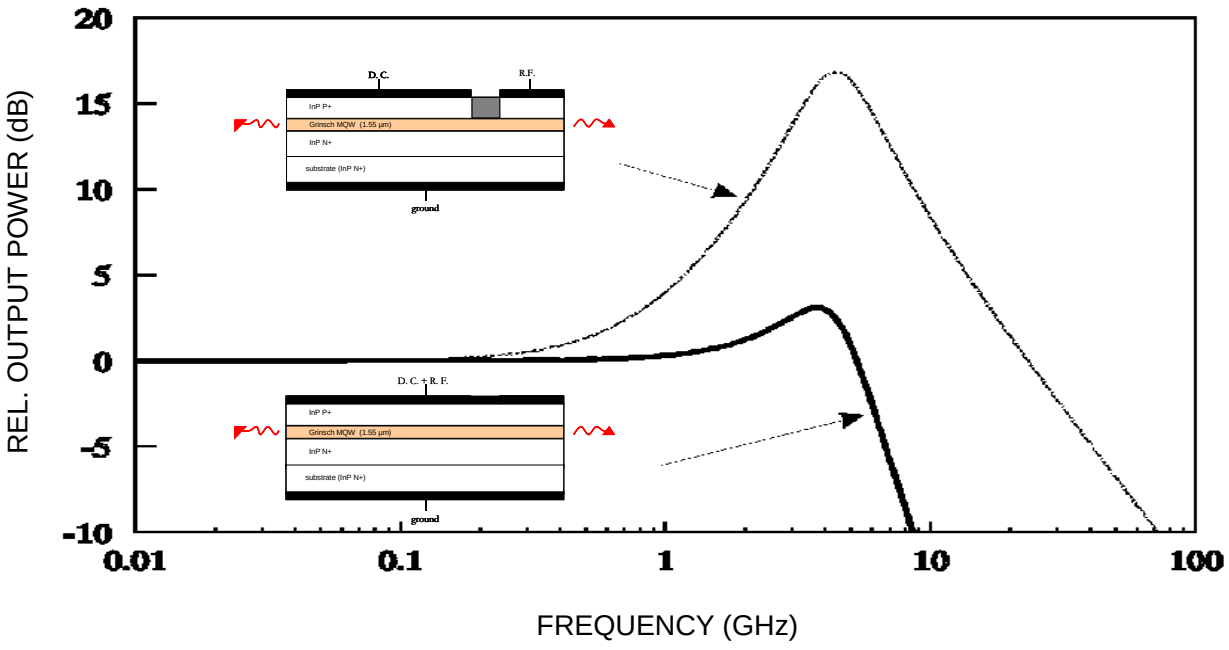

Figure 2 : Direct modulation and parametric modulation characteristics of semiconductor laser diodes.

An alternative to this approach is the laterally coupled dual laser. This new solution is currently studied in the frame of the FALCON TMR European project (coordination: prof. H. Lamela, university Carlos III –

Madrid). The principle is here to integrate inside the same laser cavity two parallel active zones. The first fabricated prototype is a 1.3 µm MQW InP Fabry-Perot laser with two active regions defined by the two parallel electrodes and by rib etching of the upper layer to get the optical confinement (figure 3). Depending on the distance between the two ribs, the optical coupling between the two laser active zones can be adjusted.

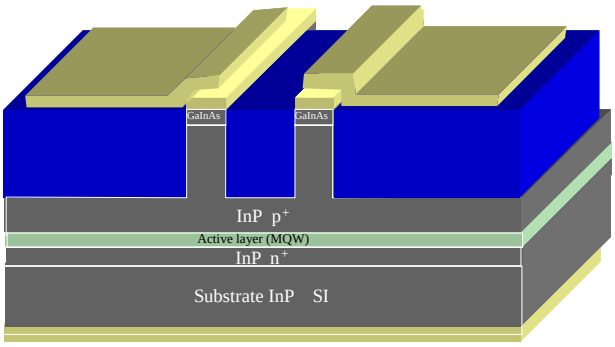

Figure 3 : Schematic view of a laterally coupled semiconductor laser.

It was theoretically predicted that a strong enhancement of the bandwidth could be achieved by applying the modulation current to one electrode and a DC current to the other one [3]. The bandwidth enhancement can be explained by a phenomenon similar to the bandwidth increase of coupled oscillators. First experimental results do not confirm theoretical bandwidth improvements. But a splitting of the optical modes into two lines could be observed, the frequency separation depending on the electrodes biasing. This result can be used to generate a microwave signal through the beating of the two optical modes into a high speed photodetector. In this experiment, the frequency of the microwave signal could be tuned with the bias currents injected into each active zone of the dual laser. The microwave signal frequency increased with the difference between the two bias currents and was only limited by the cut-off frequency (18 GHz) of the high speed photodetector. Nevertheless, due probably to the Fabry Perot multimode operation, the microwave signal was not pure enough to be useful and DFB structures seem to be promising.

2.2 External modulation:

It is an interesting alternative to direct modulation. For this scheme a CW current is injected into the laser diode and the modulation is applied to an external optical modulator. As a consequence the best (bias) conditions can be used for each function (emission and modulation). To improve the noise, hence the dynamic of the link, solid (YAG) lasers can advantageously replace the semiconductor (DFB) laser, if no limitation in place is required. Among the effort to increase the performance of the optical modulators, the bandwidth is an important feature. We can class modulators in two main types: electro-absorption and electro-optic modulators. For the first type an electric field, modifies the transparency (or absorption) of a III-V material for an optical signal wavelength close to its bandgap wavelength. Thanks to Franz Keldish effect a change of bandgap energy occurs under applied voltage and for a good choice of signal wavelength, the semiconductor material changes its transmission state from transparent to absorbing. Multiquantum well PIN structures introduced into optical waveguides are used to increase this phenomenon (Quantum Confined Stark Effect). With this kind of devices bandwidth above 40 GHz are obtained, combined to a modulation voltage close to 1 V. The efficient modulation / voltage ratio is a consequence of a (resonant) exitonic effect and thus the optical bandwidth of the modulator is limited to several 10 nm. In spite of a low modulation voltage, which makes these devices attractive, they are in general strongly nonlinear and the quality of the microwave optical link can be degraded.

It is the reason why electro-optic modulators, based on the modulation of the phase of the optical signal via the electro-optic Pockels effect, is also under studies. To get an amplitude modulation, the electro-optic device is based on the principle of the Mach-Zehnder interferometer: the optical signal is divided into two arms (equal length) and recombined at the output. The device is fabricated in integrated optics, with an electrooptic material. Electrodes are placed along one (or both) arms. When a voltage is applied to one arm, a corresponding optical phase change is obtained; if the difference of phase at the output of the two arms is π, a null occurs (which defines V_π voltage). Different materials are used: $LiNbO_3$, III-V, polymers... $LiNbO_3$

exhibits the highest optical index variation with electric field. Even in this case, the electrode must be long (over 1 cm) to get a V_π voltage still rather high (~10V). The consequence is a high capacitance, and the only solution to overcome this fundamental limitation is the travelling wave electrode. The basic idea is here to transform the long electrode into a 50 Ω transmission line loaded on a 50 Ω impedance. In principle, if the optical and microwave indices are equal, the bandwidth is unlimited. This is difficult to achieve with $LiNbO_3$ because the microwave permittivity is far from the square of the optical index; for III-V materials the condition optical index # microwave index is verified but these materials suffer from a lower electro-optic effect. Polymer based modulators are under intense research because optical and microwave indexes are equal and polymer can be deposed on metal leading to, in principle, ideal microwave microstrip lines. Electro-optic effect is induced by chromophores introduced in the polymer. To get an electro-optic activity, a poling procedure is carried out. Bandwidth over 40 GHz are obtained with the three types of materials. Due to a special electrode design ($LiNbO_3$ modulators) or advanced materials (polymer modulators), low V_π (< 1 V) and high bandwidth electro-optic modulators are demonstrated [4, 5].

2.3 Optical control of microwave oscillators :

It consists of modifying the characteristics (amplitude, phase or frequency) of a millimetre wave signal generated by the oscillator, thanks to the optical signal impinging on the oscillator. It is also possible, to optically lock the frequency of the microwave oscillator. In optical injection locking, the optical control signal is intensity modulated at a frequency close to the free running frequency of the oscillator (fundamental locking), one of its harmonics (harmonic locking), or one of its subharmonic (subharmonic locking) [6]. The modulated optical signal absorbed in the device active region gives rise to a current flow at the modulating frequency, and this acts in a very similar way to direct microwave signal injection. The use of subharmonic locking is suggested by the inherent nonlinearity of the active devices composing the oscillator, and it allows to use a diode laser which cut-off frequency is far below the frequency of the microwave oscillator (also with the possibility to neglect fibre dispersion effects). A fibre radio link was recently demonstrated based on this principle, with 7.6 dBm microwave output power, the oscillator being locked using up to the 32th subhamonic. The frequency was 10.6 GHz and the wavelength was 0.8 µm, the link being composed of a GaAs VCSEL and a GaAs MMIC [7]. Because this technique is promising for simplicity, power, conversion efficiency, intensive research are devoted to this topic for 1300 and 1550 nm operation, or for example at University of Kent at Canterbury.

2.4 Generation of harmonics with laser non-linearities:

When biased under high current or modulated at a frequency close to the resonance frequency, a laser diode is generally highly non-linear. This effect can be advantageously used to get harmonics of the modulating microwave signal at the output of the link, if the speed of the photodetector is high enough and the length of fibre low enough to overcome bandwidth limitations due to fibre dispersion effects. In practice, the laser bias current is adjusted to match the resonance frequency of the laser to the microwave modulating frequency to improve harmonics generation ; an electrical filtering at the output of the photodetector allows to select the good harmonic. In terms of phase noise, the degradation (20.Logn, where n is the rank of the harmonic) is similar to a system based on the transmission of the fundamental through the link and electrically multiplied at the output, (or other systems based on a reference multiplication). For both cases, fibre-radio systems were demonstrated [8, 9], the second solution being more tolerant to the fibre dispersion, but a more complex microwave circuit (MMIC) is required. In principle this method could be extended to non-linear photodetectors. But a photodetector (except for very small ones) is a very linear component compared to a laser diode. Non-linear photodetector behaviour needs high optical power and low bias voltage and in practice in a link, laser diodes non-linearities appear before photodetector ones.

2.5 Dual mode emitters:

Another class of the optical microwave or mm-wave generation techniques is based on the emission of an optical spectrum consisting of only two discrete tones, separated by the mm-wave frequency. Mixing the two phase-correlated tones at a square low photodetector provides a spectrally pure mm-wave carrier signal at frequency f_{mm}. Fiber dispersion only affects the phase of the detected mm-wave signal, and this approach can operate over arbitrary lengths of standard fibre at 1550 nm.

A well-known system is the one adopted within the FRANS project, supported by the European Commission ACTS programme, and developed within the RACE project MODAL [10]. This technique generates a two-tone optical signal using a Mach-Zehnder modulator as an electro-optic mixer. Knowing that the Mach-Zehnder Modulator has a raised cosine intensity response, when biased at the point of minimum optical transmission, the response of the device on the optical field can be written as : $E_{out} = E_{in} \sin (\pi V/2V_{\pi})$ [11], leading to two optical modes.

Among the number of approaches which have been proposed and demonstrated to optically generate mm-wave signals [see for example 12 – 32], a very promising solution based on optical heterodyning, was developed at BT Laboratories. It consists of a master-slave Distributed Feedback (DFB) laser arrangement, where the lasers are in a series configuration and each laser contributes a single mode for optical mixing in a high speed photodiode [25, 32]. The electrical drive to the slave laser is at a subharmonic of the beat frequency and generates a series of sidebands. The master laser mode injection locks one of these slave sidebands which results in phase noise cancellation in the output signal.

It is also interesting to mention the works on optical Single Side Band generation to overcome penalties in fibre radio system with data signal. It has been demonstrated that, by using an optical filter to suppress one of the sidebands [33], in intensity modulation schemes, dispersion effects can be reduced by the elimination of one sideband to produce an optical single-sideband. This method is limited by the filter characteristics and can be quite complex to implement. To eliminate the need of optical filtering, a novel technique recently proposed [29] uses only one dual-electrode Mach-Zehnder Modulator. The RF signal is applied to both electronics with $\pi/2$ phase shift applied to one electrode. A DC bias voltage is also applied to one electrode while the other DC terminal is grounded. The Mach-Zehnder modulator can be considered as two optical phase modulators in parallel with drive signal $\pi/2$ out of phase and with DC voltage applied to one arm. By tuning the DC voltage, modulator is biased at quadrature. The RF power degradation due to fibre dispersion was observed to be only 1.5 dB when using the technique to send 2 – 20 GHz signals over 79,6 km of fibre. Approximately at the same time, fully integrated millimetric single sideband lightwave source were demonstrated [30] increasing the attractiveness of this technique.

Obviously the disposal of monolithic integrated dual mode sources is interesting for compactness, reduction of parasitics, efficiency... One way, as said just before [30], is the monolithic association of a DFB laser and a specially designed external optical modulator. One other way is the dual mode laser. DFB laser structures for which the usual effort to lift the mode degeneracy was not taken into consideration are dual mode laser. The coupling coefficient and the total laser length are the two main parameters governing the frequency separation between the two modes. The mode separation is approximately given by the following expression: $\Delta f \sim 1.5\, c\, \kappa \sqrt{2} / (\pi\, n_e \tanh(\kappa L))$

Where Δf is the mode frequency separation of the DFB ; κ the coupling coefficient of the DFB structure and L the total laser length. For a 60 GHz mode separation for example, we need a 2 mm long laser with a 9 cm^{-1} coupling coefficient. To reduce the laser length we need to reduce the coupling coefficient as well (below 3 cm^{-1} for a 1 mm long laser). But it seems difficult to control such reduced coupling coefficients from a technological point of view and the laser could possibly turn into a multimode emission. A possible structure designed with the aim of reducing the “effective” coupling coefficient using usual technologies compatible with conventional coupling coefficients, consists of alterning DFB and FP sections pumped by a single section source (figure 4). Using such a structure we can expect to get a reduced effective coupling coefficient by increasing the FP section length. A square wave function will sample the DFB structure according to its duty cycle. So, the refractive index of this structure will be equal to the refractive index of the conventional DFB multiplied by the Fourier series expansion of the spatial square wave function. It turns out that instead of having a single reflection coefficient centred around the Bragg frequency, this structure will generate a periodic filter with a periodicity in terms of optical frequency.

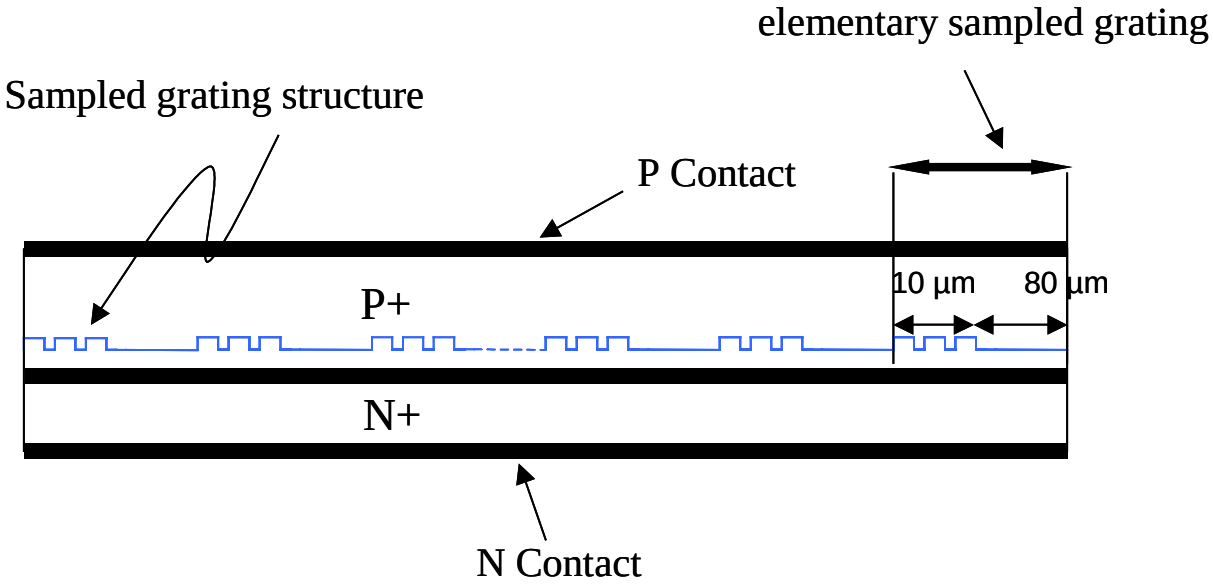

Figure 4 : Schematic of a dual mode laser based on a sampled grating structure.

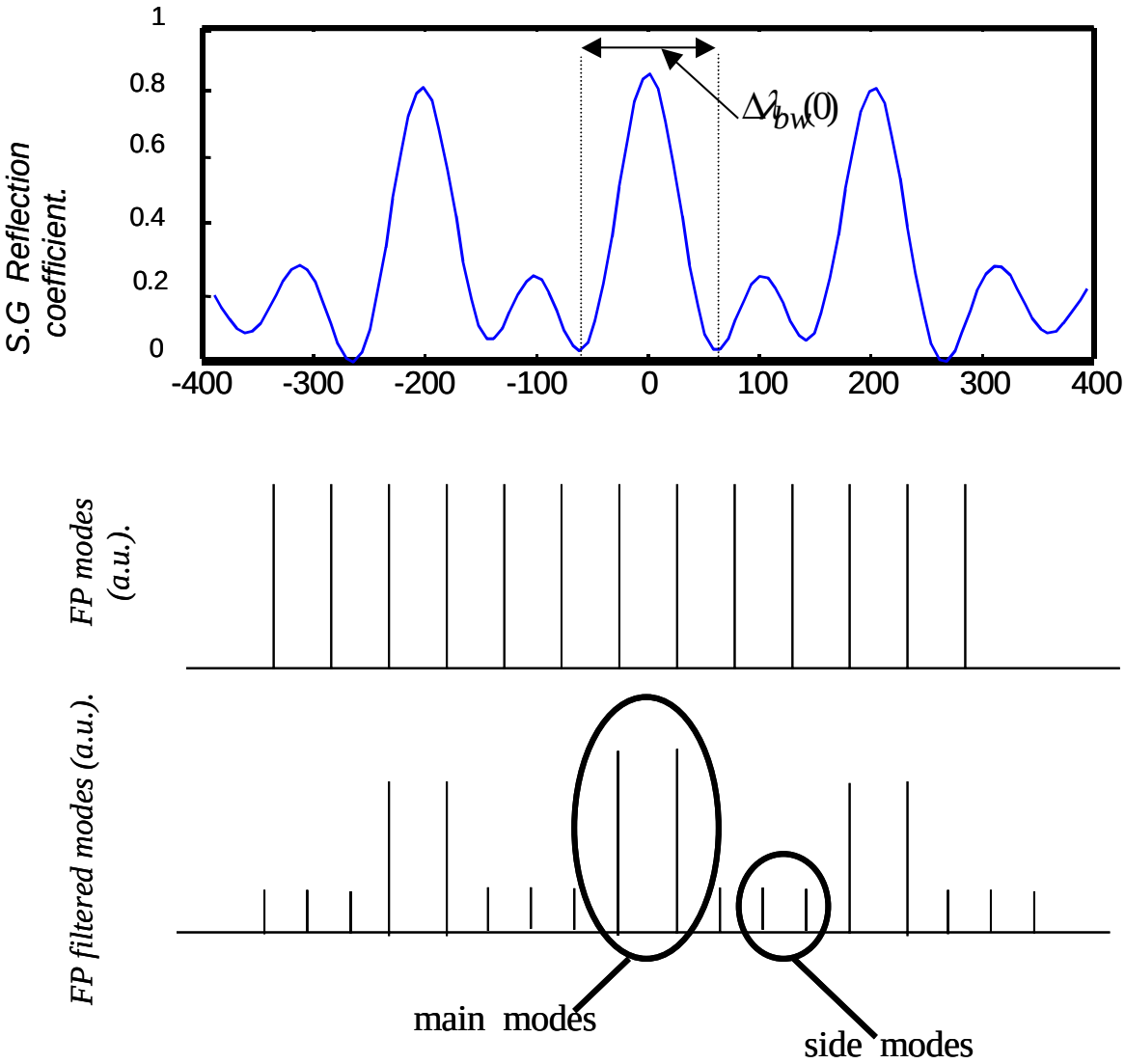

Figure 5 : Filtering of the Fabry Perot modes by the sampled grating periodic filter.

This can be illustrated by the schematic given in figure 5 where we show the modes of a Perot Fabry cavity and we superimpose the filter due to the periodic DFB section. Such a structure was modelled using the time domain model. It was shown that a good design of this structure predicts theoretically a dual mode emission with 60 GHz optical frequency separation and a dual-side mode suppression ratio of more than 35 dB [34].

3. Optical switching matrixes

An interesting example of microwave applications using optics is optical phased array antenna control. The emerging direction of array antenna beam depends on delays or phases laws. It is defined by the path differences between the physical plane of the radiating components and the virtual plane perpendicular to the beam direction.

Delays, instead of phase shifts, are needed to insure frequency independent beam steering. Usually, true time delays are obtained by the use of coaxial links or microstrip lines. In this case, the limitations are antenna dimensions and instantaneous bandwidth. Optoelectronics is one of the most promising techniques that allows antenna to fit both aerodynamic requirements and whole space survey. Different methods were proposed : for example the use of high dispersion fibre in conjunction with a widely tunable optical source to obtain the required delay variation [35], or systems where polarisation switching spatial light modulators route the optical path directly or via a corner reflector to select the delay [36]. In one system studied by Thales TRT, signal delay is optically obtained by associating switching matrixes with fibres of different lengths. Architecture properties are characterized by both temporal dynamic and resolution. Due to losses, the critical point in such systems is the number of fibre to waveguide interfaces. Thus, in order to reduce losses one possible solution is to use architecture based on high order matrixes.

Numerous optoelectronic laboratories are currently enhancing technology and properties of such devices. In particular, Westinghouse has developed a true time delay system using microwave and optical technology [37]. Thales TRT proposes a system based on integrated switching matrixes. The use of guided optics allows high order matrix implementation. Moreover, light offers an additional dimension which is wavelength. If matrixes are strictly non-blocking, which means that each input can be connected to each output independently, this dimension allows a reduction in the number of switching components proportional to the number of optical wavelengths. With this architecture, it is possible to achieve more than 4000 different paths with four 8*8 matrixes. It is characterized by a temporal dynamic of 4 ns for a resolution of 1ps.

Key components of this system are switching matrixes that fit the following specific conditions:

- light polarization insensitivity
- strictly non blocking matrix
- equivalent intra-matrix path lengths
- low power consumption.
- low insertion loss
- low excess noise (phase noise)
- low cross-talk
- short switching time

Due to high speed switching requirements, electro-mechanical (MOEMS) or thermo-optic effects (polymers) cannot be used to fabricate the switching active elements. Semiconductor optical amplifiers (SOA) is an attractive way because of its capability to high cross-talk, compensation of insertion losses and high speed. But recent experiments performed at Thales TRT shown that this component increases strongly the phase noise of microwave signals [38]. Consequently solutions using electro-optic switches driven by electrostatic modulation, carriers depletion or injection must be explored.

Among possible materials, InP based are well established for 1.3 or 1.55µm wavelength applications. An optical switching matrix is a photonic integrated circuit associating monolithically passive elements (optical waveguide with bendings,…) and switching active elements. As an example, an InP optical waveguide, grown by MBE or MOCVD on n type InP substrate, is constituted of a GaInAsP quaternary core layer inserted between InP confinement layers with a lateral confinement obtained via a rib etching (figure 7).

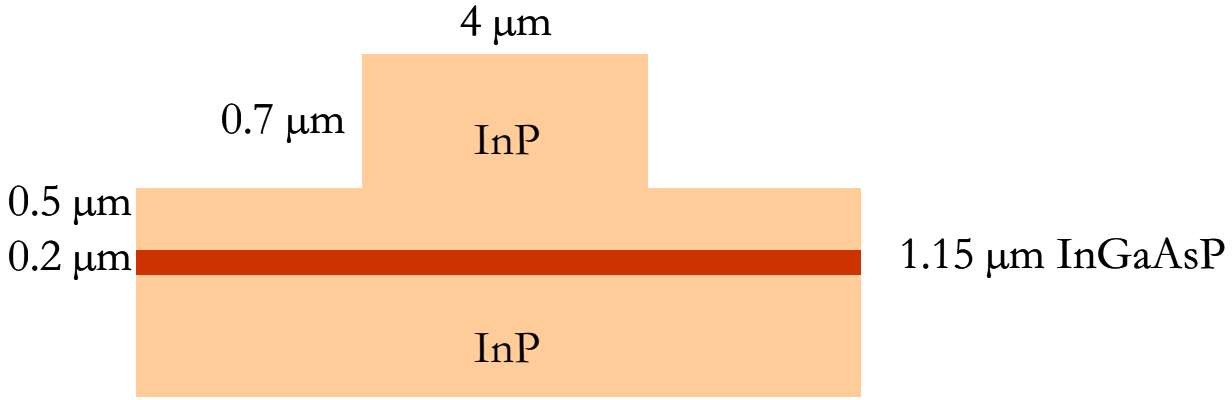

Figure 7 : Example of optical InP passive waveguide for switching matrixes.

About active elements, we used in devices fabricated at IEMN the plasma effect, obtained by injection of carriers in the optical waveguide, thanks to a PIN structure located by etching in the active zone. This effect decreases the optical index almost linearly with the density of carriers ($\cong 10^{-3}$ for 10^{17} cm^{-3}). We studied different structures : a kind of Electro-Optical Directional Coupler (EODC) that we called "cascade switch" [39-40] based on mode coupling, Digital Optical Switches (DOS) based on adiabatic mode changes [41] and a Total Internal Reflection (TIR) switch based on high reflection [42]. A 1 to 2 cascade switch (1 input, 2 outputs) is constituted of one active PIN waveguide placed closely between two passive waveguides playing the role of 1 input and 2 outputs. When no current is injected, the optical input beam is coupled to the extreme output waveguide. If current is injected into the current injection zone, the coupling is cancelled and light goes on the waveguide located just before the injection zone, here the input waveguide. This scheme can be extended to 1 to N optical switch: only one current injection will be required to obtain the light switch to any of the N outputs (figure 8).

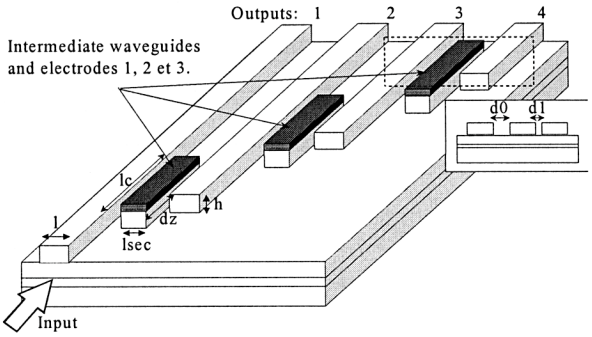

Figure 8 : Schematic view of a cascade switch

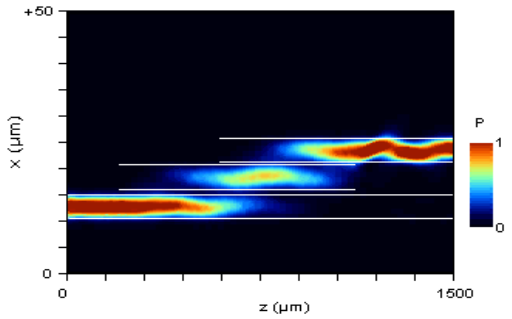

Modelling of light propagation (2D Beam Propagation Method) inside a cascade switch.

The technological fabrication [40] allows the monolithic integration of active and passive zones and is composed of three main steps: p ohmic contact realisation of the current injection zone, etching of the different guides, first level metallization and thinning and back N-metallization. The DOS is a Y junction with an electrode on each output arms. Without bias current the light is divided equally between the two arms. When a bias current is injected into one arm, optical index is reduced in this region, and light is pushed toward the other arm (figure 9).

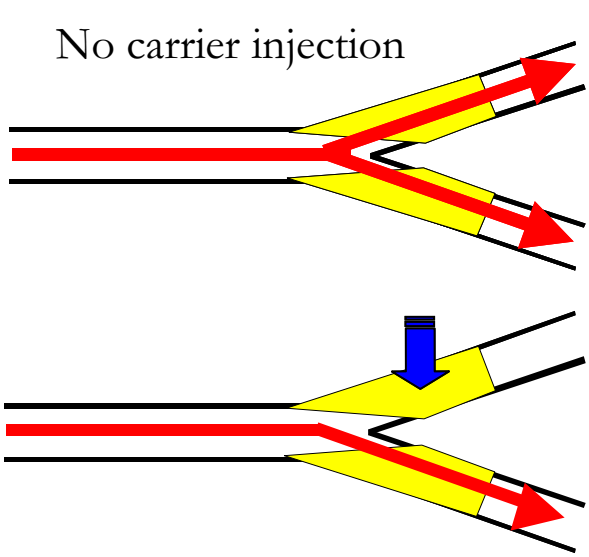

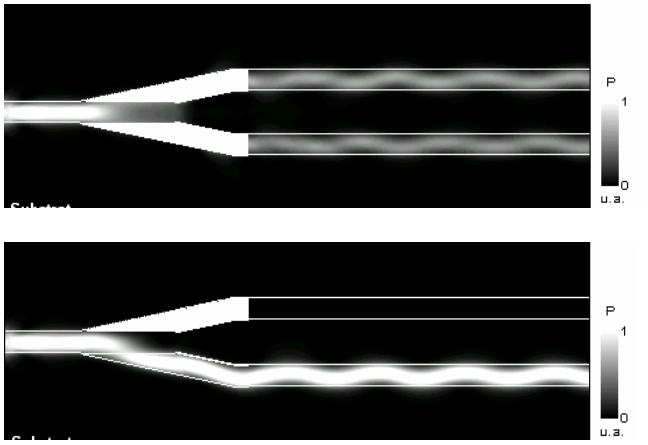

Figure 9 : Schematic view of a Digital Optical Switch

BPM modelling of the device.

The TIR is constituted of two crossing waveguides with an electrode at the crossing. Without biasing, light propagates along a straight line, an injected current acts as an electronic mirror and light is reflected into the other arm (Figure 10).

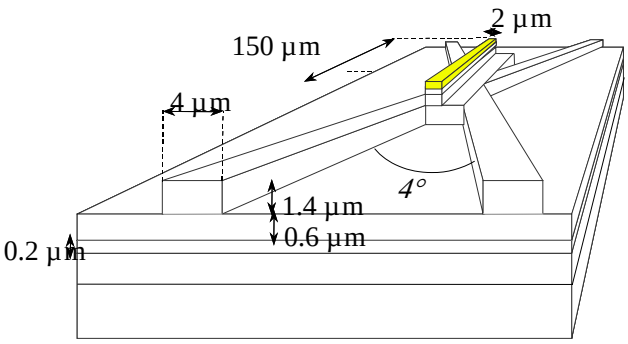

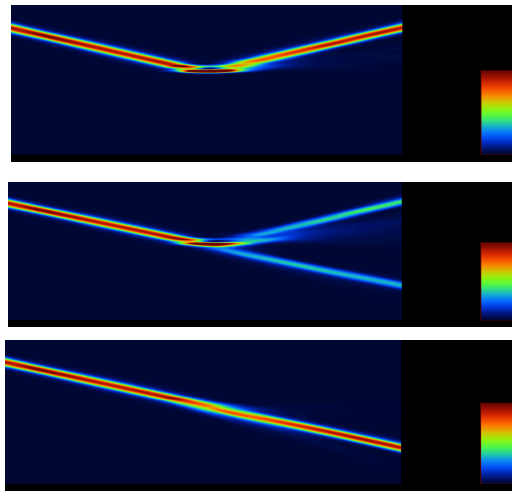

Figure 10 : Total Internal Reflection(TIR) switch

BPM modeling of the device.

. Our modelling and experimental studies show that:
- TIR switches suffer from a high consumption current (over 100 mA),
- Cascade switches offer optical cross-talk between 15-20 dB for current around 50 mA, with potentialities for 1 to N architecture with the same switching current, but suffer from a high sensitivity to technology,
- Best results are obtained with DOS. They exhibit the lowest switching currents (~20 mA for almost 1 mm long electrode and lower currents can be obtained with longer active zones) for optical cross-talk around 15 dB at 1.55 µm and around 30 dB at 1.3 µm wavelength (58 dB for a microwave signal at 9 GHz), figure 11.

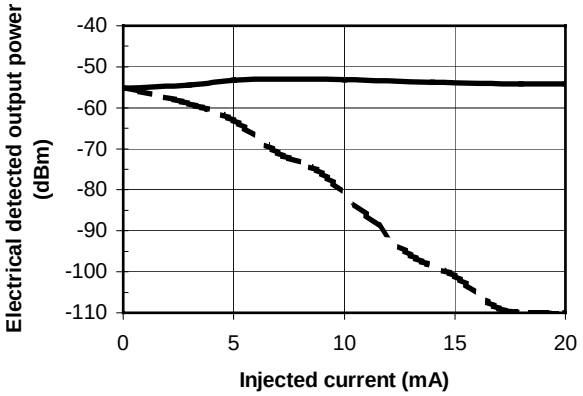

Figure 11a: Electrical output power of a 9 GHz signal issued from the switched on DOS branch (solid line) and the switched off one (dashed line) @ 1.3µm.

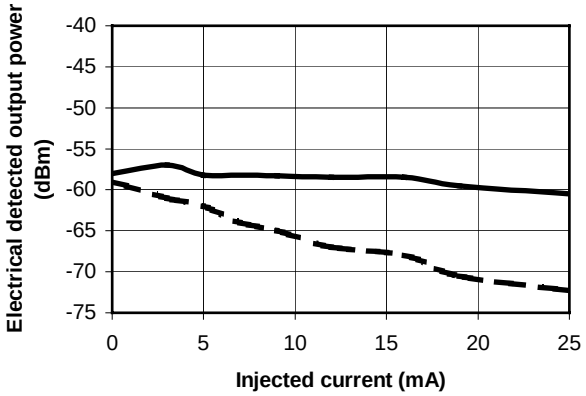

Figure 11b: Electrical output power of a 9 GHz signal issued from the switched on DOS branch (solid line) and the switched off one (dashed line) @ 1.55µm.

The difference between 1.55 µm and 1.3 µm wavelength cross-talk can be explained by band filling effects occurring for an operation wavelength close to the quaternary core layer bandgap wavelength [41] At last it was experimentally checked that the phase noise is not degraded by using DOS as shown on figure 12.

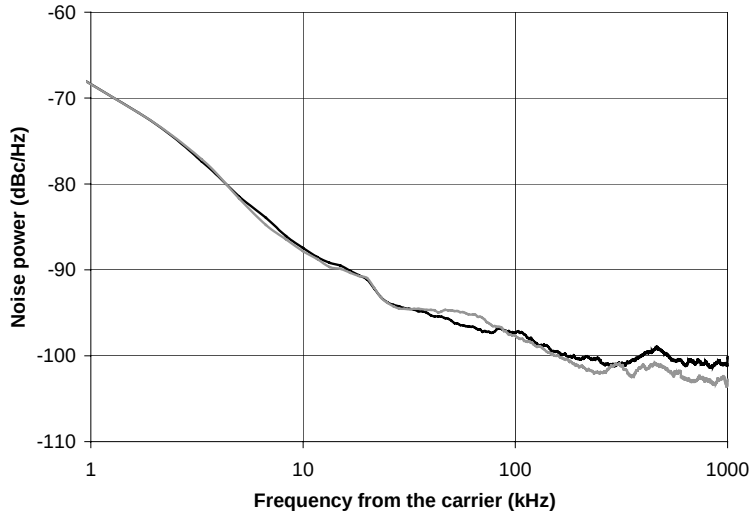

Figure 12 : Noise power level for at 9 GHz carrier@ 1.3 µm :
- gray line: switched signal (DC bias = 20 mA)
- black line: direct signal (DC bias = 0 mA)

4. High speed photodetectors

It is well known that high speed PIN photodiodes require short transit time in the active layer and small capacitance. As a consequence, for very high speed (millimetre wave) applications, the absorbing GaInAs region of InP photodiodes must be thin, typically 0.4 µm and less for cut off frequency higher than 60 GHz. With vertical illumination so thin absorbing layer leads to small quantum efficiency (figure 13a). The well known solution to overcome this trade off is the lateral illumination [43]. The photodetector is similar to an optical waveguide with an absorbing core, and is called PIN waveguide photodetector (figure 13b).

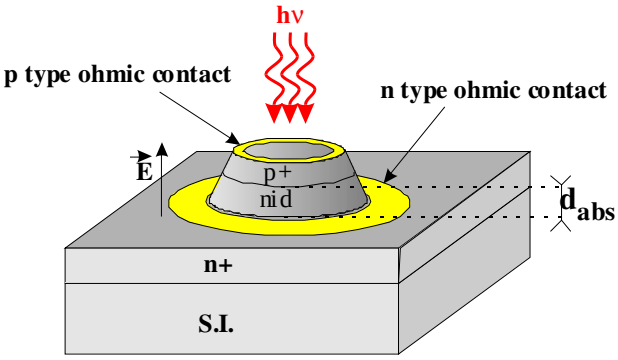

Figure 13a : Schematic view of a top illuminated PIN photodiode

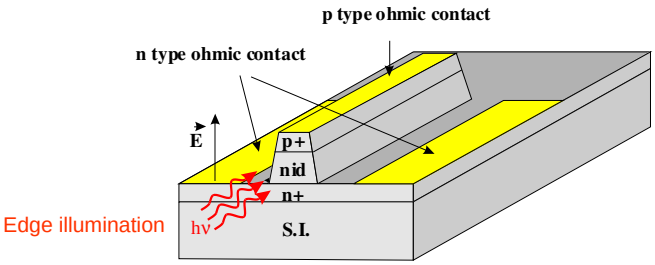

Figure 13b : Schematic view of a PIN waveguide photodiode

4.1 First problem: the optical coupling.

To get a good coupling to the optical fibre, a multimode structure is more suitable (figure 14). A typical epitaxy on InP semi-insulating substrate is then: a nid GaInAs absorbing layer between two (n and p types) GaInAsP and InP confinement layers, with a GaInAs p-type contact top layer. As an example, devices fabricated at IEMN exhibit a 4 µm etched rib waveguide, an input facet obtained by cleaving, with a total device length ranging around 10 to 20µm. With a lens-ended fibre, quantum efficiency higher than 60% without anti-reflection coating can be achieved with cut-off frequency over 60GHz [44].

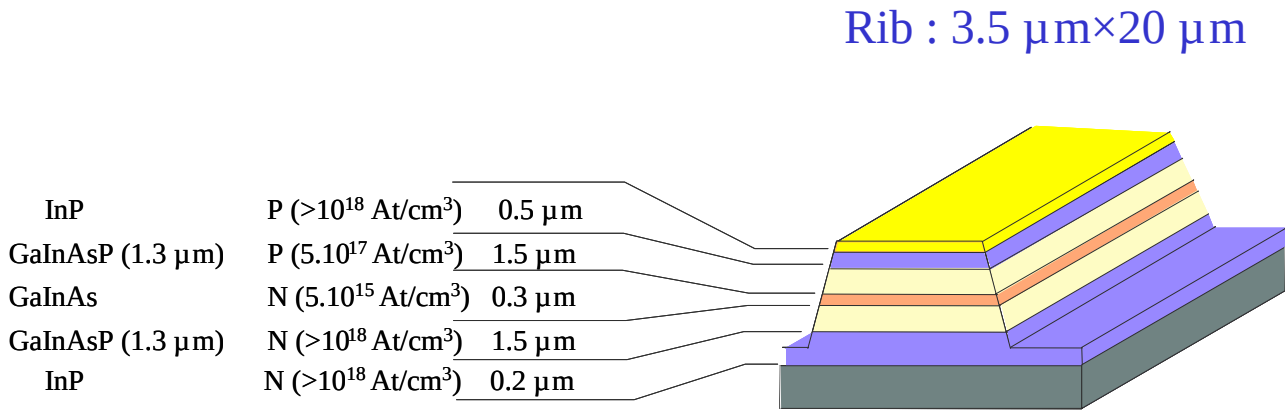

Figure 14 : multimode waveguide PIN photodiode

4.2 Second problem: the microwave or millimetre-wave access.

A semi-insulating substrate and a coplanar line improve the microwave access, by reduction of parasitics (capacitance …) (figure 15). The semi-insulating substrate allows the monolithic integration of a passive reactive network with the PIN waveguide photodiode to reduce the large impedance mismatch between the PIN photodetector and the 50Ω of the microwave world in a small bandwidth, as experimentally demonstrated for 30 GHz operating frequency by Thales TRT, in collaboration with IEMN [45].

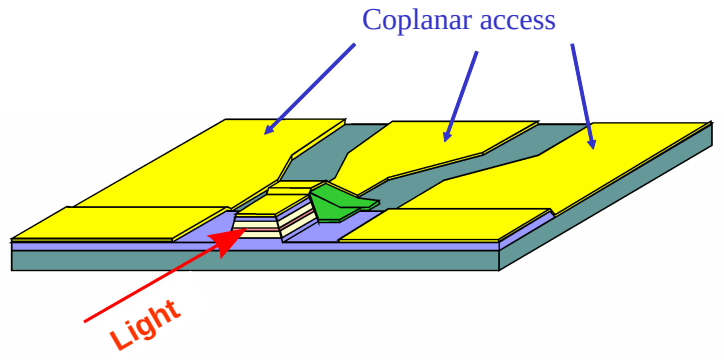

Figure 15 : coplanar microwave access.

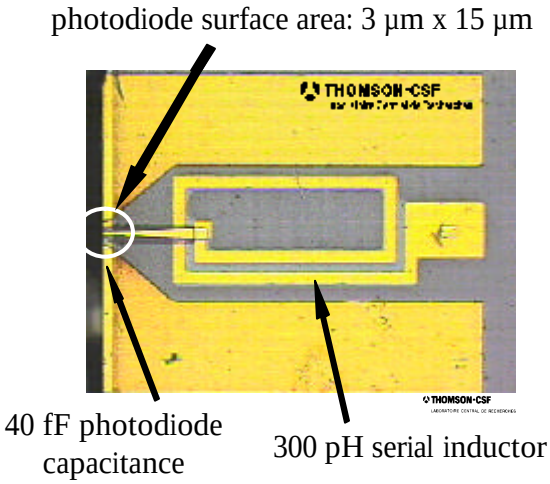

Monolithic integration of
PIN waveguide photodiode and inductor

4.3 Third problem: the power.

Power limitation (≅ 0dBm at 60GHz) [46] occur in so small devices, due to high density of photocarriers killing the electric field in the intrinsic region and high photocurrent reducing the bias voltage in the external circuit. These effects reduce the dynamic of the link. To solve this problem, two ways are possible : the travelling wave photodetector with a long length (and hence volume) with electrodes designed to get a 50Ω microwave line, and the uni-travelling carrier photodetector (figure 16) for which photodetection takes place in a thin p-type highly doped GaInAs absorbing layer. Up to date results are very encouraging [47, 48] and works are in progress at IEMN in collaboration with Thales TRT and Alcatel to get high speed, high power and high quantum efficiency devices.

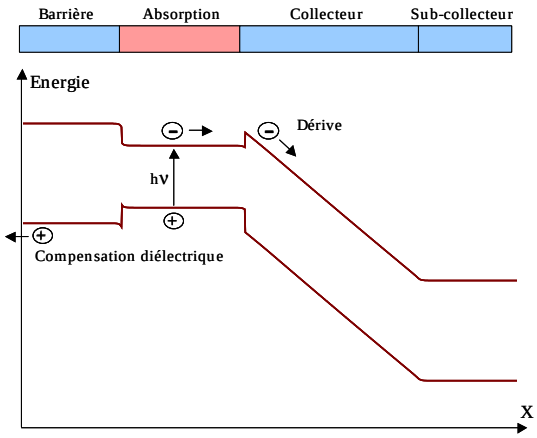

Figure 16 : band structure of an UTC photodiode.
Only electrons pass through the collector.

4.4 Fourth problem: the reliability.

The direct illumination scheme used in these devices has some known impairements: input facet fabrication with junction passivation is difficult to achieve with high reliability [49]. To overcome these impairments, high speed edge illuminated, evanescently coupled PIN photodiode was demonstrated [50]. For this last device, a taper was included in the input waveguide, leading to better alignment tolerance to the fibre. But the tapered waveguide exhibits excess loss which reduces the sensitivity. It is the reason why an attractive way is the use of a diluted multimode input waveguide, followed by the evanescently coupled PIN photodiode. The diluted waveguide is made of very thin GaInAsP quaternary epilayers introduced in InP.

The distance between the quaternary epilayers decreases from the substrate to the top of the waveguide to get a specific waveguide which can be compared to a half lens whose centre is on the top of the waveguide (figure 17). Due to numerous technological parameters and targeted performances, the device was optimised at IEMN using genetic algorithm coupled to a 2D – BPM [51]. It was fabricated at Opto^{+} and experimental results shown that high responsivities (≅ 1 A/W), low polarisation dependence (<0,5 dB) and high alignment tolerance (≅ ± 2µm) can be achieved at 1,3 and 1,55µm wavelength [52]. The cut-off frequency is in excess of 3GHz and works are in progress to extend the bandwidth up to the millimetre wave frequency range.

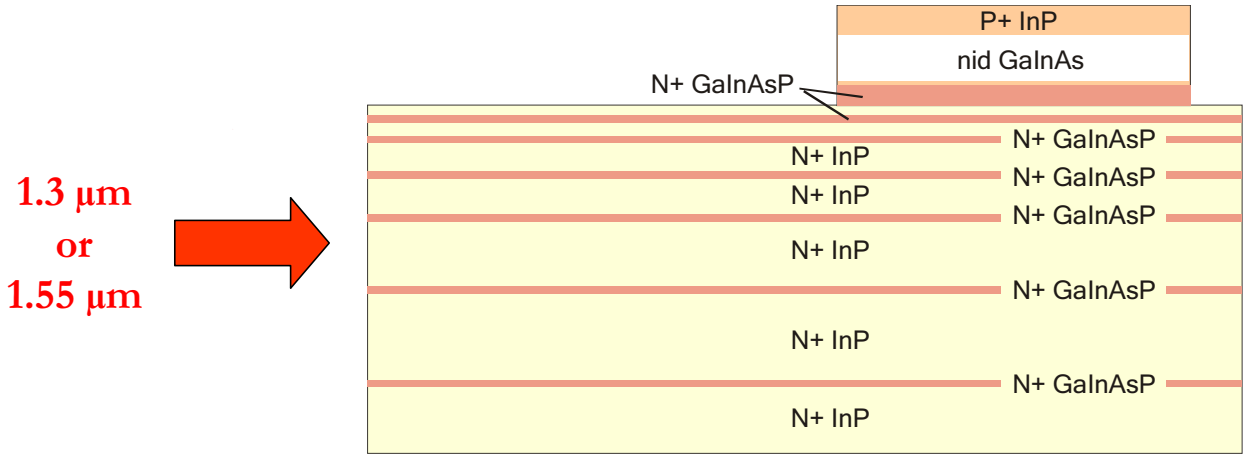

Figure 17 : multimode evanescent coupled PIN waveguide.

5. Specific microwave photonic functions: up and down conversion

5.1 Principle:

Up or down conversion is based on the existence of a non-linear element in a circuit. This element can be purely electrical and associated to the optical (or optoelectronic) component or circuit, or inside the optoelectronic component itself. We will examine various examples of non-linear functions at the emitter stage or receiver stage, demonstrating their ability for up or down conversion. The characteristic parameter is the gain conversion, which represents the comparison between the intensity of the converted line to the signal line. The goal is here to get a gain conversion (and hence a non-linearity) as high as possible.

5.2 Emitter stage:

Semiconductors lasers can be non-linear (under particular conditions such as high bias current or signal frequency close to the resonance frequency) but their characteristics are also degraded (noise...). To enhance non-linear effects and keep a good quality of emitted signals, other solutions are possible such as the association of a laser diode with an external modulator. The microwave signal is applied onto the laser and the second one onto the optical modulator. By doing this, the amplitude of the optical signal is modulated two times and contains the product of the two microwave signals amplitude. As a consequence, we find at the output of a high speed photodetector the two lines of the applied microwave signals, but also the sum and the difference of these two frequencies. Derived solutions are for example based on the use of one CW laser diode associated with two external modulators in series to apply the microwave signals. Monolithic solutions are also possible with (commercially available) DFB laser integrated with an electroabsorption modulator.

Another monolithic possible solution is the use of two-electrode lasers presented in section 2 for their enhanced dynamic response. The basic principle is to apply a microwave signal on each electrode with frequency respectively f_1 and f_2. Since the power-current characteristic depends strongly on the voltage applied onto the short electrode, the output signal will be strongly non-linear and at the output of the photodetector we measure the beat between the two frequencies. Our experiments have shown that the conversion gain ranges from -3 dB to –17 dB [53].

5.3 Receiver stage:

Photodetectors are in general linear devices (except under high power and low bias voltage, see before). It means that it seems difficult to use them directly as up or down converters. It is the reason why most of the solutions at the receiver stage are based on the association of a specific electrical (microwave) circuit to the photodetector. The optoelectronic component is then considered as a microwave signal source and the up or down conversion is made electrically with classical microwave techniques. Since many optoelectronic components are now based on InP materials (1.55 µm and 1.3 µm wavelength), their monolithic integration with microwave circuits (MMIC) is impossible, except if devices suitable for 0.8 µm wavelength are accepted. As an example, a possible solution is a specific integrated circuit associating Metal-Semiconductor-Metal GaAs photodetector with a dual gate MESFET. In spite of a rather low quantum efficiency due to shadow effects of electrodes, GaAs MSM photodetectors are known as high speed devices for 0.8 µm wavelength applications, with easy monolithic integration with field effect transistors. The use of dual gate MESFET allows to enhance the non-linear effect of the transistor and to separate the two input ports corresponding to the two microwave signals to be mixed. In this MOMIC (Microwave Optical Monolithic Integrated Circuit) fabricated at IEMN, one gate is electrically connected to one electrode of the MSM exactly as a PIN-FET and the other gate is used for the second microwave signal. The ability of this integrated circuit to up or down convert the frequency of microwave signal modulating the optical signal detected by the MSM photodetector was experimentally demonstrated [54] with conversion gain around –3 dB at 10 GHz.

The objective to monolithically integrate the non-linear microelectronics with the photodetector whatever the optical wavelength (0.8 µm, 1.3 µm or 1.55 µm) is, led to use an heterojunction phototransistor (HPT) as optoelectronic mixer. This device can be considered as a high speed photodetector with internal gain due to transistor effect. It is also an heterojunction bipolar transistor (HBT) with a base-collector junction used as a photodiode and combines monolithically the properties of an HBT and a photodiode. High speed transistor and photodetector are obtained with short transit time in GaInAs p+ base and n- collector layers. Although high speed demonstrations were made with top illuminated devices, edge illumination is suitable for high quantum efficiency and millimetre wave operation. Following previous works [55], this scheme was adopted at IEMN, since epilayers structures are compatible with an optical waveguide. For the devices fabricated at IEMN, a GaInAsP quaternary layer was introduced between GaInAs collector and InP sub-collector to get a multimode waveguide, figure 18. No quaternary layer was introduced in the emitter-base junction to keep its electrical properties. As expected, this device is a millimetre wave photodetector with internal gain (≅5dB at 40GHz) and high quantum efficiency (60% without AR coating) [56, 57]. But it is also an efficient optoelectronic mixer thanks to the non-linear behaviour of the transistor under suitable bias voltage [56, 57, 58]. More precisely, experiments carried out with a 1 GHz modulated optical signal, different optical powers (from 0 to 1 mW at the output of the fibre) and electrical DC base bias currents, shown an improvement of more than 30 dB for very small optical powers which can be explained by the gain non-linearities of the device.

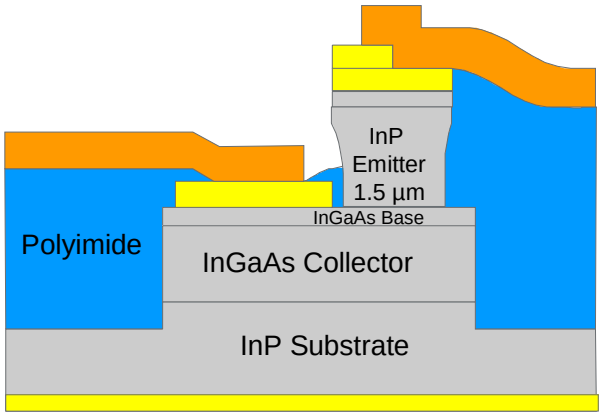

Figure 18 : Schematic view of a heterojunction phototransistor with base contact (3T-HPT).

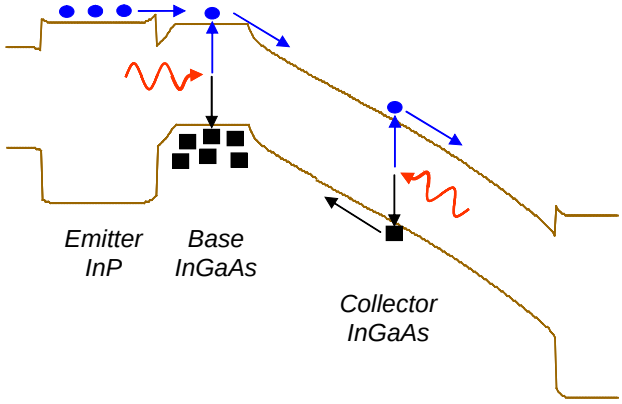

Band structure of a heterojunction phototransistor.

These non-linearities can be used to mix an amplitude modulated optical signal with an electrical one applied on the base terminal. Figure 17 shows the result of such an experiment. The intermediate frequency (IF) of the modulated optical signal is 1 GHz (with a 10 dBm power on the laser) and the local oscillator frequency (LO) is 18 GHz (with a power level of -20 dBm applied on the base). The electrical spectrum exhibits the central band at 18 GHz and the two first sidebands at 17 GHz (LO-IF) and 19 GHz (RF=LO+IF).
Another experiment was carried out with IF=8 GHz (0 dBm on the laser) and 500 MHz < LO < 10 GHz (with a power level of -10 dBm). The up-conversion gain (compared to the base-collector junction) versus LO and LO+IF is presented on figure 19. The HPT optoelectronic mixer exhibits a 6 dB up-conversion gain around LO=500 MHz and gain can be observed up to LO=7 GHz.

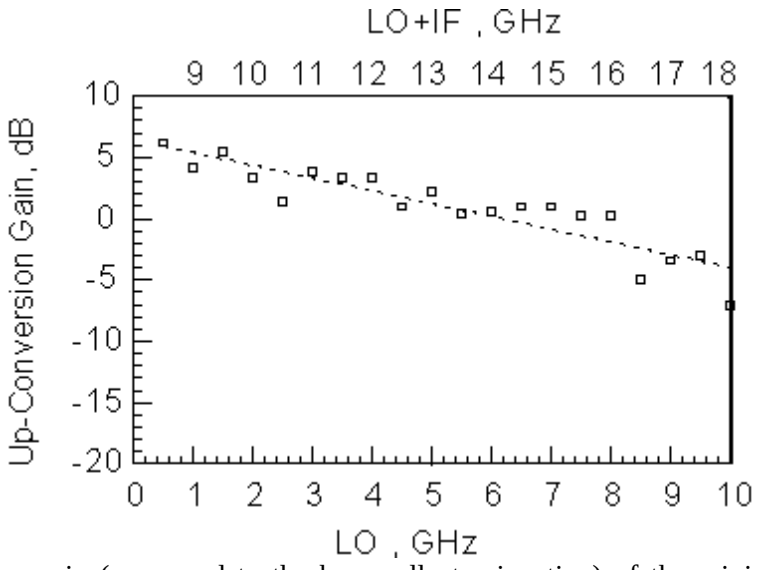

Figure 19 : Conversion gain (compared to the base-collector junction) of the mixing between an optical signal modulated at IF=8 GHz and an electrical signal applied on the base modulated at 500 MHz<LO<10 GHz (power level of -10 dBm).

For comparison, Lui, Seeds and Wake [58] reported down-conversion using a two-terminals edge-coupled InP/InGaAs HPT, with a maximum 7 dB down-conversion gain when IF=500 MHz, RF=2.5 GHz and LO=3 GHz. Suematsu *et al.* [59] reported a top-illuminated three-terminals HBT up-converting mixer with a conversion loss of 4 dB when IF=3.2 GHz, RF=30 GHz and LO=26.8 GHz. These experiments show that InGaAs / InP HPTs are promising devices to transmit a data signal up-converted to a millimetre-wave signal thanks to a mixing with a signal delivered by a local oscillator. More recently, C. Gonzales [60] and G. Eisenstein [61] demonstrated also very efficient mixing experiments using HPTs.

6. Hybrid versus monolithic integration

Microwave Monolithic Integrated Circuits are now fabricated in GaAs foundries and allow to associate, on the same substrate, a lot of different passive or active components, to get a given or several microwave functions on the same chip. Monolithic integration leads to a lot of advantages : compactness, reduction of parasitics, increasing functionality... and we could hope to get the same advantages from the monolithic integration of optoelectronic or photonic components, with microwave components to get Microwave Optoelectronic Monolithic Integrated Circuits (MOMICs). This is possible in pure microwave circuits because there is a technological compatibility (epitaxy, process...) between the various components of a MMIC. Unfortunately, this technological compatibility does not exist between the various optoelectronic (and microwave) components. For example, the structure of a high speed laser is completely different to the one of a PIN photodetector or field effect transistor. It is the reason why, in spite of a lot of technological works and researches in this field, it exists only a few examples of mature (industrial) photonic or optoelectronic integrated circuits. A well known (and may be to date the only), commercially available photonic integrated circuit, is a DFB laser integrated to an electroabsorption modulator. Even in this modest circuit (two components) complex technological steps are required. Optoelectronic circuits, associating optoelectronic components and microelectronics are not commercially available. This situation is due to completely different epitaxial structure for the optoelectronic components (2-3 µm thick) and microelectronic components (0.1 µm thick for a field effect transistor). The most advanced optoelectronic integrated circuits are probably those based on the integration of an Heterojunction Phototransistor and Heterojunction Bipolar Transistor, because these devices have the same structure, except some geometrical aspects. Here the epitaxy and the process are almost the same. The difference between microelectronic and optoelectronic devices is controlled by the design of the mask. Several high speed photoreceivers and non linear photo-mixers or photo-oscillators were experimentally demonstrated, but up to now, to our knowledge, no optoelectronic integrated circuit is commercially available.
The consequence is that optoelectronic industry has chosen the way of self-aligned flip-chip mounting technique on silicon mother-board. The basic idea is here to fabricate each component (optoelectronic, photonic...) needed for a circuit, using mature single component technology and to assemble them on a specific silicon substrate. The main problems are then: how to align the optical (optolectronic) components along the same optical axis and how to make the electrical (microwave) connections.
The first difficulty was solved using preferential silicon etching. The silicon substrate carries preferentially etched V-grooves with the angle $\alpha = 54.74°$ between the (100) and (111) crystal planes. Passive alignment of single mode fibre and waveguide devices can then be achieved. Photolithography of Si mother board allows the precise etching of V-grooves for the fibre alignment and other V-grooves for the positioning of the waveguide device. To get the alignment compatibility of the photonic device with the silicon mother board, special alignment indentation, self aligned with the waveguide stripes are achieved on the chip in the III-V material photonic device [62].
The second difficulty resides in the electrical (microwave) interconnection. One technique, compatible with the mother-board self aligned packaging, is to etch a V-groove in the silicon designed to include electrical transmission lines and solder stripes to contact and fix the electro-optic waveguide device. To reduce parasitics, the flip-chip interconnection can use small solder bumps (~20 µm in diameter). It allows to connect the pads of the two chips face to face, and operation up to millimetre frequency range occurs if no other effects introduce frequency limitations [63, 64].

7. Conclusion

Good performance improvements were obtained for various microwave optoelectronic and photonic devices during these last 10 years. Nevertheless, further works are still needed to fulfil all system requirements, for example: low noise laser, high bandwidth and low drive voltage optical modulator, high linear emitters and receivers, high speed - high cross talk – low consumption and insertion loss optical switching matrixes… No doubt that, by using together recent technological advances and modelling tools, and, may be, new concepts, it will be possible to reach these goals.
Another main aspect of the microwave photonic functions is to take advantage of hybrid or monolithic association of components to reduce parasitics, improve compactness, increase the functionality... Knowing that technological compatibility does not exist, the industrial production of Microwave Optoelectronic Monolithic Integrated Circuits, seems to date difficult, except may be for very special cases. It is the reason

why in most mature microwave photonic systems, it is more reasonable, particularly for millimetre wave applications, to reduce the difficulty of the photonic part by an increase of the complexity of the microwave (millimetre wave) part, since MMICs are commercially available. Nevertheless, with the appearance of new technological tools, it becomes now possible to fabricate very confined (sub-micron) optical waveguides, which corresponds to a reduction of 10 of the size of the waveguide (100 in section area). We can then imagine designing very small photonic components and integrated circuits which sizes are compatible to those of MMICs, with low consumption and high efficiency, and by techniques like polymer wafer bonding to associate a photonic (optoelectronic) integrated circuit with a MMIC.

References

1 - H. El kadi ; J.P. Vilcot ; S. Maricot ; D. Decoster : Microwave and Optical Technology Letter, Vol 3, pp. 379, 1990.

2 - E. Goutain ; J.C. Renaud ; M. Krakowski ; D. Rondi ; R. Blondeau ; D. Decoster : Elect. Lett., Vol 32, n°10, pp.896-897, 1996.

3 - H. Lamela, G. Carpintero, P. Acedo and A. Abella, Electronics Letters, 24th September 1992, Vol. 28,No. 20, pp. 1908-1910.

4 – Sugiyama M., Doi M., Tanugichi S., and Onaka H., Optical Fibre Communications, OFC 2002, Anaheim USA, March 2002.

5 – Chen D., Fetterman H. R., Chen A., Steier W.H., Dalton L.R., Wang W., Shi Y., Appl. Phys. Lett., vol. 70, pp. 3335, 1997.

6 - Zang X.,. Zhou X, Daryoush A.S., IEEE Transactions on Microwave Theory and Techniques, vol. 40, n°5, pp. 895-902, mai 1992.

7 - Fendler M., Descamps P., Gouy J.P., Vilcot J.P. and Decoster D, Microwave and Optical Technology Letters, june 1998.

8 – S. Mezzour, PhD thesis, Univ. of Lille 1, july 1997.

9 – S. Dupont, C. Loyez, N. Rolland, et al., Microwave and Optical Technology Letters,vol. 30, n°5, sept. 2001, pp. 307-310.

10 - R 2005 – ALC – SEL – DR – P – 031 – b1, MODAL final report and also 0'Reilly J.J., Lane P.M., Capstick C.H., Salyado H.M., Heidemann R., Hofstetter R. and Schmuck H., IEE Proceedings – J, Vol 140, n°6, pp 385 – 391, 1993.

11 - Griffin R.A., Zhang S.L., Lane P.M. and O'Reilly J.J., IEE Colloquium on Fibre Optics in Microwave Systems and Radio Access, pp 9/1 – 9/16, Birmingham, 26 june 1997.

12 - Young SP., Georges J.B., Cutrer DM., Wu T. and Lau.K., OFC'96, pp 201 – 211, 1996.

13 - Novac D. and Tucker R., Electron Letters, Vol 30, pp 1430 – 1431, 1994.

14 - Lau K.Y., J.Lightwave technol., Vol LT-7, pp 400 – 419, 1989.

15 - Walker N.G., Wake D and Smith T.C., Electron. Lett., Vol 28, pp 2027 – 2028, 1992.

16 - O'Reilly J.J., Lane P.M., Heidemann R. and Hofstetter R., Electron. Letters, Vol 28, 2309 – 2311, 1942.

17 - Goldberg L., Esman R.D. and Williams K.J., IEE Proc.J, Vol 139, pp 288 – 295, 1992.

18 - Gliese V., Nielson TN., Bruun M., Christensen E.L., Stubkjaer K.E., Lindgren S. and Broberg B., IEEE Photonic Technol. Lett., Vol 4, pp 936 – 938, 1992.

19 - Georges J.B., Park J., Solgaard O., Pepelingoski P., Sayed M and Lau K., Electron. Lett., Vol 30, pp 160 – 161, 1994.

20 - Bouyer P., Gustavson T.L., Haritos K.G. and Kasevitch M.A., Opt. Lett., Vol 21, pp 1052 à 1504, 1996.

21 - Wake D., Lima CR. and Davies P.A., IEEE Phot. Technol. Lett., Vol 8, pp 978 – 980, 1996.

22 - Manyshev P.V., Shernikov S.V. and Dianov E.M., IEEE J. Quantum Electron, Vol 27, pp 2347 – 2355, 1991.

23 - Davies P.A., Razavi K; and Pourbahri B., IEE Colloquium on fibre optics in Microwave systems and Radio Access, pp 10/1 – 10/6, Birmingham, 26 june 1997.

24 - Wake D., Lima C.R. and Davies P.A., IEEE – MTT, Vol 43, n°9, pp 2270 – 2276, 1995.

25 - Noël L., Marcenac D.D. and Wake D., Electron. Letters, Vol 32, n°21, pp 1497 – 1498, 1996.

26 - Goldberg L., Yunk A.M., Taylor H.F. and Weller J.F., Electron.Letters, Vol 21, n°18, pp 814 – 815, 1985.

27 - Pajarola S., Guekos G. and Kawaguchi H., International Topical Meeting On Microwave Photonics, MWP'97, pp 75–78, Duisburg, 1997.

28 - Kuri T.K. and Kitayama K., Electron.Letters, Vol 32, n°23, pp 2158 – 2159, 1996.

29 - Smith G.H., Novak D. and Ahmed Z., Electron-Letters, Vol 33, n°1, pp 74-75, 1997.

30 - Vergnol F., Devaux F., Jahan D. and Carenco A., Electron. Letters, Vol 33, n°23, 1997.

31 - Smith G.H., Novak D. Lim C. and Wu K., Electron. Letters, Vol 33, N° 13, 1997.

32 - Wake D., Noël L., Moodie D.G., Marcenac D.D., Westbrook L.D., and Nesset D., IEEE MTT-S Digest, TU 1B-5 pp 39 – 42, 1997.

33 - Yonenga K. and Takachio S., IEEE Photonic Technol.Letters, 5 (18), pp 949 – 951 (1993).

34 – Hussein Mourad M., Vilcot J.P., Decoster D., and Marcenac M., IEE Proc. Optoelectron., vol. 147, n°1, feb. 2000.

35 - Esman RD., Frankel MY., Dexter JL., Goldberg L., Parent MG., Stilwell D and Cooper DG, IEEE Photon.Tech.Lett.,5, pp 1347 – 1349 (1993).

36 - Dolfi D., Michel-Gabriel F., Bonn S and Huignard JP, Optics Lett., 16, pp 255 – 257 (1991).

37 - Goutzoulis A.P.., Davies D.K., Zomp J..M., Hrycak P., Hohnson A., SPIE Vol 2155 (2155-29) pp. 275 Optoelectronic Signal processing for phased array antennas IV January 1994.

38 - R. Boula-Picard, M. Bibey, N. Vodjdani, MWP 2001, Long Beach.

39 - I. Cayrefourcq : PHD Thesis, Univ. of Lille 1, 1998.

40 - Y. Hernandez ; J.P. Vilcot ; D. Decoster ; J. Chazelas : Electrochemical Society Proceedings, Vol. 2000-18, pp. 114-119.

41 - Vinchant J.F., Renaud M., Erman M., Peyre J.L., Jarry P., Pagnod-Rossiaux P, IEE Proceedings – J, Vol. 140, N°5, October 1993, pp 301-307.

42 - Cayrefourcq I., Schaller M., Fourdin C., Vilcot J.P., Harari J. and Decoster D., IEE Optoelectronic part J, july 1998.

43 - K. Kato : IEEE Transactions on Microwave Theory and Techniques, Vol.47, n°7, 1999.

44 - D. Decoster ; V. Magnin ; J.P. Vilcot ; J. Harari ; J.P. Gouy ; M. Fendler ; F. Jorge : Proceedings of SPIE, Vol. 3948 (2000), pp. 162-119.

45 - F. Jorge : PHD Thesis, Univ. Lille 1, 1999.

46 – Harari J., Journet F., Rabii O., Jin G., Vilcot J.P., Decoster D., IEEE MTT, vol. 43, n°9, pp. 2304-2330, sept. 1995.

47 - M. Alles ; V. Auer ; F.J. Tegude ; D. Jäger : IEEE – MTT S, Vol.3, 1998, pp. 1233 – 1236.

48 - H. Ito ; T. Ohno ; H. Fishimi ; T. Furuta ; S. Kodama ; T. Ishibashi : Elect. Lett., Vol. 36, n°8, pp. 747 – 748, 2000.

49 - H. Mawatari ; M. Fukuda ; K. Kato ; T. Takeshito ; M. Yuda ; A. Kozen ; H. Toba : J. Lightwave Technol., Vol 16 (12), pp. 2428 – 2429, (1998).

50 - S. Demiguel ; L. Giraudet ; P. Pagnod – Rossiaux ; E. Boucherez ; C. Jany ; L. Carpentier ; V. Coupé ; S. Fock-Yer ; J. Derobert : Elect. Lett., Vol 37, n°8, (2001), pp. 516-518.

51 - V. Magnin ; L. Giraudet ; J. Harari ; J. Decobert ; P. Pagnod ; E. Boucherez ; D. Decoster : J. of Lightwave Techn., Vol 20 n°3 ; 2002, pp. 5-16.

52 - L. Giraudet ; J. Harari ; V. Magnin ; P. Pagnod ; E. Boucherez ; J. Decobert ; J. Bonnet-Ganard ; D. Carpentier ; C. Jany ; F. Blache and D. Decoster : Elect. Lett., Vol 37, n°15 (2001), pp. 973 – 975.

53 - Hamelin R., Vilcot J.P., Gouy J.P. Decoster D., Proc. of the international topical meeting on Optical Microwave Applications, IEE MTT-S OMI 94, pp. 121-124.

54 – Van de Casteele J., PhD. Thesis, Univ. of Lille 1, oct. 1996.

55 - D. Wake ; D.J. Newson ; M.J. Harlow ; I.D. Henning : Elect. Lett., Vol. 29, n°25, pp.2217 – 2219, 1993.

56 - J. Van de Casteele ; J.P. Vilcot ; J.P. Gouy ; F. Mollot ; D. Decoster : Elect. Lett., Vol 32, n°11, pp. 1030 – 1032, 1996.

57 - V Magnin ; J. Van de Casteele ; J.P. Vilcot ; J. Harari ; J.P. Gouy ; D. Decoster : Microwave and Optical Technology Letters, Vol 13, n°6, p. 408, 1998.

58 - C.P. Liu ; A.J. Seeds ; D. Wake : IEEE Microwave and guided wave letters, Vol 7, n°3, pp. 72-74, 1997.

59 – Suematsu E., IEEE Transactions on Microwave Theory and Techniques, Vol. 44, No. 1, January 1996, pp. 133-142.

60 - Gonzalez C., Muller M., Benchimol J.L., Riet M., Jaffé P. And Legaud P., Proc. of the European Conference on Optical Communication, ECOC 2000, vol. 2, pp103-104.

61 - Lasri J., Bilenca A., Eisenstein G., Ritter D., Grenstein M., Siderov V., Goldgeier S., and Cohen S., Proc. Of the International Topical Meeting on Microwave Photonics 2000, MWP'00, Septembre 2000, Oxford.

62 – Leclerc D., Brosson P., Pommereau F., et al., IEEE Photon. Tech. Lett., vol. 7, n°5, may 1995.

63 – Wada O., Kumai T., Hamagushi H., et al., Electron. Lett., vol. 26, n°18, pp. 1484-1486.

64 – Koshuke K. Tsuyoshi H., Fumikazu O., et al., IEEE Journal of Lightwe Technology Lett., vol. 8, n°9, pp.1323-1326.

Optoelectronic Components and Integration Devices: From Concepts to Applications

D. Jäger and A. Stöhr
Gerhard-Mercator-Universität Duisburg
ZHO - Optoelektronik
Lotharstrasse 55, D-47057 Duisburg, Germany

e-mail: Stoehr@oe.uni-duisburg.de
D.Jaeger@oe.uni-duisburg.de

SUMMARY

The field of optics-microwave interactions can generally be defined as the study of high-speed photonic devices operating at microwave, millimeterwave or even THz frequencies and their use in microwave or photonic systems. In this multidisciplinary field at the interface between microwave techniques, ultrafast electronics and photonic technologies, typical investigations include, for example, high-speed and microwave signal generation, processing and conversion as well as the distribution and transmission of microwave signals via broadband optical links. From pioneering experiments in the 70´s, this field of microwave photonics has paved the way for an enabling novel technology with a number of innovative and commercially important applications.

This paper is intended to give an overview on this multidisciplinary field of microwave and millimeterwave photonics addressing specifically high speed optoelectronic components and their integration technologies and giving a glance on a few key microwave applications.

The first chapter gives as an introduction an overview on the field of microwave and millimeterwave photonics and its significance for different microwave techniques. The second chapter is devoted to the principles of microwave optical interaction devices starting with the basics of optically vertical and optical waveguide structures. Moreover, lumped elements as well as traveling wave devices are discussed furtheron. The photonic microwave component family includes photodetectors, laser diodes, modulators, mixers, etc. where different physical interactions can be employed. In particular, recent advances in electroabsorption (EA) devices such as electroabsorption modulators (EAM) and electroabsorption photodetectors (EAD) as well as EA transceivers (EAT) and photomixers (EAX) are discussed in chapter three together with the results from experiments. The fourth part addresses optoelectronic integration techniques such as monolithic integration of different functions but also fiber chip coupling techniques. It is followed by a few interesting examples of photonic microwave signal processing components and modules in chapter five. The sixth chapter is particularly devoted to basic characteristics of microwave optical links and in the last chapter several examples of optical microwave system applications are presented.

1. INTRODUCTION

Within the last decade the field of optics-microwave interactions has attracted growing interest worldwide. The specific term of microwave photonics was introduced in 1991 and used to describe novel optoelectronic components based upon the interaction of traveling optical and microwaves [1,2]. In the following, the merging of microwave and photonic

Paper presented at the RTO SET Lecture Series on "Optics Microwave Interactions", held in Jouy en Josas, France, 2-3 September 2002; Duisburg, Germany, 5-6 September 2002; Budapest, Hungary, 9-10 September 2002, and published in RTO-EN-028.

technologies was foreseen to be a new approach for future fiber radio communication systems where the RF signal is transmitted over optical carriers [3]. Since then the field of RF optoelectronics and photonics rapidly broadened: Since 1996 International Topical Meetings on Microwave Photoncis (MWP) are being held annually [4] and 1995 was the first year of an IEEE MTT Special Issue on Microwave Photonics now being published regularly [5].

Microwave photonics is an innovative multi- and interdisciplinary field combining and transfering different technologies. In particular, microwave technologies are used and employed in photonics and photonic technologies are utilized in microwave techniques. Moreover, in specific areas novel synergistic concepts have been developed.by merging both technologies which particularly holds for the field of optoelectronics as their interface. As a result of ever increasing frequencies the term microwave stands here for GHz or THz frequencies in the frequency and equivalently for ps- or fs-time scales in the time domain.

This paper is intended to give an overview on together with recent results ranging from devices and technologies to some specific systems under investigation. In particular, the following topics will be addressed by way of key examples of the synergetic mixture of the two technologies involved: (i) Ultrafast photonic components such as optical modulators and detectors with special emphasis on traveling wave devices and including integration technologies. (ii) Concepts and examples of microwave signal processing by way of using photonic technologies. (iii) Broadband and analog optical links for high-speed interconnects. (iv) Microwave photonic systems based upon the merging of microwave and optical technologies.

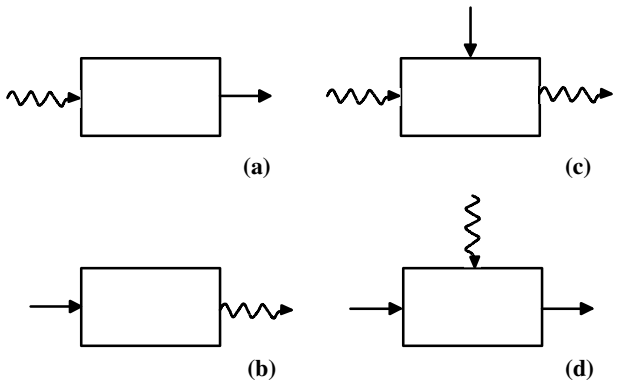

Fig. 1 Optoelectronic device family: Basic microwave-optical interaction devices: (a) Photodetector, (b) light emitting or laser diode, (c) optical modulator with electrical control, and (d) electrical modulator/device with optical control [1,2,6,7]

2. CONCEPTS OF MICROWAVE PHOTONIC DEVICES

Recent advances in the development of high speed optoelectronic devices together with the broadband and low loss transmission capability of optical fibers have in large part been responsible for the global growth of broadband communications. In particular, rapid progress has been made in the development of photodetectors and modulators that may be the key elements in the future ubiquitous high speed optical internet where the optical fiber is coming closer and closer to the customer. In the following an overview on the state of the art of ultra-fast photonic components is given with special emphasis on novel electroabsorption devices and, secondly, future trends in this emerging field of technology are addressed.

In Fig. 1 the four basic optoelectronic interaction devices are sketched. Here two types can be recognized: (i) Two port devices as converters between optical and electrical signals: the photodetector (PD) and the laser or light emitting diode (LD or LED) in Fig. 1 (a) and (b), respectively; (ii) Three port devices such as the electro-optical modulator (MOD) or the optically controlled electrical modulator in Fig. 1 (c) and (d), respectively. Please note that the two elements in Fig. 1 (c,d) are a kind of optoelectronic transistor.

Two basic concepts of microwave optical interactions may further be distinguished, see Fig. 2. As can be seen, the difference is due to different propagation directions of the optical wave. In Fig. 2 (a) the optical wave is traveling normally to the semiconductor surface, i. e. parallel to the flow of the electrical charges. This leads to a design condition where the optical interaction length is coupled and related to the distance the charge carriers are traveling. Hence, in a photodetector – as an example - the absorption length cannot be designed independently from the transit time. In Fig. 2 (b) the optical wave is traveling parallel to the surface so the penetration depth is independent from the transit time in the example of the photodetector.

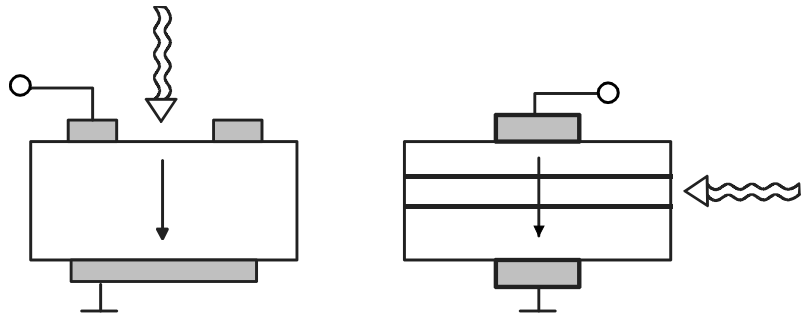

Fig. 2 Microwave optical interaction devices with vertical (a) and horizontal (b) propagation of the lightwave.

For high-speed – electrical - operation electronic devices as shown in Fig. 2 are usually scaled down with respect to the lateral dimensions of the electrical contacts in order to decrease the device capacitance and to decrease correspondingly the RC time constant thus enlarging the cut-off frequency. This procedure is usually limited by power considerations, because smaller devices will lead to smaller operating powers. A solution of this problem is the use of propagation effects of the electrical signal, i. e. to include electrical wave propagation phenomena in the design of the electronic device as well as has been described in [6] and already used in the design of high-speed integrated circuits such as RFICs and MMICs (cf. the well known traveling wave amplifiers), see Fig. 3. According to the design of such traveling wave devices the electrical contacts are realized in form of well known microstrip or coplanar transmission line. As can be seen, in these traveling wave (TW) devices wave propagation effects in the electrical as well as in the optical domain are utilized. The concept is based on the fundamentals of nonlinear optics where from a fundamental point of view interaction always takes place during wave propagation. Obviously, the bandwidths of these elements are not limited by “RC time constants”.

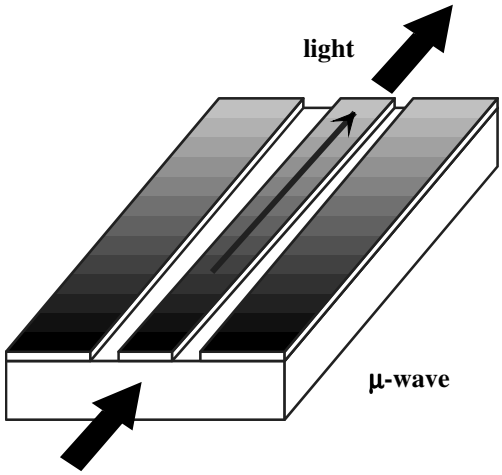

Fig. 3 Traveling wave concept

Moreover, at high frequencies the packaging of high-speed devices or circuits has basically to include electrical wave propagation effects, for example the characteristic impedance of the electrical interconnect. Additionally, the transit time and wave propagation effects of space charges have also to be regarded, especially in the development of high-speed devices. In optics on the other hand, wave propagation is the fundamental physical basis and no lumped elements exist up to now. As a consequence, the design of optical and photonic components usually include optical waveguides (see Fig. 2) and element dimensions are always large with respect to the wavelengths in optics.

In summary, in microwave photonic components an interaction between electrons, holes, electrical fields and photons take place which can be regarded as microwave-optical interactions. Consequently, different technologies meet and may - in a synergetic mixture - be merged in order to develop novel concepts with great advantages.

3. MICROWAVE PHOTONIC COMPONENTS

In the following, some key microwave optical interaction devices are discussed [7-9].

3.1 Electroabsorption modulators – Electroabsorption modulators (EAM) provide a great potential for low voltage operation, large bandwidth and monolithic integration with other components such as laser diodes. In Fig. 4 an EAM is sketched which has been designed for a wavelength of 1.55 μm using InP based semiconductor materials [9,10]. The EAM resembles electrically a pin diode, optically a waveguide is realized where the core is made of a MQW material [11-13] here sandwiched between InP cladding layers for 1.55 μm. The element in Fig. 4 is a lumped element with a coplanar input contact.

Experimental results of different devices are shown in Figs. 5 and 6. In Fig. 5, the characteristics of two digital devices exhibiting a bandwidth of ca 10 GHz and > 40 GHz, respectively, are shown. Note that non-optimised structures have been studied. Alternatively, a traveling wave design leads to a cut-off frequency of > 70 GHz [10]. In Fig. 6 the frequency dependence of a lumped EAM for sensor application and the results of SFDR measurements are plotted.

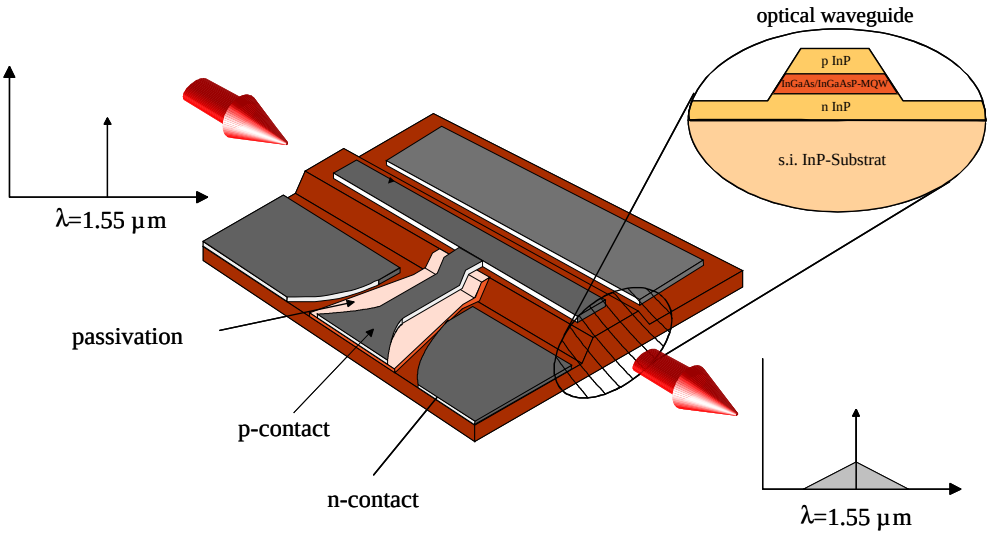

Fig. 4 Electroabsorption modulator (EAM) with cross section

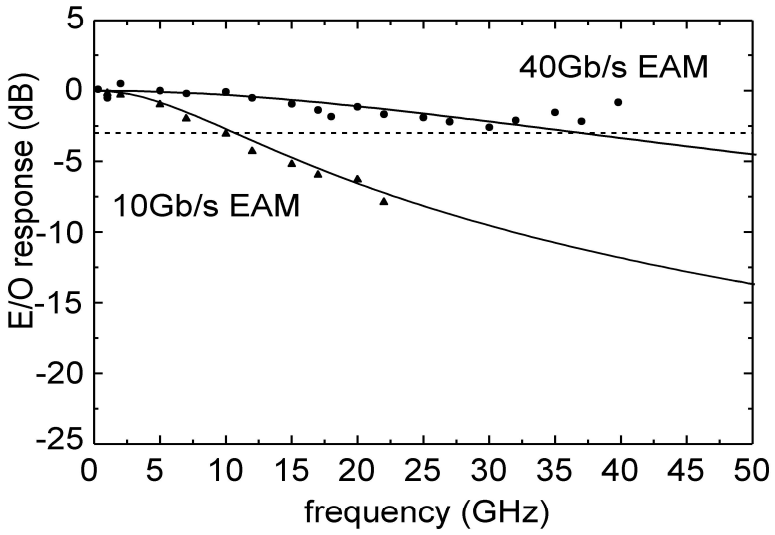

Fig. 5 Modulation of two digital EAMs.

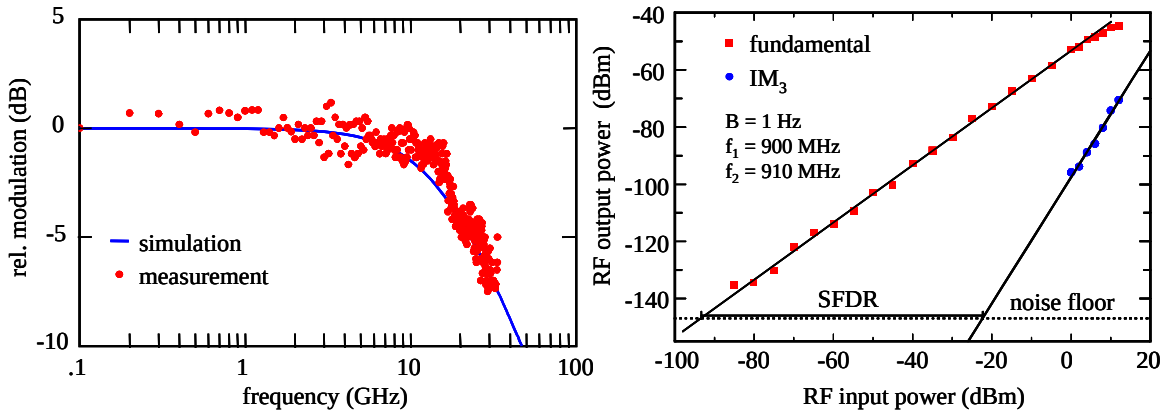

Fig. 6 Frequency dependent modulation of EAMs, (a) lumped element fabricated for sensor applications and (b) measurement of SFDR.

3.2 Electroabsorption detector - Due to the electroabsorption mechanism, i. e. the generation of charge carriers, the EAM can also be used as an – electro-absorptive - photodetector (EAD). A bandwidth of >170 GHz is experimentally demonstrated (Fig. 7) for a traveling-wave pin diode with an active multiple quantum well region. The traveling wave design [14] again includes an optical waveguide and an electrical coplanar transmission line along the optical signal path, see Fig. 3: In this case there is no optical output and no electrical input. Experimentally, a heterodyne set-up has been used where two optical input signals with a corresponding difference frequency are fed into the optical waveguide of the EAD. The photodetection process leads to a photocurrent at the difference frequency measured after down-conversion with a spectrum analyser.

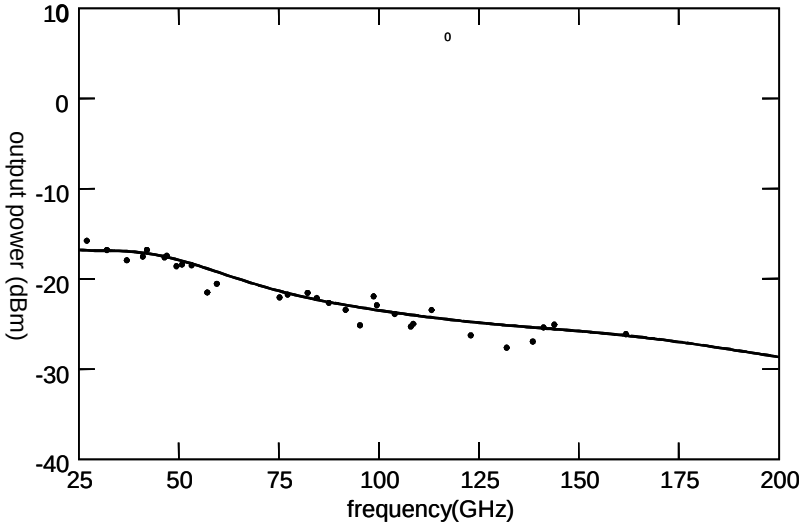

Fig. 7 Frequency response of a traveling-wave 1.55µm photodiode using electroabsorption in the MQW active material of the optical waveguide

Recently, a traveling wave photodetector has been shown to work up to 460 GHz as measured using an SIS mixer (a superconducting Josephson junction) in a THz-antenna system for radio astronomy [15]. Here the photodetector together with the two laser diodes work as a photonic local oscillator

3.3 Electroabsorption mixer - Due to the inherent nonlinearity of the photodetector where the photocurrent is proportional to the square of the electric field of the optical wave, this electroabsorptive device can further directly be employed as a photomixer (EAX). Experimental results for up-conversion at 60 GHz are shown in Fig. 8. In this experiment, again a heterodyne set-up has been used where the two laser diode signals are separated by 60 GHz and one laser diode is additionally modulated at 2.6 GHz. Obviously, the electrical output signal exhibits the RF carrier frequency as well as the side bands due to modulation.

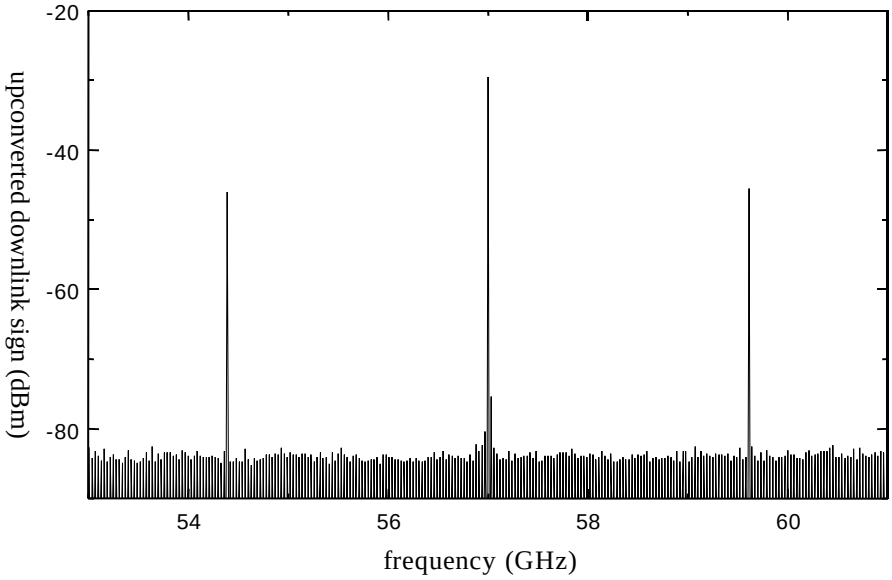

Fig. 8 Optoelectronic mixing in a photodetector, here an electroabsorption photomixer (EAX)

3.4 Electroabsorption transceiver – From the physics of electroabsorption it is concluded that the EAM can simultaneously be used as a modulator and a photodetector where for communication techniques the electrical up- and downlink signals of the device have to be frequency multiplexed. Such a dual function EAM is called electroabsorption transceiver (EAT), [16], Fig. 9. The multifunctional characteristics of such an EAT are finally demonstrated in different fiber wireless systems for broadband communications, see below.

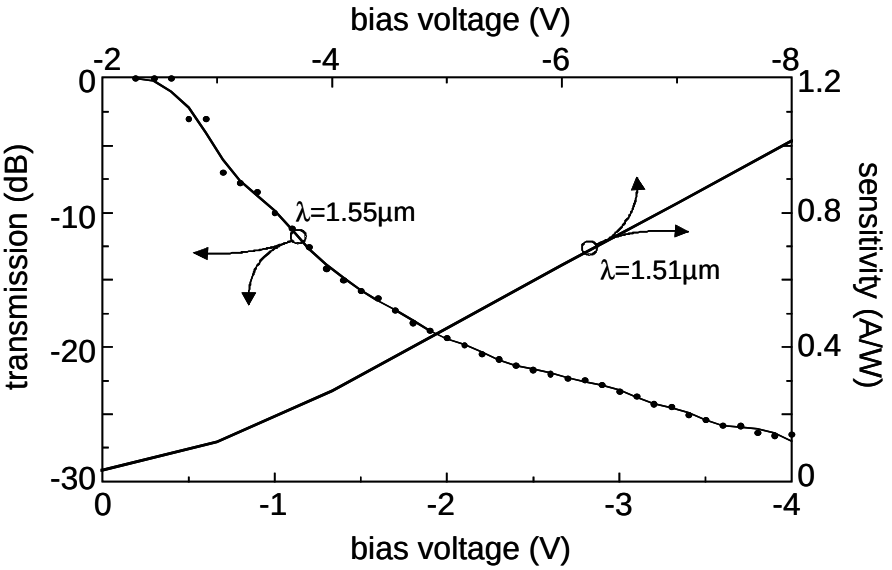

Fig. 9 Photodetection and modulation properties of an electroabsorption modulator. The device is called an electroabsorption transceiver (EAT)

3.5 Electroabsorption SEED element - An EAT can further be used to generate artificial optical nonlinearities such as optical bistability [17] which gives rise to switching, logic and memory effects. From the physical point of view this nonlinearity is caused by the internal feedback between the modulator and the photodetector properties of the device. It has been shown that this characteristic nonlinearity may be useful for multiple-GHz A/D conversion.

3.6 Microwave laser diodes - Up to now laser diodes are usually not made using a special design for microwave applications [18]. In particular, no traveling wave structures are applied although the electrical contact size is already close to the electrical wavelength for frequencies of about 10 GHz. As a result, since several years the cut-off frequency is only about 30 GHz and there is no breakthrough at higher frequencies.

4. OPTOELECTRONIC INTEGRATION TECHNOLOGIES

In an optoelectronic TW device [7,8,9] an optical waveguide (e. g. a strip loaded or a burried waveguide) is used for optical wave propagation and an electrical transmission line (e. g. microstrip or coplanar waveguide) for guiding the microwave, usually in the same direction. In the region where the electrical fields overlap, the optoelectronic interaction occurs. Note that a dc bias may additionally be applied to control the operating point. From a physical point of view the interaction is a nonlinear or active process. As discussed above, the photodetector and the laser diode are basic examples of two-port devices where optical power is converted into electrical power and vice versa. Typical three-port devices are electrically controlled optical modulators/switches or optically controlled microwave modulators/-switches. Due to the inherent nonlinearity these devices are further used for optoelectronic mixing of input electrical and/or optical signals where the output signal can be electrical or optical. As a result, such microwave optical interaction devices show a variety of optoelectronic functions where in special devices different functions may be achieved simultaneously.

A novel multifunctional device has recently been presented, the electroabsorption modulator integrated into the structure of a hetero-bipolar transistor (HBT), [19]. Such a device (Fig. 10) includes the common transistor characteristics as well as the modulator behaviour leading to a novel approach to optoelectronic integrated devices and circuits.

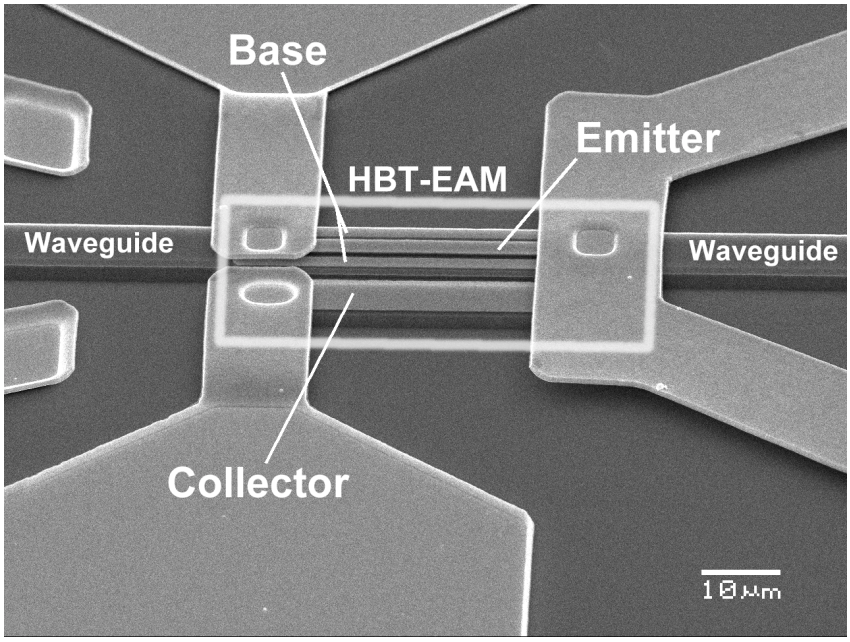

Fig. 10 SEM picture of an HBT-EAM

A further key integration technology is the optical coupling of the light between the optical waveguide and the external connection which usually is the optical fiber. This technique of fiber chip coupling includes the processing of V-grooves into the substrate or

mother board and the tapering of the optical fiber [20] A further important technology is related to the adjustment and fixing of the fiber with respect to the optical waveguide. A result of measurement is shown in Fig. 11 where a coupling loss of less than 1 dB is achieved for a MFD of about 1.5 µm. It should finally be mentioned that high frequency electrical coupling of coplanar lines with coaxial connectors requires also a careful design of wire bonding.

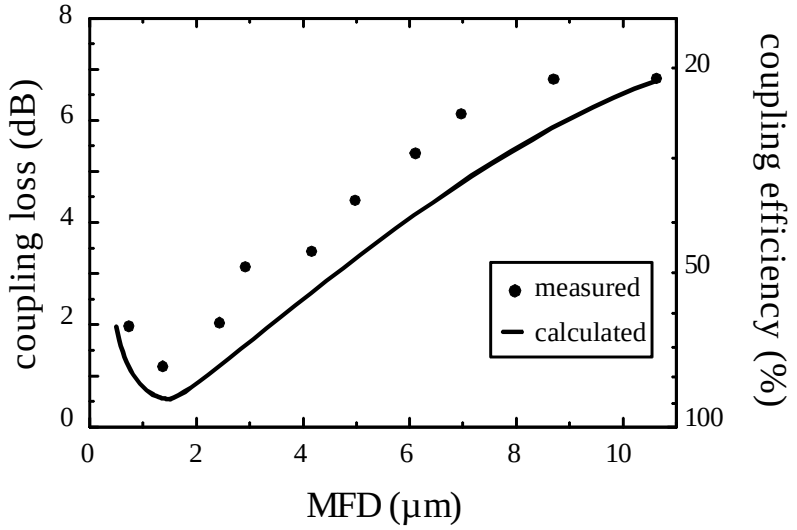

Fig. 11 Fiber chip coupling: coupling loss versus mode field diameter (MFD)

5. PHOTONIC MICROWAVE SIGNAL PROCESSING

In the following a few examples of optically controlled microwave devices and modules are discussed. The physical mechanisms are due to the optical generation of free charge carriers in a semiconductor leading to a control of some key electrical parameters determining the microwave properties.

5.1 Photonic microwave phase shifter/time delay control - In Fig. 12 electrical transmission lines- microstrip and coplanar – are sketched where the strip or the center conductor metal forms a Schottky contact with the semiconductor [6,7]. As a result the high capacitance per unit length gives rise to a slow mode behaviour and the electrical wavelength or the phase velocity are given by the width of the depletion region of the contact. This thickness of the space charge region furtheron depends critically on the applied reverse bias voltage (electrical control of the phase velocity and the delay time). When a fixed bias voltage is applied using an external series resistor, the voltage drop across the depletion layer can also be changed by absorption of an optical signal in the space charge region. As a result, the time delay is controlled optically and because it is a usual transmission line a true time delay shift occurs.

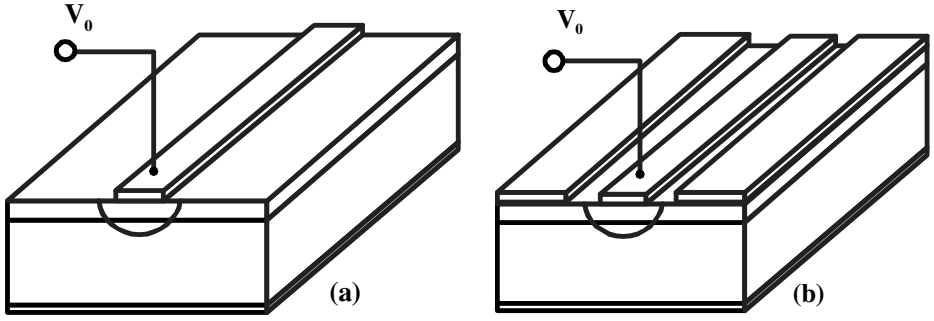

Fig. 12 Optically controlled phase shifter and time delay control using a Schottky contact microstrip line

5.2 Photonic ultrawide band (UWB) pulse generation - Fig. 13 elucidates an optically controlled generation of microwave pulses. The structure consists of a stripline resonator in the center with two gaps on each side. On the left hand side a dc or RF source is connected charging the resonator. On the right hand side an optoelectronic switch (OES) – the second gap - is provided which can optically be switched on in order to connect the output port of the resonator directly to an integrated antenna. Two operating scenarios can be distinguished: (i) Using a dc source the resonator is charged and by closing the OES a pulse is generated traveling to the antenna. The temporal width of the pulse is given by the length of the resonator (frozen wave generator). Please note that specific pulse forms are generated given by the structure of the charge line. (ii) Using a RF source the resonator is also charged and a standing wave of large amplitude, depending on the quality factor of the transmission line, is established. When the OES is optically closed, the standing wave will become a propagating wave and a short ultra broadband (UWB) pulse is generated and radiated using, for example, a broadband slot antenna [21,22]. This technique is a kind of pulse compression [23] known from nonlinear optics and soliton theory.

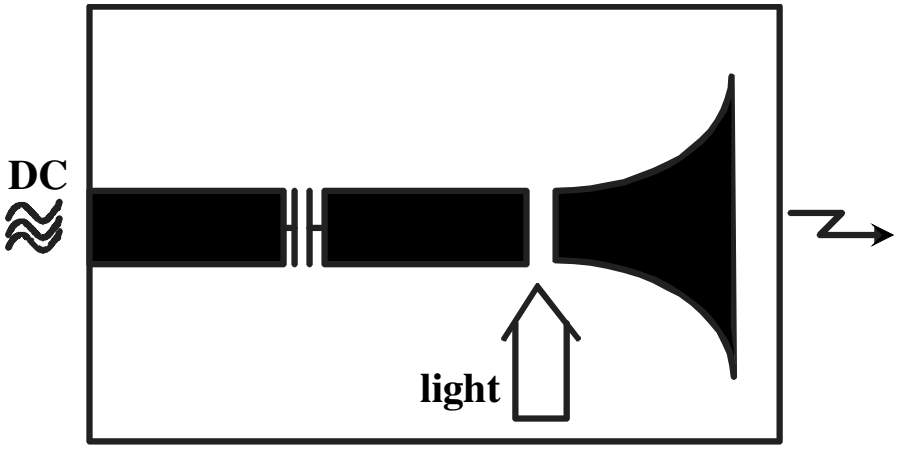

Fig. 13 Optoelectronic switching of a microwave resonator to obtain UWB signals

5.3 RF spectrum analyser - By using the techniques of 5.1 and 5.2 in an 2-dim or even 3-dim array parallel microwave signal processing becomes possible. Fig. 14 shows a microwave circuit where the input signal is divided into several channels and where each channel contains a time delay (T) and an amplitude (a) control using optical techniques as above mentioned. When the output signals are finally combined to a common connection a transversal filter results. In contrast, when the individual channels would be connected to antennas, a phased array antenna system results.

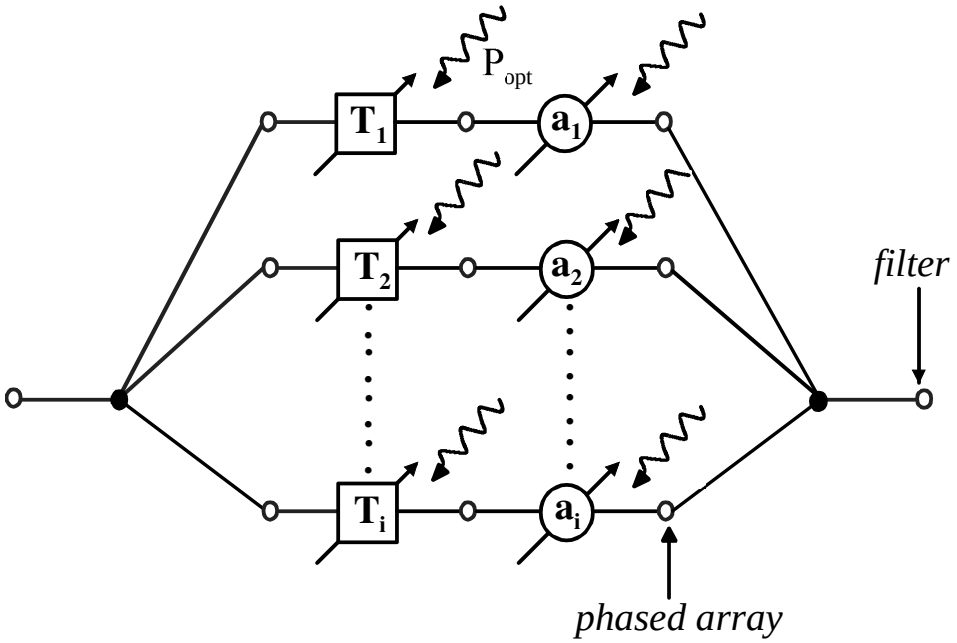

Fig. 14 Microwave signal processor

6. BROADBAND FIBER OPTICAL LINKS

An analog or digital - optical link consists of an optical transmission medium (preferably a fiber) and optoelectronic converters on both sides, see Fig. 15. The great advantage of such an optical link is that due to the broadband low-loss transmission capability the optical fiber (see Fig. 15) can ideally be used to transmit microwave signals and therefore replace other lossy metallic waveguides, see Fig. 16. Here different techniques have been explored. For example, on the transmitting side a cw laserdiode and an external modulator (electrooptic or EAM) and on the receiving side an optoelectronic photodetector can be used. Besides the bandwidth a key parameter of such a link is the link loss which depends on the conversion efficiencies of the optoelectronic elements, the optical coupling efficiencies and the attenuation and dispersion of the transmission medium [24]. Note that a link gain can easily be achieved when an optical amplifier (EDFA) and/or external modulators, preferably on both sides, are being used [24]. For high-speed and broadband operation the a. m. TW microwave photonic devices can succesfully be employed.

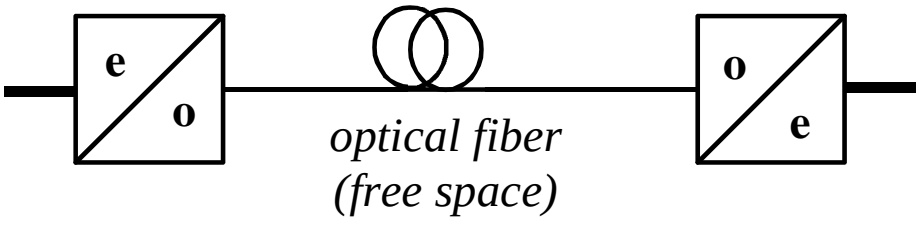

Fig. 15 Optical interconnection replacing an electrical cable

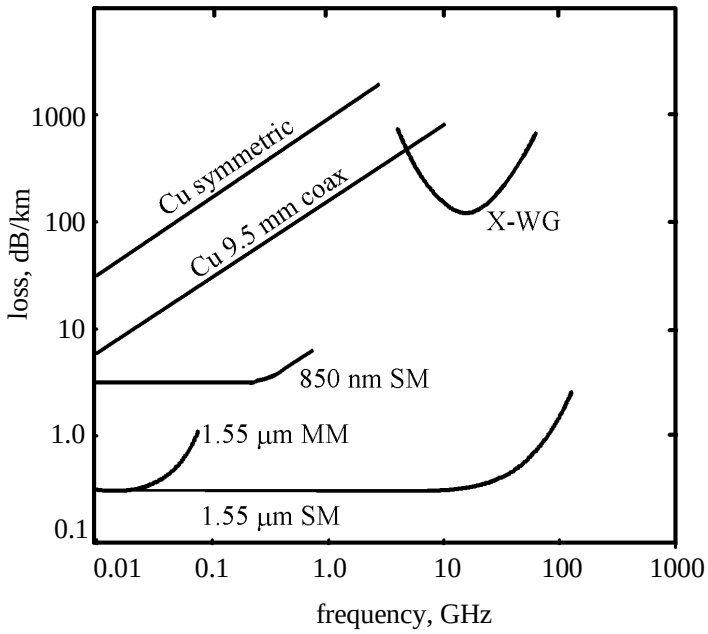

Fig. 16 Transmission loss of different transmission media

For bidirectional communications, as shown in Fig. 17, the link would require a duplication of the elements on both sides in order to provide uplink and downlink transmission. This is the conventional system architecture. But there is another solution using elements as above mentioned: Fig. 17 shows as an example also the advanced system where the base station contains only one optoelectronic element, here the transceiver, as realized by an EAT. Optically, the transceiver receives two signals, one for downlink purpose which is absorbed and one for the uplink which is modulated by the received electrical signal to be transmitted to the central station. Electrically the transceiver uses electrical frequency multiplexing saying that the up and downlink signals are at different frequencies. Given that due to the basic physical mechanisms the electrical bandwidth of the EAT is the same for the detection and the modulation process, a bandwidth of more than 170 GHz can be achieved using an TW EAT (Fig. 6).

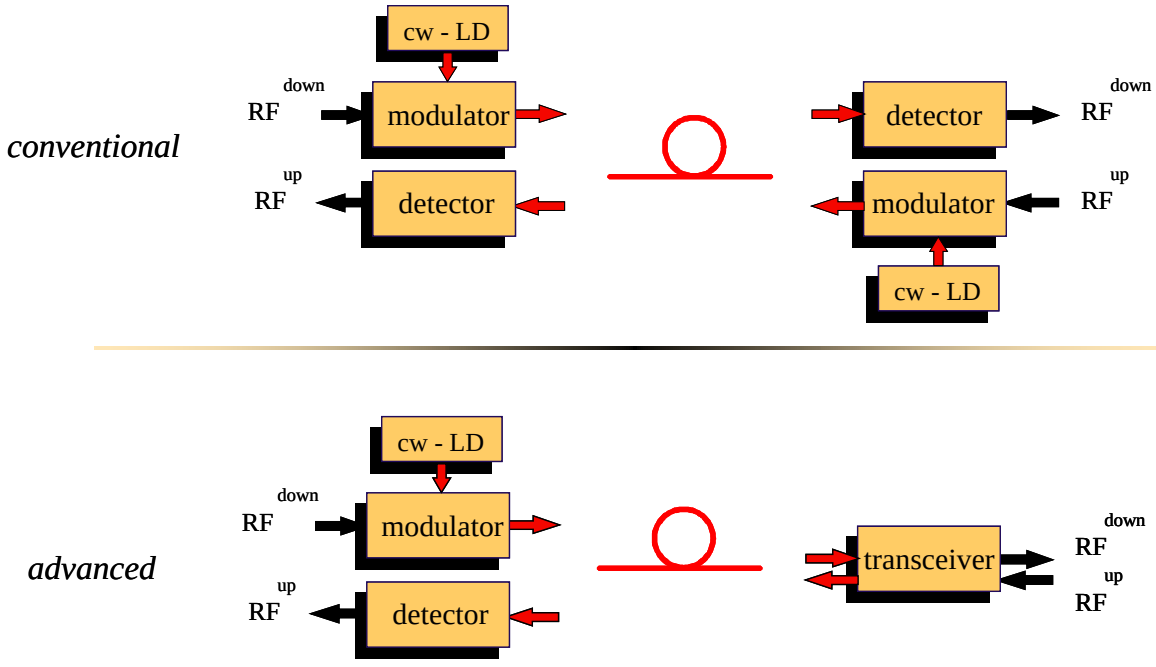

Fig. 17 Conventional and advanced IMDD scheme (IMDD is intensity modulation and direct detection)

7. MICROWAVE PHOTONIC SYSTEMS

Broadband fiber optic links are regarded to be basic building blocks for different microwave systems where specific advantages of the optical interconnections and optical signal processing capabilities are utilized. A few areas of significant applications are reviewed in the following.

7.1 Photonic local oscillators - Transmitting two optical wavelengths by using two frequency locked lasers or a two mode laser and mixing the two optical signals in a photodetector/-mixer emulates a microwave local oscillator where the difference frequency is photonically generated by heterodyne techniques and where wavelength tuning provides a bandwidth of several THz depending on the bandwidth of the detector [25]. Note also that an optically induced phase shift is directly transferred into the electrical domain. Fig. 18 shows a module fabricated for radioastronomical antennas; the module consists of a traveling-wave photomixer connected to a dc bias circuit with appropriate filters, a slot line antenna and a quasi optical lens to focus the radiated beam at 460 GHz into an He cooled SIS mixer.

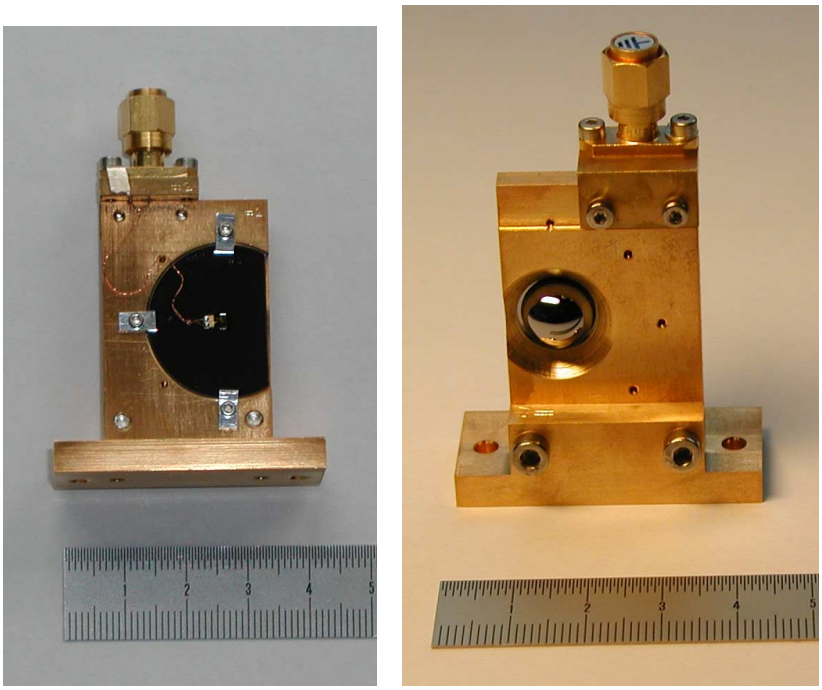

Fig. 18 Photograph of a photonic local oscillator module

7.2 EMC sensor - When the modulator at the end of a fiber is driven by an electrical input signal at the given position, the received optical signal can be used to measure the electrical signal quantitatively at the transmitter side and a field sensor results. Fig. 19 shows the circuit diagramme of such an E-field sensor for EMC applications. The sensor head consists of a dipole antenna. The output signal is fed into a transimpedance amplifier driving an EAM. The optical input signal at 1.55 μm is delivered by a laserdiode in the remote unit which contains also the photodiode to measure the output signal from the EAM in the sensor head. The dc bias for the amplifier as well as for the operating point of the EAM is provided by a photovoltaic cell (PVC) in the sensor head. A second laser diode in the read-out unit generates the necessary optical power.

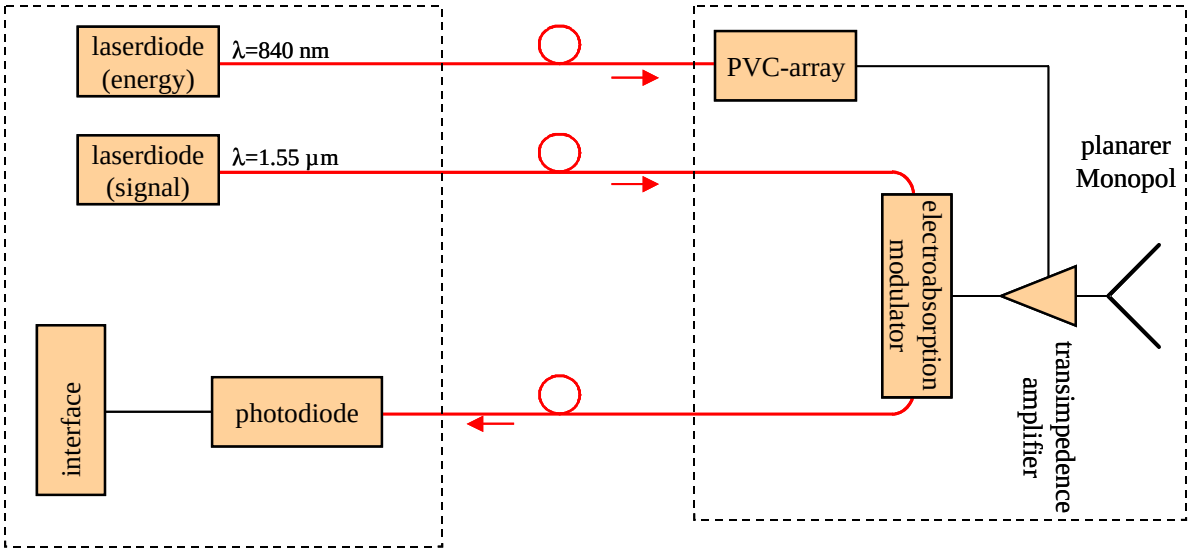

Fig. 19 EMC sensor [26,27]

7.3 Electrooptic sampling and optoelectronic testing - Using electrooptical properties of a semiconductor substrate (Fig. 20) an incoming optical beam is modulated by an applied electrical field and the reflected optical signal can be used to determine the electrical field at the position of the interaction. This set-up can directly be used to measure electrical fields, e.g. in integrated circuits, with high spatial resolution (2-dim field mapping, [28,29]) and without any mechanical contact. Moreover, characteristic sampling techniques have been presented where optical pulses in the pico- or femtosecond range are applied giving a measurement bandwidth in excess of 100 GHz. In a recently presented sensor, a microminiaturized modulator chip working in reflection mode and coupled to the end of a fiber has been applied to measure electrical fields in free space, again with high spatial resolution. Such a fiber sensor is used for contactless high-speed testing of integrated circuits or antenna radiation patterns [13] similarly to the EMC sensor mentioned before.

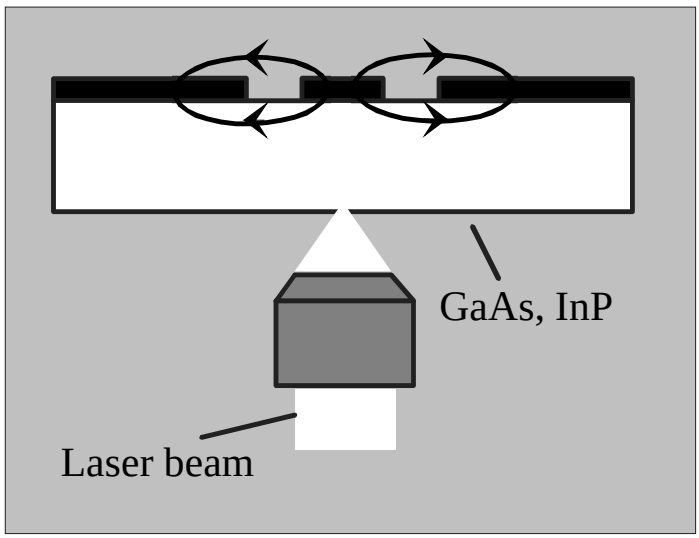

Fig. 20 Principle of electrooptic sampling

7.4 Hybrid fiber-coax (HFC) systems - In cable TV (CATV) techniques the RF signals received from TV satellites are converted into the optical domain and fed into a fiber to be transmitted over long distances with only small attenuation. The received optical signals are converted back into the electrical domain and guided to the costumer via coaxial cable. This HFC technique using again the advantages of the optical fiber transmission is continuously installed in major cities around the world where the uni-directional technique is replaced more and more by bi-directional links in order to establish a back channel, e. g. for multimedia applications.

7.5 Fiber-radio systems - It is agreed that fiber-radio access will provide a solution to the demands for a wireless connection to the costumer ("last or first mile problem"). For broadband services the frequencies are in the millimeterwave range, for example at 40 GHz or 60 GHz. Such a concept is based upon an optical link between the central office and the base stations in a picocellular structure which results from the high free space attenuation of the millimeterwave signal. As an example, 60 GHz fiber radio links have been demonstrated providing 155 Mbps and using EAMs for half-duplex and EATs for full-duplex transmission in a WDM ring network [30-32]. It is foreseen that for next generation broadband photonic communication networks, the electroabsorption modulator (EAM) and the electroabsorption transceiver (EAT) will be key elements. Experimentally, full duplex transmission in a WDM ring network and electrical frequency division multiplex (EFDM), as sketched in Fig. 21, have been studied. Here two CW LDs at different wavelengths are used to drive the modulator function of the EAT in each base station (BS) addressed by the optical wavelength (WDM technique). The other two LDs are externally modulated in the central station (CS) to provide the downlink transmission. These signals are absorbed in the EATs of the base stations to feed the wireless link. The electrical FDM technique is obvious from Fig. 17: downlink and uplink RF frequencies are 59.6 GHz and 60 GHz, respectively. The transmission quality at a data rate of 156 Mbps is finally determined and evaluated by a bit error rate tester (BERT).

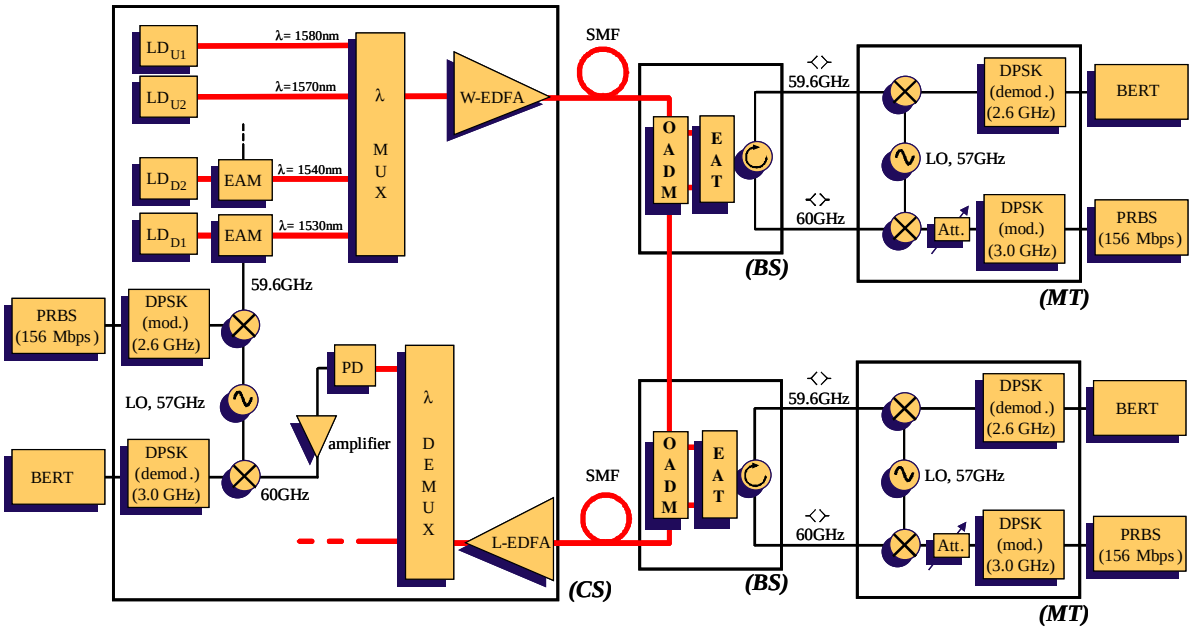

Fig. 21 Full-duplex 60 GHz mm-wave fiber wireless network employing an electroabsorption transceiver (EAT) as a key photonic component in the base station (BS)

7.6 Antenna systems – A major application of optical link technology is the remoting of antenna systems and, particularly, the optical control of array antennas, see for example

Refs. [33] and [34]. In the receiving mode a millimeterwave camera with photonic interconnection is obtained. Different applications in imaging are foreseen.

8. CONCLUSIONS

In the past decade the field of microwave and millimeterwave photonics has become a key technology extending from components and modules to systems with important applications The driver has been twofold: On one hand the broadband low-loss and high-speed transmision capability of optical fibers has led to a considerable interest in their use for distributing and controlling micro- and millimeterwave signals. On the other hand the breakthrough in the design and demonstration of several ultra-broadband photonic components has paved the way for wideband and high efficiency optoelectronic converters being important building blocks for microwave optical links. As a result, it can be foreseen that this multidisciplinary field of microwave photonics will continously be expanded and lead to further novel concepts due to the synergetic merging of different technologies.

In this contribution specific high-speed and broadband photonic components based upon the physics of electroabsorption have been discussed. In particular, electroabsorption modulators, photodetectors, mixers and transceivers have been presented. The multifunctional properties of the transceiver elements have been proven to be especially interesting. The performance of these elements has been demonstrated for example in a fiber-wireless WDM ring network by BER measurements; but the advantages will generally hold for other optical links with bi-directional transmission properties as well. The great advantage of this concept is that in the base station (in the sensor head or at the antenna side) just a single photonic component serves simultaneously as a converter for downlink and uplink communication and information transport. It is therefore concluded that these elements may play a significant and key role in fiber coupled wireless microwave and mm-wave networks and for high date rate transmission services such as in multimedia techniques.

Acknowledgement – The authors wish to thank Professor K. Kitayama, Osaka University and T. Kuri, Communications Research Laboratory, Tokyo, for their contribution to this work.

REFERENCES

[1] D. Jäger, “Traveling-Wave Optoelectronic Devices for Microwave and Optical Applications”, 1991, Proc. of Progress in Electromagnetics Research Symposium (PIERS), p. 327,
[2] D. Jäger, “Microwave Photonics”, in “Optical Information Technology”, S.D. Smith and R.F. Neale (eds.), Springer Press 1993, pp. 328-333
[3] D. Polifko and H. Ogawa, “The Merging of Photonic and Microwave Technologies”, Microwave Journal March 1992, pp. 75-80
[4] “International Topical Meeting on Microwave Photonics”, Techn. Digest, Kyoto 1996, Duisburg 1997, Princeton 1998, Melbourne 1999, Oxford 2000, Long Beach 2001
[5] IEEE Trans. Microwave Theory and Techn., Special Issues on Microwave and Millimeterwave Photonics, Sept. 1995, Sept. 1997, July 1999, June 2001
[6] D. Jäger, “Characteristics of traveling waves along nonlinear transmission lines for monolithic integrated circuits”, 1985, Int. J. Electron., vol. 58, pp. 649-669
[7] D. Jäger, R. Kremer, and A. Stöhr, “Traveling wave optoelectronic devices for microwave applications,” 1995, IEEE Int. Microw. Symp. Digest, vol. 1, pp 163-166

[8] D. Jäger, R. Kremer, A. Stöhr, “High-Speed Traveling-Wave Photodetectors, Modulators and Switches”, 1995 IEEE/LEOS Summer Topical Meeting, Keystone, USA, pp. 23-24, 1995. D. Jäger, R. Kremer, “Traveling-Wave Optoelectronic Devices for Microwave Applications”, Topical Meeting on Optical Microwave Interactions, pp. 11-14, 1994.

[9] D. Jäger, R. Kremer, O. Humbach, and A. Stöhr, “Traveling-Wave Optoelectronic Devices for Microwave Photonics”, Emerging Optoelectronic Technologies, Conference Proceedings, Editors: A. Selvarajay, B.S. Sonde, K. Shenai, and V.K. Tripathi, ISBN: 0-07-462397-4, pp. 409-413, Bangalore, July 1994, (invited paper).

[10] T.H. Wood, “Multiple Quantum Wells (MQW) Waveguide Modulators”, J. Lightwave Technol., no. 6, p. 743, 1988.

[11] O. Humbach, A. Stöhr, U. Auer, E.C. Larkins, J.D. Ralston, and D. Jäger, “Strained-Layer Multiple Quantum Well InGaAs/GaAs Waveguide Modulators Operating at 1µm”, IEEE Photonics Technology Letters, vol. 5, no. 1, pp. 49-52, January 1993.

[12] A. Stöhr, O. Humbach, S. Zumkley, G. Wingen, G. David, B. Bollig, E.C. Larkins, J.D. Ralston, and D. Jäger, “InGaAs/GaAs Multiple Quantum Well Modulators and Switches”, Optical and Quantum Electronics, vol. 25, pp. 865-883, August 1993, (invited paper).

[13] N. Mineo, K. Nagai, T. Ushikubo, “Ultra-Wideband Electro-Absorption Modulator Modules for DC to Millimeter-Wave Band”, Topical Meeting on Microwave Photonics, pp. 9-12, Jan. 2002.

[14] A. Stöhr, R. Heinzelmann, A. Malcoci, and D. Jäger, “Optical Heterodyne Millimeter-Wave Generation Using 1.55µm Traveling-Wave Photodetectors,” IEEE Transactions on Microwave Theory and Techniques, vol. 49, no. 10, part. 2, pp. 1926-1933, October 2001.

[15] A. Stöhr, A. Malcoci, F. Siebe, K. Lill, P. van der Waal, R. Güsten, and D. Jäger, “Integrated Photonic THz Transmitter Employing Ultra-Broadband Traveling-Wave 1.55µm Photodetectors”, Int. Topical Meet. on Microwave Photonics, MWP 2002, (submitted).

[16] A. Stöhr, R. Heinzelmann, T. Alder, and D. Jäger, “Electroabsorption Transceiver (EAT) for Fiber-Wireless Networks,” International Topical Workshop on Contemporary Photonic Technologies 2000 (CPT’2000), Tokyo, January 2000.

[17] D. Jäger, “Large optical nonlinearities in hybrid semiconductor devices”, J. Opt. Soc. Am. B/vol. 6, pp.588-594

[18] D. Tauber et al., “The Microstrip Laser Diode”, Phot. Techn. Lett. vol. 10, no. 4, pp. 478-480 (1998)

[19] M. Schneider, T. Reimann, R. Heinzelmann, A. Stöhr, P. Velling, S. Neumann, R. M. Bertenburg, F.-J. Tegude, and D. Jäger, “A novel 1.55 µm HBT-Electroabsorption modulator,” Tech. Digest, 2001 Int. Top. Meeting Microw. Phot. MWP `01, Long Beach, Jan. 2002

[20] T. Alder, A. Sröhr, R. Heinzelmann, and D. Jäger, “High Efficient Fiber-to-Chip Coupling Using Low-Loss Taperewd Single Mode Fiber,” IEEE Photon. Techn. Lett., vol. 12, no. 8, pp. 1016-1018, 2000

[21] R. Heidemann, Th. Pfeiffer, and D. Jäger, “Optoelectronically pulsed slot line antennas,” Electron. Lett. Vol. 19, pp. 316-317, 1983

[22] P. Paulus, W. Brinker, and D. Jäger, “Generation of microwave pulses by optoelectronically switched resonators”, IEEE J. Quantum Elecgtron. Vol. QE-22, pp. 108-111, 1986

[23] P. Paulus, L. Stoll, and D. Jäger, “Optoelectronic pulse compression of microwave signals”, IEEE Trans. Microw. Theory Techn., vol. MTT-35, pp. 1014-1018, 1987

[24] D. Jäger, “Advanced microwave photonic devices for analog optical links”, 1998, Int. Top. Meeting on Microwave Photonics Digest, Princeton, pp.

[25] A. Stöhr, R. Heinzelmann, K. Hagedorn, R. Güsten, F. Schäfer, F. Siebe, H. Stüer, P. van der Waal, V. Krozer, M. Feiginov, D. Jäger, “Integrated 460GHz Photonic Local Oscillator,” Electron. Lett., vol. 37, no. 22, pp. 1347-1348, Oct. 2001.

[26] R. Heinzelmann, A. Stöhr, M. Groß, D. Kalinowski, T. Alder, M. Schmidt, and D. Jäger, “Optically powered remote optical field sensor system using an electrabsorption modulator”, 1998, IEEE Int Microw. Symp. Digest, pp. 1225-1228

[27] A. Stöhr, R. Heinzelmann, R. Buß, and D. Jäger, “Electroabsorption Modulators for Broadband Fiber Electro-Optic Field Sensors”, in Applications of Photonic Technology 2, Eds. G.A. Lampropoulos and R.A. Lessard, Plenum Press, New York, pp. 871-876, ISBN 0-306-45808-X, August 1996.

[28] G. David, R. Tempel, I. Wolff, and D. Jäger, “Analysis of Microwave Propagation Effects using 2D Electro-Optic Field Mapping techniques,” Optical Quantum Electron. Special Issue, pp. 919-931, 1996

[29] G. David, P. Bussek, U. Auer, F.-J. Tegude, and D. Jäger, “Electro-Optic Probing of RF-Signals in Sub-µm MMIC-Devices,” Electron. Lett., vol. 31, no. 25, pp. 2188-2189, 1995

[30] K. Kitayama, A. Stöhr, T. Kuri, R. Heinzelmann, D. Jäger, and Y. Takahashi, “An approach to single optical component antenna base stations for broadband millimeterwave fiber-radio access systems,” IEEE Trans. Microw. Th. Techn, vol 48, no. 12, pp 2588-259, December 2000.

[31] K. Kitayama, T. Kuri, R. Heinzelmann, A. Stöhr, D. Jäger, and Y. Takahashi, “A Good Prospect for Broadband Millimeter-Wave Fiber-Radio Access System - An Approach to Single Optical Component at Antenna Base Station,” in IEEE MTT-S International Microwave Symposium and Exhibition, pp. 1745-1748, Boston, June 2000.

[32] Stöhr, K. Kitayama, and D. Jäger, “Full-Duplex Fiber-Optic RF Subcarrier Transmission using a Dual-Function Modulator/Photodetector”, IEEE Transactions on Microwave Theory and Techniques, vol. 47, no. 7, pp. 1338- 1341, July 1999.

[33] M. Y. Frankel and R. D. Esman, “True Time-Delay Fiber-Optic Control of an Ultrawideband Array Transmitter/Receiver with Multibeam Capability”, IEEE Trans. Microwave Theory Techn. vol. MTT-43, no. 9, pp. 2387-2394, September 1995

[34] P. J. Matthews, P.-L. Liu, J. B. Medberry, M. Y. Frankel, and R. D. Esman, “Demonstration of a Wide-Band Fiber-Optic Nulling System for Array Antennas”, IEEE Trans. Microwave Theory Techn. vol. MTT-47, no. 7, pp. 1327-1331, July 1999.

Click here to view slide presentation presented in PDF format

Wireless and Optics – A Survey and Overview of Broad Band Fiber-Fed Radio Systems

J. J. Lee
Raytheon Electronics Systems
R2-V518 PO Box 902, El Segundo CA 90245, USA

jjlee8@west.raytheon.com

Abstract – This paper was prepared for NATO's RTA Lecture Series No. 229 presented at the workshop of Optics-Microwave Interactions held in September 2002. This lecture reviews recent developments of fiber-fed radio systems, an emerging technology using fiber optic networks to distribute broad band RF and MMW signals for mobile and wireless systems over long distance and within small cells.

This lecture note is a supplement to the vugraphs package (see attachment) presented at the workshop. Basically, it is a condensed version of the text portion (annotation) attached to the vugraphs (Power Point charts).

What is "Fiber Radio?" Fiber Radio is a fiber-fed radio system using fiber optic links or networks to distribute video, voice, and data for mobile and wireless applications. Antenna remoting is an example where MMW subcarriers at 18, 24, 38, or 60 GHz with information are transmitted from central office to base stations. This emerging technology has been demonstrated for applications such as community communications and pico-cell wireless systems for both uplinks and downlinks broadcast carrying CATV, WLAN signals and data ranging from 2 to 156 Mbps.

According to a McKinsey report, August 2001, the market trend for this industry is hard to predict at this point. In general, the telecom markets have slumped for the last few years. The slowdown was caused by over-capacity and unrealistic forecast. Numerous start-ups were funded five years ago, but many stocks dropped by 80 percent or more in value since then. Many US companies have suffered great losses. However, the demand for broad band services is for sure increasing. It is estimated that the growth rate may reach 25 percent a year. Thus the over-capacity or glut may be absorbed in a few years. It can be safely remarked that the "fiber-radio" technology is attractive, but it is not a huge mature market yet.

1. Applications of Fiber-Radio Systems

Several fiber-radio system architectures have been studied and demonstrated. A typical infrastructure concept was reported by Wake, et al [Optical Generation of MMW Signals … in IEEE Trans. MTT, p.2270, 1995]. He described a system where an optical fiber system with optical couplers (splitter) was used to distribute radio signals with MMW subcarriers broadcast over many pico-cells (200 m range) for community services.

Paper presented at the RTO SET Lecture Series on "Optics Microwave Interactions", held in Jouy en Josas, France, 2-3 September 2002; Duisburg, Germany, 5-6 September 2002; Budapest, Hungary, 9-10 September 2002, and published in RTO-EN-028.

More details of similar system concepts were provided by Ogawa el al [MMW Fiber Optic Systems for Personal Radio Communications, IEEE Trans. MTT, p. 2285, 2002]. They studied and conducted an experiment reporting that excellent performance of IF links with 70 MHz QPSK and 300 MHz FM on 26 GHz subcarriers were obtained. For downlinks from central office to base stations, several modulation schemes were discussed. For uplink from base stations to central office, low frequency lasers and photodetectors could be utilized because data rate and traffics were not as high as downlinks.

Han, Kim, and Chung at Korea Advanced Institute of Science and Technology studied a multi-purpose fiber optic access network, where CATV, PCS, and base band signals were multiplexed and carried by 10 km optical fibers to various nodes for distribution. They presented the RF performance of various services with geographical and technical specifications.

Ahmed, et al [37-GHz Fiber-Wireless System for Distribution of Broad Band Signals, IEEE, MTT, p. 1431, 1997] conducted an experiment using 36 GHz carriers to broadcast audio, video, and CATV signals over short distance, establishing the feasibility of fiber-radio links for wireless systems.

Fiber-fed radio systems can also be used to study the geographic arrangement of base stations for optimum reception. Arrendonda, et al [Techniques for Improving In-Building Radio Coverage Using Fiber-Fed Distribution Antenna Networks, IEEE AP-S Symp, p. 1540, 1996] conducted a statistical study on diversity, placement, and number of antennas in a fast fading Rayleigh environment for performance improvement. They compared systems and data characteristics at 900 MHz, 1.8 and 1.9 GHz, and found that multiple distributed antennas improved coverage, reduced dynamic range required, and eliminated deep fades.

Fiber-fed radio systems may include a photonic network to distribute local oscillator signals. High frequency channels with external modulators and low frequency channels with direct modulators can be combined and distributed through the optical fiber system for various mixing and conversion functions. Photonics will be a key technology to reduce the size and weight of a complex LO distribution system for broadcast, multicast, or point to point connections.

2. Components of Fiber-Radio Systems

Several charts are included to cover the components of the fiber-fed radio systems, including MMW sources, transmitters, modulators, WDM, couplers, amplifiers, and detectors.

To be reviewed first are the schemes and performance issues of antenna remoting using direct and external modulators in the photonic links. The talk will discuss how to improve link performance with increase of laser power and photodetector output current in a link with external modulator for MMW subcarriers distribution.

To overcome the difficulty in producing high quality MMW sources by conventional RF means, one may consider optical generation by heterodyne methods (beating two optical lines) or using mode-lock lasers. Vieira et al [A Mode-Locked Microchip Laser Optical Transmitter for Fiber Radio, IEEE MTT, p. 1882, 2001] offered such a solution.

At the output side of the link, extracting 60 GHz MMW signals with a photodetector is not an easy task when efficiency, cost, and reliability are taken into account. One example was given by Rohde el al [Optical-MMW Converter for 60 GHz Radio-over-Fiber Systems.]

JDS Uniphase is one of the major companies developing key photonic components for photonic and fiber-fed radio systems. A complete photonic network requires many components, including laser sources, modulators, dense WDM, couplers (optical splitters), amplifiers, optical switches, etc. Examples will be given to realize the dimension and complexity of the key devices required for the system.

3. Issues and Performance Parameters of Fiber-Radio System

Several charts are provided to recognize the fact that the performance of a photonic or fiber-fed radio system will be judged by the same set of parameters commonly used and defined by the RF designers. These are gain, noise figure, signal to noise ratio, dynamic range, bandwidth, third order intercept point, etc. Photonic links with COTS (Commercially Off The Shelves) components for wide band and narrow band requirements will be compared with a standard RF amplifier channel using typical wide band COTS devices. It can be seen that it is still a challenging task to develop a photonic link that can compete with a conventional RF channel using the same set of performance parameters mentioned.

It can be summarized that fiber-radio is an emerging technology that will become more attractive to distribute MMW broad band signals for wireless and mobile applications. The demand for such systems is increasing for regional and community networks, but so far no major venture capitals are rushing into the market yet. In other words, no market “pain” or “killer application” has been identified to foresee a major shift in the market trend for such products. Technology for laboratory demo is maturing, but lot more product development is required to produce low cost and robust (reliable) MMW and RF photonic components. In addition, it is necessary to further improve the performance of fiber optic links for RF designers to accept and use photonics. There are many photonic scientists, but it appears that engineering schools need to train more students to become photonic system engineers.

This page has been deliberately left blank

Page intentionnellement blanche

RF Photonics for Beamforming and Array Applications

J. J. Lee
Raytheon Electronics Systems
R2-V518 PO Box 902, El Segundo CA 90245, USA

jjlee8@west.raytheon.com

Abstract – This paper was prepared for NATO's RTA Lecture Series No. 229 presented at the workshop of Optics-Microwave Interactions in September 2002. This lecture focuses on the applications of RF photonics for array antennas in signal distribution, beamforming, beam control, and antenna remoting. Examples are given to discuss the requirements, benefits, and design approaches of photonics for phased array antennas. The first demonstration of using photonics for a dual band array was conducted in 1990. Later a wide band conformal array controlled by photonics was built and tested. This example talks about the optical control of phased arrays by using fiber-optic links for RF and data remoting and a time-shift beamforming network for wide instantaneous bandwidth. Last, the talk will illustrate how photonics can be used to form a wide band feed system for multibeam arrays.

1. Background

This lecture note is supplemented with a set of vugraphs (attachment), and these charts are now summarized with the following annotations. Why RF photonics? There is growing interest in applying photonic technology to phased arrays for signal distribution, beamforming, and antenna remoting [1-6]. Recently, significant progress has been made in the reduction of RF to optics conversion loss. As a result, antenna systems can benefit in the areas of wide instantaneous bandwidth, immunity to EMI, lower transmission loss for data remoting, and eventually reduction in size and weight as a goal.

Since 1980 Raytheon and HRL have been funded by DARPA and AFRL to demonstrate several wide band arrays and feed networks using photonic technology. The concept of wide band arrays centers on the usage of a true time delay beamforming network. A large array is usually divided into many subarrays, with each subarray supported by a programmable delay line. Within each subarray, phase shifters are used on the element level, where 360 degree phase shift is provided to tilt the wave front for a given scan angle.

The first dual band array (X- and L-band) was demonstrated in 1990. The L-band array has 8 elements while the X-band array has 32 elements. Each array was divided into four subarrays. A four-channel fiber optic true time delay feed network was built to scan the beam for both frequency bands. The delay line is a 3-bit assembly consisting of a 1:8 divider with 8 lasers followed by eight fibers with different precut lengths. Scan performance will be shown to illustrate that there is no beam squint (angular change) when the frequency was switched from one band to the other by using the same set of photonic delay lines for beam steering.

Paper presented at the RTO SET Lecture Series on "Optics Microwave Interactions", held in Jouy en Josas, France, 2-3 September 2002; Duisburg, Germany, 5-6 September 2002; Budapest, Hungary, 9-10 September 2002, and published in RTO-EN-028.

After the first demonstration, a more sophisticated photonic array antenna was built and tested. The purpose of this project was to study the issues and determine the feasibility of integrating all the key photonic components into an array for system applications. The design and the wide band performance of an L-band 96-element array controlled by photonics will be discussed. The 2-D array developed for technology demo consists of 96 wideband elements, grouped into 24 columns, with each column steered by an 11-bit time shifter. The L-band array (850-1400 MHz) is capable of transmitting and receiving over ± 60° scan in the azimuth plane. It is controlled by RF and digital fiber optic links from a remote site. The design parameters of the photonic array are:

Aperture size	~ 1 x 2.7 m, conformal, 3 m radius
Frequency	L band, 850 - 1400 MHz
Bandwidth	50% at 1125 MHz center frequency
Radiation element	printed "bunny ear" elements
No. of elements	4 x 24 (96)
Element spacing	10.7 cm AZ, 21.3 cm EL
Directivity	~ 25 dBi (midband)
Beamwidth	~ 5° AZ, 15° EL (midband)
Scan limit	±60° AZ, no scan in EL
No. of T/R modules	24
Time shifters	5 bits photonic, plus 6 bits electronic
Radiated power	~ 30 W
Peak sidelobe	Transmit -13 dB AZ & EL
	Receive - 25 dB AZ, -13 dB EL

2. Photonic Beamformer

The system concept for a wideband array is quite simple -- form the beam by group delays instead of phase combining. In the 4x24 element conformal array, a T/R module with a 6-bit electronic microstrip delay line supported each column. Every three columns were combined to form one subarray, which was controlled by a 5-bit photonic time shifter. The photonic time shifter provides the long delays for the whole group of subarray, while the electronic time shifter refines the delays within one nanosecond for each column.

The system block diagram shows how the phased array is controlled by RF and digital fiber optic links from a remote site. On transmit a laser light is modulated by the RF source and transmitted through the fiber to the antenna site. The RF signal is photo-detected and amplified before it is distributed to eight subarrays. After going through the programmable 5-bit time shifter, the signal is further divided into three ways, one for each column of four elements.

The building block of the wideband beamforming network is the photonic time shift module. The programmable time shifters provide the coarse delay steps ranging from 0.25 ns to 7.75 ns for the subarrays, while the electronic delay lines in the T/R module provide fine differential delays ranging from 0.01 ns to 0.5 ns. The physical dimension of the 5-bit photonic time shift module is 10.5 x 12 x 6 cm. Key components inside the time

shifter are four semiconductor pigtailed lasers, one 4x8 fiber coupler, and two 1x4 detector arrays with FET bias switches.

During transmission, the microwave signal goes though a 1:4 RF switch and modulates one of the four lasers. The laser converts the microwave signal into light which is coupled into the 4x8 fiber coupler. After splitting by the coupler, the light is incident on all the detectors in the array. By switching on one of the 8 detectors with the bias switch, the modulated light is routed through one of the 32 preset delays before recovering the RF signal.

The RF signal is then post amplified and divided into three ways with each feeding another 6-bit time shifter in the T/R module. In the receive mode, the signal path is reversed except that the signal must be routed through two transfer switches in the photonic module so that the signal can go through the non-reciprocal 5-bit time shifter in the same direction.

In the 5-bit time shift module most of the insertion loss is incurred in the 4x8 optical coupler between the lasers and the photodetector array. The internal fan-out loss is 18 dB plus 2 dB excess loss. Further, the input impedance of the laser is only a few ohms, while the output impedance of the detector is very high, on the order of several kilo-ohms. These mismatches contribute to additional losses. To overcome these losses, matching circuits have been developed and a preamplifier and a post amplifier are usually included in the circuit to make the link appear to be transparent. Many researchers have made significant progress, and it is expected that this conversion loss will be further reduced in the future.

3. Noise Figure and Dynamic Range

Several key issues were examined in the system design and tradeoff study. The most obvious question is the impact of the high conversion loss of the time shift element on the overall noise figure of the receive system. As in a single-channel case, the overall noise figure of an array with differential weightings is primarily set by the noise figure of the LNA in each channel. Also, minimizing the front-end loss is most important because it directly affects the noise figure. This is accomplished by placing a high gain LNA right behind the radiating element. If the gain is not sufficiently large, the overall noise figure will be affected to some extent by the losses after the LNA. This is especially true for a photonic array, where the downstream loss is significant and the effect of the beam-forming network can not be overlooked.

The conversion loss of a photonic 5-bit time shifter is on the order of 40 dB without wide band input and output impedance matching. To overcome this loss, the LNA gain must be at least 45 dB or higher to reduce the overall noise figure to a reasonable level. For example, with a nominal front-end loss of 1.5 dB and a noise figure of 2 dB for the LNA, the overall system noise figure can be maintained at the level of 2.5 dB if the LNA gain is 40 dB.

The use of high gain LNA is not without limitations in terms of feedback and leakage. A lesson learned from this development is that the transfer switches in the T/R module for

the transmit and receive operation must be specially designed with very high isolation, 60 dB or more each. This results from the fact that the output of the time shifter is on the order of 0 dBm, and the power amplifier must provide 35 dB gain to boost the radiated power to two watts level specified for this application. Thus, with a 45 dB LNA, the loop gain in the T/R module is close to 80 dB, which tends to cause oscillations if the transmit and receive paths are not sufficiently isolated from each other.

There are different definitions of the dynamic range in the calculation of the radar performance. In this case, the spur free dynamic range, defined as the third order intermodulations not to exceed the noise floor, is used. Based on the beamforming network discussed, a signal to noise ratio analysis using spread-sheet program was carried out to estimate the dynamic range of the receive path.

When two amplifiers are cascaded in series, the 3rd order intercept point is somewhat degraded. To maximize the dynamic range in a cascaded system, the overall gain should be distributed properly at different stages. Lumping all the gain at the front-end is not optimal. This is especially true in the photonic array where three stages of amplification were required to overcome the loss in the receive path. In this system, an LNA in the T/R module was used to support each column; the combined output of the subarray was pre-amplified in front of the photonic time shifter, which is followed by a post-amplifier to offset the insertion loss.

Using actual device parameters in the analysis, we can optimize the dynamic range of the system to exceed 95 dB by properly distributing the gains of the amplifiers at different stages along the signal path. A high gain LNA at the front-end tends to improve the overall noise figure but reduce the dynamic range. On the other hand, a lower LNA gain will boost the dynamic range, but degrade the noise figure somewhat. Thus a tradeoff is needed to optimize the performance so that a balance on the noise figure and the dynamic range can be achieved.

Note that if the noise bandwidth increases by 3 dB the dynamic range is reduced by 2 dB, which is the two-thirds rule intrinsic to the spur free dynamic range definition. On the other hand, if the number of subarrays goes up by 15 dB, the dynamic range increases by 10 dB because the signal to noise ratio is enhanced by as much due to coherent signal combining.

Compared to an active aperture array using conventional phase shifters in the T/R modules, the optically fed array suffers about 13 dB degradation in the dynamic range due to the additional loss in the time shift module supporting each subarray. However, in spite of the high conversion loss of the photonic time shifter, many array systems can benefit from the insertion of this emerging technology to achieve wide instantaneous bandwidth, and reasonably high dynamic range at the expense of a slightly degraded system noise figure.

Now consider the effects of the conversion loss on the transmit path. The power limitations of photonic devices preclude their substitution for conventional cables or waveguides for high power distribution in the phased arrays. The concern here is how much gain is required to boost the power up to the radiation level needed for typical array

applications. Note that the maximum input power for the laser is about 10 dBm, so the input to the remote link and the time shifter is limited to this level. In the demo system, three stages of amplification were required. A post amplifier of 35 dB gain was used at the end of the remote link, followed by another post amplifier of 37 dB at the output of the time shifter. In addition, a power amplifier of 38 dB gain was used to produce one Watt radiated power for each column.

For other applications where a single channel photonic link is used with no RF fan-out loss, the transmit path will require a 10 dBm input power for the fiber optic link, followed by 30 dB post amplifier, and then a 35 dB power amplifier to produce one Watt power level at the aperture.

4. Array Performance

Antenna patterns of a nine-column test array over the specified frequency range with the beam scanned to broadside, ±30°, and ±60° showed that the beam did not squint over the bandwidth by using a true-time-delay beamforming network. A conventional array with phase shifters could not have achieved this performance.

The bandwidth of the array was studied by a new technique performed in the time domain. The basic concept is to inject a 2 ns pulse into each column of the array through a series feed and wideband couplers, and then record the waveform after the pulse propagates through all the components in the transmit or receive path. By examining the pulse shape, magnitude, and the relative time delay, we can determine the insertion loss, time delay setting, and the status of the components in each channel. This time domain reflectometry type measurement can not be used for conventional band limited arrays, but it is most suitable for a photonic time shift system.

The impulse response of a 3-column subarray consisting of 3 T/R modules and a 5-bit photonic time shifter verified that the system has a 550 MHz bandwidth, which corresponds to a range resolution of 30 cm. The pulse propagated through all the RF and optical components in the receive path, so the pulse shape revealed the true frequency characteristics of the antenna system.

The antenna patterns of the 24-column photonic array over the 850-1450 MHz band were measured. The average peak sidelobe on transmit is -15 dB, and the level on receive is -20 dB. A 10 dB edge taper was imposed on the 8:1 power combiner for the receive patterns, which produced lower sidelobes than the transmit case.

The performance of a wide band array can also be judged by its impulse response. In the antenna range test, the array was set up to receive a nono-second (500 MHz) impulse at broad side and other oblique angles. It was shown that the photonic array did not cause any waveform distortions on the impulse, while a band limited antenna with patch elements severely distort and spread the impulse. In addition, as the time shifters were commanded to cycle through various states, the impulse can be seen to shift in time domain with sub-nano-second resolution, a feature not achievable in a conventional array without a photonic true time delay feed network.

5. Multi-beam Photonic Array Feed

Photonics can also be used to support a multibeam wide band feed for array antennas. The main advantage is to reduce the complexity of the array front end. This is accomplished by replacing multiple sets of discrete phase shifters at the array element level with a simplified fiber optic Rotman lens supplemented with a RF heterodyne technique for fine scan. The feed "engine" can be used for both transmit and receive operations. On receive, the signal across the aperture is conjugatedly matched at the front end by a reverse phase gradient produced by the transmit network.

This development was motivated by the need to reduce the number of antennas on many airborne and shipboard platforms. Conventional techniques to achieve multiband and multibeam capabilities are impractical because of the size, weight, packaging density, and high cost of the beamforming networks. Packaging is difficult because of the small element spacing required for a typical 3:1 bandwidth array. It is a major challenge to package multiple sets of phase shifters, drivers, and control lines in the space available behind each element. Also, phase shifters are usually lossy, complex, and expensive to fabricate. In addition, heat dissipation imposes a heavy burden on the mechanical and thermal designs needed to achieve dense module packaging. Thus, innovative multibeam feed and independent beam scan concepts are needed.

The new beamforming system uses a simplified Rotman lens configuration supplemented with a RF heterodyne system to provide continuous scan. The configuration consists of a few feed ports to point the beams in the general directions over a ±60° range, and the heterodyne system scans the beam over a small region around the discrete offset angles. This phase-locked RF mixing feed combines the signal distribution and beam scan unit into one beamformer for both transmit and receive operations, thereby replacing the multitude of phase shifters, drivers, and beam control circuitry conventionally used. Heterodyne approaches had been studied before, but none has focused on the aspect of wide band and multibeam applications [7-16].
The basic architecture of the multifunctional, wide band beamformer will be discussed, using a 16-element array with five feed ports as an example. Each port covers a 30-degree sector over the ±60° scan range in the azimuth plane. Within any sector, each beam is steered by a heterodyne phase-locked loop, which constrains two frequencies ω_1 and ω_2 to produce a constant beat frequency, ω_0, radiated by the linear array. Frequency ω_1 is fed into the constrained lens as a reference signal. To a first order approximation, this signal provides a uniform amplitude and certain phase distribution across 16 elements along the pick-up side of the Rotman lens. The second frequency, ω_2, from an offset feed port supplies the desired phase gradient along the same 16 elements to steer the beam in the desired direction when the phase front is transferred to the array aperture. These two frequencies will mix to produce the constant ω_0. However, the spatial phase gradient is not affected by the heterodyne process. By varying ω_2 and ω_1 the phase gradient along the aperture and, hence, the beam direction, can be changed. By exciting other feed ports, one can use the same heterodyne process to generate multiple beams with different pairs of RF frequencies.

Next, the issue of bandwidth and beam broadening is considered. It can be shown that, to a first order approximation, the amount of beam squint normalized to its local beamwidth for a given bandwidth Δf_0 is given by

$$\frac{\Delta\theta_o}{BW} = \frac{N}{2}\frac{\Delta f_o}{f_{MAX}}\frac{d_R}{d_o}\,\mathrm{Sin}\theta_R\left(1-\frac{f_2}{f_o}\right) \qquad (1)$$

where N is the number of elements, f_{MAX} is the highest operating frequency of the antenna, and f_o is the current operating frequency. The element spacing is assumed to be $d_o = \lambda_{MIN}/2$ where λ_{MIN} is the wavelength corresponding to f_{MAX}. A criterion to define the bandwidth is to restrict the squint (absolute value) to be less than one quarter or one half of the beamwidth. So one can set

$$\frac{\Delta\theta_o}{BW} = \frac{N}{2}\frac{\Delta f_o}{f_{MAX}}\frac{d_R}{d_o}\,\mathrm{Sin}\theta_R\left(1-\frac{f_2}{f_o}\right) < 0.5 \qquad (2)$$

to calculate the maximum size of the array (N) for a given bandwidth ($\Delta f_o/f_{max}$) in terms of feed angle θ_R, relative element spacings, and vice versa. Note that when f_2 is equal to f_0 without heterodyne, the system degenerates into a conventional Rotman lens with infinite bandwidth, consistent with the definition of a true time delay beamformer. Also, when f_2 is varied to go above or below f_o the beam will deviate from the normal setting θ_o, scanning to the right or left depending on the frequency variation. This is the basic principle of the heterodyne beam scan system.

6. Fiber Optic Implementation

The space feed can be replaced by bundles of fibers precisely cut to produce perfect wave fronts for the directions associated with the feed ports. The fiber version of the feed makes the system compact and foldable. Using light sources of different colors will provide high isolation between independent beams. A special case of the system was described in [16], in which one set of equal-line-length fibers represents the central reference port and another set of unequal-line-length fibers of incremental length ΔL generates the phase gradient required to scan the beam by frequency control through a phase-locked loop. Multibeam operation is achieved by using laser light of different colors to carry control signals for each beam while sharing the same fiber feed system. This sharing is made possible by the use of optical wavelength division multiplexers (WDMs), which allow light signals of different wavelengths to be combined, passed through the common feed system, then separated at the output to generate independent, noninteracting beams.

The transmit (TX) manifold can be used for receive by producing a conjugate phase front to mix with the incoming wave. The TX “engine” produces an outgoing wave with a slightly offset ω_0 to heterodyne with the receive signal by another set of mixers. The IF outputs at the elements can then be added in phase with a summing network and sent to the remote site by digital photonics for further filtering and processing. Again, multiple beams can share the same beamforming manifold to reduce cost and complexity. The receive signal does not go through the entire beamforming manifold in the reverse direction. Hence, the overall noise figure is not degraded by the total loss of the beamformer in the transmit path. This is especially significant when the photonic conversion loss is still high. With the new design, the receive path bypasses most of the

transmit components so the noise figure is limited only by the front-end loss and the noise figure of the LNA. This eliminates the most severe drawback encountered in other competing designs where a conventional photonic beamformer is used.

In summary, the wide band beamformer is a low-loss, compact system for simultaneous multibeam, multiband, and wide scan operation. Multiple beams can share the same optical feed manifold without duplicating the complex network of phase shifters, drivers, and beam-control data lines of a conventional feed system. Continuous beam scan by the heterodyne process eliminates the problem of gain ripple (crossover between beams) encountered in a conventional Rotman lens. Phase shifters are replaced by Wide band mixers at lower cost and less system complexity. However, more development is required to advance the technology and verify the concept.

References

1. W. Ng, A. Walston, G. Tangonan, J. J. Lee and I. Newberg, "Optical steering of dual band microwave phased array antenna using semiconductor laser switching," Electronics Letters, Vol. 26, Page 791, 1990.
2. R. Tang, A. Popa, J. J. Lee, "Applications of photonic technology to phased array antennas," Proc. IEEE AP-S Symp., Vol. II, Page 758, 1990.
3. W. Ng, A. Walston, G. Tangonan, J. J. Lee, I. Newberg, "The first demonstration of an optically steered microwave phased array antenna using true-time-delay," IEEE Journal of Lightwave Technology, Vol. 9, p. 1124, 1991.
4. A. P. Goutzoulis, D. K. Davies, J. M. Zomp, "Hybrid electronic fiber optic wavelength-multiplexed system for true time-delay steering of phased array antennas," Optical Engineering, Vol. 31, p. 2312, 1992.
5. H. Zmuda, E. N. Toughlian, *Photonic Aspects of Modern Radar*, Artech House, 1994.
6. J. J. Lee, R. Y. Loo, S. Livingston, et al, "Photonic Wideband Array Antennas," IEEE Trans. Antennas and Propagation, Vol. 43, pp. 966-982, Sept., 1995.
7. W. R. Welty, US Patent No. 3,090,928, 1963.
8. H. Shnitkin, “Electronically scanned antennas,” p. 57, Microwave Journal, January, 1961.
9. E. Pels, W. Liang, “A method of array steering by means of phase control through heterodyning,” p. 100, IRE Trans. Antennas & Propagation, January, 1962.
10. J. L. Butler, “Variable I.F. scanning,” Microwave Scanning Antennas, Vol. III, Ed. R. C. Hansen, Academic Press, 1966.
11. K. Aamo, “Frequency controlled antenna beam steering,” p. 1549, IEEE MTT-S Digest, 1994.
12. R. Benjamin, C. Zaglanikis and A. J. Seeds, “Optical Beamformer For Phased Arrays with Independent Control of Radiated Frequency and Phase,” Electronics Letters, 1990, Vol 26, No. 22, p. 1853.
13. Seeds, A. J., “Optical Beamforming Techniques for Phased-Array Antennas,” Microwave Journal, Vol. 35, No. 7, July 1992, pp 74.
14. D.K. Paul, “Optical Beamforming and Steering Architecture for SATCOM Phased Array,” IEEE Antennas and Propag. Symp., 1996, p. 1508.
15. A. S. Daryoush and M. Ghanevati, “True Time Delay Challenge in Optically Controlled Phased Array Antennas,” IEEE Antennas and Propag. Symp., 1997, p. 732.
16. J. J. Lee, et al, “Multibeam Arrays Using RF Mixing Feeds,” IEEE Antennas and Propag. Symp., 1997, Vol. 2, p. 706.

This page has been deliberately left blank

Page intentionnellement blanche

Optical Architectures for Signal Processing - Part A

B. Cabon
IMEP, UMR 5130 INPG-UJF-CNRS
B.P.257 38016 Grenoble Cedex
France

SUMMARY:

The progress achieved in performing optoelectronic components makes feasible the generation of microwave functions using all-optical devices.

In the first part of this presentation, the principle of microwave filtering using optical interferometers is described for both optical coherent and non-coherent regimes. Optical components are addressed in terms of microwave-optical S parameters. The experimental realization of filters using fibers or integrated optics is explained.

In the second part, the use of optoelectronic techniques to control microwave devices is presented. For example, optically controlled switches and phase shifters can be useful for phased array antennas. Applications can be found also in the generation of millimeterwaves, optical probing, new microwave wide band devices …

1- INTRODUCTION

Processing microwave signals on the optical link, directly in the optical domain, avoids intermediate conversions from optics to electronics (O/E) and then back again from electronics to optics (E/O). New functions are generated at microwave frequencies by processing the RF modulating signal of the optical carrier.

By using ordinary low-cost passive optical components like interferometers, some interesting microwave functions can be generated. For example, the interference of the microwave envelope and the optical carrier generate filtering of the microwave subcarriers. Microwave filtering obtained with this method is not frequency limited unlike in the microwave domain : filtering is periodic, and extends to infinite frequency. It can be achieved in the optical domain with low cost and low-loss components. Consequently, it is interesting to process filtering optically functions at higher frequency, where it is not easily realized in the microwave domain.

1.1. All optical processing of microwave functions by insertion of an optical passive component

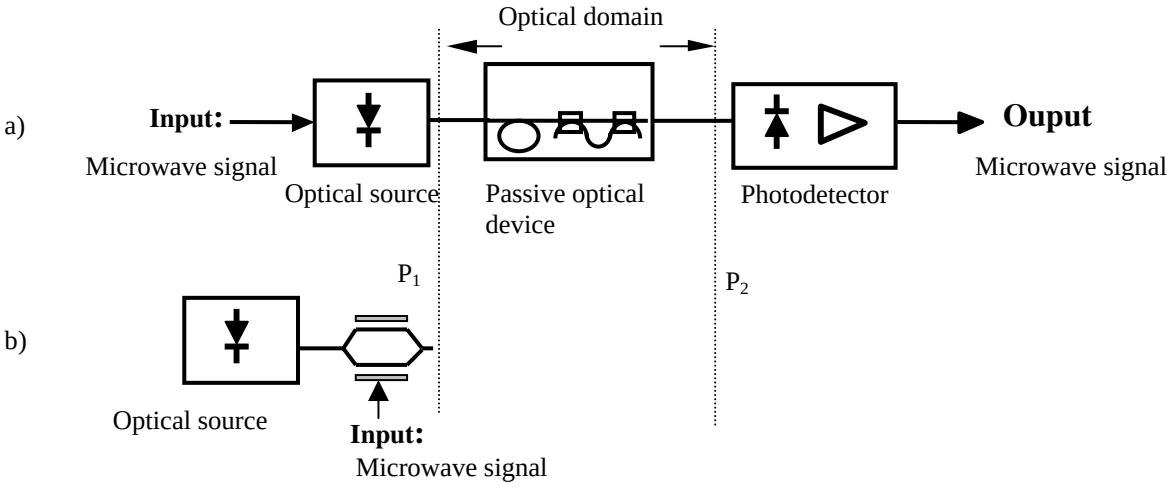

Figure 1: Insertion of optical components in the microwave link for all-optical signal processing.

In Fig. 1 is shown the point to point optical link with direct modulation (Fig. 1a), or external modulation (for example, electro-optical modulation using a Mach Zehnder interferometer, Fig. 1b). Optical passive

Paper presented at the RTO SET Lecture Series on "Optics Microwave Interactions", held in Jouy en Josas, France, 2-3 September 2002; Duisburg, Germany, 5-6 September 2002; Budapest, Hungary, 9-10 September 2002, and published in RTO-EN-028.

devices can be inserted between planes P_1 and P_2 for achieving optical processing of the microwave subcarrier. A passive interferometer inserted there, and made either of fibers and couplers or integrated optical waveguides, can realize microwave filtering. This solution is presented in section 2. In section 1.2, we discuss the transfer function of the filter in terms of S parameters and their variations with frequency.

1.2. Measurement of the optoelectronic scattering parameters

We consider here the external modulation, where the optical intensity is modulated at a microwave frequency (modulation index m).

It is convenient to define the optoelectronic S parameters as in microwave. The optical scattering waves (a_i, b_i) at each port, i , of the optical device, related to modulated optical intensity (envelope of the carrier) are :

$a_i = I_{ai} m \cos(\omega_m t + \varphi_{ai})$ and $b_j = I_{bj} m \cos(\omega_m t + \varphi_{bj})$, where φ_{ai} is the phase of the microwave envelope at port i, related to the incident wave a, and φ_{bj} relates to the emergent wave b. I_{ai} is the incident optical intensity at port i, I_{bi} the emergent optical intensity at this port.

The optoelectronic S parameters of the optical device can then be defined as :

$$S_{ij,\,opt} = \frac{b_i}{a_j} = \frac{I_{bi}}{I_{aj}} \exp j(\varphi_{bi} - \varphi_{aj}). \qquad (1)$$

These S parameters defined with the optical intensity can be measured with a microwave Vector Network Analyzer and its lightwave extension (Fig. 2).

The intensity of the light emitted by a DFB laser source (1300 nm) is modulated at the microwave frequency f_m by a microwave source modulating a MZ external modulator (E/O conversion). At the output of a rapid photodetector (O/E conversion), a synchronous detection is operated by the Vector Network Analyzer. The photocurrent detected by the photodetector is compared to a reference signal. The optoelectronic S parameters are then obtained. The microwave frequency response, the insertion loss, the group delay, etc. are finally derived.

Assuming a linear operation of E/O and O/E converters, then the optoelectronic transfer function $S_{21,\,opt}(f_m)$ of the optical device in the planes P1-P2 can be obtained by measurements. A preliminary calibration is done, then the E/O and O/E are extracted. The global transfer function T_{global} is then measured in the reference planes P3-P4 and then, the final transfer function requested in the reference planes P1-P2 is finally derived :

$$S_{21,\,opt}(f_m) = \frac{T_{global}(f_m)}{T_{E/O}(f_m).T_{O/E}(f_m)}. \qquad (2)$$

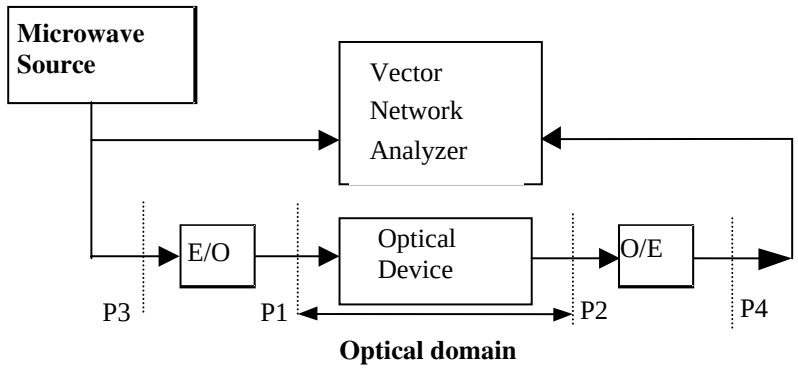

Figure 2: Measurement of optoelectronic S parameters

2- GENERATION OF MICROWAVE FILTERING

The solution presented here is based on interference (coherent regime and incoherent regime) using a directly modulated distributed feedback laser diode (DFB LD) and a passive unbalanced Mach-Zehnder (UMZ) interferometer [1]. Other solution has been presented that uses cascaded passive Mach-Zehnder (UMZ) interferometers [2].

The microwave filter consists of a single optical unbalanced Mach-Zehnder interferometer, which is composed of two optical directional 3dB-couplers separated by two unequal optical paths L_1 and L_2, when

fibers are used (Fig. 3a). It can also be realized in integrated optics on glass, with two Y junctions separated by two optical integrated waveguides of different lengths : one straight, the other curved (Fig. 3b).

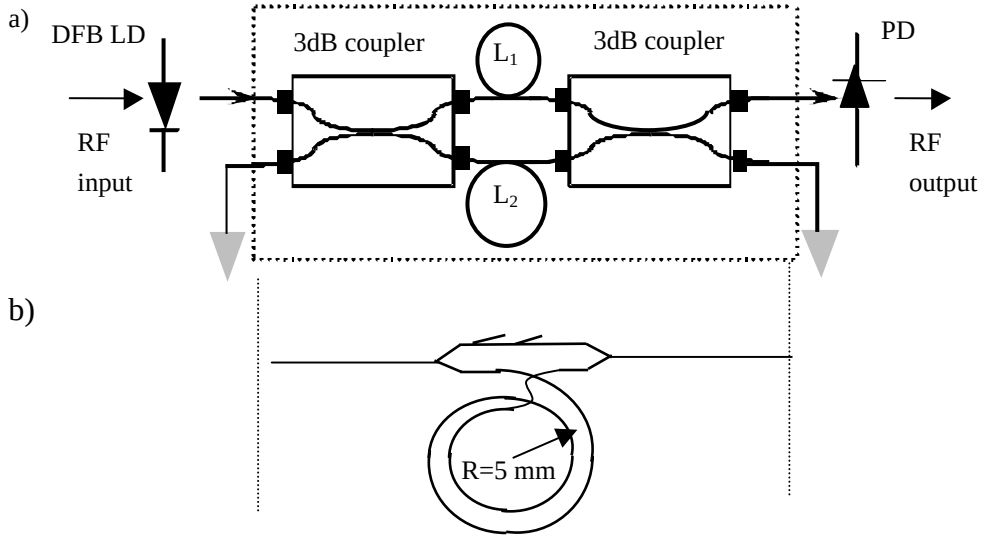

Figure 3 : UMZ: Unbalanced Mach-Zehnder used as a microwave filter made of a) fibers b) integrated optical waveguides on glass

Because of the path difference $\Delta L = L_2-L_1$ between the arms of the UMZ interferometer, two interference figures can occur at the output of the interferometer :

- microwave interference on the envelope - This occurs when two non-coherent optical pulses arrive at the same time at the output of the UMZ. This is the case when the coherent length Lc of the source is shorter than ΔL. The intensity at the output is the sum of optical intensity $I_1 + I_2$ on each arm.
- microwave interference on the envelope plus optical interference on the optical carrier - This occurs when the laser coherence length is greater than the path difference, $Lc>\Delta L$.

In each case, the RF frequency period of the transfer function $S_{21}(f_m)$ equals the FSR (Free Spectral Range) of the interferometer, which is defined as :

$$\frac{n_{eff}}{c}(L_2 - L_1) = \frac{1}{FSR} = \tau. \qquad (3)$$

The optical intensity at the output of the UMZ interferometer is

$$I(t) = I_1(t) + I_2(t-\tau) + 2\sqrt{I_1(t).I_2(t-\tau)}\cos(\Omega_0\tau).V(\tau). \qquad (4)$$

Loss of coherence in the two waves propagated on the two arms of the interferometer is illustrated by $V(\tau)$, which equals 0 in incoherent regime and is approximately 1 in the coherent regime

2.1. Non-coherent regime

The interference of the modulated intensity waves in the two arms produces a periodic transfer function $S_{21}(f_m)$ with minima and maxima. The microwave frequency of the minima is an odd integer multiple of FSR/2, that of maxima is an integer multiple of FSR.

The UMZ acts as a frequency rejection filter over a large frequency range. Filtering is periodic, period equals FSR that can be set by adjusting ΔL. A rejection ratio (maximum divided by minimum of $|S_{21}|$) greater than 50 dB electrical (25 dB optical) can be obtained.

It is worth noting that such a similar value for the rejection ratio could not be obtained in the microwave range, and moreover periodically, up to infinite frequencies if there were no limitation in the frequency response of the optoelectronic components at emission and detection sides.

2.2. Coherent regime

This regime exists when the coherence length of the source is high enough to be greater than ΔL. The coherent optical interference suffers from some additional effects :

a) influence of the optical phase of each arm and influence of the refraction index. The temperature of the component must be controlled accurately;
b) influence of the linewidth of the laser, and of the wavelength emitted (by accurate control of the DC bias and temperature of the LD);
c) influence of polarization of the light, when the optical waveguides used in the UMZ are birefringent.

2.3. Experimental results with passive UMZ interferometer integrated on glass

The example of a passive optical UMZ interferometer integrated on glass substrate by Tl+/Na+ ion exchange is presented here. The design allows a FSR of 3 GHz (ΔL=6.3 cm). The layout of the UMZ is shown in Fig. 4a, and is similar to the schematic of Fig. 3b. In the coherent regime of interference, a DFB laser diode source emitting at 1300 nm (coherence length ≈ 5m) and modulated by an external modulator (20 GHz of bandwidth is used. The optoelectronic transfer function $S_{21}(f_m)$ can be obtained, as shown in Fig. 4b.

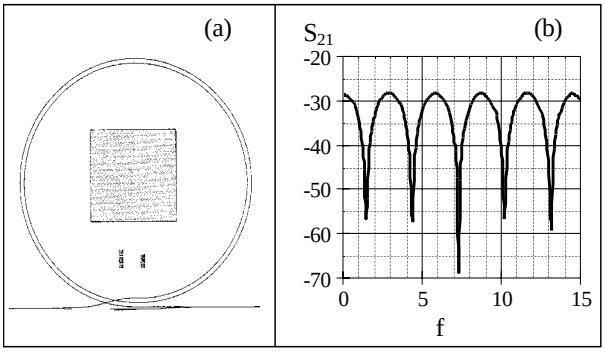

Figure 4 : layout of the integrated UMZ (a) and the corresponding measured frequency response (b).

This figure exhibits deep frequency rejections, periodical, at frequencies equal to an odd integer multiple of FSR/2 as explained before. The path difference ΔL can be adjusted (thermo or piezzo-electrical control) to have a rejection at the desired frequencies.

3. INTEGRATED OPTICALLY CONTROLLED PHASE SHIFTER

In phased array antennas, control of phase of RF signals is of major importance. Optical fibers or optical waveguides are used to distribute the control signal and offer gain of weight, of power consumption and of cost in comparison with electronic control. Thus, the introduction of these optical devices into microwave systems is very important for aircraft radar systems or in satellite communication systems where optical control of microwave devices can be applied for signal processing. A phase shifter and a microwave switch are described here. The monolithic integration of the optical waveguide offers the flexibility and precision of the optical guiding for illumination of the semiconductor device and avoids the presence of multiple beams for controlling different cells of the array.

Microwave circuits are here integrated on silicon, and their responses are modified under illumination. In the semiconductor, the light produced by a laser emitting at a wavelength in the visible range (λ=514 nm) or in the near infrared region (λ=840 nm) is absorbed, then charge carriers are generated, thus modifying the local conductivity of the semiconductor. Silicon has the advantage over GaAs to offer large carrier lifetime and important diffusion lengths. As a consequence, large variation in the conductivity of the semiconductor can be obtained for moderate illumination powers.

The optical microwave planar devices are either integrated on high resistive silicon substrate with a fiber illumination on top of the device, or they are monolithically integrated on a SOI (Silicon on Insulator) structure. In the latter case, the optical guide that illuminates the device is embedded in the structure, thus enabling a large flexibility to position the illumination wherever needed in the circuit. The novelty of this solution is that the monolithic integration results in a mixture of MMIC (monolithic microwave integrated

circuits) and OEIC (optoelectronic integrated circuits). The silicon technology chosen offers a large maturity and allows a high integration level while the SOI technology (used here for monolithic integration) is very promising for microwave applications, because of the low propagation loss. The optically passive controlled devices can be further co-integrated with MMIC on silicon, to realize sub-systems like optically controlled VCO, amplifiers...

3.1. Optical controlled microwave switch on bulk silicon

Here a high resistive (5000 Ω.cm) is used and aluminum coplanar lines are etched on top of it.

The gap (see Fig. 6) inserted in the signal line acts as a microwave phase shifter and as a switch, both controlled by the light emitted by a laser diode (λ = 840 nm). Note that here, only a bulk silicon substrate is used and illumination is made on top of the cell. The gap size is of the order of 16µmX100 µm. After on-wafer calibration, S parameters have been measured for both dark (“off”) and illuminated (“on”) states.
The variations of S_{21} with frequency are shown in Fig. 5 in the "off" and "on" state.

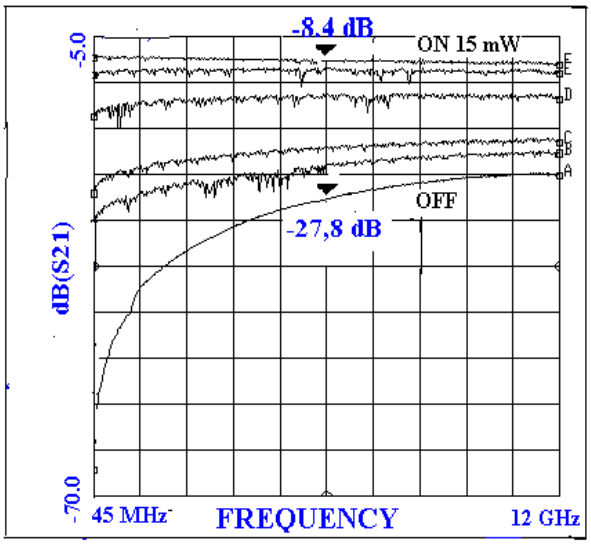

Figure 5 : S_{21}(f) for the microwave switch on bulk silicon

A large on/off ratio can be obtained; the value is 20 dB around 6 GHz with 15mW of optical power, and the insertion loss is around 8 dB.

3.2. Optically controlled switch integrated on a SOI type structure

Here, we discuss optical integration of the illuminating waveguide.

Guided wave optics based on Silicon-On-Insulator have gained interest since they offer low cost and well established technology [3] and they are compatible with monolithic microwave integrated circuits in CMOS and BiCMOS technology that works now in the GHz range. The etched buried channel optical waveguide used here and realized in this technology has been fabricated at CEA/LETI in Grenoble [4] and the fabrication procedure has been given in details in Ref. [5-6]. In the final integrated structure of Fig. 6, the polysilicon gap inserted in the signal strip of a coplanar waveguide is optically controlled by the monolithically integrated optical waveguide embedded in the SOI structure. Here, two illuminating conditions are compared : top fiber illumination with optical power of 2.4 mW and integrated illumination with optical power of 2 mW. It can be concluded from Fig. 7 that the same switching performances can be observed whatever the way of illumination is.

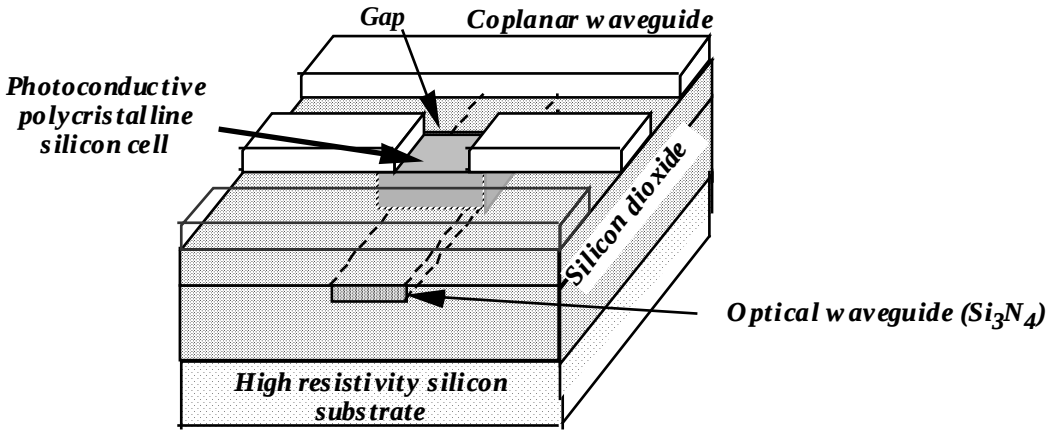

Figure 6 : Schematic view of the optical/microwave device.

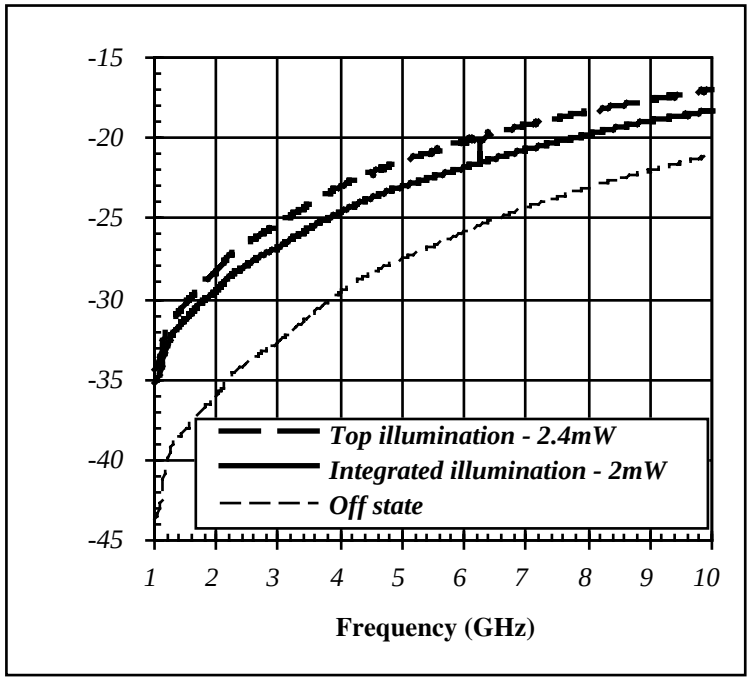

Figure 7 : Comparison of switching performances under 2mW of optical power for the full integrated structure on SOI and 2.4 mW of optical power with top illumination.

3.3. Phase shifter performances in a bulk Si structure

In the monolithic integrated device shown previously, deposited polysilicon has been used for the gap since wafer bonding (monosilicon) is difficult to realize. The performances reached with undoped silicon are better than with polysilicon because of larger values of the diffusion length and of carriers lifetime. But a compromise must be chosen between optical control efficiency and faster response of the device. In this section are discussed the performances of the phase shifter realized in bulk silicon with top illumination, having in mind that top and integrated illumination would lead to the same results as explained in the previous section. Fig. 8 shows the phase shift of S_{21}, under dark and illumination. It reaches the value of 76° at 1.4 GHz and 56° at 12 GHz for an illumination power as low as 5 mW.

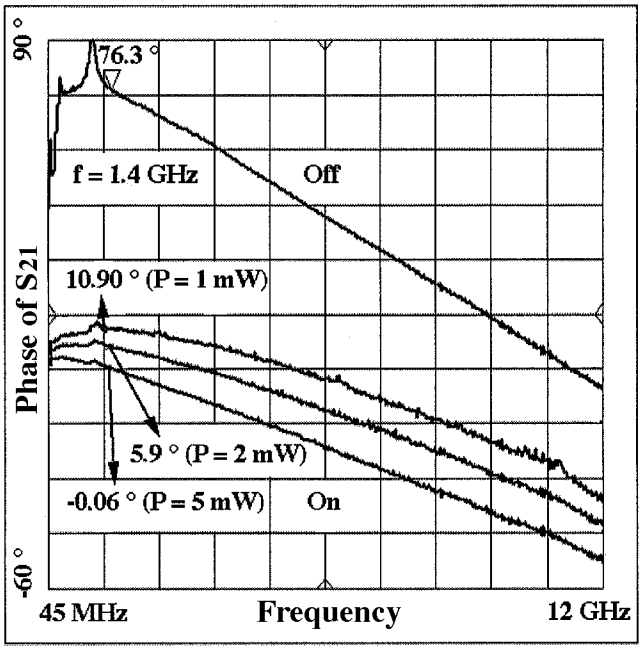

Figure 8 : Phase of S_{21} as a function of frequency in the "off" state and the "on" state for an optical power of 1, 2 and 5 mW.

3.4. Model of the phase shifter

The electron-hole plasma created in the semiconductor results in modifications of conductive as well as dielectric properties of the device. In polysilicon, these effects are limited to a thin layer near the illuminated surface, while in bulk silicon these effects are widely distributed in the substrate. Consequently, the effects observed in the illuminated gap can be modeled by an equivalent circuit composed of a Π network of series connected cells (see Fig. 9), each cell made of shunt connected resistor and capacitor. In this way, the frequency dependence of the gap response (transmission and reflection) is considered together with the modifications of the response under illumination and the distributed effects in the substrate thickness.

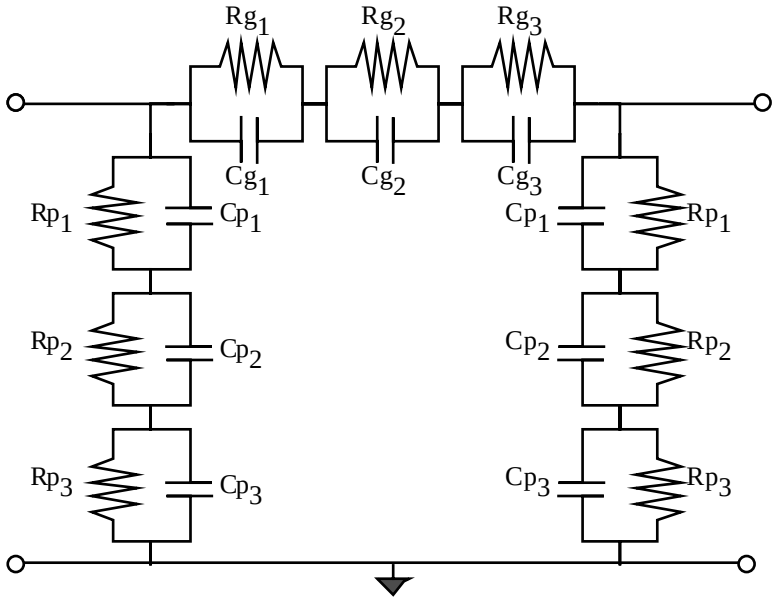

Figure 9 : Equivalent circuit of the gap.

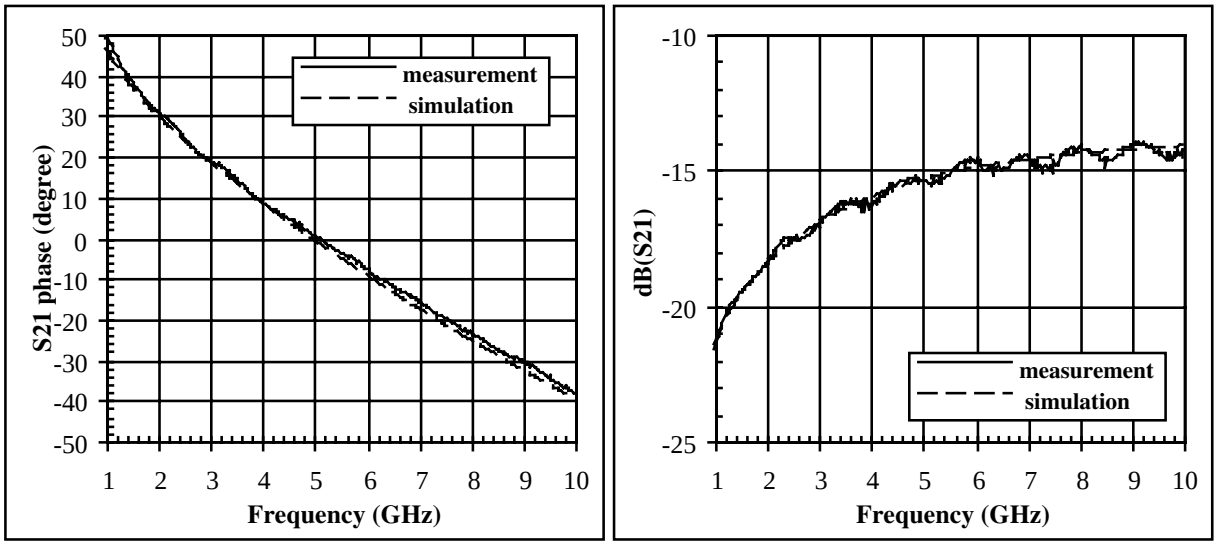

**Figure 10 : S21 magnitude and phase variations –
Comparison between simulation and experimental results related to the "on" state.**

ON state		OFF state	
Rp_1 (Ohms)=160	Cp_1(fF)=1190	Rp_1 (Ohms) $>10^8$	Cp_1(fF)=10^{-3}
Rp_2 (Ohms)=10^5	Cp_2(fF)=3370	Rp_2 (Ohms) $>10^8$	Cp_2(fF)=2.5
Rp_3 (Ohms)=130	Cp_3(fF)=25	Rp_3 (Ohms) $>10^8$	Cp_3(fF)=0
Rg_1 (Ohms)=3.10^5	Cg_1(fF)=845	Rg_1 (Ohms)=3.10^5	Cg_1(fF)=103
Rg_2 (Ohms)=3.10^5	Cg_2(fF)=829	Rg_2 (Ohms)=5.10^5	Cg_2(fF)=23
Rg_3 (Ohms)= 3.10^5	Cg_3(fF)=1109	Rg_3 (Ohms)=5.10^5	Cg_3(fF)=25

**Table 1 : R and C values under dark and illumination
for the optically controlled phase shifter on silicon.**

Simulations of the equivalent circuit related to the optically phase shifter on silicon have been carried out using Advanced Design System software (ADS) from Agilent Technologies. From Fig. 10, it can be seen that the modeled S_{21} phase and magnitude values are in very good agreement with experimental results. The values of modeled capacitances and resistances under dark and illumination are indicated in Table 1. It can be concluded that both capacitances and resistances exhibit a great variation under illumination.

4- CONCLUSIONS

It has been demonstrated that microwave functions can be generated with all optical components. Photonics-microwave rejection filters with high extinction ratio, not limited in frequency range, have been presented. They use a passive unbalanced Mach-Zehnder interferometer, low loss and low cost.

Optical control of a microwave switch and phase shifter has been presented. The phase shift of 76° has been confirmed in a silicon gap structure under an optical power as low as 5 mW. The optical control avoids physical connection to the circuit and avoid biasing components that are usually used in electrical switches. These optically controlled systems are advantageous for wide-band signal transmission and produce novel microwave systems of enhanced capabilities. They can also be applicable to fiber optic fed microwave systems such as phased array antennas.

References

[1] An Ho Quoc, “Etude et Réalisation de Dispositifs Tout-Optiques pour le Traitement de Signaux Rapide”, PhD thesis, INPG Grenoble, France, July 1996.
[2] T.A. Cusik, S. Iezekiel, R.E. Miles, S. Sales, J. Capmany, “*Synthesis of All Optical Microwave Filters Using Mach Zehnder Lattices*”, IEEE Trans. on Microwave Theory Tech., vol. MTT-45, pp. 1458-1461, August 1997.
[3] U. Hilleringmann and K. Goser, “*Optoelectronic System Integration on Silicon, Photodetectors and VLSI CMOS Circuits on One Chip*”, IEEE Trans. Electron Devices, vol. 42, pp. 841-845, 1995.
[4] P. Mottier, “*Integrated Optics at LETI*”, International Journal of Optoelectronics, Vol. 9, Nr 2, pp. 125-134, 1994.
[5] S. Chouteau, B. Cabon and J. Boussey “*Integrated Optics on Silicon substrate for Microwave Applications*”, 28 th European Microwave Conference, Amsterdam 6-8 October 1998, Proc. pp. 70-74.
[6] S. Chouteau, J. Boussey, B. Cabon, A. Illiadis, “*Optoelectronic Microswitch on SOI Based Structure*”, IEEE International SOI Conference, 1995, Proc. pp. 40-41.

This page has been deliberately left blank

Page intentionnellement blanche

Optical Processing of Microwave Signals - Part B

Jean Chazelas
Thales Airborne Systems
2 Avenue Gay Lussac,78851 Elancourt Cedex
Daniel Dolfi, Sylvie Tonda-Goldstein, Jean-Pierre Huignard, Thales Research & Technology
91401 Orsay Cedex, France

Abstract

The availability of optoelectronic components operating up to 20 GHz brings attractive perspectives for optical processing of microwave signals. Furthermore optically carried microwave signals can experience large time delays, especially in fiber based systems, providing time-frequency products in the range between 10^2-10^3. Owing to their inherent parallel processing capabilities, optoelectronic architectures are well suited for the implementation in radar and electronic warfare systems of basic functions such as spectrum and time delay analysis, adaptive and programmable filtering, correlation and waveform generation.
This document is prepared for the NATO's RTA Lecture Series 299 on Optics and Microwave Interactions to be presented in September 2002

1. Programmable transversal filtering- Thales approach

A transversal filter optimizes the detection in a signal $x(t) = S(t) + N(t)$ of a given signal S(t) with duration T, in presence of a stationary noise N(t) or permits jammers rejection from detected signals. These signals are often processed in a sampled form using digital electronic delay lines, allowing a rather large number of sampling points (up to 10^2 - 10^3), but with a frequency bandwidth limited to the low and intermediate frequencies (100 MHz-1 GHz). This frequency bandwidth can be extended up to the 10 GHz region using optoelectronic architectures, especially in fiber based systems, but with the limitation of a number of sampling points in the range 10-10^2.
Therefore, we propose a free space optical architecture of a programmable filter which could provide a large number of samples of about 10^3 and which may process signals over a frequency bandwidth as large as 20 GHz. The operating principle of this programmable filter is shown in figure 1.

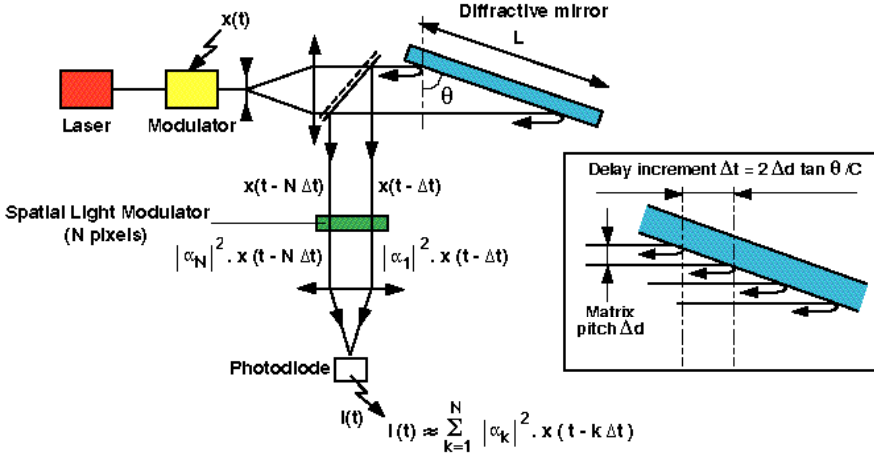

Figure1 Programmable transversal optical filter

Paper presented at the RTO SET Lecture Series on "Optics Microwave Interactions", held in Jouy en Josas, France, 2-3 September 2002; Duisburg, Germany, 5-6 September 2002; Budapest, Hungary, 9-10 September 2002, and published in RTO-EN-028.

A CW laser diode is coupled into an integrated optic amplitude modulator, excited by a microwave signal x(t). This provides an optical carrier of this signal x(t). This optical carrier is expanded and reflects off a diffractive mirror, which operates in the Littrow geometry and provides the necessary time delays. This reflected beam, extracted with a beam-splitter, passes through a one dimensional LCSLM of N pixels providing parallel weighting. Finally the channelized beam is focused onto a photodiode. The response time of the proposed programmable filter is mainly determined by the response time of the liquid crystal SLM (in the range 10-100 µs for ferroelectric or chiral smectic LC). In order to meet radar or EW systems requirements in term of adaptive processing speed in the range 10 ns - 10 µs, it would be necessary to use multiple quantum well SLMs or to take advantage of the high resolution of LCSLMs. Furthermore, it is possible to extend the concept to a 2D geometry including a photodiode array in order to provide high speed processing and large time delays, i.e time-frequency products up to 10^3-10^4.

As a proof of concept a simple rejection filter is implemented using a CW fiber laser (40 mW at 1550 nm). It is coupled to an integrated optic Mach-Zehnder modulator, excited by a CW microwave signal. An image of two slits is displayed onto the SLM, providing two out-of-phase signals. The diffractive mirror operates in the double pass geometry, providing a measured maximum delay of 750 ps. In these conditions, using a multimode-fiber pigtailed photodiode, it is possible to measure at 1.3 GHz a 52 dB signal rejection as shown in figure 2.

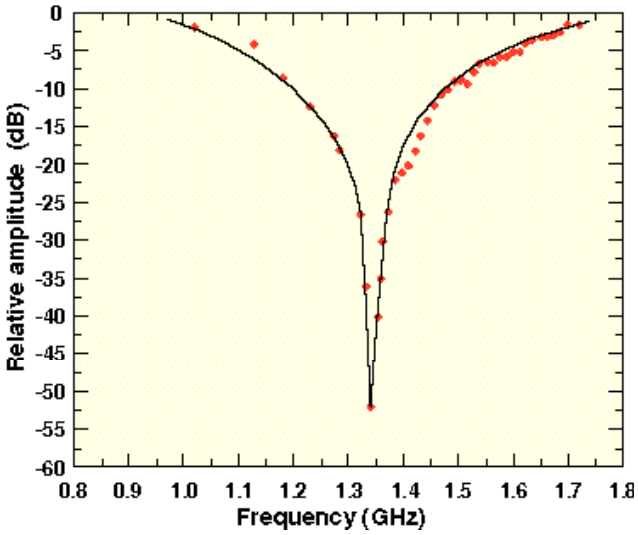

Figure 2 52 dB stop-band filter at 1.3 GHz

2. Optical waveform generation

In order to increase the resolution and the jamming robustness of radar systems, highly complex synthetic waveforms are needed to perform sophisticated signal processing functions at high speed. Typical nowadays solutions are based on digital processing techniques requiring high speed sampling of the signals. Hundreds of thousands sampling points with 8 to 10 bits coding are required because the radar pulse typically lasts 1 to 10µs for radar frequency of 10GHz in 1GHz-bandwidth. A new realistic solution would be to exploit and combine the flexible numerical processing strengths of electronics with the communication and parallel processing strengths of optics to accomplish computationally intensive tasks with

high processing speed. We propose and demonstrate an arbitrary waveform generator based on the heterodyne detection of optically carried microwave signals whose phase and amplitude is optically controlled through the use of LCSLMs.
The operating principle of controlling the amplitudes and phases of optical carriers of microwave signals using heterodyne detection is depicted in Figure 3. It is based on a combination of the basic principles already illustrated in the previous applications. A single-frequency laser beam (ω) is focused through an anisotropic acousto-optic Bragg cell (BC), excited by a continuous microwave signal at pulsation 2πf.

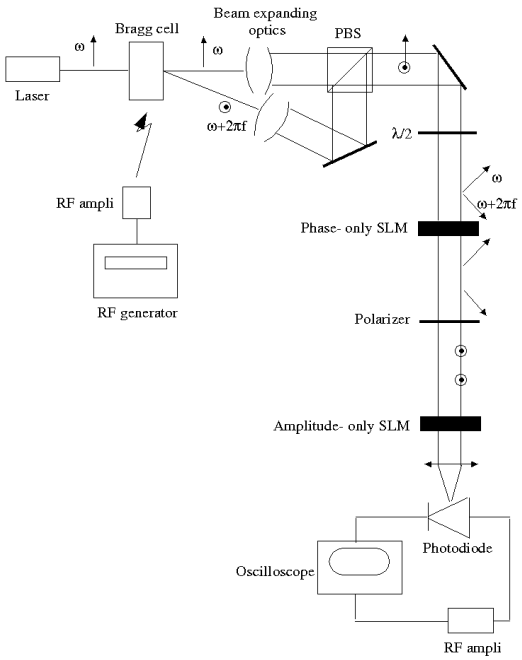

Figure 3:Experimental set-up of the control of amplitudes and phase of optically carried microwave signals.

The transmitted beam (ω) and the diffracted beam (ω+2πf) at the output of the Bragg cell are cross-polarized. They are recombined without loss on a polarizing beam splitter (PBS) to get a dual-frequency optical carrier for the microwave signal. When a photodiode detects this dual-frequency beam through a 45°-oriented polarizer, a microwave beating signal at frequency f is observed. The dual-frequency beam intercepts a first nematic liquid crystal (NLC) spatial light modulator (SLM1) of P pixels providing P channelized beams. This phase-only SLM permits, independently on each channel, an analog phase control of the optically carried microwave signal by changing the relative optical phase of the cross-polarized components of the dual-frequency beam. Next, a twisted nematic liquid crystal (TNLC) SLM (SLM2) of P pixels, placed between two crossed polarizers (polarizing beam splitter PBS at input and exit polarizer at output of SLM2), provides the amplitude control of the microwave signals. Images up to 8 to 10 bits are displayed on the TNLC cell, so that the transmission of each pixel of SLM2 is changed. By control of the displayed grey levels onto the TNLC cell, the amount of light passing through the exit polarizer is controlled, giving an amplitude-controlled output microwave signals. At the output of SLM2, the beating signal is detected at the photodiode. According to the set-up features (photodiode area, optical wavelength, number and size of the SLM pixels and focal length), the amplitudes of the optical signals are coherently summed onto the photodiode, thus also generating coherent summation in the electrical domain of the optically carried microwave signals.

For microwave signals composed of several frequencies, as it is the case for radar pulses, the acousto-optic Bragg cell has to be excited by several continuous microwave signals at different frequencies f_k, (k=1 to N). Each diffracted beam, frequency-shifted by f_k passes through one given pixel i (i=1 to P) of the SLMs'. We control independently the features of each microwave frequency component f_k (phase and amplitude) by the control of the transmission law of the SLMs'. When attributing one frequency to a given pixel i and when doing so for all the frequencies of a given radar spectrum, one can generate any arbitrary waveform. In practical case, a radar antenna transmits a coherent pulse train e(t) that has a pulsewidth T and an interpulse period PRI=1/PRF. The Fourier transform of the pulse train has a sinc(u) envelope, modulating a series of spectral lines f_k spaced by the PRF of the radar ($f_k=f_a+kPRF$, k=-∞..+∞). The peak of this response is at the radar center frequency f_a, and the zeros of the sinc(u) envelope are located at frequencies $f_a \pm j/T$ (j=-∞..+∞) where T is the pulse width. At the output of the SLMs', and on channel i, the expression of the modulated microwave signal is :

$$s(t) = \frac{1}{2}\sum_{k=0}^{+\infty} a_{k,i} E_k \left(\cos(2\pi f_{k,i} t + \phi_{k,i}) + \cos(2\pi f_{-k,i} t + \phi_{-k,i})\right)$$

where the coefficients $a_{k,i}$ are the attenuations of the frequencies $f_{k,i}$ due to the pixel i of the amplitude-only SLM2 and $\Phi_{k,i}$ the phase shifts introduced by the pixel i of the phase-only SLM1. The E_k coefficients are the Fourier coefficients of the coherent pulse train. The frequency $f_{k,i}$ is associated to the pixel i and $f_{-k}=f_a-kPRF$ and $f_{+k}=f_a+kPRF$. We decompose the output signal s(t) onto the kPRF frequencies of the envelope in order to be able to modify s(t) by arbitrary changing the parameters (a_k,Φ_{+k} and Φ_{-k}).

According to the Fourier Transform of the radar pulse train, two consecutive frequencies f_k and f_{k+1} are spaced from only PRF=1/PRI, that is in the range of a few tens of kHz. In order to cope with this low resolution, we propose an alternative optical architecture (Figure 7) that combines an acousto-optic Bragg cell (BC) with a moving grating that diffracts multiple orders. The moving enforced to the grating is driven by applying a periodical signal on the grating. We consider as for the frequency of the applied signal, the frequency of the radar pulse train: f_s=PRF.

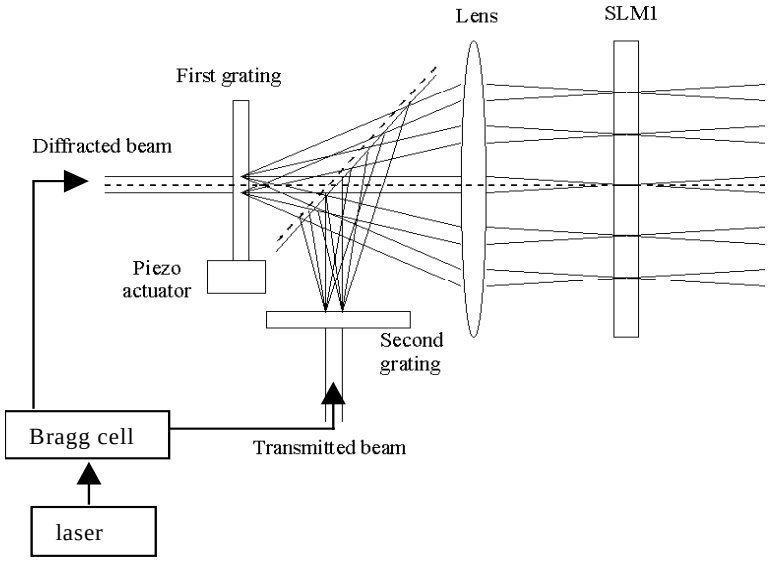

Figure 4: kHz rate architecture with two gratings, that drives each frequency component at kPRF towards each pixel.

In order to modulate the maximum number of frequencies, the grating should diffract many orders. The second grating in the Figure 4 is a fixed one that diffracts the transmitted beam coming from BC. This architecture has the advantage to discriminate the optical beams on the

assumption of SLMs' with classical sizes of pitches (larger than 40μm). According to the required kHz frequency shift, the Raman-Nath grating (first grating) is moved using a piezoelectric actuator, excited with a sawtooth signal of pulsation $2\pi f_s$. This moving grating creates a Doppler shift resulting in diffracted orders at pulsation $\omega+2\pi kf_s$. Owing to the capabilities of the Bragg cell combined with the moving grating, the optical architecture enables us to drive each frequency f_k shifted by kPRF towards each pixel i of the SLMs'. The microwave carrier f_a and the frequency spectrum of the radar f_s are respectively transposed on the optical carrier by the Bragg cell and the moving grating. Figure 5 presents the complete optical architecture of the proposed arbitrary waveform generator.

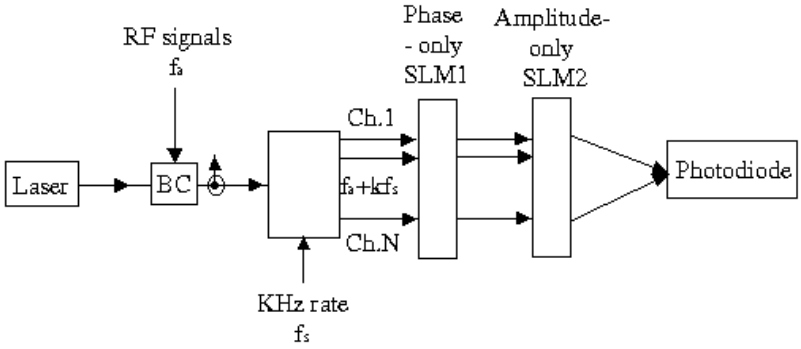

Figure 5: Complete optical architecture of the proposed arbitrary waveform generator

A proof of concept is experimentally demonstrated using two computer-controlled SLMs of 4x4 pixels. Each pixel is 3.5x3.5mm^2 and exhibits an optical transmission of 95%. It permits to explore amplitude and phase ranges of 30dB and 2π rad respectively. The Bragg cell central frequency is 2GHz with bandwidth of 2GHz. Our aim was to control independently the features of the two frequencies (phase and amplitude). We used two RF generators and a combiner to sum the two RF signals. Owing to an appropriate set-up, the two diffracted beams at the output of the Bragg cell were made to travel in parallel through two different pixels of the 4x4 pixel SLM. The signal detected at the photodiode was composed of a carrier at frequency $(f_1+f_2)/2$ and an envelope at frequency $(f_1-f_2)/2$. By switching off independently pixel 1 or pixel 2 of the amplitude-only SLM, we were able to attenuate of 25dB either the spectrum line 1 or the spectrum line 2 of a dual-frequency signal (Δf=45MHz).
We also demonstrated the control of a pulse train (pulsewidth T=12ns and interpulse period PRI=77ns, PRF=13MHz). Because the pixel sizes of the SLM we used were quite large (3.5x3.5mm^2), the signal modulation could only be realized with two pixels. Figure 9 shows the sinc(u) envelope when the light beams travel through the two pixels. The spectrum lines are spaced of 13MHz. We first verified that switching off all the pixels causes all the spectrum lines to disappear (top of Figure 6), next, that switching off one pixel causes a part of the spectrum to disappear (bottom of Figure 6). For example, the extinction of pixel 1 leads to the attenuation of the left lines with respect to the central line. And the extinction of pixel 2 leads to the attenuation of the right lines. The attenuation of the lines was about 25dB, which is close to the SLM maximum attenuation.

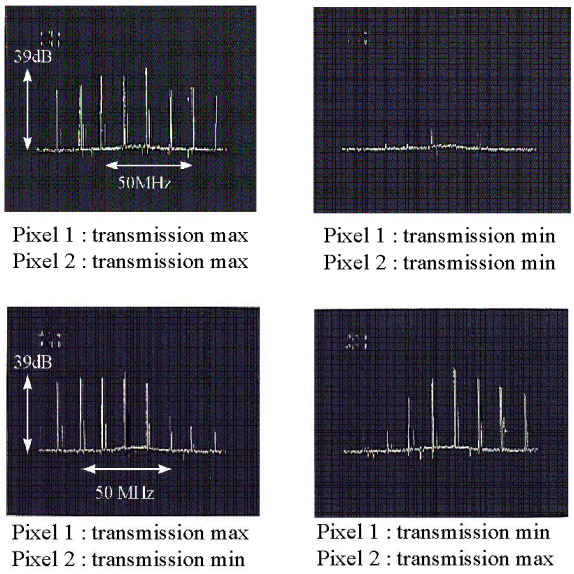

Figure 6: Amplitude modulation in case of a pulse train (T=12ns, PRI=77ns).

We have finally demonstrated with the experimental set-up of Figure 5 that the moving grating controlled by a piezoelectric material permits us to increase the resolution of the architecture. A 1µm-step grating was used that combine the transmitted zero-order beam with the 1-order and 2-order beams. The periodic electrical signal was at 10kHz. The beating signals were detected at frequencies 10kHz for the 1-order beam and 20kHz for the 2-order beam.

3. Spectrum analysis and correlation

Acousto-optic spectrum analyser

The operating principle of an acousto-optic spectrum analyser is presented on figure 10

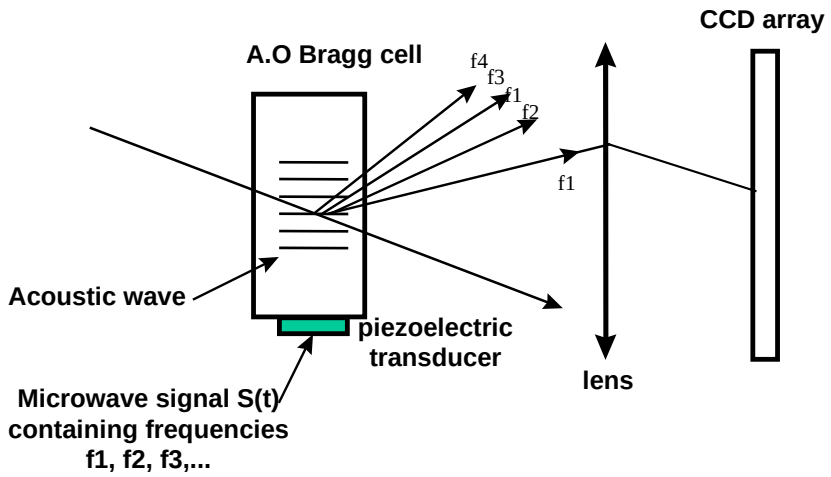

Figure 8.10 - Acousto-optic spectrum analyser

The microwave signal to be analysed is applied onto a piezoelectric transducer, glued on an elasto-optic material. In such a material, the refractive index is changed according to the locally applied pressure. Through the piezo-transducer a pressure wave (i.e an acoustic wave) is generated . It results in a travelling refractive index grating. Since this mechanism is a linear one, each frequency contained in the applied signal S(t) will results in a corresponding grating with a period $\Lambda_i=v/f_i$ (where v is the speed of the acoustic wave). In fact, each diffractive grating is a "frozen image" of the microwave signal. When a collimated laser beam travels through these superposed gratings, each grating will diffract the light in a given direction corresponding to the period Λ_i, with an efficiency proportional to power of frequency f_i. Those diffracted beams are then collected and "Fourier transformed" through the use of an optical lens on a CCD array. An image of the microwave spectrum is then displayed onto the CCD.

Typical performances of such systems are shown in the following list:

- central frequency F: typ. 1 to 2 GHz (up to 9 GHz, University Saratov)
  - mainly limited by the piezo transducer thickness (typ. few µm) and the acoustic absorption
- frequency bandwidth DF: 0.5 to 1 GHz (up to 3 GHz)
  - mainly limited by the acousto-optic/Bragg conditions
- frequency resolution : 1 to 3 MHz
  - linked to the central frequency and the time.frequency product
- diffraction efficiency: typ. 10% / W RF
  - maximum microwave power mainly limited by the piezo transducer thickness
- linear dynamic range: typ. 30 - 40 dB
  - mainly limited by the CCD array (acoustic linear dynamic range typ. 70 dB)

One of the main interest of the acousto-optic spectrum analysis was its wide instantaneous bandwidth and its low power consumption. Now a day, purely digital spectrum analysis can bring quite the same performances, taking advantage in addition of an extended compatibility with other digital processing functions.
According to the dynamic range limitation and the long access time (about 100 µs, linked to CCD response time and to the necessary propagation of the acoustic wave in the crystal) practical use of acouto-optic microwave spectrum anlyser is limited to radioastronomy (both ground based and spaceborne).

Frequency filtering

The combination of acousto-optic components with spatial light modulators permits the implementation of processing functions such as adaptive frequency filtering. The operating principle of such an architecture is shown on figure 11.

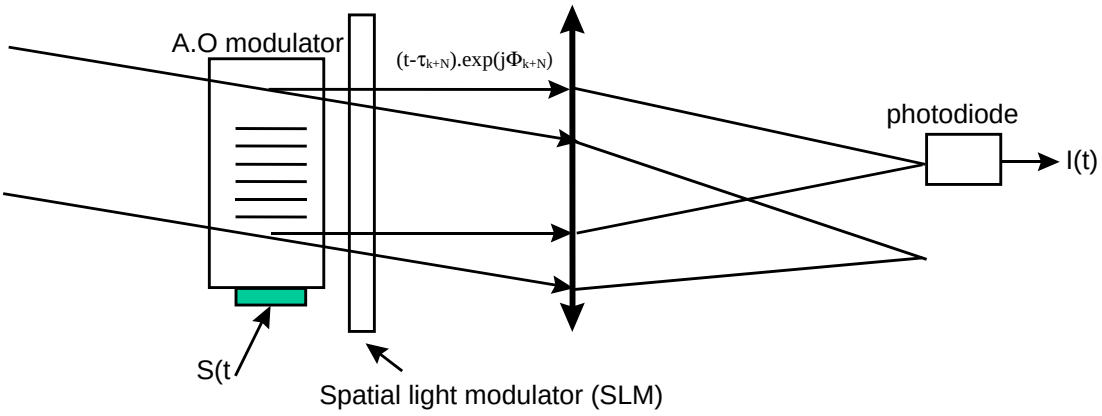

Figure 8.11 - Adaptive frequency filtering architecture

According to the spatial resolution of the SLM, this last one is arranged close to the Bragg cell or in the Fourier plane of the lens. Considering resolutions of about 100x100 pixels (obtained for example with liquid crystal SLMs), most of the experimental demonstrations were performed with the « SLM close to the Bragg cell » architecture.

The collimated laser beam diffracts off an acoustic replica of the electrical signal S(t) applied on the piezoelectric transducer. According to the propagation of the acoustic wave, each portion of the laser beam, along the acoustic column, will diffract with an efficiency proportional to the amplitude of the sample $S(t-\tau_i)$. Through the use of the SLM, it is possible to control the phase of the optical carrier of the microwave signal, for each sample. These sample are then coherently summed onto a high speed photodiode.
Considering the capability offered by 2D SLMs to provide reconfigurable complex phase law, sophisticated programmable filters can be performed with this type of architecture.
Typical parameters of experimental demonstrations of adaptive filtering are listed below :

- central frequency: 140 MHz
- max. duration of the signal: 2 µs
- frequency bandwidth: 90 MHz
- 256 pixels SLMs with phase delays up to 7π

Main limitations of this approach are :
- central frequency of about few hundreds MHz. In order to use high efficiency A .O Bragg cells, providing in addition acoustic column lengths corresponding to time of propagation of about few µs, it is necessary to operate with frequency lower than 300 MHz

– response time of liquid crystal SLMs of few tenth of milliseconds. It corresponds to the time of reconfiguration of the filter.

With this kind of performances, once again, now a day corresponding digital architectures offer better and more exploitable performances. But an increase of the operating frequency up to 1 GHz (potentially possible with low loss materials) combined for instance with SLMs response as low as 0.1µs would provide performances largely exceeding those of numerical filters.

Acousto-optic correlators

The operating principle is described on figure 12

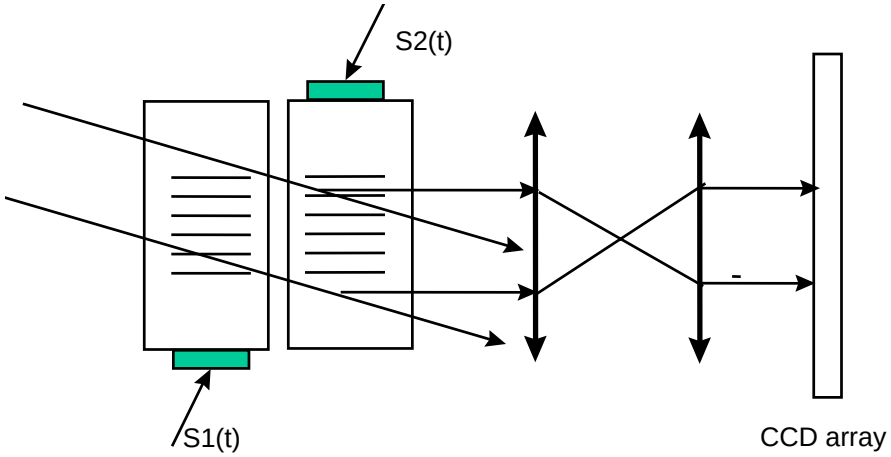

Figure 8.12 - Acousto-optic correlator principle

The microwave signals $S_1(t)$ and $S_2(t)$ are respectively applied on two acousto-optic Bragg cells, in which the acoustic wave propagate in opposite directions. In this case, on each pixel of the CCD, the detected, and potentially integrated, amount of light will be propotional to $S_1(t).S_2(t-\tau_i)$.

Another way to implement the same function would be to use the following architecture.

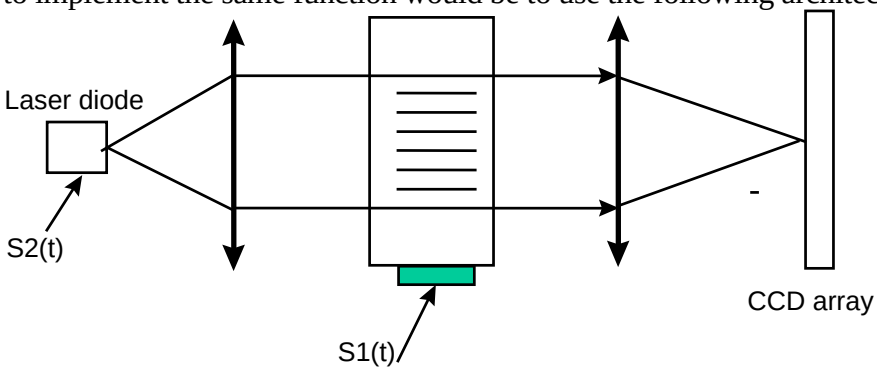

In this case the first A.O cell is replaced by a modulated (directly or externally) laser source which is fed with signal $S_1(t)$.

In both cases the correlation function of the two signals appear as a spatially varying function along the CCD array.

Main advantage of this type of correlator is to permit the analysis of long microwave pulses (up to few hundreds of milliseconds). Most of the practical implementations are thus devoted to radioastronomy applications with the following typical performances :

- central frequency: 100 MHz
- frequency bandwidth: 10 MHz
- time of integration : 10 ms

Time of integration up to 100 ms - 1s (corresponding to time.frequency products and compression coefficients of 10^6 = 10 MHz x 100 ms) can be obtained through the association of a CCD array with a digital memory.

4. REFERENCES

1. D. Norton, S. Johns, C. Keefer and R. Soref, "Tunable microwave filtering using high dispersion fiber time delays", *IEEE Photon. Tech. Lett*., vol 6, pp. 831-832, 1994.
2. M.Y. Frankel and R.D. Esman, "Fiber-optic tunable transversal filter", *IEEE Photon. Tech. Lett*., vol 7, pp. 191-193, 1995.
3. D. Dolfi et al, "Optical architectures for programmable filtering and correlation of microwave signals", *IEEE Trans microwave Theory Tech.* Vol 45, pp. 1467-1472, 1997.
4. .P. Foord, P.A. Davies and P.A. Greenhalgh, "Synthesis of microwave and millimetre-wave filters using optical spectrum-slicing", *Electron. Lett*., vol 32, pp. 390-391, 1996.
5. J. Capmany, D. Pastor and B. Ortega, "Fibre-optic microwave and millimetre wave filter with high density sampling and very high sidelobe supression using subnanometre optical spectrum slicing", *Electronics Letters*, 1999, pp. 494-496.
6. J. Capmany, J. Cascón, D. Pastor y B. Ortega, "Reconfigurable fiber-optic delay line filters incorporating electrooptic and electroabsorption modulators", *IEEE Photonics Technology Letters*, 1999, pp. 1174-1176
7. G.A. Ball, W.H. Glenn and W.W. Morey, "Programmable fiber optic delay line", *IEEE Photon. Technol. Lett*., vol 6, pp. 741-743, 1994.
8. Molony, C. Edge and I. Bennion, "Fibre grating time delay for phased array antennas", *Electron. Lett.*, vol 31, pp. 1485-1486, 1995.
9. D.B. Hunter and R.A. Minasian, "Reflectivity tapped fibre-optic transversal filter using in-fibre Bragg gratings", *Electron Lett*., vol 31, pp. 1010-1012, 1995.
10. D.B. Hunter and R.A. Minasian, "Tunable transversal filter based on chirped gratings", *Electron. Lett*., vol 31, pp. 2205-2207, 1995.
11. D.B. Hunter and R.A. Minasian, "Microwave optical filters using in-fiber Bragg grating arrays", *IEEE Microwave and Guided Wave Lett*., vol 6, pp. 103-105, 1996.
12. D.B. Hunter and R.A. Minasian, "Photonic signal processing of microwave signals using active-fiber Bragg-grating-pair structure", *IEEE Trans. Microwave Theory and Techn*, vol 8, pp. 1463-1466, 1997.
13. J.L. Cruz, B. Ortega, M.V. Andres, B. Gimeno, D. Pastor, J. Capmany and L. Dong, "Chirped fibre Bragg gratings for phased array antennas", *Electron. Lett*., vol 33, pp. 545-546, 1997.
14. D.B. Hunter and R.A. Minasian, "Microwave optical filters based on fibre Bragg grating in a loop structure", *Proc OFC '97*, paper TH2-2, pp. 273-275.
15. D.B. Hunter and R.A. Minasian, "Microwave optical filters based on fibre Bragg grating in a loop structure", *Proc OFC '97*, paper TH2-2, pp. 273-275.

16. D.B. Hunter and R.A. Minasian, “Photonic signal processing of microwave signals using active-fiber Bragg-grating-pair structure”, *IEEE Trans. Microwave Theory and Techn*, vol 8, pp. 1463-1466, 1997.
17. S.C. Kim, et al, “Recirculating fiber delay line filter using a fiber Bragg grating”, *IEEE LEOS ’98 Digest*., pp. 328-329, 1998.
18. D. Pastor and J. Capmany, “Fiber optic tunable transversal filter using laser array and linearly chirped fibre grating”, *Electronics Letters*, 1998, pp. 1684-1685.
19. J. Capmany, D. Pastor and B. Ortega, “Experimental demonstration of tunability and transfer function reconfiguration in fibre-optic microwave filters composed of a linearly chirped fibre grating fed by a laser array”, *Electronics Letters*, 1998, pp.2262-2264
20. W. Zhang, J.A.R. Williams, L.A. Everall and I. Bennion, “Fibre-optic radio frequency notch filter with linear and continous tuning by using a chirped fibre grating”, *Electron. Lett*., vol 34, pp. 1770-1772.
21. W. Zhang, J.A.R. Williams, L.A. Everall and I. Bennion, “Tuneable radio frequency filtering using linearly chirped fibre grating”, *proc ECOC ’98*, pp. 611-612, 1998.
22. D.B. Hunter and R.A. Minasian, “Tunable microwave fiber-optic bandpass filters”, *IEEE Photon. Technol. Lett*, vol 11, pp. 874-876, 1999.
23. N. You and R.A. Minasian, “Synthesis of WDM grating based optical microwave filter with arbitrary impulse respose”, *Int. Top. Meeting MWP ’99 Digest*, pp. 223-226, 1999.
24. N. You and R.A. Minasian, “A novel high-Q optical microwave processor using hybrid delay line filters”, *IEEE Trans. Microwave Theory Tech*., vol 47, pp. 1304-1308, 1999.
25. R. Minasian, “Photonic signal processing of high speed signals using fiber gratings”, *Int. Top. Meeting MWP ’99 Digest*, pp. 219-223, 1999.
26. W. Zhang, J.A.R. Williams, L.A. Everall and I. Bennion, “Tuneable radio frequency filtering using linearly chirped fibre grating”, *proc ECOC ’98*, pp. 611-612, 1998.
27. K.J. Williams, J.L. Dexter and R.D. Esman, “Photonic microwave signal processing”, *Int. Top. Meeting MWP ’98 Digest*, pp. 187-189. 1998.
28. W. Zhang, J.A.R. Williams and I. Bennion, “Recirculating fiber-optic notch filter employing fiber gratings”, *IEEE Photon. Technol. Lett*., vol 11, pp. 836-838, 1999.
29. J. Capmany, D. Pastor and B. Ortega, “Efficient sidelobe supression by source power apodisation on fibre-optic microwave filters composed of linearly chirped fibre grating fed by laser array”, *Electronics Letters*, 1999, pp. 640-642.
30. J. Capmany, D. Pastor, B. Ortega, “Applications of fibre Bragg Gratings to Microwave Photonics”, *IEE Colloquium on fibre gratings 1999*, Birmingham, UK.
31. J. Capmany, D. Pastor and B. Ortega, “New and flexible fiber-optic delay line filters using chirped Bragg gratings and laser arrays”, *IEEE Trans. Microwave Theory Tech*., vol 47, pp. 1321-1327, 1999.
32. P.J. Mathews and P.D. Biernacki, “Photonic signal processing for microwave applications”, *IEEE MTT-S Digest*, paper WE1B-1, pp. 877-880, 1999.
33. D. Pastor, J. Capmany and B. Ortega, “Experimental demonstration of parallel fiber-optic-based RF filtering using WDM technique”, *IEEE Photonics Technology Letters*, 2000, pp. 77-79.
34. R.A. Minasian, “Photonic signal processing of high-speed signals using fiber gratings”, *Opt. Fib. Tech*., vol 6, pp. 91-108, 2000.
35. W. Zhang, J.A.R. Williams and I. Bennion, “Optical fibre delay line filter free of limitation imposed by optical coherence”, *Electron.Lett*., vol 35, pp. 2133-2134, 1999.
36. Ho-Quoc, S. Tedjini and A. Hilt, “Optical polarization effect in discrete time fiber-optic structures for microwave signal processing”, *IEEE MTT- Symposium Digest*, pp. 907-910, 1996.

37. F. Coppinger, S. Yegnanarayanan, P.D. Trinh and B. Jalali, “All-optical incoherent negative taps for photonic signal processing”, *Electron. Lett*., vol 33, pp. 973-975, 1995.
38. M. Tur and B. Moslehi, “Laser phase noise effects in fiber-optic signal processors with recirculating loops”, *Opt. Lett*., vol 8, pp. 229-231, 1983.
39. M. Tue, B. Moslehi and J.W. Goodman, “Theory of laser phase noise in recirculating fiber optic delay lines”, *IEEE J. Lightwave Technol*, vol 3, pp. 20-30, 1985.
40. M. Tur and A.Arie, “Phase induced intensity noise in concatenated fiber-optic delay lines”, *IEEE J. Lightwave Technol.*, vol 6, pp. 120-130, 1988.
41. B. Moslehi, “Analysis of optical phase noise in fiber-optic systems employing a laser source with arbitrary coherence time”, *IEEE J. Lightwave Technol*., vol 4, pp. 1334-1351, 1986.
42. J.T. Kringlebotn and K. Blotekjaer, “Noise analysis of an amplified fiber-optic recirculating delay line”, *IEEE J. Lightwave Tech*

Opto-Microwave Signal Processing: Up and Down Conversion Techniques

Tibor Berceli
Márk Csörnyei
Budapest University of Technology & Economics
1111 Budapest
Goldmann György tér 3, Hungary

1. Introduction

This application note introduces the concepts of opto-microwave signal processing used in several communication systems today. Emphasis is placed on optical-microwave up- and down conversion techniques.

In today's and future mobile- or local area networks (LAN) there is a need for optically supported network technologies with a few sophisticated central stations serving a big number of quite simple and cheap optical terminals, such as small base-stations in millimeter-wave optical-wireless local multipoint distribution systems (LMDS), computer or CATV networks. The right answer for all of these challenges is the subcarrier modulated optical transmission.

The subcarrier optical data transmission method offers several advantages over the generally applied TDMA (time division multiple access) system. In a TDMA system the transmitters of the stations are operated on a time sharing basis. In the receivers direct optical detection is used. In a high bit rate data communications network a digital signal processing system with complete capacity should be applied both in the transmitters and in the receivers. That is a big disadvantage which limits the future enhancement of the network capacity.
In case of the subcarrier type optical data communications the transmission capacity of the network can be increased by applying new subcarriers, and thus the digital signal processing system can be kept with unchanged bit rate. The transmitters are used in a continuous operation and in the receivers a heterodyne type detection can be applied which provides a lower noise figure. The continuous operation of the transmitters makes possible several connections working at the same time.
The present method used for reception is rather complex and therefore somewhat troublesome because it applies a tuned filter. Utilizing an opto-microwave mixer there is no need for a tuned filter and thus it is suitable for monolithic integration.

1.1. SUBCARRIER TYPE DATA COMMUNICATIONS

The principle of the subcarrier type data communications is presented first. Each transmitter has its own subcarrier frequency (or frequencies); however, the receivers are tuned to make connection with any transmitter. Thus there is no need for switching in the network because the requested connection is established by tuning the receiver to the wanted subcarrier frequency.
To establish a connection between the stations a signaling channel and a central control unit are applied [1], [4]. An individual subcarrier serves for that purpose applying on/off modulation with a low bit rate and time sharing for the transmitters and receivers. A control unit has a photodetector for the reception of the calling signals coming from the transmitters. The control unit emits ringing signals and control signals for the receivers. The control signal contains the information which subcarrier frequency has to be received by the specific receiver.
The block diagram of the transmitter is shown in Fig. 1. The information signal is modulating the subcarrier frequency. The signaling information is transmitted in a similar way. The subcarrier frequency of the signaling channel is the same for all of the transmitters and receivers. That common signaling channel is used on a time sharing basis. However, the subcarrier frequencies of the information channels are different.

Paper presented at the RTO SET Lecture Series on "Optics Microwave Interactions", held in Jouy en Josas, France, 2-3 September 2002; Duisburg, Germany, 5-6 September 2002; Budapest, Hungary, 9-10 September 2002, and published in RTO-EN-028.

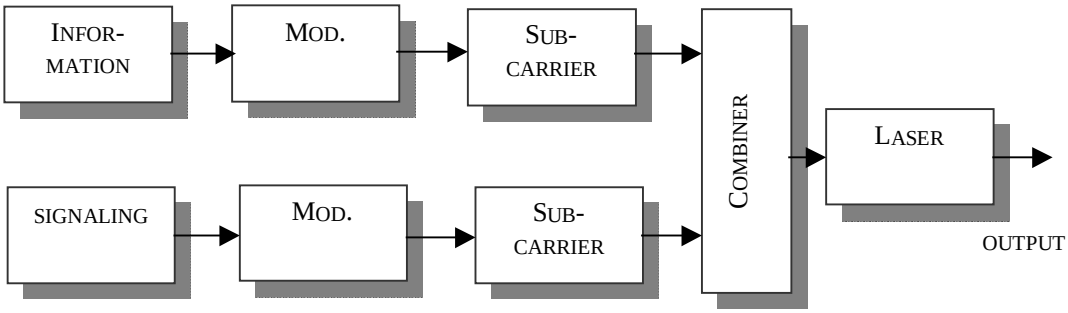

Fig. 1 Block diagram of the transmitter

The block diagram of the receivers is shown in Fig. 2. The received optical signal is detected by a photodiode and the required channel can be selected by a tuned filter. A tuned oscillator is used for further down-conversion. The calling and controlling signals are received in the signaling channel which is transmitted via a fixed frequency subcarrier, and therefore a fixed filter is used in the signaling channel.
As Fig. 2 shows in the conventional direct detection optical receivers there is a need for a tuned filter which makes the high quality realization and MMIC integration quite difficult. Using an opto-microwave mixer in place of the photodetector heterodyne reception scheme can be obtained.

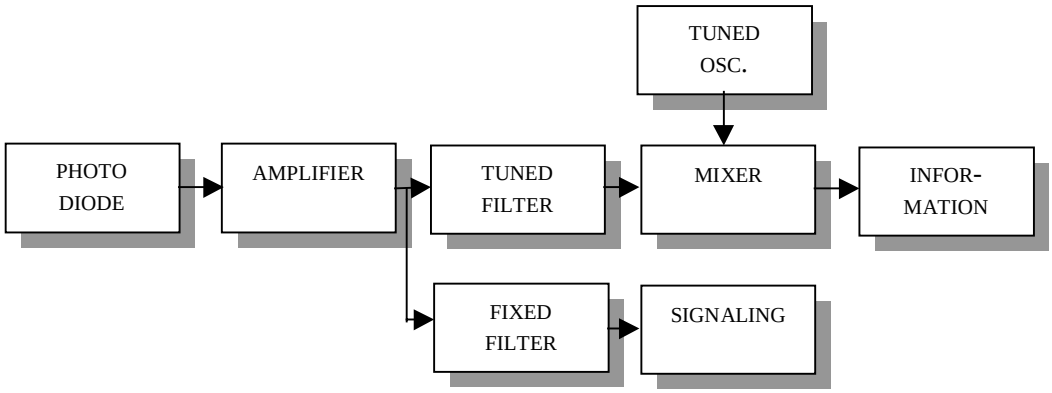

Fig. 2 Block diagram of the receiver

The block diagram of the new receiver is shown in Fig. 3. Instead of a detecting photodiode a mixing device (FET field effect transistor, HEMT high electron mobility transistor, UMZ unbalanced Mach-Zehnder modulator, PIN diode) is used for combined optical-microwave mixing. In such mixers the signal of the tuned local oscillator and the subcarrier of the modulated light are mixed with each other by the device nonlinearities.
The microwave local oscillator is tuned to an off-set frequency of the subcarrier to be received. Thus heterodyne reception is obtained. The unwanted other subcarriers are suppressed by filtering. As seen the new arrangement of Fig. 3 is simpler than the more conventional one of Fig. 2. In the new arrangement there is no tuned filter which is a big advantage.

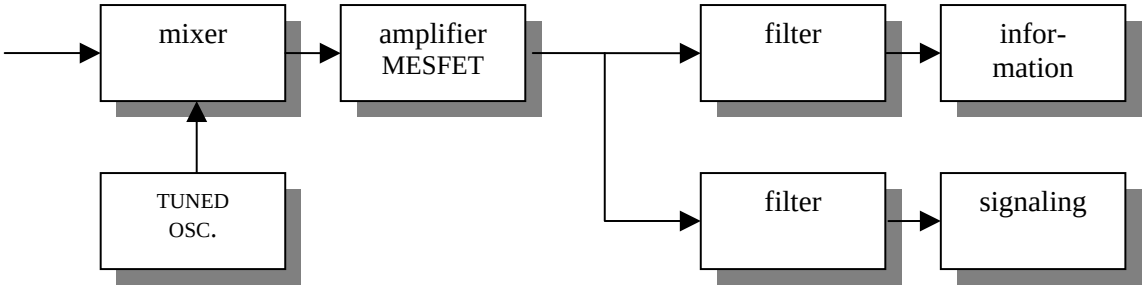

Fig. 3 Block diagram of the receiver with opto-microwave mixer

2. Opto-microwave mixing by MESFETs

This chapter presented here concerns the mixing of a microwave signal with a modulated optical signal in a MESFET. A brief theoretical analysis of the mixing mechanism is given in terms of the input signal parameters and device characteristics. Experimental results for the IF response of the MESFET as a function of RF frequency, incident optical power, optical modulation depth and gate bias voltage are shown.

The basic motivation for the research presented here is the chip-level integration of microwave and photonic components. It is demonstrated that a microwave signal can be mixed with a modulated optical signal in a MESFET, the most commonly used device in MMIC's, for the up- and down-conversion of microwave signals.

2.1. PHOTORESPONSE OF THE MESFET

The following discussion is based on recent work by Malone and Paolella at.al. [1] and [3] related to the internal photovoltaic effect in the MESFET, which gives rise to photoresponse in the device. In the internal photovoltaic effect, illustrated in Fig. 4, the absorbed photons modulate the channel-substrate barrier, thereby modulating the channel height. In effect, the light acts as an "optical gate." We take advantage of this effect to mix an optical signal with a microwave signal in the device.

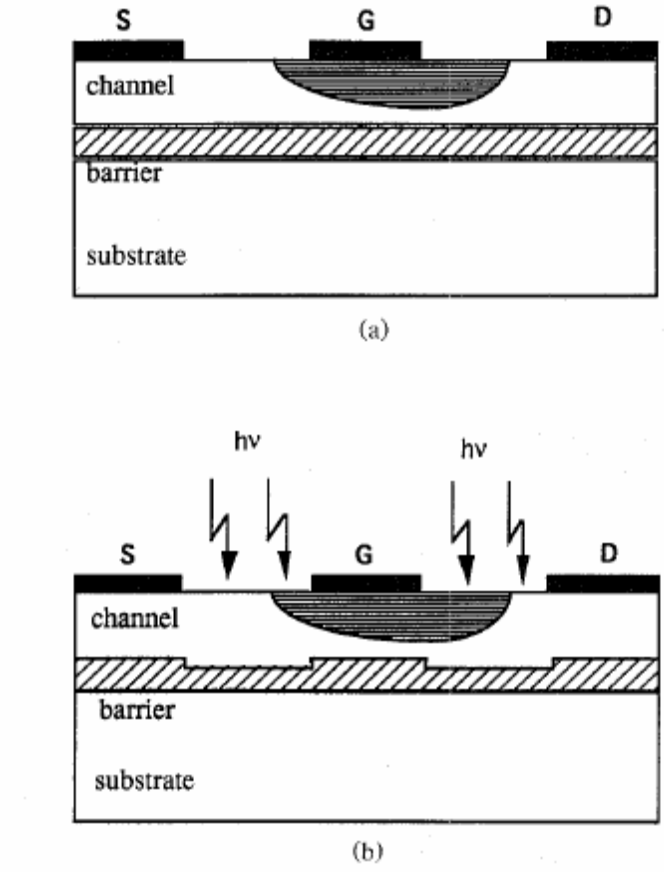

Fig. 4 Internal photovoltaic effect in a GaAs MESFET. The difference in doping level between the epi and substrate layers produces a potential barrier in the standard MESFET, as shown in (a). When illuminated the potential barrier is reduced, as depicted in (b), thereby increasing the channel height (optical gate).

The drain-source current photoresponse for a MESFET was measured as a function of gate-source voltage. The optical signal can be derived from medium power laser operating at 850nm. An optical attenuator controls the power to the MESFET. The optical signal is routed to the MESFET via a cleaved output fiber positioned over the MESFET.
The measured results are presented in Fig. 5. The drain current photoresponse is determined by the measurement of the drain current in the dark and the drain current under illumination, and is expressed as

$$I_{ph} = I_d(\text{illuminated}) - I_d(\text{dark}) \tag{1}$$

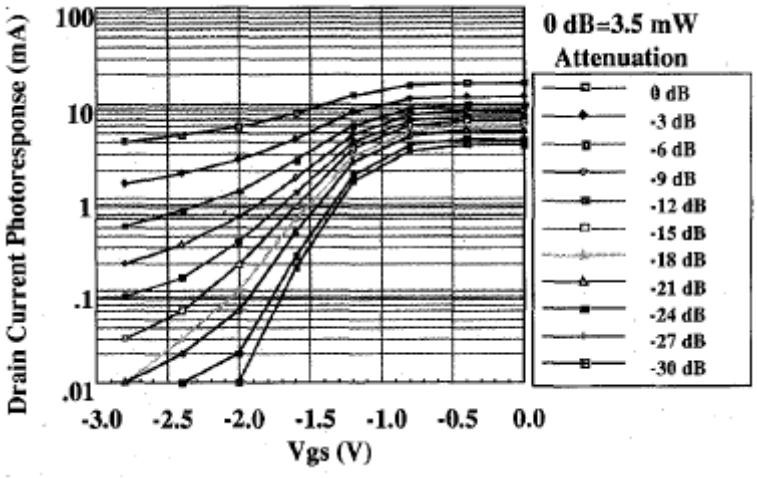

Fig. 5 Drain current photoresponse of the MESFET as a function of gate-source voltage

The photoresponse of the drain current is due to the internal photovoltaic effect and is given as

$$I_{ph} = g_m V_{ph} \tag{2}$$

where g_m is the transconductance of the device. V_{ph} is the optically induced photovoltage[1],[14], which can be written approximately as

$$V_{ph} \approx c_1(L_0)P + c_1 p(L_0)^{(p-1)}(L - L_0) + \ldots \tag{3}$$

where L is the optical intensity, and L_0 is the optical intensity at the operation point. The higher power terms are omitted. The coefficients c_1 and p depend on the specific MESFET. To obtain the coefficients, the photovoltage was measured as a function of optical intensity. The measured relationship was approximated using a curve fitting method.
In Fig. 5 the maximum optical intensity of 3.5mW is used as the 0dB reference, and for each successive curve the intensity is attenuated by 3dB. Under small signal conditions the photoresponse follows the transconductance (g_m) of the device, which is essentially constant with gate bias from 0 to -0.5V. The photoresponse is dominated by the product of the internal photovoltage and g_m when no external resistance is connected to the gate (i.e., R_g=0). As optical intensity is increased, there are contributions to the photoresponse from the substrate photocurrent and the photoconductive current in the channel. The internal photovoltage which is an exponential function will be large resulting in a significant photoresponse well beyond the pinch-off.

2.2. MIXING MECHANISM IN THE MESFET

The mixing effect is the result of the device nonlinearities. In general all elements of the internal equivalent circuit exhibit some nonlinearity, however the dominating factor is the nonlinearity of the drain-source current versus gate-source voltage characteristics. A small effect is obtained from the nonlinear gate-source capacitance as well.

The drain-source current is expressed as a power series of the gate-source voltage at a constant drain-source voltage

$$I_d = I_{db} + a_1 V_{gl} + a_2 (V_{gl})^2 + a_3 (V_{gl})^3 + \ldots \quad (4)$$

where a_1,a_2 and a_3 are coefficients that depend on the drain-source voltage and I_{db} is the dc quiescent point. V_{gl} is the gate-source voltage under illumination.

The effect of illumination on the drain-source current is taken into account by introducing the optically induced photovoltage V_{ph} which is dependent in the light intensity. Thus in case of illumination the gate-source voltage is the sum of the electrically applied voltage and the photovoltage

$$V_{gl} = V_g + V_{ph}. \quad (5)$$

The lightwave illuminating the device is modulated:

$$L = L_0 [1 + m \cos(\omega_1 t)] \quad (6)$$

where L_0 is the average optical intensity, and ω_1 and m are the modulation frequency and depth, respectively.

A microwave signal is simultaneously applied across the gate and source

$$V_g = V_{s0} \cos(\omega_2 t) + V_{gb} \quad (7)$$

where V_{s0} is the amplitude, ω_2 is the angular frequency of the microwave signal, t is the time, and V_{gb} is the biasing gate-source voltage.

Thus the gate-source voltage under optical illumination is the sum of the electrically and optically induced voltages

$$V_{gl} = V_{gb} + V_{ph0} \cos(\omega_1 t) + V_{s0} \cos(\omega_2 t) \quad (8)$$

where V_{ph0} is the amplitude of the photovoltage

$$V_{ph0} = c_1 pm(L_0) P. \quad (9)$$

The mixing product in the drain-source current at the intermediate frequency ω_2-ω_1 is obtained by substituting (5) into (4)

$$I_{dmix} = a_2 V_{ph0} V_{s0}. \quad (10)$$

For this result we assume that the second order nonlinear term of (4) is much larger than the higher order terms (i.e. small-signal case). This simplified theoretical derivation shows the dependence of the mixing product in the drain-source current on all the parameters of the microwave input V_{s0}, optical input L_0, and m, as well as the device characteristics, a_2, c_1, and p.

The other nonlinearities of the device can also influence the mixing product; however, their contribution is small. Nevertheless, some effect is obtained from the nonlinearity of the gate-source capacitance. The two signals, i.e. the electrically and the optically induced signals are mixed in the nonlinear gate-source capacitance and then they are amplified due to the transconductance of the device. The capacitive mixing product in the drain-source current is expressed as

$$I_{dnux/cap} = \alpha c_c V_{s0} V_{ph0} / 2 \quad (11)$$

where α is a coefficient presenting the part of the optically induced voltage V_{ph} which effects the gate-source capacitance, and $c_c = \partial C_{gs} / \partial V_g$ being the derivative of the gate-source capacitance with respect to the gate-source voltage. The parameter c_c, represents the part of the photovoltage which influences the gate-to-source capacitance. That influence was measured and a curve fitting method was used to obtain c_c. The parameter α was estimated based on the construction of the FET used. The mixing products in the drain-source current are presented in Fig. 6 based on the measurements performed recently to determine the elements of the MESFET under optical illumination [1]. In Fig. 6 the conversion ratio is plotted with and without capacitive mixing as a function of the gate-source voltage. The conversion ratio is defined as

$$Cr = I_{dmix} / V_{s0} V_{ph0.} \quad (12)$$

As seen in Fig. 6 the contribution of the nonlinear gate-source capacitance is quite small. Some noticeable effect is only observed around the minimum conversion ratio where the drain-source current nonlinearity produces a small mixing product.

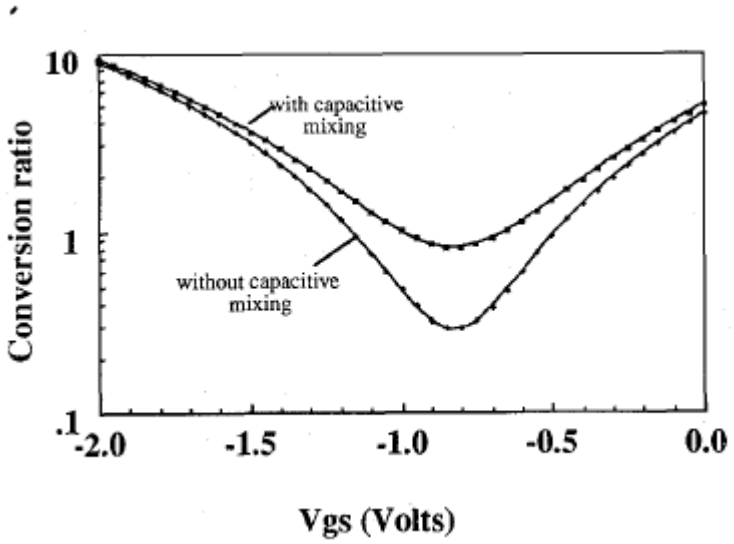

Fig. 6 Conversion ratio as a function of the gate-source voltage with and without capacitive mixing

2.3. COMPARISON OF "DIRECT" AND "INDIRECT" MIXING

There are two basic experimental setups concerning the MESFET as an O/E up- or down-converting front-end in the optical receiver. In an "indirect" mixing configuration (Fig. 7), the MESFET serves as a detector for the optical signal and the up- or down- conversion is performed in a conventional Schottky barrier mixer. However, by taking advantage of the inherent nonlinearities of the MESFET, both detection and frequency conversion of the modulated optical signal can be achieved in the device. This direct mixing approach, shown in Fig.8, is in the focus of this note.

In both of the setups of Fig. 7 and 8 an 850nm wavelength laser can be used. This wavelength is defined by the photosensitivity of the GaAs. The light is directly modulated by the RF Source 1 and positioned on the gate fingers of the MESFET. In case of commonly used microwave transistors, the device should operate with a reverse bias, for example with 0.5 volt at the gate and a drain-to-source voltage of 2 volts. As shown in eq. 9 and 10, the IF or the upconverted term of the drain current is dependent on the optical modulation depth m.

For the indirect mixing configuration, shown in Fig. 7, the MESFET was used as an optical detector. The detected signal from the MESFET was mixed with the signal from RF Source 2 in an additional mixer. As a baseline of comparison, indirect mixing can also be accomplished with a PIN photodetector in place of the MESFET (the conventional optical detection followed by microwave mixing).

For the direct mixing configuration, in addition to the optical input, a signal from RF Source 2 was applied to the gate of the device and the IF output was measured at the drain using a spectrum analyzer with an appropriate resolution.

2.4. EXPERIMENTAL MIXING RESULTS

As an example there are some experimental mixing results for direct mixing with MESFET as an opto-microwave mixer and for indirect mixing accomplished with p-i-n photodetector and a Schottky barrier mixer. The MESFET in the example [1] is an ITT GTC213-1 with four 75μm wide gate fingers, a gate length of 0.8μm and a dopant concentration of $3x10^{17}$ cm^{-3}. The device was operated with a reverse bias. For the direct mixing approach, the signal from an 850nm wavelength laser with an 8GHz bandwidth was directly modulated by an RF source and conveyed to the MESFET by an optical fiber. To maximize the IF response, 100% modulation depth was used on the laser, which has an average optical output power of 1.8mW.

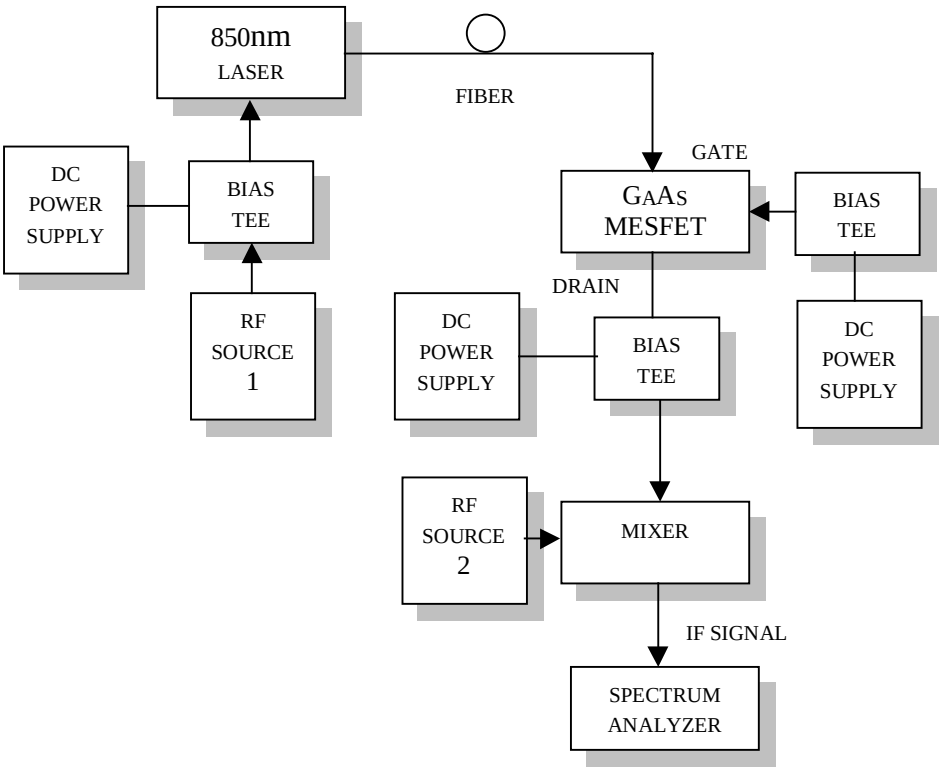

Fig. 7 Indirect mixing configuration

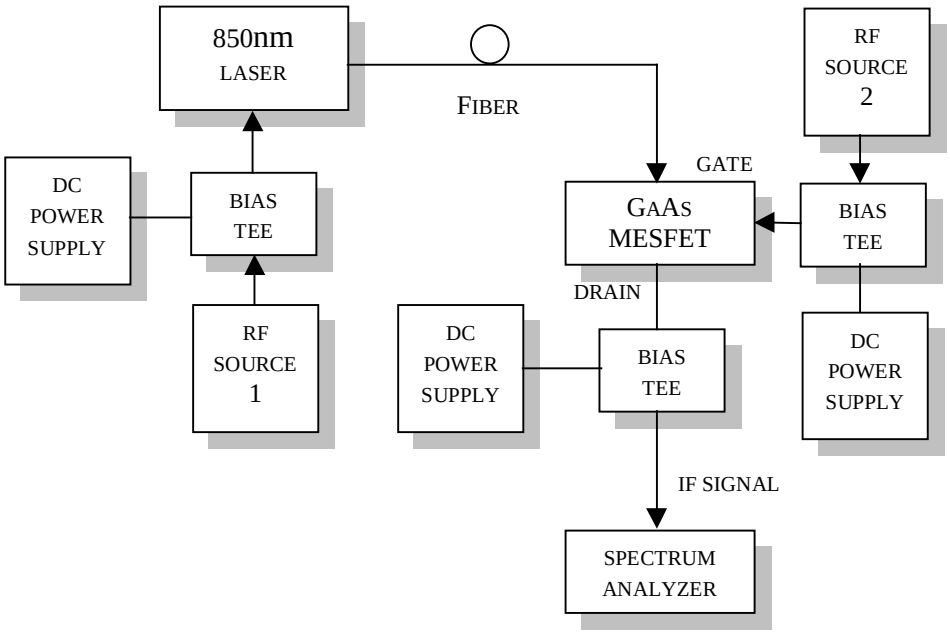

Fig. 8. Direct mixing configuration

The results of optical mixing with MESFET and the conventional detection and mixing with a p-i-n diode and an additional mixer are depicted in Fig. 9. The p-i-n photodetector had a 10GHz bandwidth, a responsivity of 35mA/mW and a diameter of 25μm. The p-i-n operates in this example with a reverse bias of 8V.

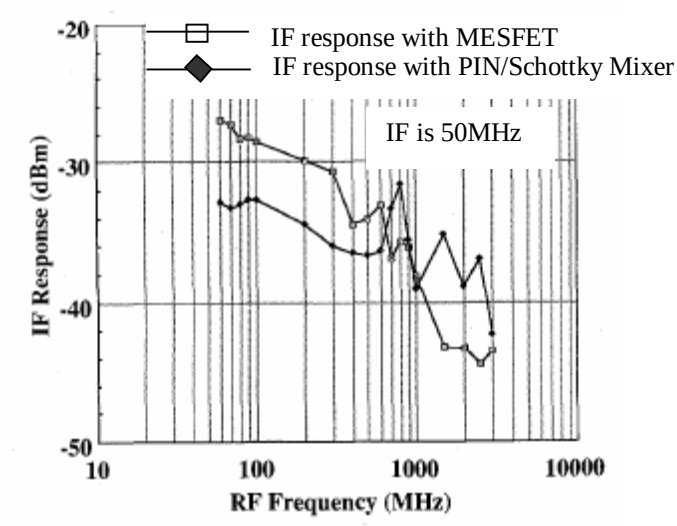

Fig. 9 IF response of the two mixing configurations

In that results of [1] IF response of the MESFET exceeds that of p-i-n/Schottky mixer combination up to an RF frequency of about 700MHz. The IF response emulates the photoresponse spectrum of the device with a conversion loss in range of 7-11dB. Under the same conditions the Schottky mixer had a conversion loss in the range of 4-10dB (See Fig.10). Clearly, as these results show, the MESFET can be used as mixer with optical and microwave inputs. Depending upon the particular application, the data may be an optical signal and the local oscillator an electrical signal, or vice versa.

The dependence of the IF response of the device on the average incident optical power and the RF drive power to the laser is shown in Fig. 11. The slope of the lines indicates that a 1dB decrease in optical power incident on the device translates into a 2dB decrease in the IF response, as expected with square law behavior. The figure also indicates that the IF response decreases linearly with RF drive power to the laser (modulation depth). The conversion response of the MESFET is also strongly dependent on the gate bias voltage. A plot of the IF response versus source-gate voltage at various RF frequencies is shown in Fig. 12. The IF response is maximized when the gate is reverse biased at around 0.5V, which is also the bias voltage at which the transconductance of the device is maximized. Larger reverse bias voltage on the gate decreases the IF response significantly due to a reduction in the gain. However, at bias voltages larger than 1.8V the IF response increases again. This is most likely due to the voltage dependence of the nonlinear coefficient a_2.

The system noise figure is presented in Fig. 13 as a function of the RF frequency. In the figure 3 curves are plotted: one for the p-i-n/Schottky mixer configuration and two for the MESFET with different bias voltages. The noise is significantly smaller with a bias voltage close to pinch-off because then the drain-source current is also smaller. As seen the system noise figure below 1000MHz is smaller in the case of the MESFET than with the p-i-n/Schottky mixer configuration if a bias voltage close to pinch-off is used. However, the system noise figure above 1000MHz is higher in the case of the MESFET compared to the p-i-n/Schottky mixer setup.

2.5. COMPARISON OF DYNAMIC PROPERTIES OF DETECTION AND MIXING, BY FET DEVICES

According to the detection measurements of Berceli et.al. [5] by FET devices, the detected signal exhibits a decay with increasing modulation frequency. The decay is relatively slow at low modulation frequencies. The measurement result is in accordance with the recently published theoretical and experimental investigations.

The decrease in the detected signal with increasing modulation frequency is due to the time constant of the barrier depletion region between the substrate and the epitaxial layer.

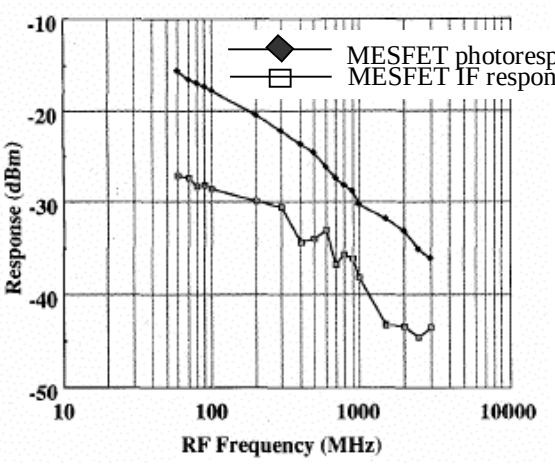

Fig. 10 Photo- and IF response of the MESFET

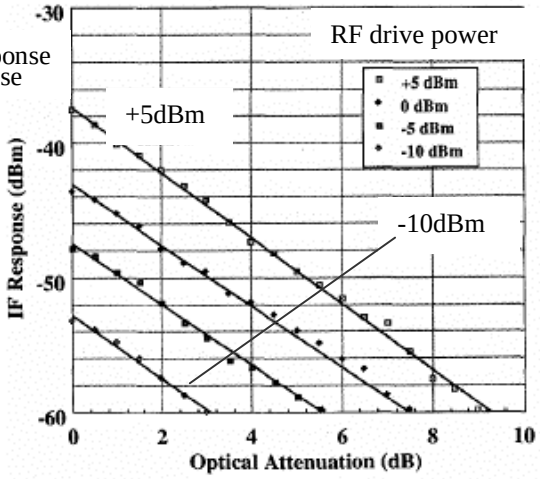

Fig. 11 IF response of the MESFET versus optical attenuation at various RF drive levels. The incedent optical power to the MESFET is 1.8mW.

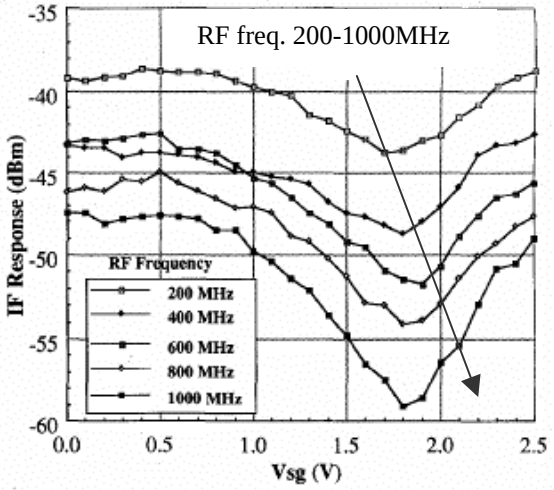

Fig. 12 IF response of the MESFET versus source-gate voltage

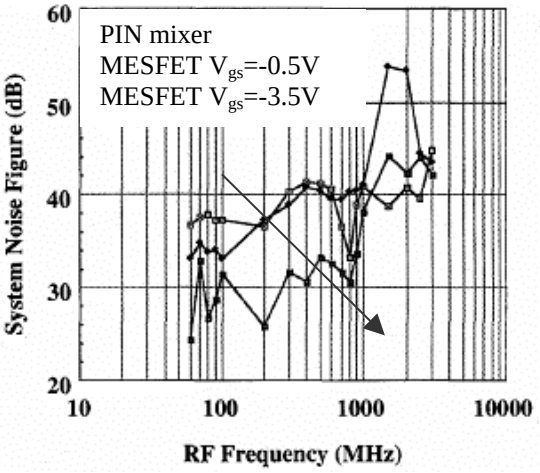

Fig. 13 System noise figure as a function of the RF frequency

The next question is whether the dynamic properties in the detection mode and in the conversion mode of operation are the same.
In the tests investigating the dynamic properties of opto-microwave mixing by FET's, both the optical and microwave gates are driven by signals. Between the gate and source a microwave signal is applied while the intensity modulated signal of a semiconductor laser diode is used to illuminate the active device. The frequency dependence is different, the decay in the converted signal is much higher at low modulation frequencies, and it is more pronounced with increasing modulation frequency compared to the frequency response of the detected signal.
Another significant deviation is that the decrease in the converted signal is proportional to modulation frequency, however, the decrease in the detected signal is developed slowly when the modulation frequency in increasing. The reason of the differences in the dynamic characteristics is the following.
In the detection mode of operation the optically generated charge carriers are contributing to the detected electric current in both depletion regions below the gate and between the substrate and the epitaxial layer by changing the height of the conductive channel. Beside that effect the charge carriers generated in the substrate are also participating in the detected current. Therefore, the frequency dependence of the detected signal is determined by the conductive channel and the substrate currents.
On the other hand, in the mixing mode of operation the contribution of the substrate current in the generation of the mixing product is negligible because in the substrate there is neither a nonlinear nor a parametric effect. The mixing products are created mainly in the conductive channel. This way their power level is somewhat lower and their frequency dependence is higher. There are two reasons for it: the time constant exhibited by the depletion region between the substrate and the epitaxial layer and optically induced substrate current which is increasing with the modulation frequency and doesn't contribute to the mixing effect.

2.6. SINGLE SIDEBAND OPTICAL-MICROWAVE MIXERS

As mentioned in section 2.2 the mixing product in the drain-source current at the difference of the input frequencies (ω_2-ω_1) is:

$$I_{dmix-} = a_2 V_{ph0} V_{x0} \tag{13}$$

The mixing product in the drain-source current at the sum of the input frequencies (ω_1+ω_2) is obtained as follows [4]:

$$I_{dmix+} = a_2 V_{ph0} V_{s0}^{*} \tag{14}$$

V_{s0} is the complex amplitude and V_{s0}^{*} is the conjugate of the complex amplitude of the microwave signal applied across the gate and source. V_{ph0} is the amplitude of the photovoltage.
Comparing these equations it can be seen that there is a phase difference between the mixing product current amplitudes I_{dmix-} and I_{dmix+} because of the conjugation of the microwave signal amplitude in the second case. That makes possible to construct a single sideband optical-microwave mixer arrangement if two mixers are applied in the two branches of a hybrid and 90° phase difference is established between the outputs of the hybrid driving the mixers by the microwave signal. Due to the conjugation of the microwave signal the mixers will provide 180° phase shift in the mixing product current amplitudes which makes possible their separation by another hybrid. A switch is used for choosing the right mixing product for further signal processing.
The principle of the single sideband optical-microwave mixer is presented in Fig. 14, [4].
For the subcarrier type signal reception an important requirement is the high suppression of the image frequency. This is achieved if the mixing products in the two branches are of equal amplitude with a 180° phase difference. However, both the amplitude and the phase of the mixing product are frequency dependent.

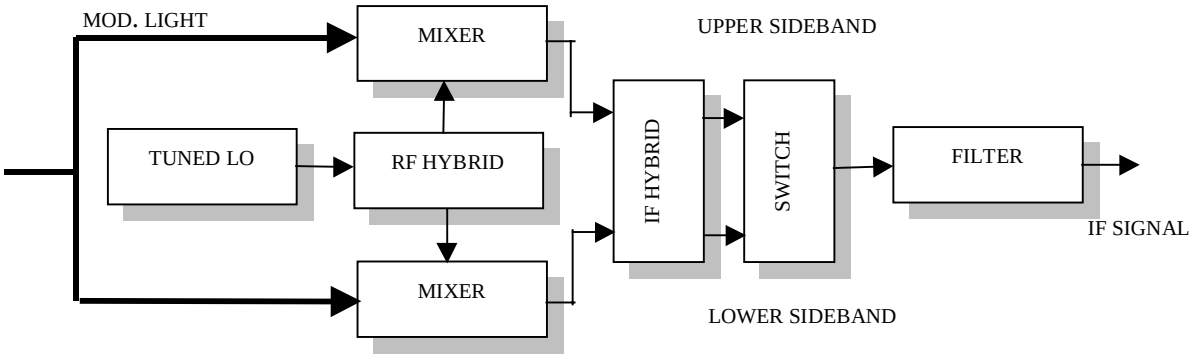

Fig. 14 Block diagram of the new single sideband optical-microwave mixer

3. Optical-microwave double mixing by PIN diodes

The commonly used optical receivers apply mainly photo-diodes to detect the optical intensity modulated signal. A relatively high sensitivity is achieved by properly matched transimpedance or distributed amplifiers.
In another method the modulated optical signal is mixed with a microwave signal in the photodiode producing an intermediate frequency signal. Thus, heterodyne type reception is feasible. However the mixing conversion has a higher loss compared to the direct detection.
In the double optical microwave mixing approach the conversion loss is much less than that of direct detection offering a significant improvement in the reception sensitivity. The mixing product is even further increased by resonance enhancement providing 20dB improvement in comparison to direct detection.

3.1. DOUBLE MIXING PRINCIPLE

This method of Berceli and Járó [7] utilizes simultaneously two effects: a direct and an indirect mixing of the modulated optical signal and the microwave local oscillator signal. For direct mixing the bias is chosen close to the zero voltage where the photo current is highly dependent on both the illumination intensity and applied voltage. Therefore the mixing product is high. At the same time a detection of the optical signal is also obtained which produces a detected signal in the base band. If this signal is reflected back to the photodiode it will also be mixed with the microwave local oscillator signal. Thus the output signal is the resultant of two mixing procedures: an optical-microwave and an electrical mixing (after optical detection).
The double mixing approach [7] is experimentally presented utilizing a 1A358 type CATV p-i-n photodiode. The setup of optical-microwave circuit is shown in Fig. 15.

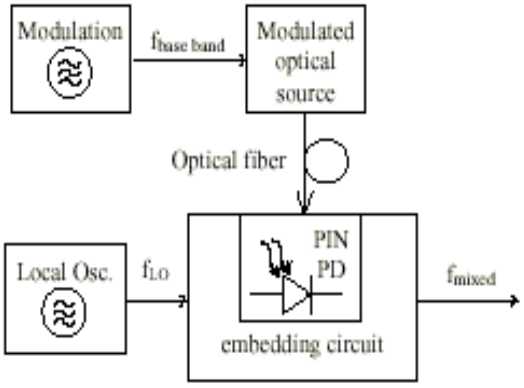

Fig. 15 Optical-microwave mixing setup

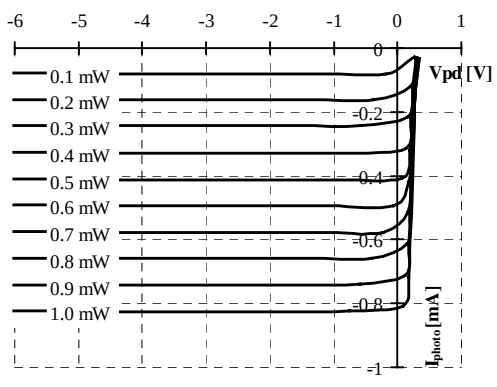

Fig.16 Measured DC characteristic of the pin photodiode

The embedding circuit can be optimized for detection or mixing. The dc characteristics of the p-i-n photodiode is shown in Fig. 16. Here the detected photocurrent is plotted as a function of the bias voltage for different illumination intensities. As seen close to the zero voltage bias point the curvature of the characteristics exhibits a maximum. At this bias voltage the dependence of the photo-current on the light intensity is also maximal. This coincidence ensures the high mixing product in the double mixing approach.The p-i-n photodiode is embedded into a microwave circuit where the detected base band signal is reflected. The photo diode is driven by a microwave local oscillator signal and at the same time it is illuminated by an intensity modulated optical signal. The result is presented in Fig. 17.
Here the mixing product is depicted as a function of the bias voltage. The frequency of the applied local oscillator was 3GHz and the modulation frequency of the intensity modulated optical signal was 540MHz. As seen, about 10dB mixing gain can be achieved biasing the photodiode close to zero voltage.

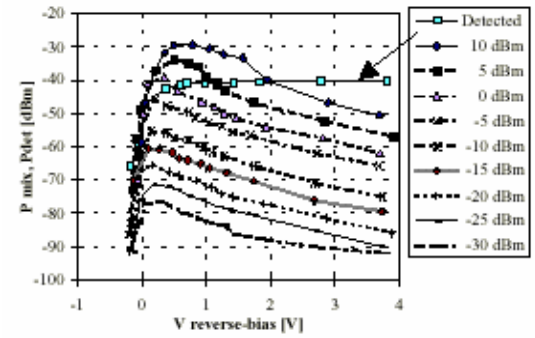

Fig.17 Measured power level of the upconverted signal versus the reverse bias voltage (parameter is the LO power)

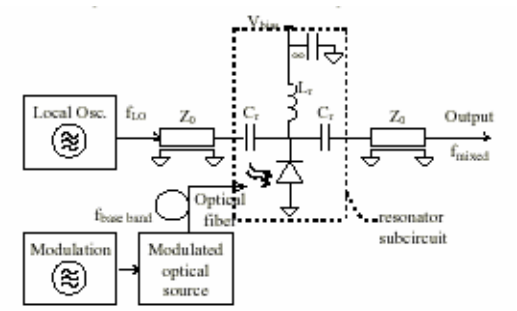

Fig. 18 Measuremtn setup for resonant mixing using a "transmission setup"

3.2. RESONANT ENHANCEMENT

For further improvement the resonant enhancement method can be utilized. The base band and the microwave band are separated by a branching filter as shown in Fig. 18. The reflection in the base band can be adjusted using a sliding short circuit (varying inductance). This way the mixing product is enhanced in a narrow band. The spectrum of the upconverted signal is plotted in Fig. 19.
In the investigations by [7], the frequency of the local oscillator is 2GHz, the photodiode is biased at –0.2V and the series capacitor is 4.7pF. With these settings there is a resonant peak around 50MHz as shown in the figure.

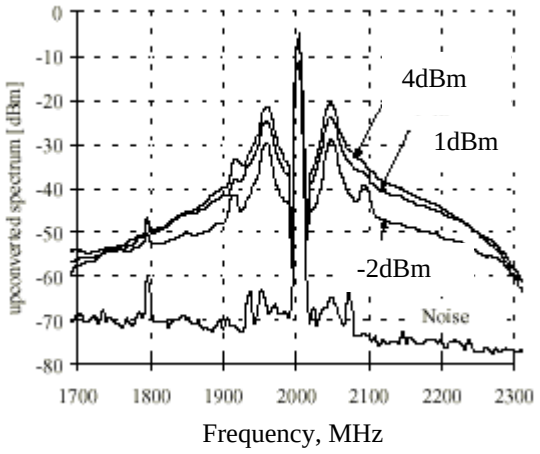

Fig. 19 Measured power level of the upconverted signal (parameter is the LO power) (transmission setup)

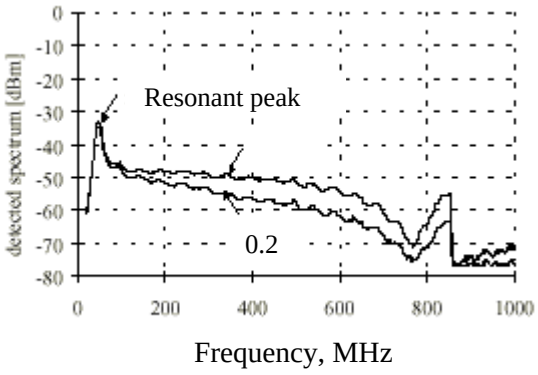

Fig. 20 Measured power level of the detected sigal in resonant condition (parameter is the reverse bias voltage)

The resonance can be measured at base band too. The measured detected spectrum at base band is shown in Fig. 20 at different bias voltages. The peak of the detected spectrum is only an attenuated signal after the series capacitor of the resonator. For comparison Fig. 21 shows the upconverted spectrum using the same configuration setup without resonator subcircuit. In this case the embedding circuit was optimized for detection. Comparing the curves of the Fig. 19 and 21 the effect of the resonance can be seen.

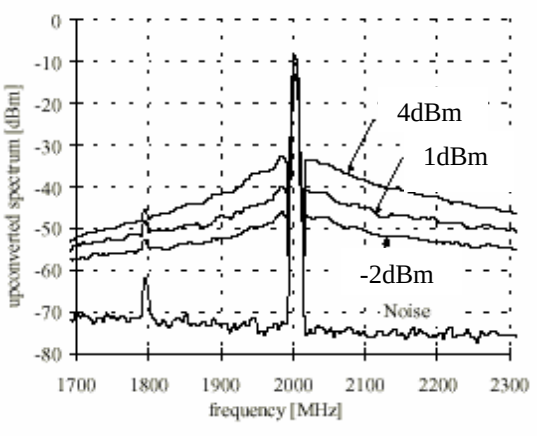

Fig. 21 Measured power level of the upconverted signal without resonator (parameter is the LO power)

4. Frequency conversion methodes by optical interferometer and photodiode

According to [10], there is a comparison of the performance of two different optoelectronic configuration, both used for frequency conversion in the microwave frequency range. In the firs case, mixing is achieved by a Mach-Zehnder (MZ) interferometer, while in the second case, photodiode mixing is presented.

4.1. MIXING WITH UMZ/PD

In the firs case, the optical system used for microwave mixing is a distributed feedback (DFB) laser diode (LD) directly modulated by two microwave frequencies, f_1 (f_{LO} corresponding to the LO signal) and f_2 (in this case, f_{RF}) followed by an unbalanced MZ (UMZ) and a photodetector (PD). The system is shown in the upper portion of Fig. 22.
The basic principle is the nonlinear (sinusoidal) intensity response of the UMZ interferometer/PD combination as a function of the frequency of the optical field. Direct modulation generates FM, which is then converted to AM using the UMZ interferometer working in the coherent regime. The PD detects the optical intensity which is a quadratic function of the optical field, so frequency mixing is obtained. The originality of this solution is the use of a passive optical device inserted in the optical link which generates mixing with better conversion than classical solutions using active MZ modulators.

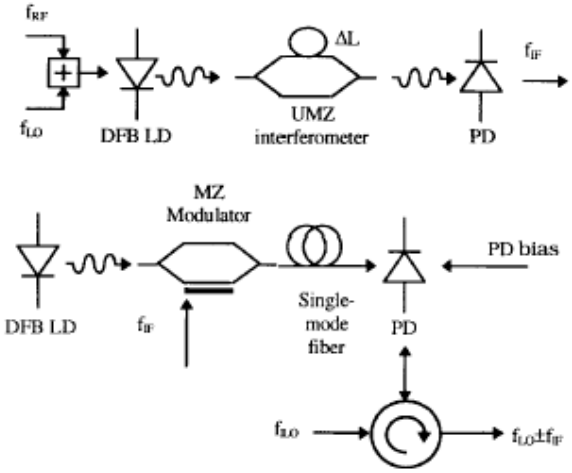

Fig. 22 Optical systems used for optical-microwave mixing

Considering a linear LD operating regime and neglecting AM, the intensity at the output of the interferometer, with delay time τ between both arms is given by

$$I(t)=\frac{E_0^2}{2}\left\{1+V(\tau)\cos\left[2\pi\nu_0\tau+\beta_1\sin\left(\omega_1\frac{\tau}{2}\right)\cdot\cos\left(\omega_1\left(t+\frac{\tau}{2}\right)\right)+\beta_2\sin\left(\omega_2\frac{\tau}{2}\right)\cdot\cos\left(\omega_2\left(t+\frac{\tau}{2}\right)\right)\right]\right\} \quad (15)$$

where $\beta_{1,2}$ is the FM index, $\omega_{1,2}$ is the angular modulation frequency, and $V(\tau)$ reflects the loss of choerence between electric field in both arms of the interferometer. In the coherent working regime $V(\tau)=1$ and in the incoherent regime $V(\tau)=0$. As can be deduced from the equation, in the coherent working regime, when the interferometer is balanced on bright or dark fringe, i.e., when $\cos(2\pi\nu_0 t)=\pm1$ (condition 1), the rsulting intensity is generated at harmonics and intermodulation products of even order, and in particular, at the mixing frequency f_{IF}. Condition 1 is then the first condition to obtain the best mixing at frequency $f_{IF.}$

To be optimized, the output spectrum of the optical intensity must exhibit the maximum power of the mixing frequency and the minimum power of the input frequencies. This second condition (condition 2) is fulfilled when

$$f_1=(2k+1)\frac{FSR}{2} \quad (16)$$

and

$$f_2=(2k'+1)\frac{FSR}{2},(k,k')\in N^2 \quad (17)$$

where $FSR=1/\tau=c/(n_{eff}\Delta L)$. Therefore, f_2-f_1 must be as close as possible to a multiple of the free spectral range (FSR). For given input microwave frequencies, the ΔL must be chosen to match these two conditions.

The response at the PD output is periodic with the input frequencies, which means that the device does not optimally work for all frequencies but for particular frequencies in any frequency range. Within a period, the 3dB bandwidth approximates FSR/2. However, in some applications, it is advantageous since the UMZ acts as a microwave filter too.

4.2. PRINCIPLE OF OPTICAL-MICROWAVE MIXING BY PHOTODIODES

The optoelectronic system explored for opto-microwave mixing is shown below the UMZ/PD system in Fig. 22. The mixing was analyzed based on the dc characteristics at different optical intensities illuminating the device. To achieve good detection, the PD is used in its linear regime where the applied reverse bias is usually several volts. However, even in this regime a noticeable nonlinearity is present at higher light injection levels.

Simultaneously injecting a microwave signal at the electrical port of the PD and a modulated optical signal results in the mixing of the two signals. The optimal bias points for efficient mixing and for efficient detection are significantly different. The mixing process is explained as a result of the nonlinearity of the PD current-voltage relationship. Due to the fact that the characteristics exhibit the maximum nonlinearity in the vicinity of 0V, it is the optimal operation point for efficient mixing. Nonlinearity of the PD generates several mixing products of the microwave driving signal f_{LO} and of the photo-induced signal f_{IF}. By injecting an LO signal $f_{LO}>f_{IF}$, the detected optical signal is upconverted.

Fig. 23 represents the voltage dependence of the detection and of the mixing products at $f_{LO}+f_{IF}$. In this experiment, f_{LO}=3GHz was used and the light was intensity modulated by f_{IF}=150MHz. Optimal detection is achieved by high reverse bias and a plateau is observed at bias points $V_{PD}<0$. In the absence of electrical excitation, the power of the second harmonic was considerably small, taken into account also the contribution of the modulator part. However, the most efficient mixing is obtained at a bias close to V_{PD}=+0.3V, having a sharp optimum. Conversion loss of the electro-optical mixing process is defined as the ratio of the power at f_{IF} (using the PD in its linear regime as a PD) and of the signal levels at $f_{LO}\pm f_{IF}$ frequencies upconverted by the PD nonlinearity.

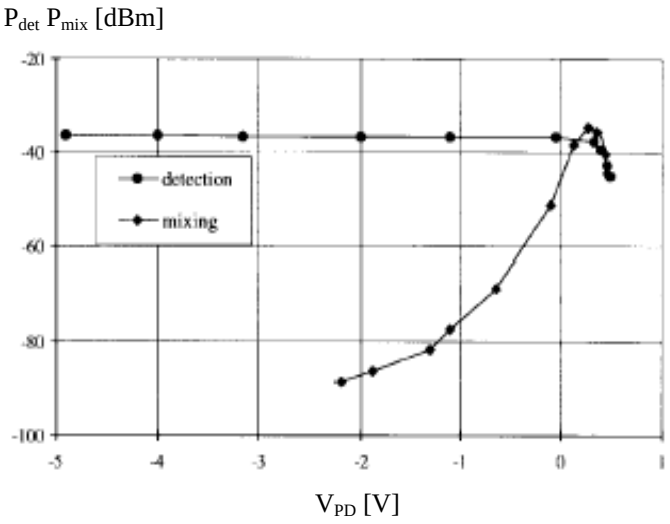

Fig. 23 Voltage dependence of the detected power and of the upper-sideband mixing product.

4.3. EXPERIMENTAL RESULTS WITH UMZ/PD

Measurements were made in [10] with a DFB LD emitting at λ=1300nm, having an I_{th}=13mA and a maximal oscillation frequency of 2.5GHz. The dc-bias current was 22mA and the optical power coupled in the interferometer was 420µW.

To operate in the coherent regime as wanted, the UMZ was realized using only two connectorized –3dB fiber directional couplers. In this case, ΔL=1.6cm, which corresponds to FSR=13GHz.

The LO frequency was F_{LO}=1.9GHz, with a power of –4dBm. The other modulation frequency, f_{RF} was swept from 2 to 2.5GHz and had a power of –18dBm. Fig. 24 shows the power spectrum of the intensity detected by the PD and measured by a spectrum analyzer. In Fig. 24, the lower sideband of the mixing product, f_{LO}-f_{RF}, as well as the third order intermodulation product, was significantly increased by inserting the UMZ. However, the input frequencies f_{LO} and f_{RF} are not rejected. In fact, to obtain an optimal rejection of the fundamentals, condition 1 should first be fulfilled, which was not the case under the conditions of operation. The relative optical phase shift between the two arms is very sensitive to ambient variations, and during the experiments the operating regime continuously varies between minimum and maximum transmission including the quadrature. Secondly, the closer f_1 would be to FSR/2=6.5GHz, the larger the rejection would be, and here f_1=f_{LO}=1.9GHz (limitation due to the LD)

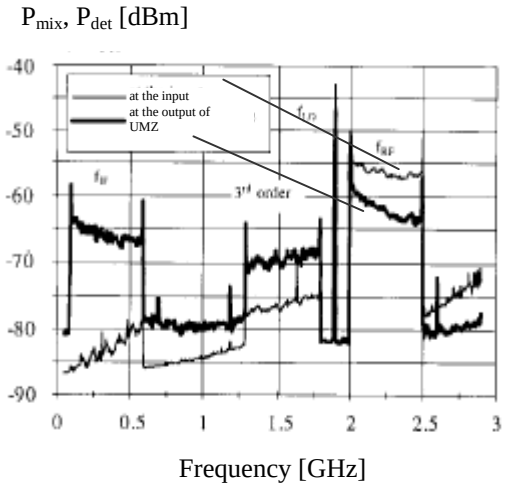

Fig. 24 Power spectra of detected signals with and without UMZ

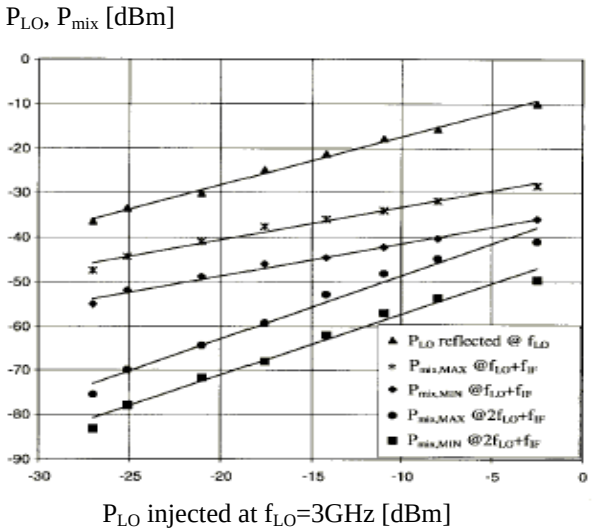

Fig.25 Levels of first and second harmonic mixing as a function of P_{LO}, m=25%(MIN), and m=75%(MAX)

4.4. EXPERIMENTAL RESULTS WITH PD

Investigating the frequency conversion, a PD was illuminated by a DFB laser according to [10]. The LO signal was fed to the PD through a wide-band circulator or a directional coupler separating the LO input and the RF output. No amplifier was used to avoid additional nonlinearities.
Fig. 25 shows the first and second harmonic mixing of f_{IF} and f_{LO} frequencies as a function of the injected LO power measured by a spectrum analyzer. The LO frequency was f_{LO}=3GHz while the optical intensity was modulated by f_{IF}=150MHz. The driving LO signal reflected at the PD is shown as well. A slight saturation effect is observed at P_{LO} close to 0dBm and a proportional increase of the mixing products is shown for greater optical modulation depth (OMD). Results of Fig. 25 demonstrate the interest of exploring the generation of second or higher harmonics for mixing purposes. It can find applications in systems where the LO is received from a remote site. Using subharmonically pumped mixing, only the subharmonic of the LO signal has to be transmitted.

4.5. COMPARISON OF THE TWO METHODS

The principle of the frequency conversion is different in the presented methods. In the first case, the f_{LO} and f_{RF} signals are optically converted by FM, mixed by UMZ, and transmitted. Applications are at the emission side of a fiber-optic link. In the second case, mixing is realized at the reception of the optical link. Only the frequency f_{IF} is transmitted by optical IM.

5. Summary

In this notes a short recapitulation of optical-microwave frequency conversion techniques was given. Optical-microwave signal processing and optical-microwave mixing is one of the most important fields of research regarding todays and future optical-wireless networks and local area networks.

We analyzed a wide spectrum of potential solutions depending on up- or down-conversion and on different device structures, such as MESFETs, p-i-n diodes, unbalanced Mach-Zehnder Interferometric modulators.

On the basis of the widespread references it is possible to make further investigations in the field.

6. References

[1] S.Malone, A.Paolella, P.R. Herczfeld, T.Berceli: “MMIC Compatible Lightwave-Microwave Mixing Techniques.”, *IEEE MTT-S Digest* 1992

[2] T.Berceli: “Dynamic Properties of Optical-Microwave Mixing Processes Utilizing FET Devices”, *IEEE Transactions on Microwave Theory and Techniques*, Vol. 43, No.9, September 1995

[3] A.Paolella, S.Malone, T.Berceli, P.R.Herczfeld: “MMIC Compatible Lightwave-Microwave Mixing Technique”, *IEEE Transactions on Microwave Theory and Techniques*, Vol. 43, No.3, March 1995

[4] T.Berceli: “New methods for subcarrier type optical reception applying new single sideband optical-microwave mixers”, *IEEE MTT-S Digest* 1994

[5] T.Berceli, B.Cabon, A.Hilt, A.Ho-Quoc, É.Pic, S.Tedjini: “Dynamic Characterization of Optical-Microwave Transducers”, *IEEE MTT-S Digest* 1995

[6] C.P.Liu, Y.Betser, A.J.Seeds, D.Ritter, A.Madjar: “Optoelectronic Mixing in Three-Terminal InP/InGaAs Heterojunction Bipolar Transistors”, *IEEE*

[7] T.Berceli, G.Járó: “A New Optical-Microwave Double Mixing Method”, *IEEE* 1998

[8] C.P.Liu, A.J.Seeds, D.Wake: “Two-Terminal Edge-Coupled InP/InGaAs Heterojunction Phototransistor Optoelectronic Mixer”, *IEEE Microwave and Guided Wave Letters*, Vol. 7, No.3, March 1997

[9] Lu Chao, Chen Wenyue, J. Fu Shiang: “Photonic Mixers and Image-Rejection Mixers for Optical SCM Systems”, *IEEE Transactions on Microwave Theory and Techniques*, Vol. 45, No.8, August 1997

[10] G.Maury, A.Hilt, T.Berceli, B.Cabon, A.Vilcot: “Microwave-Frequency Conversion Methods by Optical Interferometer and Photodiode”, *IEEE Transactions on Microwave Theory and Techniques*, Vol. 45, No.8, August 1997

[11] A.S.Daryoush, K.Sato, K.Horikawa, H.Ogawa: “Efficient Optoelectronic Mixing at Ka-Band Using a Mode-Locked Laser”, *IEEE Microwave and Guided Wave Letters*, Vol. 9, No.8, August 1999

[12] H.Ogawa, Y.Kamiya: “Fiber-Optic Microwave Transmission Using harmonic Laser Mixing, Optoelectronic Mixing, and Optically Pumped Mixing”, *IEEE Transactions on Microwave Theory and Techniques*, Vol. 39, No.12, December 1991

[13] H.Kamitsuna, H.Ogawa: “Monolithic Image Rejection Optoelectronic Up-Converters That Employ the MMIC Process”, *IEEE 1993 Microwave and Millimeter-Wave Monolithic Circuits Symposium*, 1993

[14] A.Madjar, P.R.Herczfeld, A.Paolella: “Analytical Model for Optically Generated Currents in GaAs MESFETs”, *IEEE Transactions on Microwave Theory and Techniques*, Vol. 40, No.8, August 1992

[15] H.Ogawa, Y.Kamiya: “Fiber-Optic Microwave Transmission Using Harmonic Modulation and Optoelectronic Mixing/Optically Pumped Mixing”, *IEEE MTT-S Digest*, 1991

[16] K.Matsui, E.Suematsu, T.Takenaka, H.Ogawa: “A One-Chip Integrated Optical/RF Transducer Using a HEMT Optomicrowave Mixer and a Slot Antenna” *IEEE MTT-S Digest*, 1994

This page has been deliberately left blank

Page intentionnellement blanche

Fiber Optic Distribution Networks for Military Applications

Afshin S. Daryoush
Department of Electrical and Computer Engineering
Drexel University, Philadelphia, PA 19104, USA

Daryoush@ece.drexel.edu

ABSTRACT

A number of military applications require ad-hoc wireless communication and networking systems that employ low phase noise reference signals for up- and down-conversion of communication signals and further processing of data signals. High performance fiber optic link s are important for distribution of signals while phase noise degradation induced by AM-PM conversion in fiberoptic links impacts phase coherency of local oscillator (LO) signals in distributed systems. This paper focuses on issues associated with directly and externally modulated fiber optic links and their performance limitations in terms of gain, noise figure, nonlinearity, and dynamic range. The performance-cost aspects of both types of links are compared and it is pointed out that directly modulated links meet performance-cost requirements in most applications. Analysis of phase noise degradation of frequency reference is presented for directly modulated fiber optic distribution networks. SRS induced fiber nonlinearity is also discussed. Since the response of a Fabry-Perot laser diode can be altered by adding an external feedback, resulting in a resonance peak, results of a monolithically integrated FP laser are discussed. Finally, opto-electronic mixing of IF and LO signals are also demonstrated for the mode-locked case.

1.0. INTRODUCTION

Recently a lot of efforts has been directed toward increase in global interconnectivity through electronic media and many market studies has identified a significant increase in demand for personal communication services in the 21st century. One of the most important proponents of this market is in the inter-office communication, where the high-speed fiberoptic local area networks (LAN) are combined with wireless communication to provide interconnectivity among many users.

Conceptual system architecture of a hybrid wireless and fiber optic LAN with applications to both civilian and military systems is shown in Fig. 1. In this figure, personal computers (PC) are networked together through this hybrid wireless and fiberoptic networks. The digital data from the PC is up-converted by a millimeter wave (MMW) stable carrier and is then radiated by a low cost omni-directional antenna. The modulated received RF signal is then down-converted to the coded digital signals using the same stabilized MMW local oscillator (LO). The coded digital signal is then networked to other users through a high-speed fiberoptic network. The fiber-optic LAN is envisioned to operate either in analog format or digital data rates well above Gb/s.

An important component of a reliable inter-office communication for the portable PC is the use of the low power consuming frequency translation circuits, which up- and down-converts the information without any degradation in the its spectral purity. Frequency stability of the local oscillators used in the MMW wireless communication, and the clock recovery circuits used in the decision circuits, are critical in accurate data retrieval.

Paper presented at the RTO SET Lecture Series on "Optics Microwave Interactions", held in Jouy en Josas, France, 2-3 September 2002; Duisburg, Germany, 5-6 September 2002; Budapest, Hungary, 9-10 September 2002, and published in RTO-EN-028.

This paper first reviews the performance of directly and externally modulated fiber optic links. First analytical expressions are presented for gain, noise figure, and dynamic range and sources of phase noise degradation in directly and externally modulated FO links are presented. Cost and reliability performance of fiberoptic links in harsh military environment is also reviewed. Next performance of a long F-P laser structure that is monolithically integrated with electro-absorption modulator is reviewed where efficient transmission of data and carrier signals with high SFDR and low phase noise degradation are achieved.

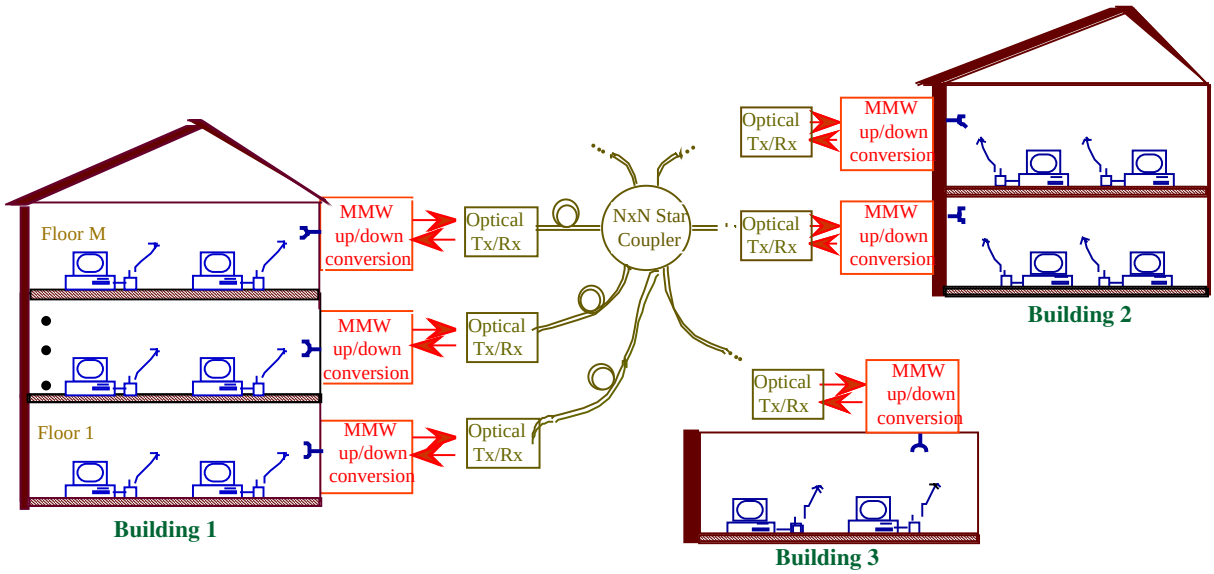

Fig. 1. Conceptual diagram of hybrid fiberoptic and wireless local area distributed network system. (Optical fiber distribution, electrical distribution, free space distribution).

2.0. FO LINK PERFORMANCE

Fiber optic (FO) links are employed for distribution of frequency reference as well data communications in distributed systems, where these links need to provide RF signals with high dynamic range and low phase noise degradation. The FO link gain and noise performance will impact signal to noise performance, while the nonlinearity of various elements in the optical system will contribute to a limited dynamic range. The nonlinear phase and amplitude variation with input RF power will results in AM-AM and AM-PM conversion.

Directly Modulated FO Link: The gain of a fiber-optic link can be calculated in terms of microwave scattering parameters using the signal flow diagram (SFD) technique [1]. The transducer gains of the optical transmitter and optical receiver are derived separately and then combined to yield the gain of the complete link. The link gain is expressed as

$$G = \frac{P_{out,Tx}}{P_{av,\,Rx}} = G_{Tx} \times |H_L|^2 \times G_{Rx}$$

$$= \frac{|S_{21D}|^2 \; |S_{21L}|^2 \, (1 - |\Gamma_{las}|^2) \; (\eta_L K_L L K_D \eta_D)^2}{|1 - \Gamma_{las} \, S_{22L}|^2 \; |1 - \Gamma_{SD} \, S_{11D}|^2} \, .$$

When a directly modulated semiconductor laser diode is employed in the optical transmitter, the SFD is obtained by considering the forward-bias junction resistance of the laser diode to be the port two termination of a two-port network consisting of the microwave impedance-matching and driving circuit combined with the other device

parameters of the laser. Whereas a reverse-biased p-i-n photodiode is employed in the optical receiver, the SFD is obtained by considering the junction resistance of the diode to be the port one terminating load to a two-port network consisting of the microwave impedance-matching circuit and the other device parameters of the detector. The link current transfer function, H_L, is defined as the ratio of detector current to RF current across the laser. This is a measurable quantity that is a function of the electro-optic device quantum efficiencies as well as optical attenuation and coupling efficiency, where η_L is the laser diode external quantum efficiency, η_D is the detector responsivity, L is the optical attenuation in the fiber, and K_L, K_D are the laser-to-fiber and fiber-to-detector coupling efficiencies, respectively. At the moment nonlinear fiber performance due to Stimulated Brillouin and Raman Scattering processes for long fiber length L is ignored, but this issue is to be discussed later.

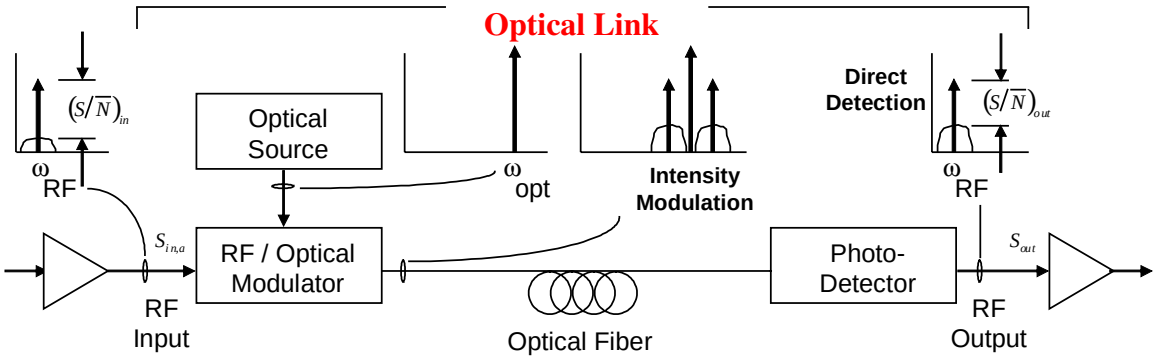

Fig. 2. Overall structure of a fiberoptic link. Note for directly modulated system the optical source is internally modulated whereas in externally modulated link the electro-optic property is used to perform intensity modulation in a MZ modulator.

The four contributions to the noise power of the directly modulated fiber-optic link. The total noise power at the output of the detector is the sum of all these individual noise powers,

$$N_{out} = N_{RIN} + N_{shot} + N_{thtx} + N_{thrx} = N_{RIN} + N_{shot} + N_{th}.$$

The dominant term is the laser RIN noise power, which is expressed as:

$$N_{RIN} = RIN(f)\,(I_b - I_{th})^2\,(\eta_L K_L L K_D \eta_D)^2 \frac{|S_{21D}|^2}{|(1 - \Gamma_{SD} S_{11D})|^2} B Z_0$$

The next dominant noise source is shot noise of the detector, including dark current noise,

$$N_{shot} = 2e\left[(I_b - I_{th})(\eta_L K_L L K_D \eta_D) + I_d\right] B \frac{|S_{21D}|^2}{|(1 - \Gamma_{SD} S_{11D})|^2} Z_0$$

followed with the thermal noise of the transmitter,

$$N_{thtx} = 4kT_a B (\eta_L K_L L K_D \eta_D)^2 \,\mathrm{Re}\{Y_{thl}\} \frac{|S_{21D}|^2}{|(1 - \Gamma_{SD} S_{11D})|^2} Z_0$$

Finally the thermal noise of the detector,

$$N_{thrx} = 2kT_a B\left(1 - |\Gamma_{in}|^2\right).$$

The only noise source at the input of the link is the thermal noise in the transmitter circuitry; i.e., $N_{in} = kT_aB$. Noise Figure of the fiber-optic link is defined as

$$NF_{Link} = \frac{(SNR)_i}{(SNR)_o} = \frac{P_{in} * N_{out}}{P_{out} * N_{in}} = \frac{1}{G_{Link}} * \frac{N_{out}}{N_{in}} \qquad (1)$$

Externally Modulated FO Link: The small-signal gain of an externally modulated fiber-optic link is derived using the SFD technique as was applied to direct modulation. When a Mach-Zehnder interferometric modulator is employed in the optical transmitter to impress a microwave signal upon the optical carrier in a single-mode fiber, the transmitter SFD is obtained by considering the capacitance C_M across the modulator terminals to be the port two termination of a two-port network consisting of the microwave impedance-matching circuit and the other device parameters in the equivalent circuit of the modulator. The output power of a fiber-optic link depends on the amplitude of photocurrent, I_{det}, generated in the detector, which is in turn proportional to the RF voltage V_M across the capacitor C_M. This gain is represented as:

$$G = \left(\frac{\pi \, L \, K_D \, \eta_D \, P_{in,op} \, Z_0}{2 \, V_\pi} \right)^2 \frac{|S_{21M}|^2 \, |S_{21D}|^2 \, |1 + \Gamma_M|^2}{|1 - S_{22m} \, \Gamma_M|^2 \, |1 - S_{11D} \, \Gamma_{SD}|^2}.$$

Where V_π = bias voltage required for 100% modulation and $P_{in,op}$ is the optical output of the modulator. Figure 3 compares the achievable gain of directly and externally modulated fiber optic links. Note that a higher gain is achieved when optical source and detector with efficient light coupling and responsivity are employed. Finally, gain of the externally modulated FO link monotonically increases as optical power squared. Four noise sources contribute to the output noise power of the link. The dominant term in the case of large input optical power is the shot noise followed with excess RIN noise of the laser. The shot noise of the detector, including dark current, is expressed as:

$$N_{shot} = 2e\left[\left(\frac{\eta_{op} \, \eta_D \, P_{in,op}}{2}\right) + I_d\right] B \frac{|S_{21D}|^2}{|1 - \Gamma_{SD} \, S_{11D}|^2} Z_0$$

The excess noise of the laser is related to optical source RIN noise which could be significantly lower than the semiconductor laser diode.

$$N_{excess} = \left[RIN\left(\frac{\eta_{op} \, \eta_D \, P_{in,op}}{2}\right) - 2e\right] \times \left(\frac{\eta_{op} \, \eta_D \, P_{in,op}}{2}\right) B \frac{|S_{21D}|^2}{|1 - \Gamma_{SD} \, S_{11D}|^2} Z_0$$

The thermal noise sources of the transmitter and of the detector are presented respectively as:

$$N_{thtx} = kT_a \, B \left(\frac{\pi \, \eta_{op} \, \eta_D \, P_{in,op} Z_0}{2 \, V_\pi}\right)^2 \frac{|S_{21m}|^2 \, |S_{21D}|^2 \, |1 + \Gamma_M|^2}{|1 - \Gamma_M \, S_{22m}|^2 \, |1 - \Gamma_{SD} \, S_{11D}|^2}$$

$$N_{thrx} = 2kT_a \, B \left(1 - |\Gamma_{in}|^2\right)$$

The total noise power at the output of the detector is the sum of all these individual noise powers. As in the direct modulation case, the noise power at the input to the external modulation link is simply kT_a B. Therefore the noise figure is given by equation (1). Note the total shot noise increases as optical power, therefore signal to noise ration increases as optical power increases in the externally modulated links. However, the challenge is developing high-speed high-power handling photodetectors.

Fig. 3 depicts comparison measured and analytical calculated gain results of directly and externally modulated fiberoptic links. The optical power can be high in externally modulated fiberoptic links when a solid state laser is employed as optical source. Note a low V_π MZ modulator and operation in the quadrature point of $V_b = V_\pi/2$ (i.e., $\phi = 90^o$) along with a high power handling photodiode allows for the highest reported gain for FO links. Naturally a higher responsivity (i.e. η_L and η_D) laser diode and photodiode result in a lower insertion loss.

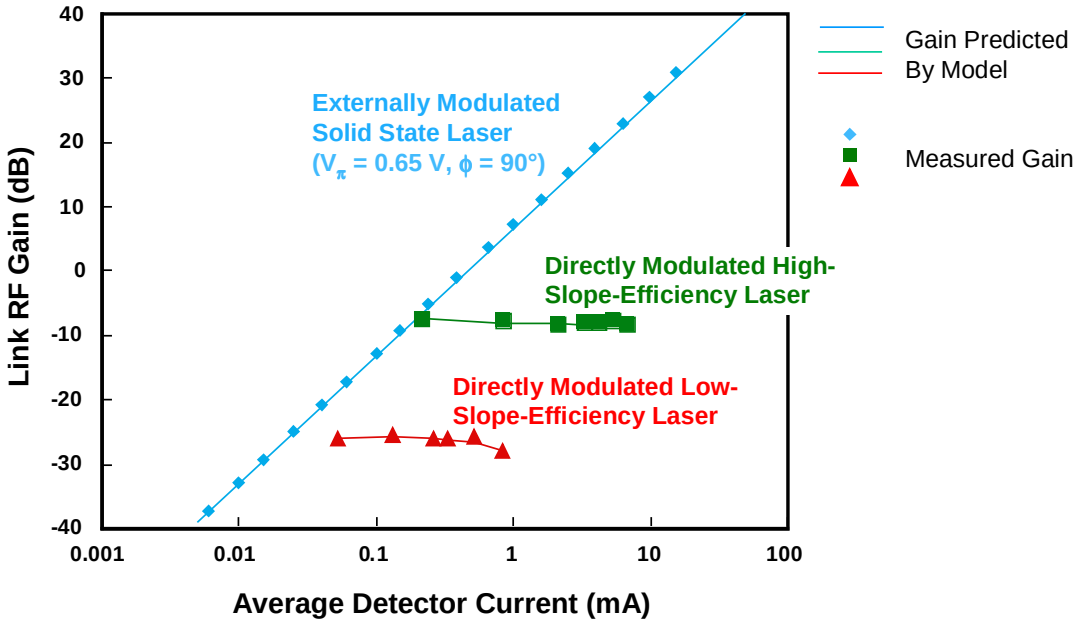

Fig. 3. Comparison of experimental and simulation results of directly and externally modulated fiber optic links at HF [2]. (Courtesy of Ed Ackerman of Photonics Inc).

Dynamic Range: Spurious free and compression dynamic range are directly related to linearity off the optical modulator (i.e., laser diode in the case of directly, and MZ modulator in the externally modulated FO links). The 3rd order intercept point and 1 dB compression point for the directly modulated are calculated [1] based on the optical modulation index m,

$$P_{in,int} = \frac{m_{int}^2 (I_b - I_{th})^2 \left| 1 - S_{22L}\Gamma_{Las} \right|^2 Z_0}{|S_{21L}|^2 \left(1 - |\Gamma_{Las}|^2\right)}$$

$$P_{in,1dB\ CP} = \frac{m_{1dB\ CP}^2 (I_b - I_{th})^2 \left| 1 - S_{22L}\Gamma_{Las} \right|^2 Z_0}{|S_{21L}|^2 \left(1 - |\Gamma_{Las}|^2\right)}$$

In a similar fashion, the 3rd order intercept point and 1 dB compression point are derived for externally modulated fiberoptic links as:

$$P_{in,int} = \frac{8 V_\pi^2 \left| 1 - S_{22m}\Gamma_M \right|^2}{\pi^2 Z_0 |S_{21m}|^2 \left| 1 + \Gamma_M \right|^2}$$

$$P_{in,1dB\ CP} = \frac{0.950454^2 V_\pi^2 \left| 1 - S_{22m}\Gamma_M \right|^2}{\pi^2 Z_0 |S_{21m}|^2 \left| 1 + \Gamma_M \right|^2}$$

Using the derived relationship for intercept and compression points, Spurious Free and compression dynamic range are calculated using the following expressions:

$$SFDR = \frac{2}{3} \times 10\ Log_{10}\left[\frac{P_{out,int}}{kT_aG\ NF}\right]\ \ dB.Hz^{2/3}$$

$$CFDR = 10\ Log_{10}\left[\frac{P_{out,1dB\ CP}}{kT_aG\ NF}\right]\ \ dB.Hz$$

Fig. 4 represents the calculated dynamic range of externally and directly modulated fiberoptic links as a function of frequency and makes comparison against the measured results at various operating frequencies. Moreover, references are made to various practical military and civilian applications at those frequency bands. As seen the externally modulated fiber optic link with high power and low RIN noise solid state laser as source combined with high power handling photodetectors provide for the highest dynamic range. However, note that at lower frequencies, externally modulated link using DFB lasers as source outperforms solid state laser due to its RIN resonance peak about MHz. In the directly modulated links, a higher dynamic range is obtained in DFB laser based systems where a lower RIN noise is obtained compared to FP laser diodes.

On the other hand, Fig. 5 compares cost vs DR performance of directly and externally modulated links reported. The dashed line corresponds to the current cost-performance limit of the reported FO links. In addition a number of civilian applications are identified in this figure. As indicated, even though externally mdulated links will meet the stringent requirements of many commercial applications, however due to its high-cost can not be considered economically viable. Therefore, the derive needs to be either improving performance of directly modulated links or through manufacturing innovations drive the price of externally modulated links down.

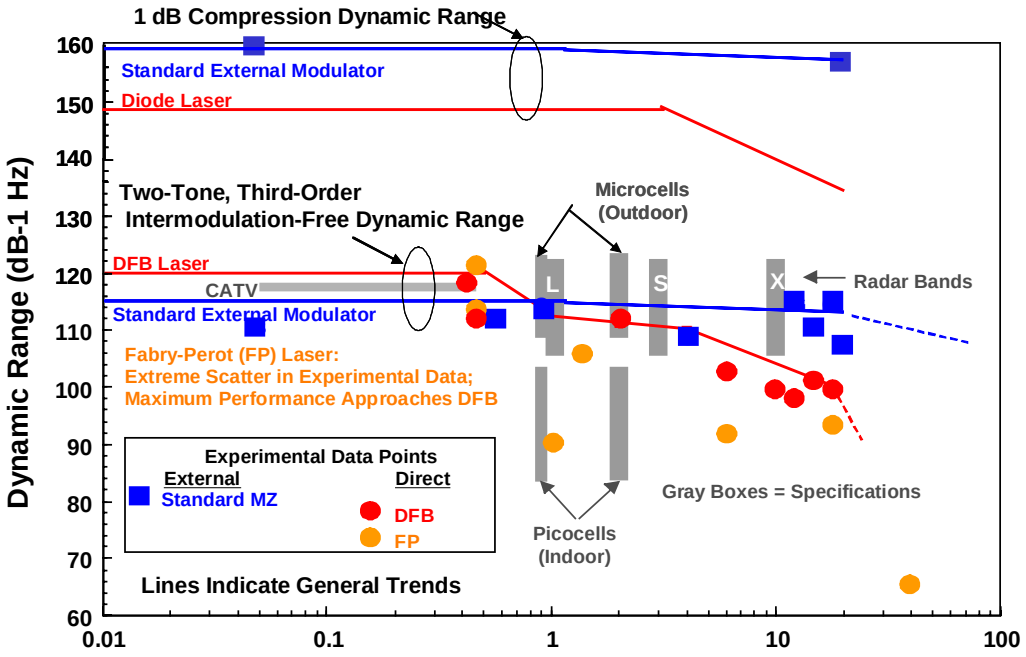

Fig. 4. Comparison of measured and calculated dynamic range for directly and externally modulated fiber optic links [2]. (Coustesy of Ed. Ackerman of Photonics Inc.)

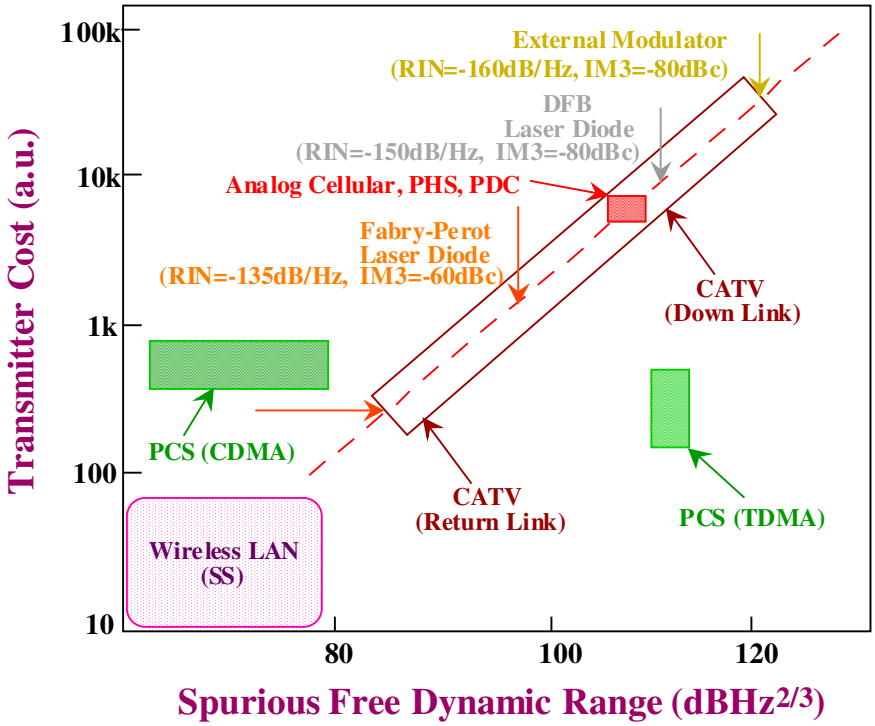

Fig. 5. Cost-Dynamic Range comparison of directly and externally modulated fiber optic links for a variety of civilian applications [3].

Fiber Nonlinearity: WDM optical systems are employed in optically controlled phased array antenna applications, where long length of optical fibers are employed for true time delay devices in large apertures. In pushing these systems to the limits of transmission capability, aspects such as fiber nonlinearities need to be understood. These aspects include the nonlinear fiber phenomena of SRS (stimulated Raman scattering) [4], SBS (stimulated Brillouin scattering) [5], and XPM (cross phase modulation) [6]. These nonlinear effects become noticeable particularly in WDM subcarrier multiplexed (SCM) systems that may cover a lot of closely packed video channels cover long distances. These nonlinearities result in optical power transfer to higher and lower optical frequencies. Each nonlinear effect creates a distortion level that becomes intolerable above the acceptable threshold level. Threshold requirements are based on electrical nonlinear distortion requirements, composite second order (CSO) and composite triple beat (CTB) (particularly CTB), which have been determined in published works such as [8, 9].

Fig. 6 shows the SRS crosstalk level for a two channel WDM system, while the fiber length is varied and for 9.4 nm channel spacing, an input power of 4 dBm, a dispersion of 17 ps/nm/km, and a subcarrier frequency of 152 MHz. The two curves in the figure represent the high and low dispersion fibers. The more dispersive fiber generates lower XT due to the walk-off effect. As is expected, the crosstalk level begins to increase as the fiber length increases. However, the XT level reaches a peak value and then decreases as the length is increased further. As the length is increased beyond 70 km, eventually the SRS level reaches a steady state value. This behavior shows a sinusoidal dependence of crosstalk on fiber length for dispersive fiber but a monotonic increase in for the dispersion shifted fiber. The importance of this result is that due to the walk-off effect, the crosstalk level for a length of fiber may not increase as the fiber length increases. Hence, the crosstalk level can be reduced or increased depending upon the fiber length. In comparison of the measurement and simulation (based on Wang [8] and Phillips [9] models), the maximum error is less than 5 %. Measurement results of the

SRS crosstalk while increasing the RF frequency from 50 to 725 MHz in steps of 50 MHz is depicted in Fig. 7. Also included in the figure is a simulation of the Phillips model [9]. Figure 7 shows that as the frequency is increased, the SRS crosstalk level changes following a behavior similar to a sinc function [i.e., sinx/x] squared fashion.

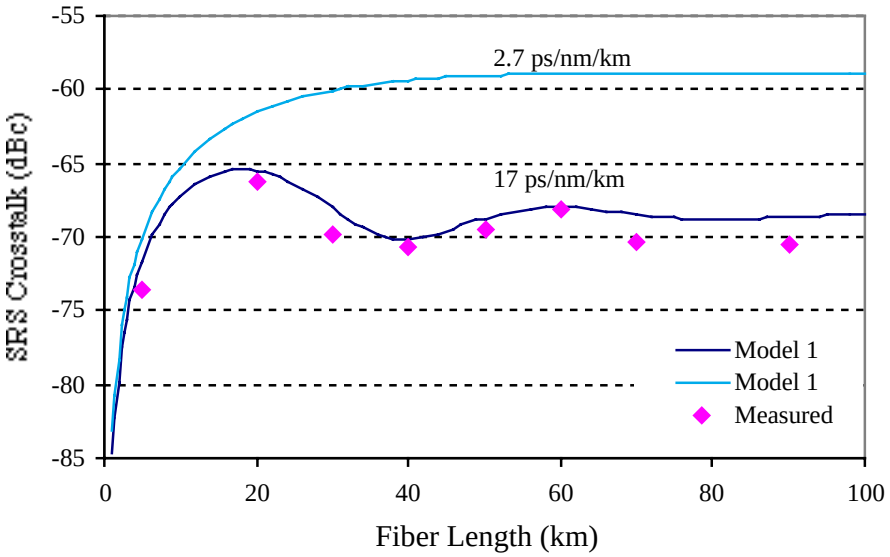

Fig. 6 Measured and simulated SRS induced crosstalk versus fiber length for an input optical power level of 4 dBm, fiber dispersion of 17 ps/nm/km, RF frequency of 151.85 MHz, and a channel spacing of 9.4 nm.

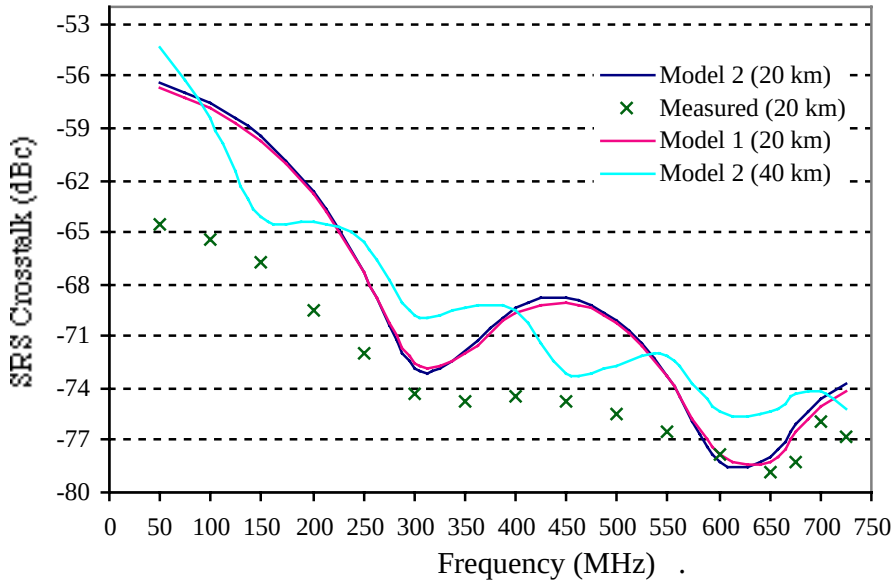

Fig. 7 Measured and simulated SRS crosstalk versus RF frequency with a fiber length of 20 km, fiber dispersion of 17 ps/nm/km, channel spacing of 9.4 nm, and a 4 dBm (2.5 mW) input power per channel, also a simulation of 40 km using only the Phillips model.

The problem of crosstalk becomes more aggravated as the number dense WDM channels increases. Even though analytical models were developed by Wang [8] to address N optical channels, but there are certain deficiencies associated with this model. An “alternative technique” was used to predict that for an 8 channel system, the crosstalk level could easily violate the acceptable cross talk. Specifically, for an input power of – 4 dBm, a subcarrier frequency of 50 MHz, a channel spacing of 1.6 nm (λ_8 = 1541.4 and $\Delta\lambda$ = 11.2 nm), and a fiber length of 40 km, the – 65 dBc threshold is violated. However,

by taking advantage of the walk-off effect, it is feasible to reduce the crosstalk level. For example, the simulation technique has predicted a greater than 10 dB decrease in crosstalk level by increasing the subcarrier frequency from 50 to 250 MHz, and decreasing the channel spacing from 1.6 to 0.8 nm. Therefore, the walk-off effect shows good potential for crosstalk reduction through control of its various parameters. The channel spacing not only affects the walk-off but also the Raman gain coefficient, thus, it offers substantial crosstalk reductions.

A four wavelength channels, ranging from 1531.90 nm to 1541.35 nm in steps of 3.2 nm, is characterized and simulated for 40 km fiber and the results are displayed in Fig. 8. The simulated curves are represented as solid lines and are labeled as XTi(2), XTi(3), XTi(4), and Alt. Tech (4), where the numbers represent the wavelength in order from the shortest wavelength (channel 1 at 1531.9 nm). In the same figure the measured and simulated crosstalk levels are presented for the second, third and fourth wavelength, while the pump wavelength is not shown (XT(1) level is expected to be much lower). Results from the measurement show some agreement with theory in that the longest wavelength channel receives the most SRS crosstalk distortion, while the shortest wavelength channel receives the smallest distortion. This alternative model provides more accuracy in the predicted distortion in a multi-channel system.

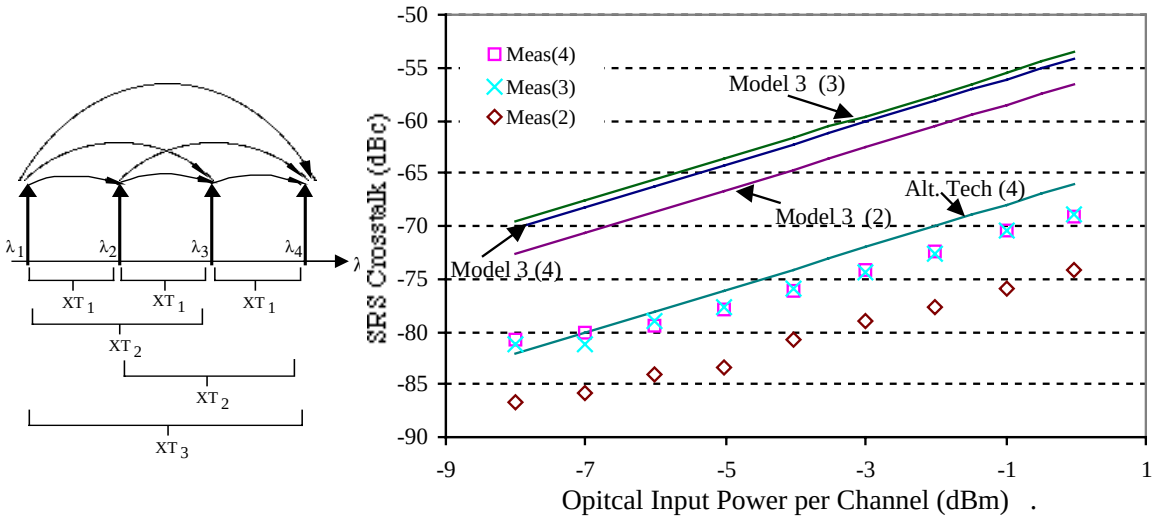

Fig. 8. Measured and simulated crosstalk versus optical input power per channel. The simulations represented include the three longest channel simulations using Wang's equation and the longest channel simulation using the alternate technique. Other parameters are a subcarrier frequency of 151.85 MHz, a dispersion of 17 ps/nm/km, a channel spacing of 9.4 nm, and a fiber length of 40 km. All discrete points are measurement points, whereas all solid lines are simulations.

Phase Noise Degradation: The FO distribution link contributes residual phase noise to the reference signal, which is a function of operation frequency. This impact is mostly significant in the directly modulated fiber optic links where the RIN of the optical source is far stronger than the externally modulated FO links. Moreover, directly modulated fiber optic links due to its lower cost than externally modulated links. The phase noise of the reference signal could be degraded if residual phase noise is too close to the signal noise floor level. Therefore, an appropriate selection of reference frequency is necessary to avoid being degraded significantly after passing through the FO link. For example as shown in Fig. 9, to generate a 12 GHz local oscillator (LO) at front-end, a reference signal at frequency of 100 MHz (UHF), 4 GHz (C-band), and 12 GHz (X-band) can be

sent through FO link. Since the phase noise contributions for FO links are different at these frequencies, an optimum frequency for reference signal can be found to have the least phase noise degradation due to FO link.

The optical spectra of a modulated optical signal are expressed as: $P_{opt}\left\{1+\mathbf{m}\cos\left(\omega_{\mathbf{m}}\mathbf{t}+\delta\phi_{\mathbf{m}}(\mathbf{t})\right)+\mathbf{n_{RIN}}(\mathbf{t})\right\}\cos\left(\omega_{opt}t+\phi_{opt}(t)+\delta\phi_{opt}(t)\right)$, where P_{opt} is the averaged optical power, $\mathbf{m}$ is the optical modulation index at modulating microwave carrier, ω_m. The focus of present work is $\delta\phi_m$, the residual phase noise added to the microwave carrier from the laser diode noise source. $\mathbf{n}_{RIN}$ is the relative intensity noise; ω_{opt} is the optical frequency; ϕ_{opt} is the optical phase signal due to side modes and modulation, and $\delta\phi_{opt}$ is the phase noise of the optical signal. Since most fiber-optic links for antenna remoting applications use intensity detection, only the noise signals in optical intensity affect the microwave carrier signal, namely, $\delta\phi_m$ and $\mathbf{n}_{RIN}$. The $\mathbf{n}_{RIN}$ could contribute to the FM noise of the reference signal through nonlinear AM/PM conversion [10].

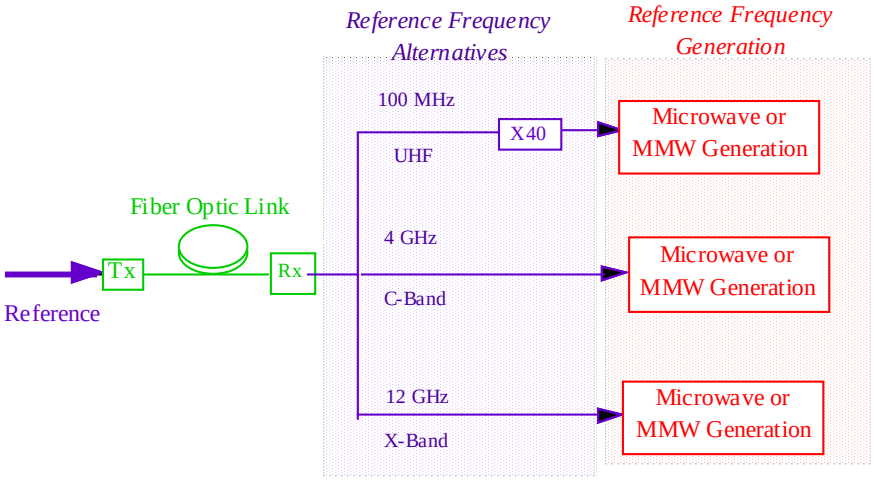

Fig. 9. Distribution of frequency reference and generation of MMW signal using various frequency references used in a FO based local oscillator (LO) synchronization network.

The laser diode SSB phase noise of the nth harmonic of the modulating signal, $£_{out}$, has contributions from three noise terms: i) the input reference signal phase noise, $£_{in}$; ii) the low frequency noise of laser diode up-converted to the carrier frequency, $£_{up}$; and iii) the RIN noise at the offset microwave carrier, $£_{RIN}$. This behavior is quite analogous to microwave systems [11]. Therefore at angular offset carrier frequency of Ω, $£_{out}$ can be approximately expressed as [12]:

$$£_{out,n\omega}(\Omega) = n^2£_{in,\omega}(\Omega) + n^2£_{up,\omega}(\Omega) + £_{RIN,n\omega}(\Omega) \qquad (2)$$

The factor of n is the harmonic order of the modulation signal, if any nonlinearity of laser diode is exploited to generate the nth harmonic [10]. (If the fundamental frequency is employed then n=1.) The subscript ω indicates the modulation frequency. The up-conversion factor of low frequency RIN to phase noise is the dominant noise source. The calculation of this up-conversion factor depends on the derivative of the RF phase with respect to the RF derive amplitude and is $C_{up,\omega} = 1/2(\partial\theta(\omega)/\partial P_o)^2P_o^2$, which θ is phase of optical signal at the modulating frequency ω. The dependence of phase on the optical output power in directly modulated system is a bit more complicated than externally modulated system since the nonlinear behavior is dependent on modulation index of laser

diode and relationship of its operation frequency compared to the relaxation oscillation frequency. This process is nonlinear and at certain frequencies results in AM-PM compression. The results are related to modulation index through “a” parameter, which is a function of modulation frequency and averaged optical power [1].

Since in semiconductor laser diodes RIN noise are strong up to 100 MHz because of mode partition noise, it is predicted that the spectral purity of the UHF reference signal is greatly degraded, resulting in a higher FM noise. Moreover, the X-band modulating signal is close to the relaxation oscillation frequency where RIN is peaked. The best frequency for reference signal distribution through DMFO link is the C-Band signal as depicted in Fig. 10, where the phase noise of the 12 GHz LO signal is generated from the reference signal through the above mentioned DMFO link. Clearly, the signal generated from a C-band signal has the best phase noise performance. The signal from UHF reference degrades greatly because the residual phase noise of the FO link is higher than the reference phase noise at offset frequency higher than 100 Hz.

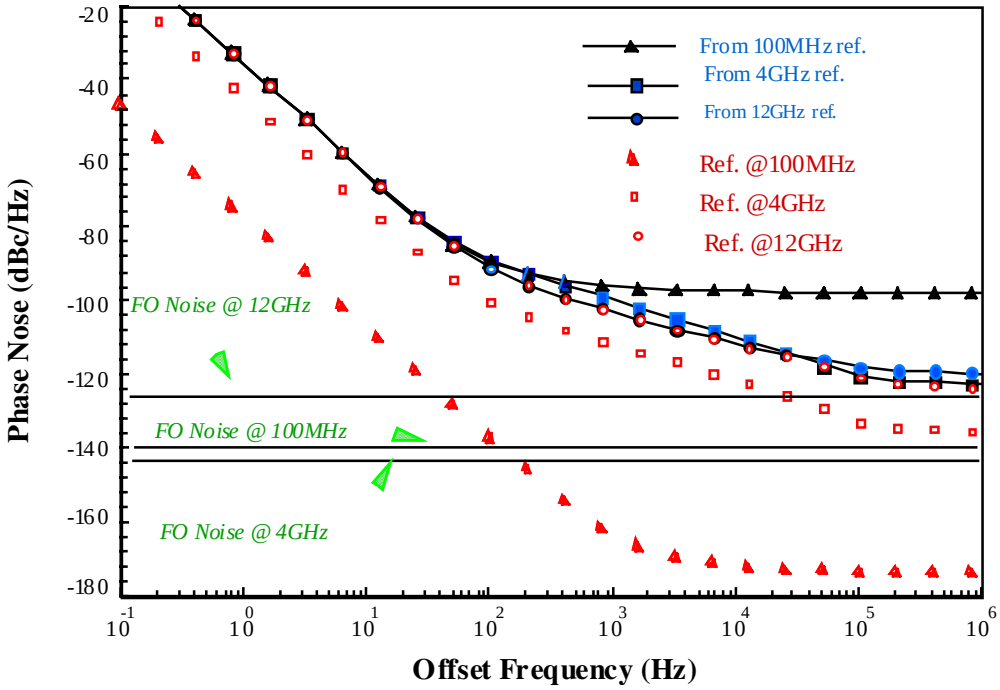

Fig. 10. The simulated phase noise of a LO signal at 12 GHz, which is generated from different reference signals through a directly modulated FO link as depicted in Fig. 9.

3.0. Semiconductor Laser Diodes with Self-Resonance

It is attractive to achieve optical systems that provide a performance analogous to the electrical functions. For example, a laser source with oscillation at millimeter wave frequencies along with the opto-electronic mixing would resemble the SOM circuit. A F-P laser with optical feedback has provided this feature and was first reported by Lau [13]. This resonance frequency is stabilized using a modulating frequency fundamentally or harmonically related to the self-resonance frequency. A thorough characterization and explanation of FM noise degradation of the frequency reference in the laser is also reported by Ni et al [12].

A monolithic version of laser with external cavity is realizable using semiconductor fabrication process and reported by a number of researchers. Fig. 11a shows a schematic drawing of the monolithic laser with an integrated EA modulator. Stacked structure consisting of two MQW layers, a MQW for laser diode (MQW-LD) and a MQW for EA

modulator (MQW-MD) are employed. The F-P cavity length for our experiment is cleaved approximately for a length of 2170μm. This total length is composed of 1970 μm long gain section, 150 μm long modulator, and a 50 μm long separation region. The facet of the modulator section is coated with high reflective film (R≈85%). The facet of the gain section is as cleaved. The laser is mounted in a high-frequency package. The schematic diagram of the long FP laser with integrated EA modulator is shown in Fig. 11b.

The gain section of the laser diode is forward biased at different bias currents and the EA section is reverse-biased by different voltage levels. The natural frequency response of the laser is measured at various laser bias currents, ranging from I_b=80mA up to I_b=150mA for bias voltage of V_m=0V. A resonance peak is observed that is associated with the longitudinal mode separation in the long FP laser. The longitudinal mode separation is calculated as $\Delta f=c/2nL\approx 19.3$GHz, where c=300mm.GHz is speed of light in free space, n≈3.5 is index of refraction of wave-guide, and L≈2.17mm is the F-P cavity length. This resonant frequency has a frequency tuning sensitivity of ≈1MHz/mA.

One could stabilize the optical oscillations using injection-locking process as demonstrated [13]. As the gain section is modulated by a synthesized frequency reference (HP83640A) of P_m≈-1dBm at f_m=19.258GHz, a single oscillation peak appears. The familiar one-sided injection-locking spectra are observed outside the injection locking range and the close-in to carrier phase noise is significantly reduced within the locking range. The measured close in to carrier phase noise degradation at 100Hz offset carrier is depicted in Fig. 12, where 31dB and 6dB degradation are measured for the injected power of P_m=+0.5dBm in the resistively- and reactively-matched modules respectively. However for injected power level of +4.5dBm, a close-in to carrier phase noise identical to the reference source is measured for the reactively-matched case.

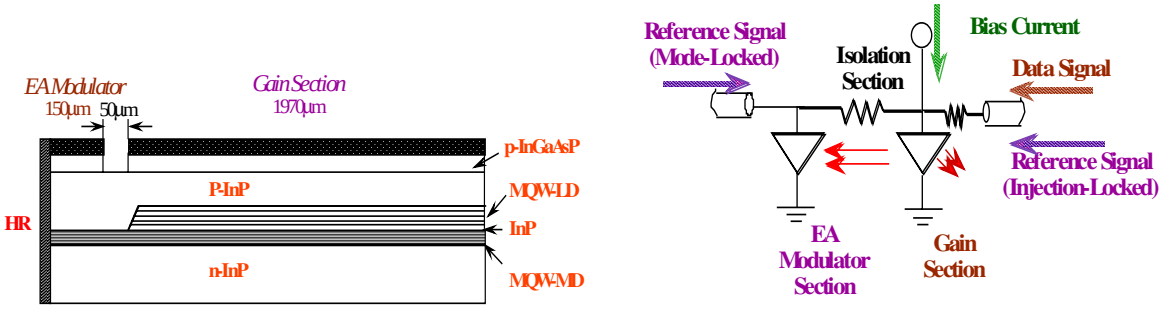

(a) (b)

Fig. 11. a) Conceptual representation of the long F-P laser integrated with an electro-absorption modulator; b) mechanical fixture used for mounting of the laser diode for injection locking, mode locking and opto-electronic conversion evaluations.

The 19.3 GHz resonant frequency has a frequency tuning sensitivity of ≈1MHz/mA. The resonance frequency is stabilized using fundamental mode-locking by modulating the EA section by a synthesized source. The close-in to carrier phase noise are measured and comparison is made against the reference signal from an HP83640A source. The results are summarized in Table I for different laser operation points. As indicated a very small phase noise degradation is observed, however the results for V_m= – 1 V is better that the results for V_m =-4.5V for the same laser current of I_b=140mA.

		£(Ω)(dBc/Hz)		Δ(dB)	
f_m (GHz)	V_m (V)	Ω=100Hz	Ω=1kHz	Ω=100Hz	Ω=1kHz
19.13400	-4.5	-75.4	-81	2.6	2.4
19.29469	-2.5	-77.0	-82	1.0	1.1
19.29406	-1.0	-77.6	-82	0.4	0.4

Table I. Phase noise degradation of the LO signal as a function of various offset frequencies and laser operation points.

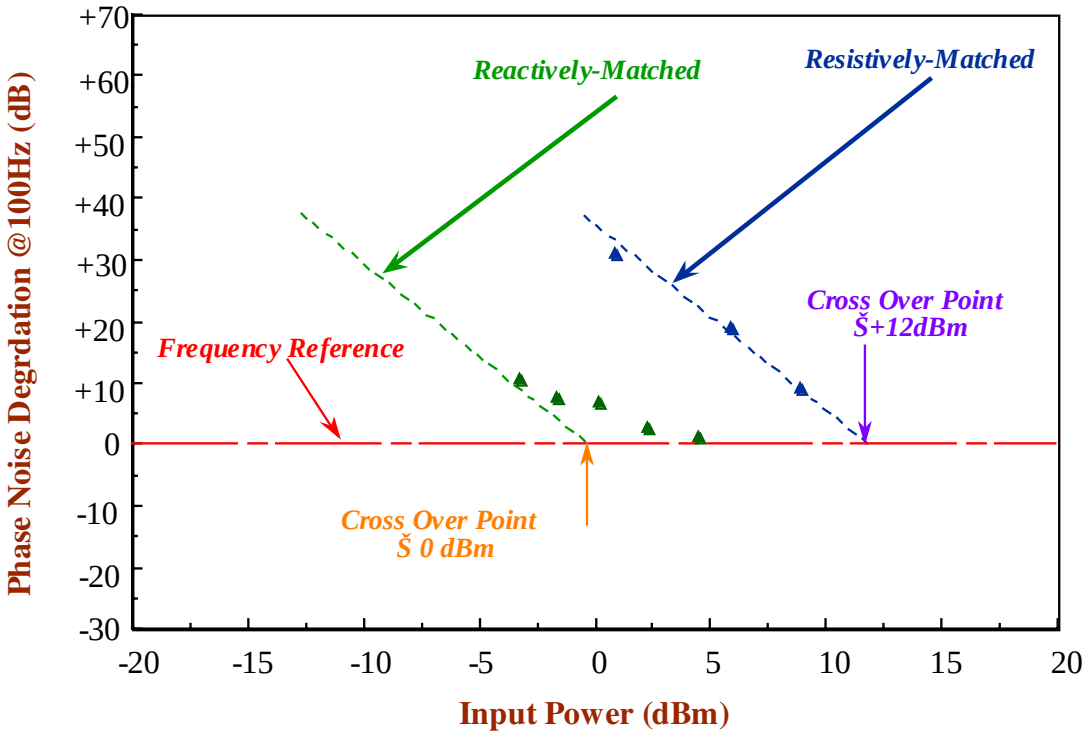

Fig. 12. Measured FM noise degradation at 100Hz offset carrier for the injection locked intermodal oscillation. The measured injection locking power of the long F-P laser diode are also depicted at the cross over point for the resistively- (▲) and reactively-matched (▲) lasers.

Since this stabilized signal has much cleaner close-in to carrier phase noise than the free-running oscillation, it could be employed as the LO signal. The laser diode's gain section is forward biased (I_b = 140 mA) and the EA modulator section is reverse biased (V_m = -1V). This operating point is selected because of the efficient mode-locking process while maintaining the least amount of phase noise degradation of the carrier signal. The laser diode optical output is collimated to a single mode optical fiber using a polarizing collimator with an overall fiber coupling efficiency of 12%. The optical fiber output is connected to an optical receiver integrated with RF analyzer (HP70004A system). Note that HP70004A system automatically de-embeds the calibrated optical

receiver response from the measurement and displays it in the optical domain. The electrical domain power levels, in dBr, are easily calculated by multiplying the depicted optical domain results, displayed in dBm, by a factor of 2.

Next the gain section of this laser is modulated by S-band signals (2.2 GHz ± 50 MHz). Strong nonlinearity of the mode-locked laser at the LO signal of 19.3 GHz up-converts the S-band signals to 17.1 GHz and 22.5 GHz as shown in Fig. 13. The data modulation power level is changed over a wide range. An optical conversion loss is defined as the ratio of the generated mixed RF signal (19.3 ± 2.2 GHz) to the IF signal (2.2 GHz). The optical conversion loss is as low as 1.4 dB resulting in the electrical conversion loss of 2.8 dB. The opto-electronic conversion loss for the lower side-band (LSB) at 17.1 GHz is higher than the upper side-band (USB) of 22.5 GHz by 1.3 dB (i.e., 2.6 dB electrical) [14].

On the other hand, a modulation loss greater than 51 dB is measured when the gain section is directly modulated by the RF signal at 17.1 GHz. The spurious-free dynamic range (SFDR) of this opto-electronic mixer is also evaluated. The intermodulation distortion (IMD) measurements are conducted for two modulating tones which are 5 MHz apart (e.g., f_1 = 2.200 GHz and f_2 = 2.205 GHz). Both tones are up-converted by stable LO signal of 19.360 GHz and IMD of the up-converted RF signals are measured at LSB and USB frequencies. Based on the mode-locked laser IMD and RIN noise measurement results for the up-converted RF tones, SFDR LSB and USB RF signals are ≈ 88 dB.Hz$^{2/3}$ and 89 dB.Hz$^{2/3}$ respectively.

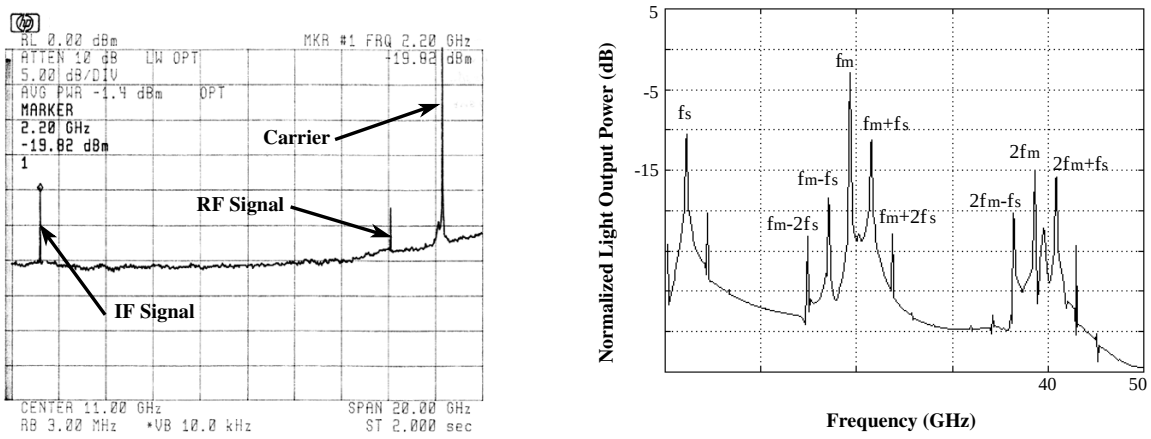

(a) (b)

Fig. 13. Opto-electronic mixing of data signal with local oscillator signal in the mode-locked long FP laser diode. a) Experimental results for the operating condition is I_b = 140 mA, V_m = -1 V, f_m = 19.360 GHz, P_m = +15 dBm, f_{data} = 2.200 GHz, and P_{data} = -25 dBm. Data, lower side-band RF, and local oscillator signals (center frequency of 11.0 GHz and frequency span of 20.0 GHz); b) simualtion results based on travelling wave rate equation [15].

4.0. CONCLUSIONS

Fiber fed wireless communication is considered for mobile and fixed-point communications in micro and pico-cellular as well as many military ad-hoc WLAN scenarios. This paper has addressed fiber optic distribution of analog data in terms of link gain and dynamic range and frequency reference signal for generation of a coherent local oscillator signal in terms of AM/PM conversion. Moreover, distortion induced by SRS in

dense WDM systems is discussed. Fiber optic links based on directly modulated could meet cost-performance for many applications, even though monolithically integrated EA modulators are becoming very attractive. (This topic is discussed in a paper in this proceedings dealing with the state-of the-art of devices and circuits by Prof. Dieter Jaeger.)

A monolithically integrated FP laser with EA modulator is employed to simultaneously transmit frequency reference of data signals. The analytical models indicate that stabilized LO signal at 19.3 GHz can be attained using injection locking and mode-locking. The achieved close-in to carrier phase noise of the stabilized LO signal is lower in the case of injection locking than mode-locking for the same modulating power level. The opto-electronic mixing of 19.2 GHz LO and S-band data is also feasible using this device with SFDR as high as 90 dB. $Hz^{2/3}$. Moreover, optoelectrnic mixing can occur in a mode-locked laser, creating possibility of generating RF signal from frequency reference and data signals, thus bypassing the need for integration with electrical mixers in the up- and down-conversion. (A similar approach using attractive microchip laser is presented in this proceedings by Prof. Tibor Berceli.)

ACKNOWLEDGMENT

The author wishes to acknowledge the contribution of many of his students, partciularly Dr. Edward Ackerman, Mr. Adam McInvale, Dr. Tsang Der Ni, Dr. Xiangdong Zhang, and Dr. Joong Hee Lee.

REFERENCES

[1] A. S. Daryoush, E. Ackerman, N. Samant, D. Kasemsat, S. Wanuga, "Interfaces for High-Speed Fiber Optic Links: Analysis and experiment," *IEEE Trans. on Microwave Theory and Techniques*, vol. 39, no. 12, Dec. 1991.

[2] Edward Ackerman, Photonics Inc., Private Communications.

[3] K. Emura, “Technological Choices in Optical Fiber Feeding Wireless Access Systems,” Microwave Photonics Satellite Workshop, Dec. 1996, Kyoto, Japan.

[4] A.R. Chraplyvy, P. S. Henry, "Performance degradation due to stimulated Raman scattering in wavelength-division-multiplexed optical-fiber systems," *Electron Lett.*, Vol. 19, No 16, August 1983.

[5] A.R. Chraplyvy, “Limitations on Lightwave Communications Imposed by Optical-Fiber Nonlinearities,” *J. of Lightwave Technology*, Vol. 8, No. 10, Oct. 1990.

[6] Z. Wang, et. al., “Effects of Cross Phase Modulation in Wavelength SCM Video Transmission Systems,” *Electronics Lett.*, Vol. 31, No. 18, August 1995.

[7] T. E. Darcie et. al., “Lightwave Multi-channel Analog AM Video Distribution Systems,”*IEEE International Conference on Communications*, Boston, MA, June 1989.

[8] Z. Wang, A. Li, C.J. Mahon, G. Jacobsen, and E. Bodtker "Performance Limitations imposed by Stimulated Raman Scattering in Optical WDM SCM Video Distribution Systems", *IEEE Photonics Techn. Lett.*, Vol. 7, No. 12, December 1995.

[9] M.R. Phillips and D.M. Ott, “Crosstalk Due to Optical Fiber Nonlinearities in WDM CATV Lightwave Systems,” *J. of Lightwave Technology*, Vol. 17, No. 10, Oct. 1999.

[10] X. Zhang, T.D. Ni, and A.S. Daryoush, “Laser Induced Phase Noise in Optically Injection Locked Oscillator,” *Digest of IEEE 1992 MTT Symposium*, pp.765-768, 1992.

[11] X. Zhang and A.S. Daryoush, "Bias Dependent Low Frequency Noise Up-Conversion in HBT Oscillators", *IEEE Microwave and Guided wave Letters*, vol. 4, no. 12, pp. 423-425, Dec. 1994.

[12] T.D. Ni, X. Zhang, and A.S. Daryoush, "Experimental Study on Close-in carrier Phase Noise of Laser Diode with Coherent Feedback," *IEEE Trans. Microwave Theory and Techniques*, vol. 43, no. 9, pp. 2277-2283, Sept. 1995.

[13] K. Lau, “Short-Pulse and High-frequency Signal Generation in Semiconductor Lasers,” *IEEE Journal of Lightwave Technology*, Vol. 7, No. 2, pp. 400-419, Feb. 1989.
[14] A.S. Daryoush, K. Sato, K. Horikawa, and H. Ogawa, “Efficient Opto-electronic Mixing at Ka-Band using a Mode-locked Laser,” *IEEE Microwave and Guided Wave Lett.*, vol. 9, no. 8, pp. 317-319, August 1999.
[15] A. S. Daryoush, et al., “Applications of Opto-Electronic Mixing in Distributed Systems” Digest of *2001 Topical Symposium on Millimeter Wave, TSMMW2001*, Yokosuka, Japan, pp. 175 – 178, March 2001.

Novel Microwave Photonic Techniques in the Future Military Systems

Afshin S. Daryoush
Department of Electrical and Computer Engineering
Drexel University, Philadelphia, PA 19104, USA

Daryoush@ece.drexel.edu

Abstract

This paper reviews a number of novel applications of microwave photonic techniques in future military systems. One category is light interactions with microwave devices and circuits, which has contributed to the beginning of microwave photonics. The performance of HBT is the most attractive over FET and HEMT devices, due to its I-V dependence on high bandwidth and optical sensitivity. Moreover, different techniques of optical ADC are reviewed and among them all-optical ADC has the greatest promise of achieving high bit resolution. Microwave spectroscopy of biological tissues provides opportunity to create tomographic images of brain and breast, which leads to low-cost and reliable health monitoring of military personnel. A higher spatial resolution is obtained when a higher modulating frequency is employed. Finally, a new microchip laser is developed to generate frequency agile sources at microwave photonics. Optical sources operating at a fixed temperature will correspond to a beat signal, where a low phase noise beat signal is produced.

1. Introduction

In the last few years novel microwave photonics techniques are developed that lead to superior performance over purely electronic systems. Some examples of these techniques are reviewed that may form the basis of future robust military systems. The first approach is based on light interactions with microwave devices. A review of the previously established optically controlled devices and circuits are made and example of clock recovery circuit up to 100Gb/s is discussed. Next the concept of optical analog-to-digital converter is presented with capability of reaching 50 GSPS. Finally an approach based on diffused photon near infrared imaging technique is discussed leading to monitoring systems for pilot overload. As the modulation frequency expands in to upper microwave frequencies, spatial resolution increases. A microchip laser is presented which can be used as a chirped laser source with applications in lidar and medical imaging.

2. Light Interaction with Devices and Circuits

From early beginning of optical control of TRAPPAT and IMPATT in 1970, optical control of semiconductor devices has provided the promise of remote control along with isolation of optical source from other electrical sources. Over time a number of techniques have been developed to control performance of a number of devices and circuits using optical interactions. Various optically controlled microwave subsystems

Paper presented at the RTO SET Lecture Series on "Optics Microwave Interactions", held in Jouy en Josas, France, 2-3 September 2002; Duisburg, Germany, 5-6 September 2002; Budapest, Hungary, 9-10 September 2002, and published in RTO-EN-028.

have been demonstrated in the last twenty years, such as OCO and optically tuned filters [1], phase shifter [2], amplifiers [3], switches[4], and antennas [5]. Even though these techniques are intriguing, but have not found significant applications yet. More recently, spurred by rapid developments in fiberoptic based networks (MAN and LAN), the chip level integration of photonic and microwave components for high performance optical receivers have gained attention. PIN-amplifier configurations, such as PIN-HEMT [6] have been reported, and lately high performance PIN -HBT combinations have been realized by Aitken et. al. [7]. The three terminal microwave devices are attractive to perform photodetection and control functions in the receiver front-end [8, 9]. This configuration enhances receiver performance by reducing parasitics, requires less pre-amplification due to intrinsic gain of transistors, and has lower power consumption and less costly fabrication.

The key to these developments and related applications in communications and control of microwave systems is the understanding of the optical properties of microwave devices. Professors Seeds and Salles provided an excellent overview on this topic in 1990 [10]; however, since then the developments of HBT have brought more emphasis on the subject. Particularly photo-response of HBT, MESFET and HEMT could be unified and a comparison is made in terms of inherent photo-detection mechanism, gain, sensitivity, and bandwidth.

Static Analysis: Table I summarizes various effects that contributes to the photoresponse of the HBT, MESFET, HEMT, and its comparison to PIN photodiode. (The performance of PIN photodiode is considered as baseline.) For PIN photodiode the photoresponse current is determined by the photo-generated electron-holes pairs in the intrinsic region and no current gain is experienced. The light level directly controls the photocurrent in a linear fashion. On the other hand in HBT, in addition to photo-generated electrons at the collector depletion region, there is an increase in the effective base current due to the drift of photogenerated holes from the collector depletion region to the base. This source of this term is change in current injection rate due to change in base voltage and hence is labeled as internal photoconductive effect; since this increase occurs under constant bias current, it results in current gain. The photoresponse of the HBT is linear with optical power.

	Ipvi		**Ipvx**		**Ipc**		**Ipci**		**Ipd**	
	gain	**speed**	**gain**	**speed**	**gain**	**speed**	**gain**	**speed**	**gain**	**speed**
PIN	------	------	------	------	-----	-----	------	------	none	very fast
HBT	------	------	------	------	-----	-----	moderate (linear)	fast	none	very fast
FET	large (log)	slow	large (log)	very slow	small	fast	------	------	------	------
HEMT	large (log)	slow	large (log)	very slow	small	fast	------	------	------	------

Table I . Sources of photo-detection mechanisms in popular microwave semiconductor transistors and their comparison to PIN photodiode as baseline.

On the other hand, the photoresponse in both field effect transistors (MESFET and HEMT) is attributed to three mechanisms [11]. The photogenerated carriers collected at the gate yield a photovoltage V_{phx}, when passing through an external resistor. Thus the *external photovoltaic* increases in gate bias, which opens the channel and results in a photocurrent of $I_{pvx} = g_m V_{phx}$. The *internal photovoltaic effect* results in $I_{pvi} = g_m V_{ph}$, where for MESFET [12] V_{ph} is a light-induced modulation of the channel height and in the case of the HEMT, V_{ph} represents a shift in the quasi-Fermi level [13]. The *photoconductive effects* I_{pc} are very small, and are neglected. The optical responsivity of microwave semiconductor transistors is compared in Fig. 1. At low illumination the logarithmic response of FET devices provides large gain. However, photoresponse saturates rapidly, which limits their dynamic range. The HBT, which has relatively large dark current, but low noise [14], performs best at moderate and high illuminations.

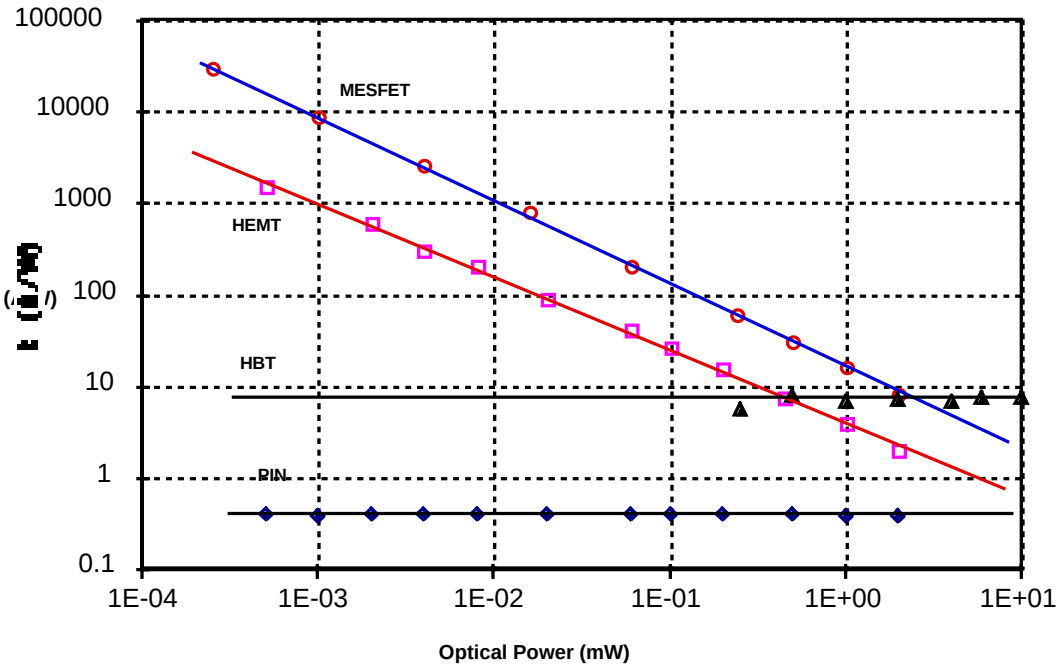

Fig. 2 Comparison of the static light responsivity for microwave transistors and their performance comparison to PIN Photodiode as a baseline. (Courtesy of Prof. P.R. Herczfeld of Drexel Univ.)

Dynamic Response: The frequency response of a PIN is limited by the carrier transit time, where a shorter intrinsic region yield a faster response but this behavior is at the expense of quantum efficiency for vertical devices. (Traveling wave photodiodes are designed to simultaneously meet high power handling, speed, and efficiency requirements.) The speed of the HBT is governed by sum of different time constants associated with the charging time of the B-E junction, the base transit time, the charging time of the B-C junction, and the transit time across the collector depletion region. The optical response of the HBT is fast since these time constants are the same as those which determine the HBT ultra high-speed response. Whereas for the FET devices the external photovoltaic effect is very slow because of the long charging time of the gate external circuit. The MESFET's dynamic response is dominated by the dynamics of the internal photovoltaic effect, which is defined by the RC time constant of substrate resistance and

the epi-layer/substrate junction capacitance [14]. For the HEMT, on the other hand, the RC time constant, determined by the buffer resistance and the change in electron concentration in the 2-DEG channel [12], defines the speed. It is important to note that the speed of photoresponse of the FETs is independent of their microwave speed.

The measured and calculated frequency response for these devices is depicted in Fig. 2. At low frequencies FETs perform well, but the intrinsically slow photovoltaic effect yields a small gain-bandwidth product. The speed of the HBT and PIN is comparable. Note, increasing the coupling of efficiency of the HBT from 1% to 10%, which is a feasible task, will reduce the link insertion loss by 20dB, and thus supersedes that of the PIN. Using devices with larger β (e.g. 250 instead of 25) will also give additional advantage to the HBT.

Recent publication on nonlinear behavior of high-temperature superconducting film as photomixer has provided opportunity to generate THz signals using the kinetic inductive photoresponse [15]. These new applications maintain interest in light interaction with microwave circuits.

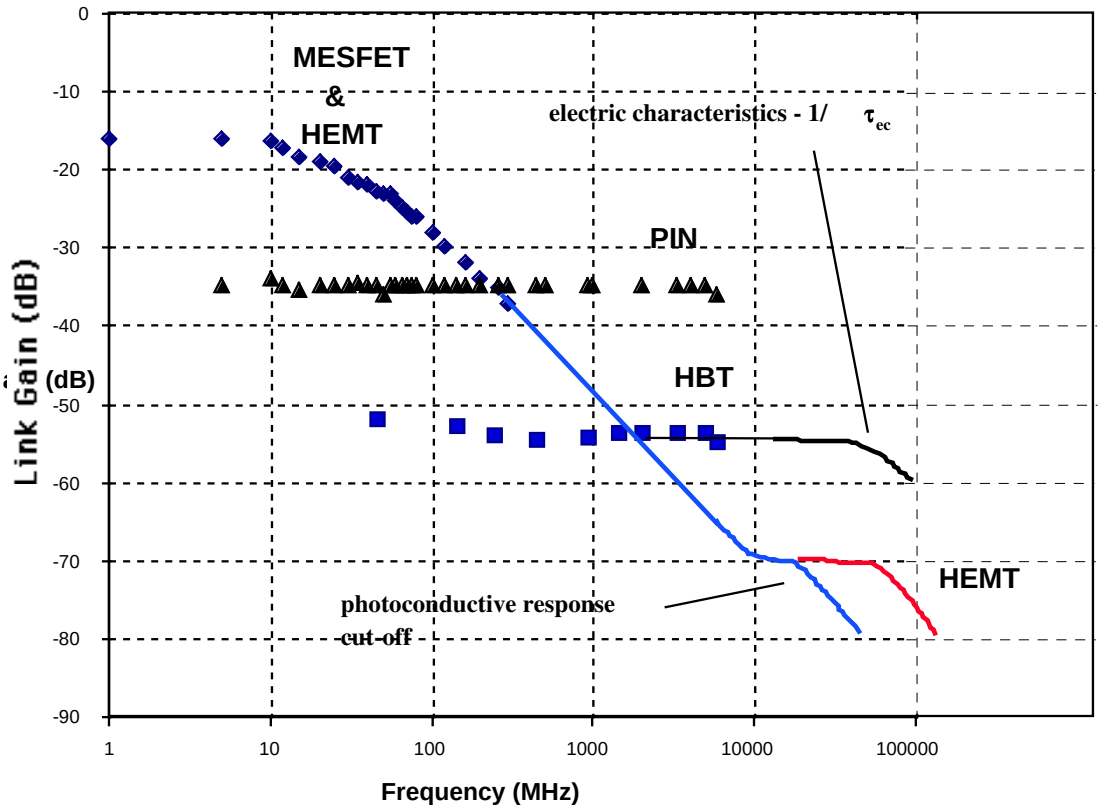

Fig. 2. Frequency response of microwave devices, measured data is represented by discrete points and theory by solid lines. The optical coupling efficiencies were calculated to be less than 1% for the HBT, 4% for the MESFET and the HEMT and 60% for the PIN. (Courtesy of Prof. P.R. Herczfeld of Drexel Univ.)

3. Optical ADC Techniques

Optoelectronic devices have demonstrated ultra-fast switching speed and mode-locked lasers have achieved high-speed and accurate optical pulses. With capability of sampling electrical signals at resolutions of sub-picoseconds, implementation of optical Analog-to-Digital Converter has long intrigued many researchers due to it s following advantages. Since optical sampling has time jitter that is about 2 orders lower than electronic clock. Second, optical sampling decouples sampling electrical signal and sampled optical signals. Third, optical sampled or quantized signal is easy to distribute by fiber and remotely controlled. Also, many photonic ADC approaches also produce output as Gray-codes directly, eliminating the need for additional encoding circuits. However optical quantization is generally limited to resolution of a few bits and this remains a big challenge. There are two approaches to quantize the information after sampling by optical signal: i) hybrid optic-electronic ADC, where electrical quantizers are employed; and ii) all-optical ADC, where optical quantization is implemented.

Hybrid optic-electronic ADC: Hybrid optic-electronic ADC, or called optically assistant ADC, employs optical sampling followed by electronic quantization. It attempts to combines advantages of both optical and electronic ADC technologies: high-speed rate of optical sampling and high resolution of electronic quantization. But the speed of electronic devices is much lower than the optical sampling rate. So the sampled optical signal has to be down converted to lower speed and channeled to parallel electronic quantizers. For example, 100 GSPS sampled pulses can be split into 8 channels in time domain, and the pulse rate in every channel is 12.5 GSPS. Most optical sampling transducers are implemented with Mach-Zehnder modulators [16], where the output intensity of the Mach-Zehnder interferometer is function of the applied voltage:

$$I_{out} = I_i \cos^2(\frac{\varphi_0}{2} - \frac{\pi V}{2V_\pi})$$

where $\varphi_0=2\pi nL/\lambda_0$, the optical distance of a branch, and V_π is the half-wave voltage, defined as the applied voltage at which the phase shift changes by π. Optical sampling operates in a small range around V_π, the output is approximately linearly proportional to applied voltage V. To extend the linear range of Mach-Zehnder modulator, a number of linearization approaches were demonstrated. In photonic ADC, the linearization can be implemented in digital domain by directly inverting the transfer function in DSP.

The key issue in hybrid opto-electronic ADC is to channelize high speed sampled optical pulses and ensure channels matching in amplitude and time. Based on approaches of channelization, three major schemes are proposed as: a) time interleaving [17], b) WDM channelized [18], c) time stretched [19]. The optical sampling and time interleaving is employed by Juodawlkis et al to implement an ADC with bandwidth up to 505 MSPS by using 1:8 optical demultiplexers and 14-bit electrical quantizers. A dual-output $LiNbO_3$ MZ modulator is used for linearization processing and a 65 dB SFDR and 47 dB SNR, corresponding to an effective resolution of 7.5 bits. The sampled optical pulses are split into 8 channels by optical time division demultiplexers, which are composed of 3 stages of 1×2 switches controlled by 505 MHz driving signals. Therefore the 16 parallel high-resolution electronic quantizers are working at 63 MSPS [18]. To achieve an interleaving SFDR of 80 dB, the converter-to-converter gains must be

matched to ~0.01%, the offset must be matched to ~0.01% of the signal amplitude, and the converter-to-converter crosstalk must be less than one part in 10^4.

On the other hand using optical dispersive components, multi-wavelength optical wave is smeared (for continuous spectrum) or split (for discrete wavelengths) in time, borrowing concept from WDM communication, the sampled optical signal can be channelized in both wavelength and time domains. The RF signal is sampled by the WDM pulses and then channelized by a WDM demultiplexer. Clark et al demonstrated a 100-GSPS photonic ADC based on the time- and wavelength-interleaved scheme [18] using mode-locked fiber laser (MLFL) that generates 12.5 GHz pulse train, and 100-GHz sampling optical pulses is obtained by an 8× multiplexer. The pulses propagate through different fiber delays and attenuators which then are recombined in the WDM. The delay fibers and attenuators can be adjusted for time matching and amplitude equalizing respectively. The time interweaved pulse train is then demultiplexed in to 8 channels according to wavelengths. The resulting parallel pulses are then to be quantized by >12.5 GSPS quantizers, but an 8-bit ADC operating at only 781 MSPS was achieved with SNR of 22~26 dB, which corresponds to about 4 bits. The resolution of wavelength channelized ADC is still limited since it faces to similar difficulties as the time interleaving ADC does. The time uncertainty and amplitude uniformity between channels are difficult to control.

Bhushan et al demonstrated a record ultra-fast sampling rate of 130 GSPS using time stretching approach [19]. The idea behind this ADC is similar to wavelength channelized ADC, but in time stretched RF input signal modulates a broadband optical continuous wave (CW) other than is sampled by optical pulses with discrete wavelengths. The detected analog optical signal is sampled and quantized by electronic ADC. Fig. 3 shows a limited time application of time stretch preprocessing, where a passively mode-locked fiber laser with 20-MHz repetition rate followed by a 17 nm filter is used to generate broadband short pulses. The optical pulse propagates through a dispersive fiber of length L1 and dispersed in time to get 0.8 ns time aperture. The wave is then modulated by RF signal to be converted. The modulated wave is sent to another piece of dispersive fiber of L2 to be stretched in time domain. The ADC obtain a stretch ration of M=16.2 by proper choosing L1 and L2, where then the stretched signal is detected and digitized by a single 8-GSPS electronic ADC of an oscilloscope. So the effective sampling rate is about 130 GSPS (8GSPS × 16.2) with SNR of 45 dB, corresponding to 7.5 bits of resolution.

On the other hand for continuous signals in time, a parallel architecture must be used in order to preserve the information. In this process an arrayed waveguide grating (AWG) is employed to sample a portion of the optical spectrum and since each optical wavelength corresponds to a different propagation time delay, the filter performs sampling in time. Then each segment is time stretched by the same factor M prior to entering a slow electronic ADC, however both time alignment and amplitude in balance between various arms of are crucial.

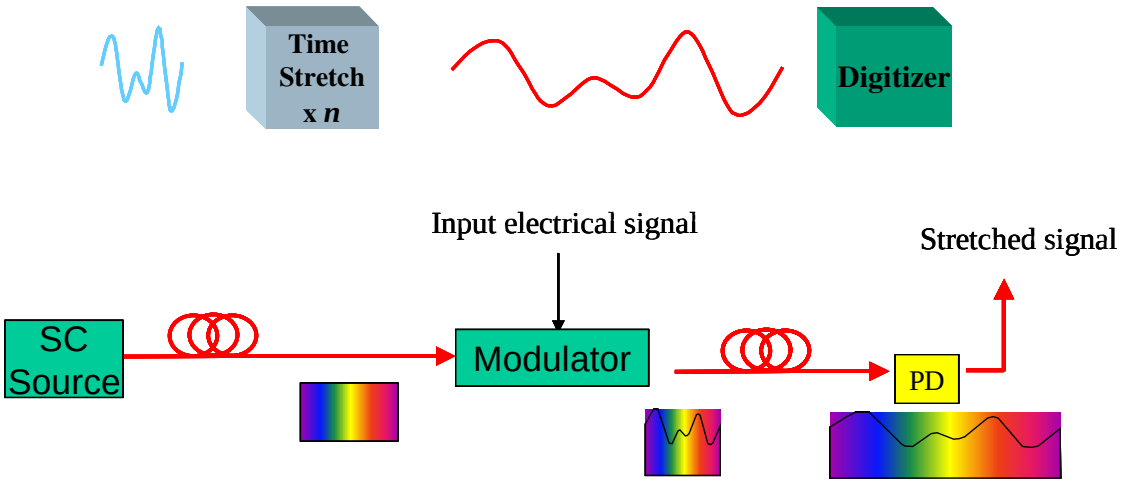

Fig. 3. Time limited signal converted by time stretching ADC [19]. (Courtesy of Prof. Jalali from UCLA)

All-optical ADC: There are quite a few ways to implement optical quantization, but probably the best known photonic ADC is based on by Taylor patent of 1977 [20]; a revised design called optical folding flash ADC in 1995 [21]. Fig. 4 shows a block diagram of a 4-bit optical folding-flash ADC. The geometrical scaling of V_π or electrode length is eliminated by a parallel-serial combined configuration. This scheme uses identical electrode length but sets DC bias at different points on the interferometer transfer characteristic curve. The resulting transfer function of MSB-2 and LSB branch is obtained by multiplying the functions of all stages at different bias and show doubled frequency comparing to previous bit. However this scheme also presents some additional challenges. First the MSB is susceptible to high noise because of the slow changing slope at digital edges. Second, the transit time limitation is still not eliminated; moreover, the hardware complexity increases exponentially in term of interferometer number as $2^{(b-1)}+1$ and it strongly relies on accurate bias.

Another way to quantize optical signal is to exploit variable electro-absorption semiconductor modulators demonstrated by Hayduk et al [22]. The quantization is achieved using an architecture that relates the

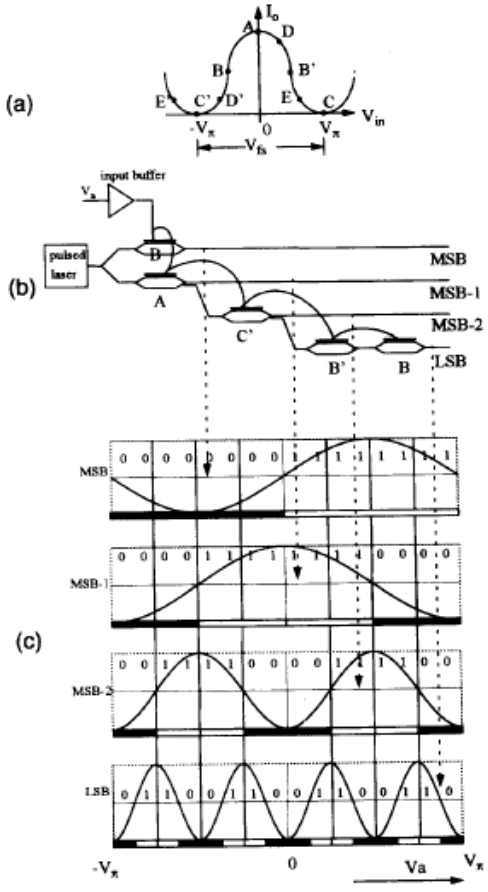

Fig. 4. Optical folding-flash ADC [21]. a) various bias points of all optical ADC, b) realization of MZ modulators for quantization, c) the received signal levels for each significant bit.

received analog voltage to an optical intensity, which shares the same idea with electronic flash ADC, in which 2^N-1 comparators with different threshold are used. The use of the passive materials in this flash photonic ADC architecture with no external voltage requirement makes this module very low power dissipation. The authors claim that the ADC has potential to operate at more than 100 GSPS combined with resolution as high as 12-14 bits. But this scheme is susceptible to amplitude fluctuation and unbalanced energy splitting. A similar idea is also employed in all-optical ADC quantization using photodetectors with different sensitivities [23].

In the two ADC schemes mentioned above, RF signal is sampled and quantized by optical amplitude. However the amplitude errors are strongly depends on source fluctuation, device linearity and loss along the optical link. So it is hard to build high resolution all-optical ADC based on optical amplitude. An all-optical ADC working in spectrum domain is demonstrated by Zmuda et al [24], as shown in Fig. 5. The input signal is sampled by a tunable laser and quantized by processor filters with binary behavior. The output wavelength of the tunable laser is modulated by the applied electrical field so the electrical amplitude is represented as wavelength in spectrum domain. The post-sampled light is processed by a parallel optical filter array. If the spectrum line falls into the pass band, the output is represented as "1", otherwise a "0" will be read. Each filter has periodic equally spaced passband and stopband and organized in a Gray code manner.

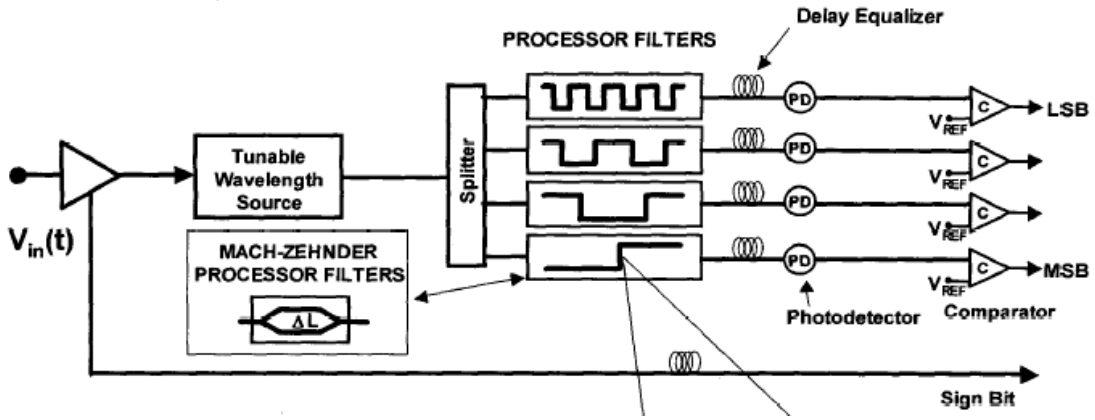

Fig. 5. Optical ADC using tunable laser and filters [24].

The major challenges for this scheme are the filter design of sharp transition and tunable laser. A 4-bit optical ADC using Bragg grating filters and ring cavity tunable laser is proposed and analyzed. Because of the convergence time limitation of Fabry-Perot cavity, only 4 bits of resolution can be achieved at 10 Gs/s. And the performance of Bragg grating filters (Fig. 6) show limited resolution. The authors proposed a folding circuit to enhance its resolution, where a Mach-Zehnder interferometer performs the optical folding circuit and first- or second-order linearization circuit corrects the nonlinear folded signal. So two low resolution ADCs are coupled with the folding circuit to achieve M+N bits of resolution. The author claimed the ADC would be able to operate at conversion speeds in excess of 10 GHz with up to 10- to 12-bits of resolution. However, it is not clear how the upper M-bit ADC achieved the additional 6 to 8 bits. But it indicates a promising way to perform analog-to-digital in spectrum domain.

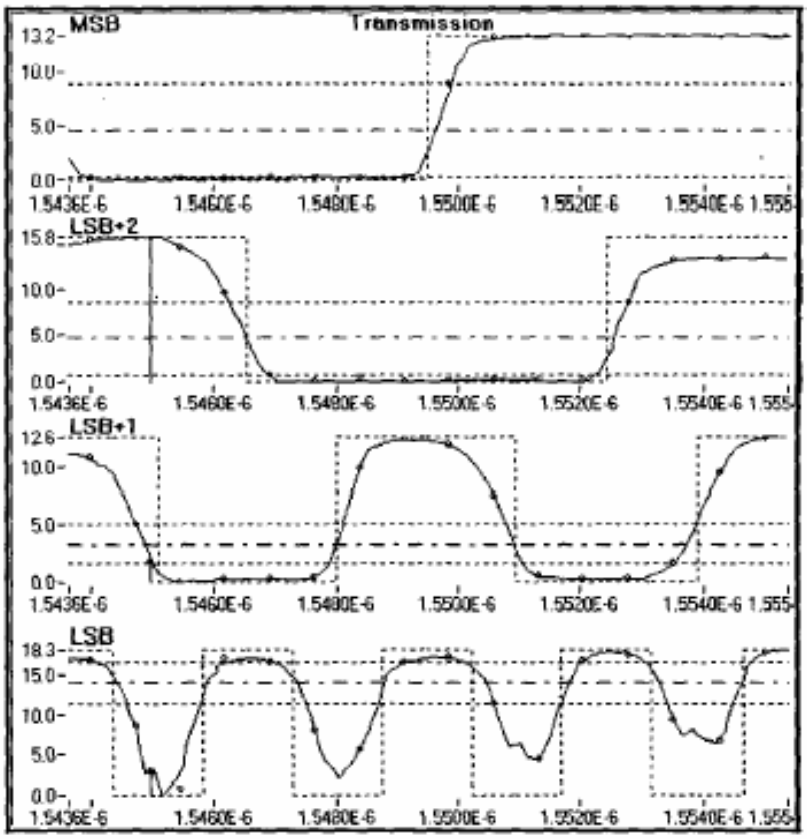

Fig. 6. Performance of Bragg grating filters [24].

4. Near IR Optical Spectroscopy

Near Infrared (NIR) spectroscopy is a new, non-invasive technique to analyze living tissue. In NIR spectroscopy, the main aim is to extract the optical properties (absorption and scattering) of the living tissue. Absorption information is used to characterize the concentration of biological chromophores, such as hemoglobin (in oxy and de-oxy forms), which in turn indicates the physiological changes in blood. This approach could be employed for health monitoring purposes, such as pilot overload in combat aircrafts. Scattering information provides information on composition, density, and organization of tissue structures, such as cells and sub-cellular organelles [25, 26]. Therefore, NIR techniques provide information about disease-related functional and structural changes. More specifically, it has been shown recently that physiological changes such as ischemia, necrosis and malignant transformation can produce

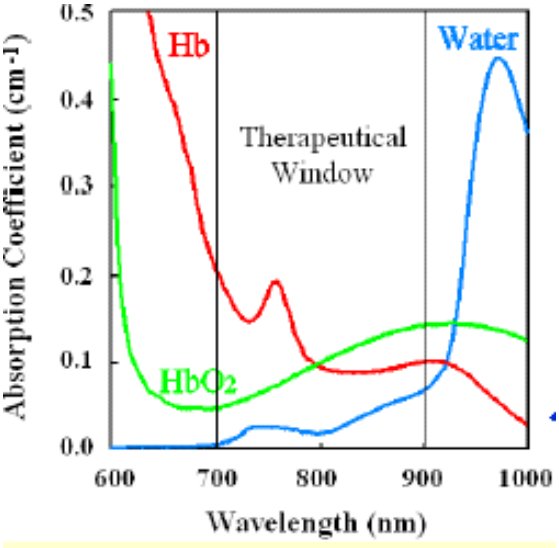

Fig. 7. Absorption spectrum of Hb (deoxy-hemoglobin), HbO2 (oxy-hemoglobin), and water in the NIR region.

important perturbations in tissue optical properties [27]. The importance of NIR spectrum lies in the fact that in this region tissue absorption is much lower than the other parts of the spectra (see Fig.7). Apart from tissue information content, this region is attractive since NIR instruments are inexpensive to construct and are easily portable. These features allow NIR instruments to be an attractive alternative to other techniques, such as MRI. Moreover, NIR light is not an ionizing radiation; therefore, it can be used as a usual clinical monitoring of patients in radiation therapy.

The modulated NIR could be employed for greater spatial and temporal information and could be explained based on the following physical foundation. When photons enter a turbid (multiply scattering) media, the photons scatter randomly in all directions, diffuse through the medium, and get absorbed during this diffusion process. When source detector separation is large enough and scattering is dominating absorption, diffusion theory is very well suited approximation for photon transport:

$$\frac{1}{c}\frac{\partial \Phi(r,t)}{\partial t} - D\nabla^2\Phi(r,t) + \mu_a\Phi(r,t) = S(r,t),$$

where Φ is the fluence rate (W/cm^2), c is the speed of light in the tissue, S is the source term, μ_a is the absorption, and D is the diffusion constant, which is related to reduced scattering constant, μ_s', by $D = 1/(3\cdot\mu_s')$. In an infinite medium for a point source photon diffusion wave (PDW) can analytically be expressed as:

$$\Phi(r,t) = \frac{S}{4\pi D}\frac{\exp(ikr)}{r}$$

where k is the complex wave vector, (i.e., $k = k_{real} + ik_{imag}$) and is described as combination of modulating frequency, diffusion, and absorption coefficients as: $k = \sqrt{-\mu_a / D + i\omega/(c\cdot D)}$. The back-scattered PDW has phase lag and amplitude attenuation relative to the source as:

$$\Theta_{lag}(r,\omega) = k_{imag}.r$$

$$A_{att}(r,\omega) = \exp(-k_{real}r)/(4\pi Dr)$$

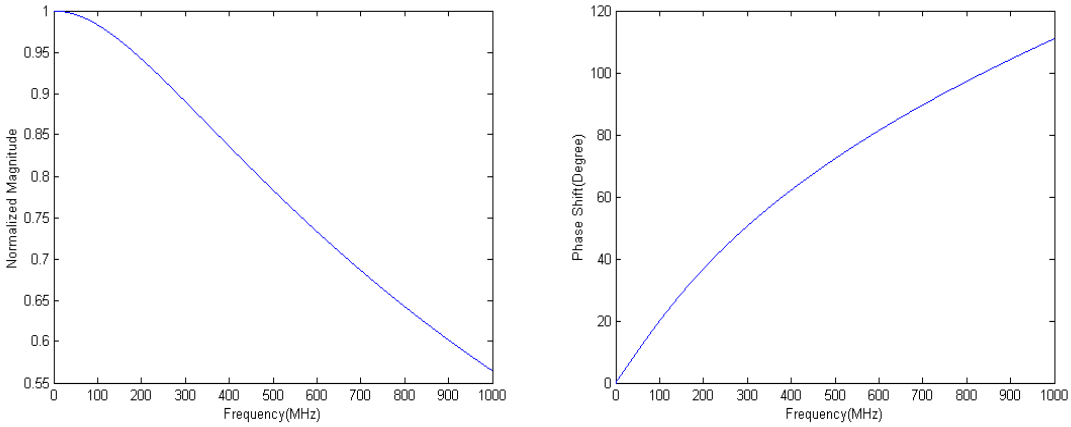

Fig. 8. Normalized amplitude attenuation (left) and phase-shift (right) of photon density waves as a function of frequency.

Fig. 8 shows the solution of amplitude attenuation and phase-shift of photon diffuse waves with respect to frequency (up to 1 GHz) for a breast tissue with optical absorption and scattering coefficients properties of $\mu_a = 0.05 cm^{-1}, \mu_s' = 10 cm^{-1}$. NIR techniques are also being used for brain imaging a seen in Fig. 9 [28, 29]. The image on the left is BOLD image from MRI. The image on the right is obtained from diffuse optical tomography.

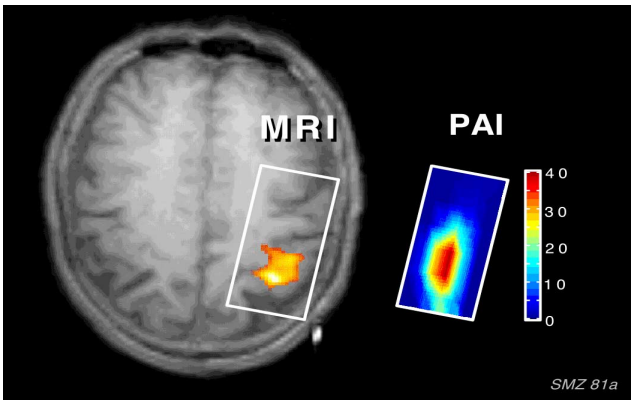

Fig. 9. Brain activation image. MRI image is shown on the left and the image from diffuse optical tomography is depicted on right. (Courtesy of Prof. Britton Chance of Univ. of Pennsylvania.)

NIR technique uses constant wave (CW), time-domain, and frequency domain instruments according to their applications and information content. The CW systems are very inexpensive, however suffers from limited resolution. Frequency domain instruments are more compact, cheaper, and algorithms are easier to handle than time-domain techniques, hence frequency-domain instruments are more attractive. In frequency-domain photon migration concept is easier too. When light is modulated with modulation frequencies in megahertz region, diffuse photon density waves (PDW) are generated, propagating with a wavelength of several centimeters [30-33]. At the detector one measures the amplitude decay and phase shift data of these waves (see Fig. 8). Amplitude and phase data are used to map the optical absorption and scattering properties of the medium. Optical constants in turn are used to obtain hemoglobin concentration, blood volume and oxygen saturation. More accuracy of the extracted results is achieved when a frequency swept mode is employed, and as the modulation frequency increases to microwave region a higher spatial resolution is attained.

5. Tunable Microchip Lasers

Compact, efficient solid-state microchip lasers, with high spectral quality, show great potential as optical transmitters for rapidly tunable sub-carrier sources in biomedical imaging and hybrid lidar-radar applications. Optical heterodyning of two ring-oscillators has been reported for millimeter-wave generation [34] using PZT tuning, which are essentially very slow processes. An alternative design topology is developed by Prof. P.R. Herczfeld and his group at Drexel University.

The basic microchip laser configuration is depicted in Fig.10, where two identical optical cavities are formed by depositing dielectric mirrors on opposite ends of a single

$Nd:YVO_4/MgO:LiNbO_3$ crystal assembly [35]. This configuration is comprised of a 0.3mm long $Nd:YVO_4$ crystal, which serves as the gain medium, and a 1.2 mm MgO:LiNbO3 crystal, which is the tuning section. The two side-by-side lasers are pumped by an 808nm high power laser diode source. Electrodes are deposited on the top and the bottom of the 1.2 mm MgO:LiNbO3 tuning section. The outputs of the two lasers are combined, coupled into a single mode fiber and transmitted to a high-speed optical detector. By applying an electrical field to one of the lasers, its refractive index is modulated, which modulates its lasing wavelength resulting at a millimeter wave signal. The difference in the optical wavelengths of two lasing sections, $\Delta\lambda_{opt}$, leads to the millimeter wave beat frequency, $f_{mm}=c\ \Delta\lambda_{opt}/\lambda_{opt}^2$. The monolithic configuration gives the device simplicity, compactness, stability, and reduced sensitivity to external temperature fluctuations. The actual device, mounted on a brass fixture, is depicted in Fig. 11.

The measured laser output power vs. pump power characteristic is depicted in Fig. 12. The threshold pump power is found to be 160mW, and the overall efficiency at 250mw pump power is approximately 12%. The frequency shift of the laser output as a function of temperature is shown in Fig. 13. From this measurement a temperature sensitivity of about 4GHz/^{o}C is measured. Considering the monolithic configuration of the device, it is expected that two laser sections are at the same temperature, and temperature drift will affect both sections similarly. Realization of two laser sections in a single crystal assembly dramatically improves the temperature stability. By varying pump current, the crystal temperature or the applied electric field the beat frequency can be tuned from DC to 90 GHz. The optical spectrum of the two laser outputs is depicted in Fig. 14. To obtain this spectrum first the two lasers are adjusted so that their lasing frequencies were identical, then one of the lasers was tuned until the peak optical powers of the two lasers were 0.3 nm apart, which corresponds to 90 GHz beat frequency.

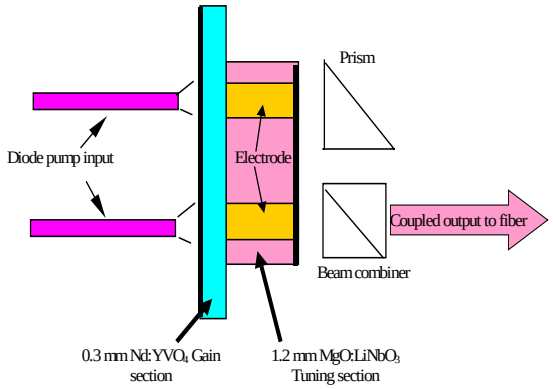

Fig. 10. The monolithic microchip laser structure [35].

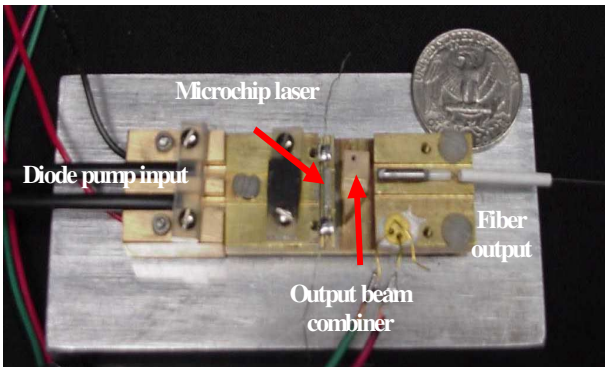

Fig.11. Picture of the heterodyne transmitter [35].

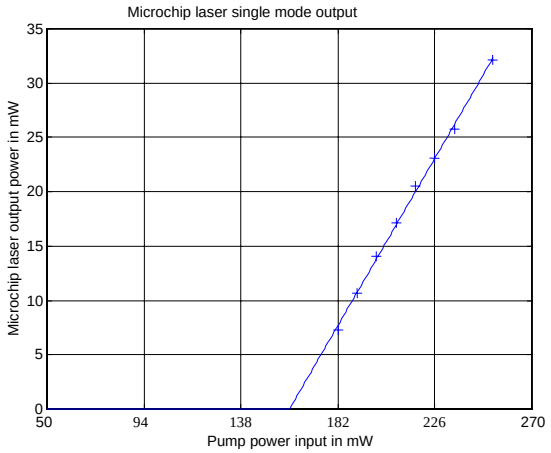

Fig. 12. The laser output power characteristics. The measured threshold pump power is 160mW [35].

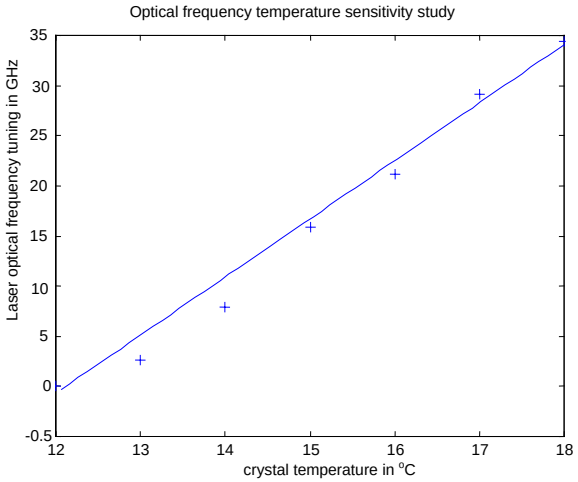

Fig. 13. Optical frequency temperature sensitivity. The optical frequency at 12°C is used as reference [35].

Chirped Heterodyne Transmitter: The experimental setup for the characterization of the chirped heterodyne transmitter is shown in Fig. 15. To generate a chirped signal, an electrical ramp voltage signal is applied to one laser while the other laser sees no electric field. Since the applied electrical field shifts the optical frequency of the laser, a chirped beat frequency is generated in the detector. The electrical voltage tuning is a very fast process, resulting in a fast chirp.

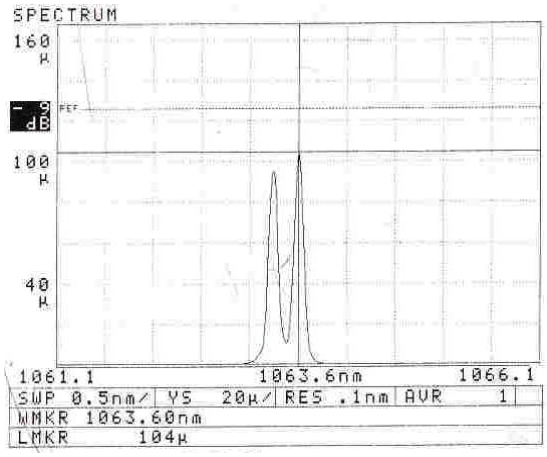

Fig. 14. Optical spectrum of the combined laser outputs. The wavelength separation is 0.3 nm [35].

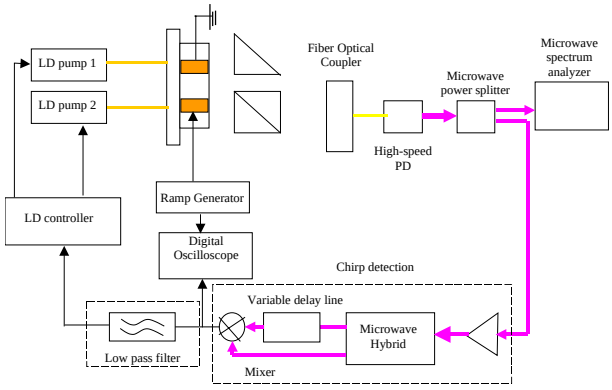

Fig. 15. The transmitter and measurement block diagram [35].

Although the monolithic laser structure provides for stability, fluctuations of the pump power can result in noise in the beat frequency. To obtain a stable signal, a feedback scheme using a microwave homodyne discriminator is introduced. The microwave homodyne discriminator is also used to recover the chirping signal. A low pass filter with stop band of 500 Hz is used to separate the slow random frequency drifting terms and fast tuning voltage induced FM terms. By this way, the feedback only tracks the low frequency drifting and it has not effect to the fast voltage tuning process.

The transmitter was tested with the beat frequency ranging from 7 to 10 GHz. Fig. 16 shows the microwave spectrum with a beat frequency of 7.889GHz. The transmitter electrical tuning sensitivity is characterized by applying 10KHz, 5volt peak-peak ramp tuning signal and measuring the output from microwave homodyne discriminator. The result, shown in Fig. 17, indicates a sensitivity of 8.8MHz/volt.

For the chirping measurement a 1MHz 10 Volt peak-peak ramp signal is applied to one of the lasers. Fig. 18 shows the recovered frequency chirping as well as the applied ramp signal in a sampling oscilloscope. A frequency beat sweep of 88.9 MHz over 0.5 μs time period was obtained. This corresponds to a 177.8GHz/ms sweeping rate. The frequency chirping resembled the ramp signal except for some distortion due to the system noise.

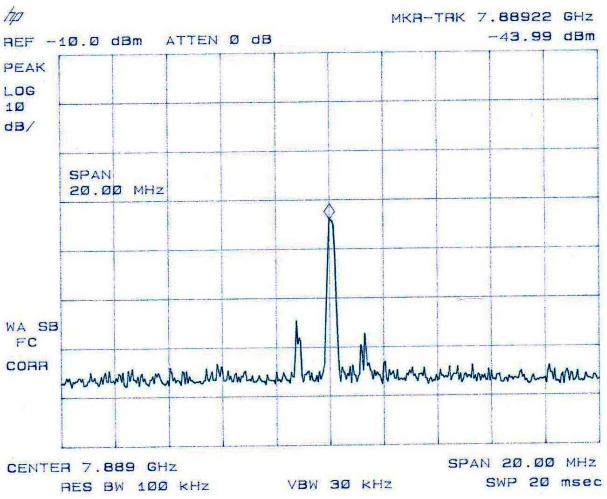

Fig. 16. Microwave spectrum of the beat frequency with no tuning signal [35].

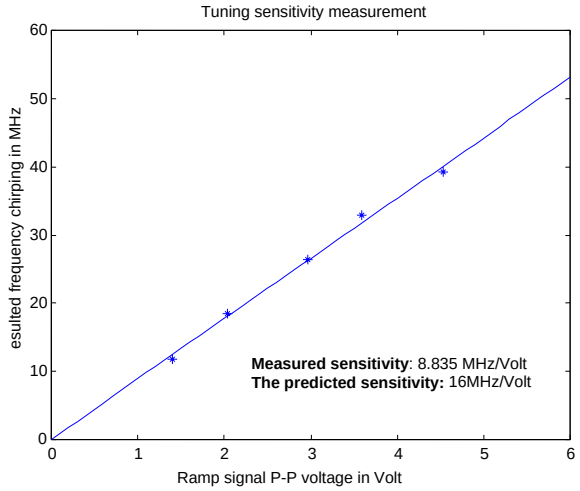

Fig. 17. Transmitter voltage tuning sensitivity [35].

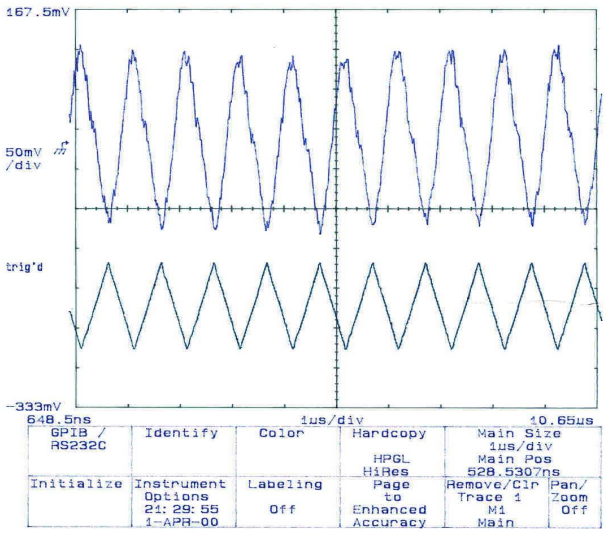

Fig. 18. Measured 1MHz repetition rate 10-volt peak-peak ramp signal modulation response. The upper trace is the recovered frequency-chirping signal. The lower trace is the applied ramp signal [35].

Conclusions

Novel devices are introduced that will lead the microwave photonics applications to a number of future military system applications. Light interaction with microwave devices and circuits will see a new resurgence, particularly in applications dealing with integrated optical detectors with microwave functions as optical clock recovery circuits and multifunction circuits such as optoelectronic mixers. HBT based devices (heterojunction photo transistor) seems to provide high gain and speed performance. Another application of microwave photonics is in development of optical ADC, where various methodologies are considered in achieving high resolution GSPS analog to digital converters. Among these approaches all optical ADC has the greatest promise. An important military application of microwave photonics is the use of photon density waves for medical imaging. The RF modulated light at microwave frequency provides a higher spatial resolution for medical imaging based on the calculated scattering and absorption parameters. The measured results will lead to blood volume of both oxy- and deoxy-hemoglobin, which enable us to develop monitoring systems to assess the pilot overload. Finally, microchip lasers are introduced where a tunable high-speed optical transmitter has been introduced. The transmitter consists of two microchip lasers co-located on the same crystal assembly. The outputs of the two lasers are heterodyned to produce a tunable millimeter wave signal. The composite cavity design provides single mode operation, while maintaining excellent efficiency. The monolithic configuration of realizing two lasers within one microchip crystal makes the transmitter more tolerant to the environmental fluctuations. A novel frequency stabilization scheme is used. The measured tuning sensitivity is around 8.8MHz/Volt. Chirping operation up to 2MHz repetition rate is achieved with good result. Thus we can conclude the tunable optical transmitter provides a good solution to chirped lidar-radar, optical/wireless communications and biomedical imaging.

References

[1] M. Belaga, *Application of an Optically Controlled PIN Diode in Microwave Circuits*, MS Thesis, Drexel University, Philadelphia, PA, 1987.

[2] P. Cheung, D.P. Neikirk and T. Itoh, “Optically controled coplanar waveguide phase shifters,” *IEEE Trans. on Microwave Theory & Techn.*, Vol.38, No.5, pp.586-595, 1990.

[3] R. Simons, “Microwave performance of an optically controlled AlGaAs/GaAs high electron mobility transistor and GaAs MESFET,” *IEEE Trans. on Microwave Theory & Techn.*, Vol.35, No.12, pp.1444-1455, 1987.

[4] A. Rosen and F.Zutavern, *High-power Optically Activated Solid-state Switches*, Artech-House Inc., 1994.

[5] A. S. Daryoush, K. Bontzos and P. R. Herczfeld, "Optically Tuned Patch Antenna for Phased Array Applications," *IEEE International APS Symposium Digest*, Philadelphia, PA, 1986.

[6] Y. Akatsu, “High-speed monolithically integrated pin-HEMT photoreceivers,” *Proceedings of the 1995 IEEE/LEOS Summer Topical Meeting*, ICs for new age lightwave communications, pp.33-34.

[7] A.L. Gutierrez-Aitken, K. Yang, X. Zhang, G.I. Haddad, P. Bhattacharya and L.M. Lunardi, “16-GHz bandwidth InAlAs-InGaAg monolithically integrated p-i-n/HBT photoreceiver,” *IEEE Photon. Tech. Lett.*, Vol.7, No.11, pp.1339-1341, Nov.1995

[8] S. Chandrasekhar, L. Lunardi, A.H. Ganuck, R.A. Hamm and G.J.Qua, “High-speed monolithic p-i-n/HBT and HPT/HBT photoreceivers implemented with simple phototransistor structure,” *IEEE Photon.Tech.Lett.*, Vol.5, No.11, pp.1316-1318, 1993.

[9] J. Lasri, D. Dahan, A. Bilenca, G. Eisenstein, and D. Ritter, “Clock Recovery at Multiple Bit Rates Using Direct Optical Injection Locking of Self Oscillating InGaAs/InP Heterojunction Bipolar Photo-transistor,” *IEEE Photon. Tech. Lett.*, Vol. 13, pp. 1355-1357, 2001.
[10] A.J. Seeds and A.A.A. de Salles, “Optical control of microwave semiconductor devices,” *IEEE Trans. on Microwave Theory & Techn.*, Vol.38, No.5, pp.577-585, 1990.
[11] A. Madjar, P. Herczfeld and A. Paolella, “A novel analytical model for optically generated currents in GaAs MESFETs,” *IEEE Trans. on Microwave Theory & Techn.*, Vol.40, No.8, 1992.
[12] M.A. Romero, *Modulation doped field effect photodetectors*, Ph.D. Thesis Dissertation, Drexel University, Philadelphia, PA, 1995.
[13] H. Ogawa, S. Banba, E. Suematsu, H. Kamitsuna and D. Polifko, “A comparison of Noise performance between a pin diode and MMIC HEMT and HBT optical receivers,” *the 1993 IEEE International Microwave Symp. Digest*, pp.225-228, Atlanta, GA.
[14] A. Paolella, A. Madjar and P. Herczfeld, “Modeling the GaAs MESFET’s response to modulated light at radio and microwave frequencies,” *IEEE Trans. on Microwave Theory & Techn.*, Vol.42, No.7, pp.1122-1130, 1994.
[15] A.H. Madjedi, S.K. Chaudhuri, and S. Safavi-Naeini, “Optical-Microwave Interaction Modeling in High-temperature Superconducting Film,” *IEEE Trans. on Microwave Theory & Techn.*, Vol. 49, No. 10, pp. 1873-1881, 2001.
[16] B. L. Shoop, *Photonic Analog-to-Digital Conversion*, Springer 2001.
[17] P.W. Juodawlkis, J.C. Twichell, G.E. Betts, J.J. Hargreaves, R.D. Younger, J.L.Wasserman, F.J. O'Donnell, K.G. Ray, R.C. Williamson, “Optically sampled analog-to-digital converters” *IEEE Trans. Microwave Theory & Techn.*, Vol. 49, No. 10, pp. 1840 -1853, Oct. 2001.
[18] T.R. Clark, J.U. Kang, R.D. Esman, “Performance of a time- and wavelength-interleaved photonic sampler for analog-digital conversion**,”** *IEEE Photon. Tech. Lett.*, Vol. 11, No. 9, pp.1168 -1170, Sept. 1999.
[19] A. S. Bhushan, P. V. Kelkar, B. Jalali, O. Boyraz and M. Islam, “130-Gsa/s Photonic Analog-to-Digital Converter with Time Stretch Preprocessor”, IEEE Photonic Technology Letters, Vol. 14, No. 5, May 2002, pp684-686
[20] H. F. Taylor, “Electro-Optic A/D Converter, US patent 4058722
[21] B. Jalali and Y. M. Xie, “ Optical folding-flash analog-to-digital converter with anlog encoding”, *Opt. Lett.*, Vol. 20, No. 18, pp1901-1903, 1995.
[22] M. J. Hayduk, “Photonic Analog-to-Digital Conversion Using Light Absorption” US patent # 6326910.
[23] J. T. Gallo, “Photonic A/D converter using parallel synchronous quantization of optical signals”, US patent # 6188342.
[24] H. Zmuda, E.N. Toughlian, G. Li, P. Li Kam Wa, “A photonic wideband analog-to-digital converter**”,** *Proceedings of the 2001 IEEE Aerospace Conference*, Vol. 3, pp. 1461 -1472.
[25] B. Chance, M. Cope, E. Gratton, N. Ramanujam, B. Tromberg, “Phase measurement of light absorption and scatter in human tissue,” *Rev. of Sci. Inst.* 69, 3457-3481 (1998).
[26] B. Tromberg, N. Shah, R. Lanning, A. Cerussi, J. Espinoza, T. Pham, L. Svaasand, and J. Butler, “Non-Invasive In vivo Characterization of Breast Tumors Using Photon Migration Spectroscopy,” *Neoplasia* 2, 26-40 (2000).
[27] J.B. Fishkin, O. Coquoz, E. Anderson, M. Brenner, and B. Tromberg, “Frequency-domain photon migration measurements of normal and malignant tissue optical properties in a human subject,” *Appl. Opt.* 36, 10-20 (1997).
[28] B. Chance, E. Anday, S. Nioka, S. Zhou, L. Hong, K. Worden, C. Li, T. Murray, Y. Ovetsky, D. Pidikiti, and R. Thomas, “A novel method for fast imaging a brain function, non-invasively, with light,” *Opt. Express*, 2, pp. 311-423.
[29] V. Ntziachristos, A.G. Yodh, M. Shnall, and B. Chance, “MRI-guided diffuse optical spectroscopy of malignant and benign breast lesions,” *Neoplasia* (in press).
[30] J.B. Fishkin, and E. Gratton, “Propagation of photon density waves in strongly scattering media containing an absorbing semi-infinite plane bounded by a straight edge,” *J. Opt. Soc. Am.*, A 10, pp. 127-140 (1993).

[31] Fantini S, Franceshini M, and Gratton E, “Semi-infinite-geometry boundary problem for light migration in highly scattering media: a frequency-domain study in the diffusion approximation,” *J. Opt. Soc. Am.*, B 11, pp. 2128-2138 (1994).
[32] J.B. Fishkin, S. Fantini, M.J. vandeVen, and E. Gratton, “Gigahertz photon density waves in a turbid medium: Theory and experiments,” *Phys. Rev.*, E 53, P. 2307 (1996).
[33] T.H. Pham, O. Coquoz, J.B. Fishkin, E. Anderson, and B. Tromberg, “Broad bandwidth frequency domain instrument for quantitative tissue optical spectroscopy,” *Rev. Sci. Inst.* 71, 2500-2513(2000).
[34] G.J. Simonis and K.G. Purchse, “Optical Generation, Distribution, and Control of Microwaves Using Laser Heterodyne”, *IEEE Trans. Microwave Theory & Techn.*, Vol. 38, No. 5, pp. 667-669, May 1990.
[35] Y. Li, A.J.C. Vieira, P. Herczfeld, A. Rosen, W. Janton, “Rapidly tunable millimeter-wave Optical transmitter for Lidar-Radar”, *IEEE Trans. Microwave Theory & Techn.*, Vol. 49, No. 10, October 2001.

This page has been deliberately left blank

Page intentionnellement blanche

Optical Beamforming Networks for Radars & Electronic Warfare Applications

Jean Chazelas
Thales Airborne Systems
2 Avenue GayLussac
78851 Elancourt Cedex
France

Daniel Dolfi, Sylvie Tonda-Goldstein
Jean-Pierre Huignard
Thales Research & Technology
91401 Orsay Cedex
France

Introduction

Future microwave systems will be generally based on active electronic antennas. This evolution is determined by requirements of improved performances of these equipments in terms of reliability, jamming resistance, flexibility for the beamforming in the transmit and in the receive mode.

Such antennas will be use in a large number of applications such as radar, communication and electronic warfare. In order to satisfy this multifunctional aspects, it will be necessary to distribute these antennas on ground based areas as well as the aircraft surface. Multistatic systems will impose multiple remoting of antennas with respect to their processing units.

In all cases, it appears a need for low loss link able to remote the control of the antennas as well as distribution and processing of very wideband microwave signals (typ. 1-20 GHz).

Maturity and performances (in terms of spectral purity or phase noise, dynamic range linearity) of optoelectronic components permit to envisage the optical transmission and the optical processing of these signals.

Today, the optical transmission of microwave signals offers in conjunction with their low loss propagation over very wide frequency bandwidth, a high immunity to electromagnetic perturbations, which opens new avenues for the insertion of new concepts and photonic architectures in microwave systems.

Photonics and microwave technologies offers new opportunities for controlling many thousand array elements together with handling the wide bandwidth of shared aperture antennas. Photonics technologies will provide an interconnect solution for future airborne phased array radar antennas, which have conformality, bandwidth, EMI immunity, size,and weight requirements increasingly difficult, if not impossible, to meet using conventionnal electrical interconnect methods.

The first set of applications envisaged for the microwave optical links is the replacement of coaxial cables and especially of wideband coaxial cables. It requires low insertion loss and low noise figure.
The second set is associated to a remote control of antennas or processing equipment
It requires simultaneously for a single microwave channel both low insertion loss and high dynamic range and for multichannel phase pairing

Paper presented at the RTO SET Lecture Series on "Optics Microwave Interactions", held in Jouy en Josas, France, 2-3 September 2002; Duisburg, Germany, 5-6 September 2002; Budapest, Hungary, 9-10 September 2002, and published in RTO-EN-028.

Remoting of narrow band signals for radar antenna remoting and wideband antenna remoting and phase pairing for interferometry (ESM function).

The third set of applications is the delay function. In the microwave domain this function is of paramount importance due to the actual lack of digital function able to store a wide bandwidth signals. This represents the memory of microwave signals

Distribution of microwave signals

In future generation phased array radars, signal distributions will have to fulfil strict performance criteria. These include high isolation from both electromagnetic interference and crosstalk between module or subarray feeds with increased instantaneous bandwidths; dramatic reduction in size and weight regarding present fielded radars; and performance compatible with growing requirements such as low phase noise and high dynamic range.

The 1 to N distribution of microwave is extensively used in the telecomuunication or digital signals networking for send informations from one central board to N secondary ones.
In conventional telecommunications networks as well as in long distance networks it is required to detect and re-amplify the signals in order to avoid any distortions (low BER (bit error rate)) . The first application of optical amplifiers (see chapter II) is linked to the distribution of high speed digital signals.
In phased array antennas, an equivalent of this situation is found. In order to distribute local oscillators to active antennas arrays, we require to distribute high spectral purity signals. In complex environment (constraints of volume), optoelectronic technologies could bring a strong advantage to phased array antennas.

Optical architecture for phased array antennas

The beamforming, over a wide frequency instantaneous bandwidth of a phased array antenna requires a control of delay or at least a combination of phase and delay. The large amount of delay ($\approx$ 10 ns in order to compensate for the size of large antenna and $\approx$ 6 to 8 bits of phase between 0 et 2π to obtain the low level of secondary lobes secondaires) do not allow the use of control architectures based on microwave technologies (dispersion and insertion losses of microwave waveguides, interconnection complexity).

1 Review of Optical beamforming networks architectures

1.1 Optical Architectures : state of the art

As pointed out True Time Delay (TTD) beamforming is required when wide band operation is combined with significant beam steering offset. In this case there is a need of low loss transmission links allowing the remote control of the antennas and the distribution of large bandwidth microwave signals. This need is fulfilled today by microwave optical links, owing to an increase in the modulation bandwidth and the dynamic range of optical emitters and detectors. Furthermore, optoelectronic architectures, because of their inherent parallel processing capabilities, bring attractive perspectives for radar signal control and processing.

According to these considerations, a large number of Optical Beamforming Networks (OBFN) have been proposed during the last decade. One can classify these architectures according to five generic approaches :

- switched delay lines
- laser/photodiode switching
- wavelength coded architecture: dispersive delays/Bragg grating delays
- 2D optical delay lines.
- coherent OBFN

For each approach we will detail in the following a typical demonstration that already includes a built array. This overview is completed with related published references.

1.1.1 Coherent beamforming network

This approach is based on the generation of the phase delays to be distributed onto the antenna, through the use of dual frequency optical carrier of the microwave signal.
This concept can be illustrated by the experiment performed by Tamburrini & al.

Two mutually coherent, frequency offset optical beams are obtained by injection locking a slave laser (SL) with the emission of a master laser (ML), which was frequency shifted by a Bragg cell operating at frequency f = 3.2 GHz. These thus beams interfere and give rise to a moving interference pattern. A regularly spaced array of multimode fibers is used to spatially sample the moving pattern and to transmit the optical signals to the antenna plane. The light intensity coupled into each fiber varies at the beam frequency f with a microwave phase depending linearly of the fiber position and of the angle between the interfering beams. Phased array beam steering is achieved by changing the angle between the beams, thereby changing the spatial period of the interference pattern. The far field pattern of a 7 element linear antenna was characterised.

This concept was revisited (see references) but all these different approaches are based on the optical control (integrated optics, free space,...) of the microwave signal by changing the relative phase of the optical components of a dual frequency beam. It provides generally simple structures but does not permit a large frequency bandwidth operation of the antenna since these architectures only perform phase scanning.

1.1.2 Switched delay lines

This approach is based on the optoelectronic switching of fiber delay lines. This switching provides a digital control on the path lengths experienced by an optical carrier microwave signal and thus permits a true time delay control of a phased array antenna. This concept can be illustrated by the experiment performed by Goutzoulis et al. The operating principle is shown in the following figure 2.

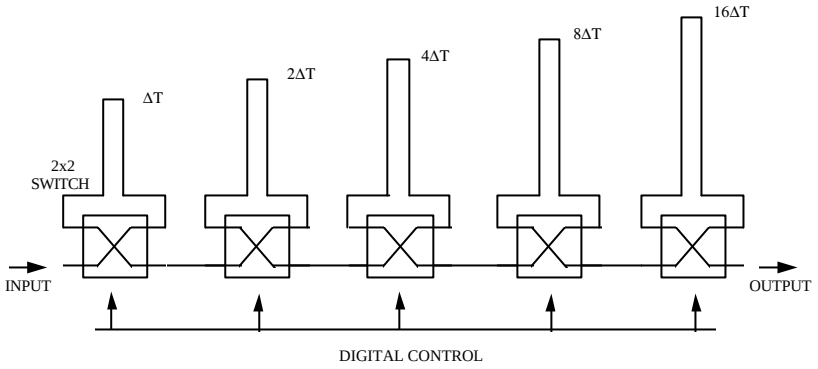

Figure 2: switched fiber delay lines

In the binary fiber optic delay line (BIFODEL) architecture, the optical carrier of the microwave signal is optically routed through N fiber segments whose lengths increase successively by a power of 2D. The required fiber segments are addressed using a set of N 2x2 optical switches. Since each switch allows the signal to either connect or bypass a fiber segment; a delay T may be inserted which can take any value, in increments of ΔT, up to a maximum value T_{max} given by :

$$T_{\max} = (2^N - 1)T$$

For each reading element or subarray of a phased array antenna it is necessary to implement such a BIFODEL. It yields that this technique is very well adapted to a TTD control of a subarrayed antenna.

The performances of this concept can be extended, mainly for an antenna divided in subarrays, according to the use of optical wavelength multiplexing. This approach is the one proposed by Westinghouse in its proof of concept demonstration (Goutzoulis et al,).

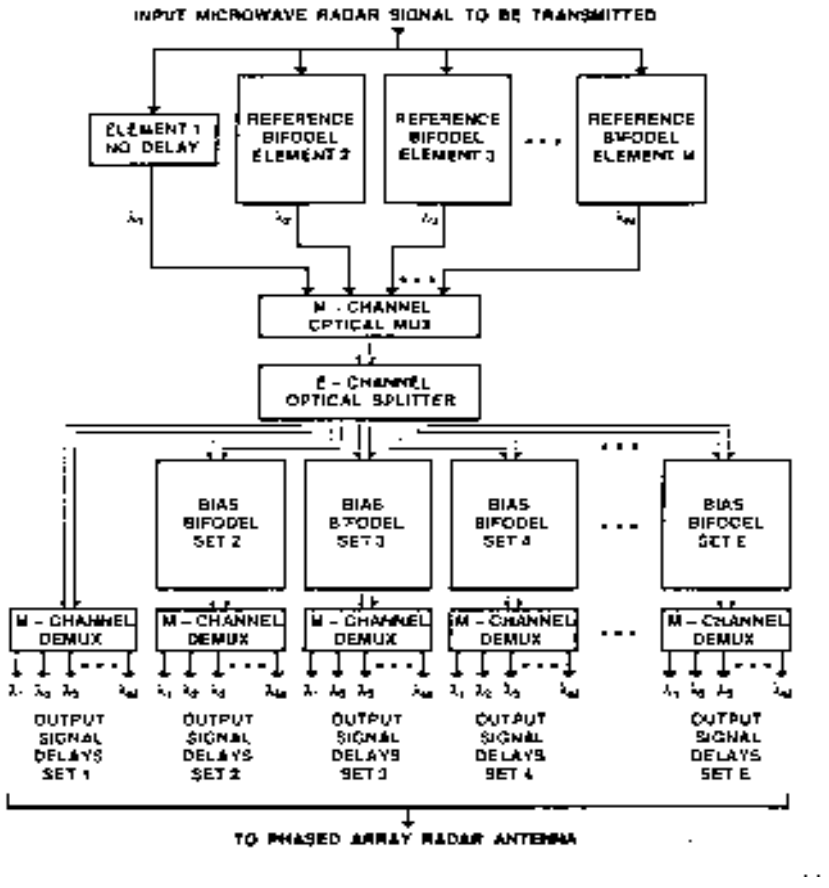

Figure3: BIFODEL architecture

The partioned phased array concept can be implemented using optical WDM in conjunction with all optical programmable delay lines. Furthermore it is reversible since the hardware can be used for both transmit and receive modes.

In the transmit mode *M-1* BIFODELs with outputs at wavelengths λ_2, ..., λ_M are driven in parallel radar signal. The *M-1* BIFODEL outputs, along with an undelayed output at wavelength, λ_1, are multiplexed via an *M*-channel multiplexer (MUX), the output of which is divided into *E* channels vie a 1:*E*-channel optical divider.
All but one of the divider outputs independently drive a bias BIFODEL, each of which is followed by an optical *M*-channel demultiplexer (DEMUX) output will also contain *M* wavelengths, λ_1, λ_2, ..., λ_M. The outputs of the nonbiased DEMUX contain the *M* progressively delayed signals required for the set 1.The outputs of each the remaining DEMUXs contain a similar set of signals but they are further delayed via the bias BIFODELs.
Similar wavelength outputs drive similar location elements in each set. All BIFODELs must have
$N = \log_2 R$ cascaded segments and different time resolution T_{imin}. The latter is determined by the location of the specific element, the antenna geometry, the radar characteristics, and so on. Similar comments apply to the bias BIFODELs, which have time resolutions $(i-1)T_{\text{Mmin}}$. In the receive mode, the same architecture is used, but in reverse. Here, the output of each element of the phased array drives an LD of a different wavelength. Elements with similar locations in different sets drive LDs of the same wavelength.

The experimental demonstration of this concept was performed at Westinghouse (Northrop-Gruman) for a 16 element linear antenna (16 elements for the transmit mode, 8 elements for the received mode). The far field pattern was characterised for both modes over the frequency range 600-1500 MHz for the distribution of the microwave signals. The antenna is divided in 4 subarrays. The microwave signal is first divided in parts, 3 of them can be electrically delayed (from 8 ps to 1500 ps with a 1.5 ps accuracy). The output of the non delayed line end of the 3 delayed lines are used to feed 4 directly modulated semiconductor lasers at different wavelengths.

1.1.3 Thales Approach

Inisde Thomson-CSF, this approach is under evaluation and development.
One of these is an architecture essentially 1D based on the delay switching (figure 4 - in this case, switching matrices base on cascade InP (IEMN - Lille) and WDM).

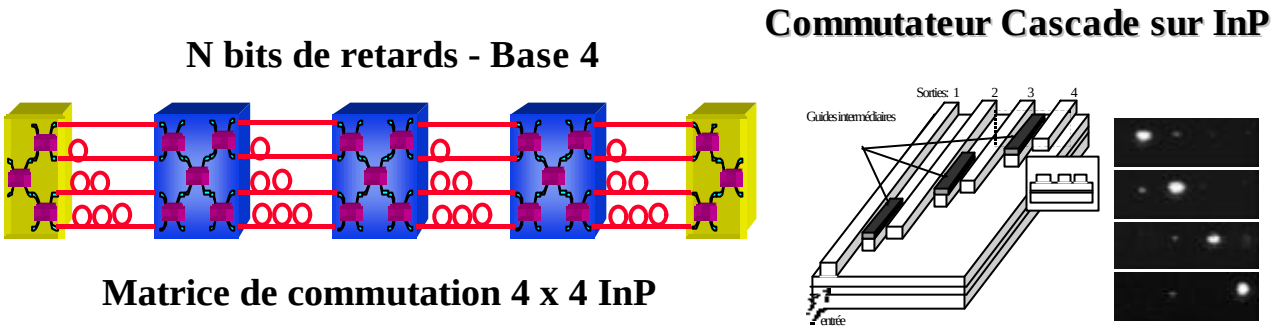

Figure 4: Base 4 switched delay lines

1.1.4 Laser / photodiode switching

In this approach (originally proposed and demonstrated by Hughes Aircraft), the delay path of the optical carrier of the microwave signal is defined, for each radiating element or subarray, by selectively turning on a laser and detector located respectively at the beginning and end of an analog optical link.

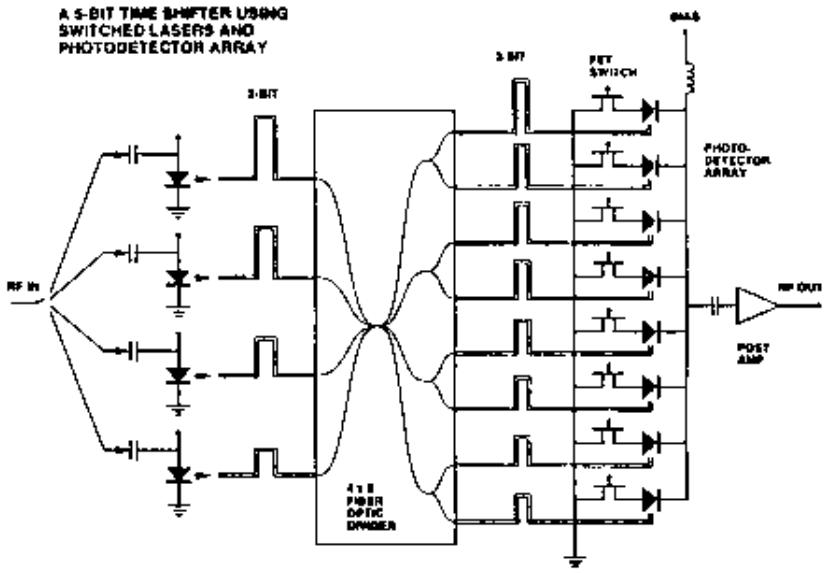

Figure 5: 5-bit time shifter

Combining laser and detector switching the network of the above figure (figure 5) provide 32 delay options (i.e 5 bits of resolution). This 5 bit time shift module is the building block of a wide band feed network. The programmable time shifters (8) provide the coarse delay steps ranging from 0.25 ns to 8 ns (5bits) for the 8x3 subarrays of a 96 element antenna. Electronic delay lines in the T/R modules provide fine differential delays ranging from 0.01ns to 0.5 ns (6 bit precision).
According to this concept both transmit and receive modes of a 2D conformal antenna were characterized over the frequency bandwidth 850 – 1400 MHz. This proof of concept is, at the moment the most achieved demonstration of optical remote control and beamforming of a large bandwidth antenna.

1.1.5 Dispersive delays / Bragg grating delays

1.1.5.1 Dispersive delays

In this approach, the time delays experienced by optically carried microwave signals are provided by the use of one or several tunable wavelength lasers in conjunction with a wavelength selective material. This material is either an optical fiber including permanent Bragg gratings (Lembo et al. from TRW, Smith et al. From GEC-Marconi) or an optical fiber used in its dispersive region (Frankel et al. from the Naval Research Lab.).

In the following we will detail the NRL approach, since it is already demonstrated with a radiating antenna.

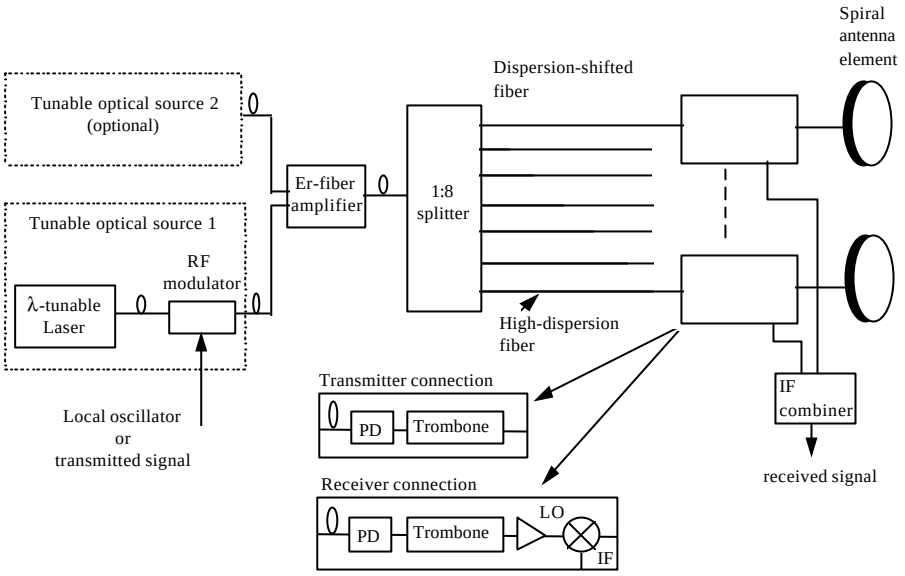

Figure 6: dispersive delays

The microwave signal driving the antenna elements is transmitted on a single wavelength-tunable optical carrier via a bank of dispersive fiber optic links. The TTD function is realized by tuning the carrier wavelength to vary the group velocity of the propagating signal. Each fiber link feeding an array element incorporates an overall amount of dispersion proportional to the element position. A set change in the carrier wavelength provides the necessary proportional time delay for all array elements with a single wavelength control input.

This approach seems to be very well adapted to linear antenna, with a number of elements in the range 10-100. It was experimentally demonstrated, for the transmit mode, with a very large bandwidth antenna (2 – 18 GHz) of 8 radiating elements. Receive mode operation is also possible with this concept when the optical beamformer is used to generate a properly phased local oscillator. In this case, a tunable laser is used in the module.

This fiber prism technique has since been shown to transmit multiple simultaneous beams and has been extended to a two-dimensional arrangement that operates over the full 6-18 Ghz band.

1.1.5.2 Bragg grating delays

Several laboratories have investigated the use of Bragg fibre gratings to provide true time delay beam steering in optically controlled phased array antennas. These studies have considered the performance of single channel discrete multi grating arrays (C.Edge & I Bennion) as shown in the following figure, chirped grating beamformers and full transmit /receive antenna systems.

Generation of TTD using multi element or chirped gratings is advantageous since all of the required delays for a single antenna element can be provided on one fibre rather than the more complex switched time delay modules described in the previous section. There are significant disadvantages however including the manufacturing reproducibility of fibre gratings, the requirement for highly wavelength stable tunable laser sources (only currently available in bench top form and with slow tuning speeds) and the ability to achieve suitable close-to-carrier phase noise performance within a system (BAES).

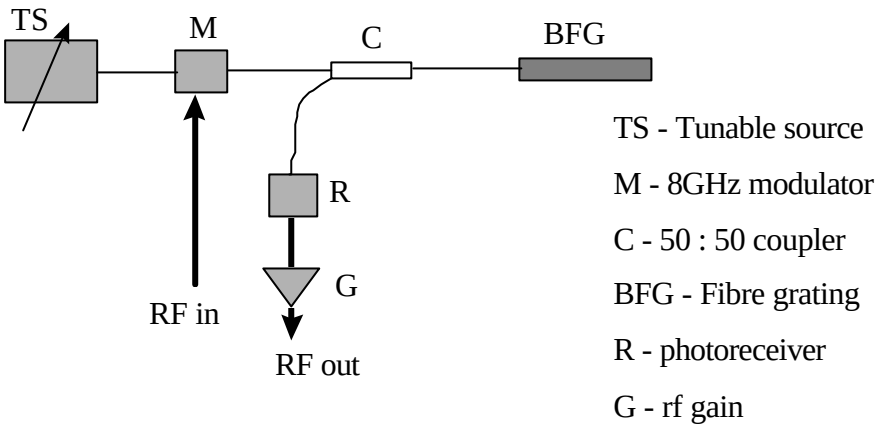

Figure 7: 8 element (3-bit) Bragg fibre grating test configuration

1.1.6 2D optical delay lines

A 2D optical delay lines has been implemented and demonstrated (cf Dolfi & Riza).
In this approach the time delays are provided by free space delay lines, switched using 2D spatial light modulators (SLM).

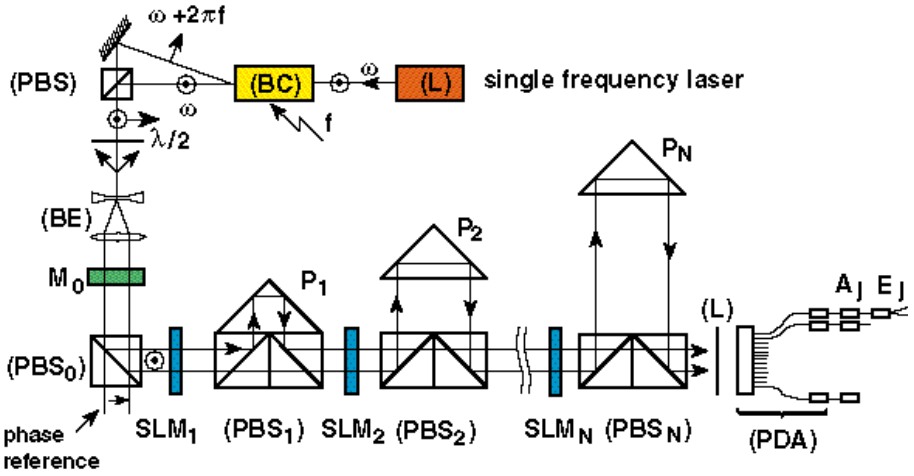

Figure 8: 2D optical delay lines

A dual frequency laser beam is the optical carrier of the microwave signal. This beam is expanded and travels through a set of SLMs whose number of pixels (pxp) is the number of radiating elements of the antenna. M_O is a parallely aligned nematic liquid crystal (LC) SLM. It controls the phase of the microwave signal by changing the relative optical phase of the cross polarized components of the dual frequency beam.
At the output of M_O, the linearly polarized dual frequency beam intercepts a set of spatial light modulators SLM_i, polarizing beam splitters PBS_i and prisms P_i. They provide the parallel control of the time delays assigned to the antenna. The beam polarization can be rotated by 0° or 90° on each pixel. According to the polarization, PBS_i is transparent (and the light beam intercepts the next SLM_{i+1}) or reflective (and the microwave signal is delayed). The collimated beam travels through all the (PBS_i) and is focused by an array of microlenses (L) onto an array of pxp fiber pigtailed photodiodes (PDA).

For a given photodiode, the phase of the microwave beating signal is determined by the applied voltage on the corresponding pixel of M_O and by the choice of the PBS_i on which the reflections occur. Since the positions of prisms P_i provide delay values according to a geometric progression (t, 2t, 4t..), the beating signal can be delayed from 0 to $(2^N-1)t$ with step t.

Experimental demonstration of an optically controlled phased array antenna, operating between 2.5 and 3.5 GHz. The 2D architecture is implemented with 6 SLMs of 4 x 4 pixels. It provides 32 delay values (5 bits), an analog control of the phase [0,2p] and permits the control of a 16 element phased array antenna. Furthermore, when far field patterns at different frequencies are superposed for a given scan direction , one can notice the absence of any beam squint.

1.2 Optical Beamforming Receive Mode – Thomson-CSF 2D Approach

We propose and experimentally demonstrate two optical architectures performing processing of the receive mode of a p×p element phased array antenna. They are based on free space propagation and switching of channelized optical carriers of microwave signals. The first architecture assumes a direct transposition of the received signals in the optical domain. The second one is based on the optical generation and distribution of a microwave local oscillator matched in frequency and direction. Preliminary experimental results at microwave frequencies of about 3 GHz are presented.
The review presents an original architecture dedicated to the processing of the receive mode, using a similar concept as the one demonstrated in for emission. In the Direct Architecture, the received microwave signals are optically carried and travel back through the same time delay network as the one used for the transmit mode. In the Matched Local Oscillator Architecture (MLOA), a channelized microwave local oscillator, time delayed and optically carried, is mixed, at the antenna level, to the received signals. It provides an heterodyne filtering, matched in frequency and direction, to the received signal. Such an approach was recently considered with quite different implementations. We propose here a third implementation, fully programmable and based on the optical generation of simultaneous complementary delays for both the transmit signal and the Local Oscillator (LO).

When now using this architecture in the receive mode, the microwave signal reflected by the target travels back to the antenna, and is detected by an array of p×p microwave receivers. The signals issued from each receiver are used to feed an array of modulated lasers (direct or external modulation). For a radar detection in the same direction as for emission, the received signals, optically carried, have to travel through the same time-delay network as the one used for the emission mode. It permits in-phase addition over a large frequency bandwidth of all the microwave signals received by the antenna. An array of p×p photodiodes then extracts the microwave information from the optical carriers for processing.

This detection mode leads to some important problems. Indeed, robustness to jamming requires opto-electronic elements able to handle high power microwave signals. In the same time, they must be able to detect very low level signals, corresponding to the target signatures in limit of range. The ratio jammer signal to lower signal requires linearity of opto-links in the range 100 – 120 dB. This corresponds to spurious free dynamic range (SFDR) in the range 70 – 80 $dB/MHz^{2/3}$. Such performances are still difficult to attain over large bandwidth with

currently available opto-components. This first architecture, using direct transposition of the received microwave signals, is operating with a time-reversal approach. In the following, we then detail an approach using a Matched Local Oscillator that operates in a similar way as phase conjugation (Fig.9).

In order to overcome this dynamic range limitation, we have developed the MLOA, in which a channelized microwave local oscillator, optically carried, is used for mixing with the received microwave signals. The operating principle is shown on Fig.9. In a similar way as the one on Figure 8, two optical beams are excited by a microwave signal at f_e and f_{LO} respectively. In the emission mode, for a frequency f_e and a time-delay τ_k, the phase of the radiating element *k* is

$\varphi_k^e(t)=2\pi f_e(t-\tau_k)$. (1)

After a round-trip time 2T from the antenna to the target, receiver *k* detects a signal of phase :

$\varphi_k^r(t)=2\pi(f_e+f_D)(t-2T+\tau_k)$ (2)

where $f_D<<f_e$ is the Doppler frequency due to the target velocity. In the following, $f_r=f_e+f_D$ is the received frequency associated to f_e. As for the emitted signal, the microwave LO, with (principal) frequency f_{LO}, is channelized and optically carried through the time-delay network. The carriers are detected by a p×p photodiodes array. Each photodiode provides a microwave signal of frequency f_{LO}, time-delayed according to the law given by the delay network. Each of those channelized microwave signals is then mixed, at the T/R module level, with the corresponding component of the received signal. It results in a low-frequency microwave signal of phase :

$\varphi_k^s(t)=\varphi_k^{LO}(t)-\varphi_k^r(t)$ (3)

where φ_k^{LO} is the phase of the Local Oscillator. The delay law experienced by the LO is chosen to perform in-phase addition of all the low intermediate frequency signals coming out of the mixers. To achieve this condition, a remarkable property of an optical architecture based on liquid crystal SLMs can be used here. When two cross-polarized beams travel along the same channel, their polarizations stay cross-polarized, and they experience complementary paths. One of the two beams is delayed by τ_k, the other (cross-polarized) by $(\tau_M-\tau_k)$, where τ_M is the maximum time-delay. According to (1), if we choose the LO complementary to the emitted signal, the phase of the LO will be:

$\varphi_k^{LO}(t) = 2\pi f_{LO}(t-(\tau_M-\tau_k))$. (4)

According to (2), (3) and (4), the resulting mixed signals will have the phase

$\varphi_k^s(t)=2\pi(f_i(t+\tau_k)-f_{LO}\tau_M+2f_rT)$, (5)

where $f_i=f_{LO}-f_r$ is the intermediate frequency, and the term $2\pi(f_it-f_{LO}\tau_M+2f_rT)$ is common to all the channels. In the case of an homodyne detection, where we would have $f_{LO}=f_r$, the phase, at the output of each channel, reduces to $\varphi_k^s(t)=2\pi(f_{LO}\tau_M+2f_rT)$, and ensures that all the channels are added in phase. Note that for an emitted signal with a large frequency bandwidth, the condition $f_{LO}=f_e$ is satisfied for each component of the spectrum, by using a large frequency bandwidth local oscillator. By this way of complementary path, we can therefore generate a perfectly matched LO. In order to avoid any crosstalk between emission and reception, the wavelength of the LO and the emission optical carriers have to be different. At the output of the delay network, a dichroïc mirror switches the carriers on two different photodiodes. One will provide the signal to be emitted, the other one the microwave LO signal.

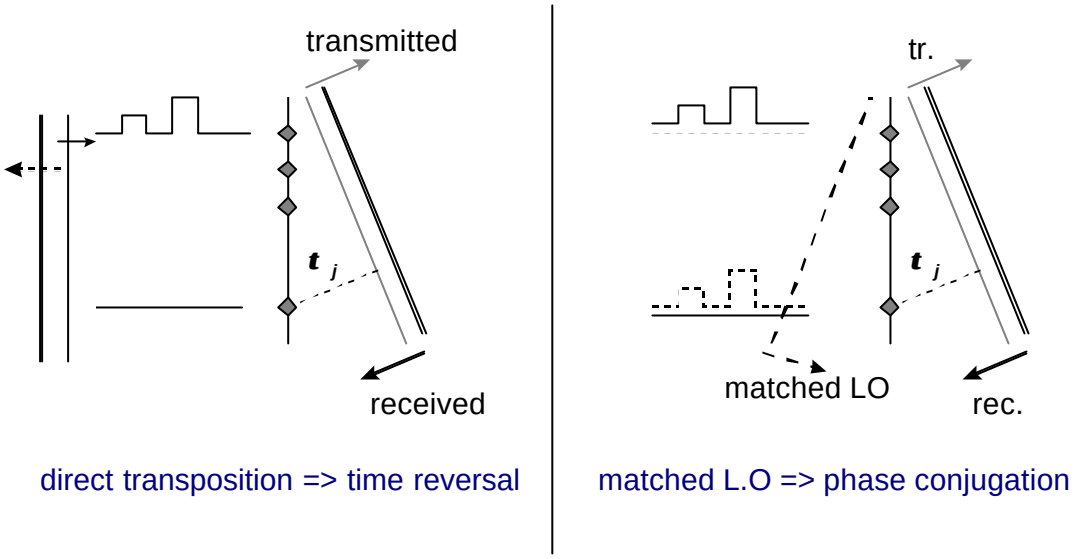

Figure 9 Matched local oscillator principle (a)

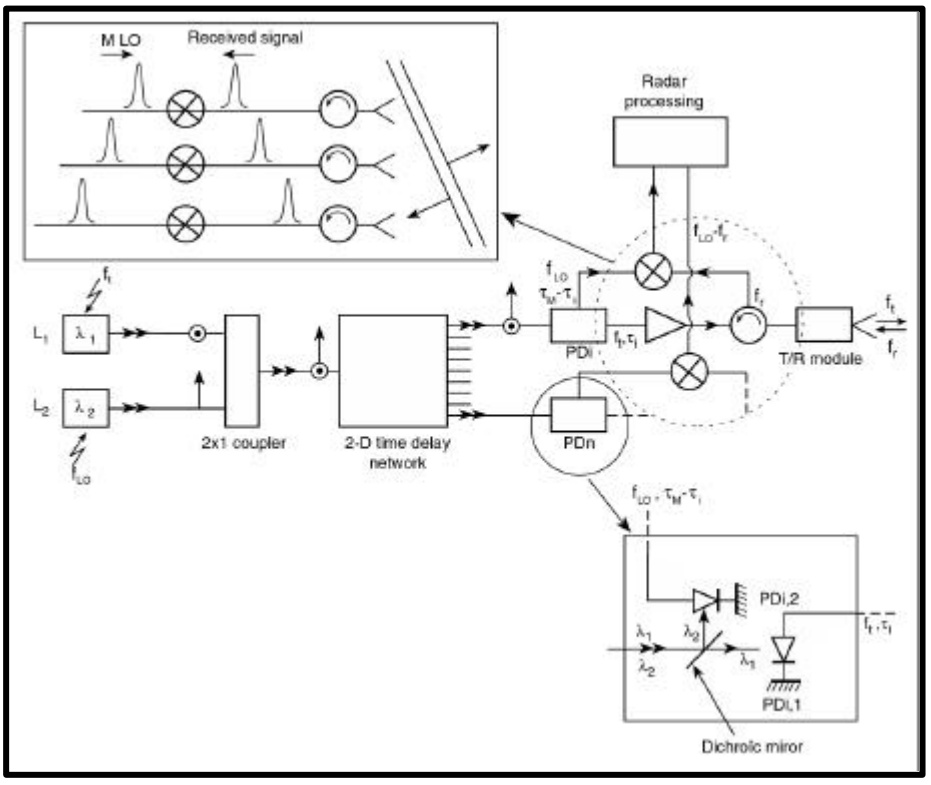

Figure 9 Matched local oscillator architecture (b)

2 References

- **Coherent beamforming networks**

M. Tamburrini, M. Parent, L. Goldberg, D. Stillwell « Optical feed for a phased array microwave antenna », Electron. Lett., 23, 680, 1987.
J.L. Guggenmos, R. L. Johnson, B. D. Seery «Optical distribution manifolds for phased array antennas », Proc. SPIE, vol . 886, 214, 1988.
E. N. Toughlian, H. Zmuda, Ph. Kornreich « Deformable mirror based optical beam focusing system for phased array antenna » IEEE Photon. Tech. Lett., 2, 444, 1990.
M. J. Wale, C. Edge, M. G. Holliday, R. G. Walker, N. S. Birkmayer, B. Hösselbarth, T. Jakob « Optoelectronic beamforming for a space borne phased array antenna », Proc. SPIE, vol. 1703, 368, 1992.
M. F. Lewis « Coherent optical RF beamforming » Proc. IEEEE Microwave Photonics'97, 23, 1997.

· **Switched fiber delay lines**

A. Goutzoulis, K. Davies, J. Zomp, P. Hrycak, A. Johnson « Development and field demonstration of a harware compressive fiber optics true time delay steering system for phase array antennas » Appl. Opt., 33, 8173, 1994.
K. Horikawa, I. Ogawa, T. Kitoh « Silica based integrated planar lightwave true time delay network for microwave antenna applications », OFC'96 Technical Digest, 100, 1996.
C. T. Sullivan, S. D. Mukherjee, M. K. Hibbs-Brenner, A. Gopinath, E. Kalweit, T. Marta, W. Goldberg, and R. Walterson « Switched time delay elements based on AlGaAs/GaAs optical waveguide technology at 1.32 μm for optically controlled phased array antennas » SPIE, vol. 1703, 264, 1992.
G. A. Magel and J. L. Leonard « Phosphosilicate glass waveguides for phased-array radar time delay » SPIE, vol. 1703, 373, 1992.
E. Ackerman, S. Wanuga, D. Kasemset, W. Minford, N. Thorsten, and J. Watson « Integrated 6-bit photonic true-time delay unit for light weight 3-6 Ghz radar beamformer » in MTT-Symposium Digest (Institute of Electrical and Electronic Engineers, New-York, 1992, pp. 681-684.

· **Laser / photodiode switching**

W. Ng, A. Walston, G. Tangonan, J.J. Lee, I. Newberg, N. Bernstein «The first demonstration of an optically steered microwave phased array antenna using true time delay», IEEE J. Lightwave Technol., LT9, 1124, 1991.
J.J. Lee, R.Y. Loo, S. Livingston, V.I. Jones, J.B. Lewis, H.W. Yen, G. Tangonan, M. Wechsberg, «Photonic wideband array antennas», IEEE Trans. Antenna Propag., 43, 966, 1995

· **Dispersive delays / Bragg grating delays**

Frankel, R.D. Esman, «True time delay fiber optic control of an ultrawideband array transmitter/receiver with multibeam capability», IEEE Trans. Microwave Theory and Tech., 43, 2387, 1995
M. Wickham, L. Lembo, L. Dozal, J. Brock, «Fiber optic grating true time delay generator for broad band RF applications», Proc. SPIE vol. 2844, 175, 1996
B. Smith, M. Nawaz, «Evaluation of Bragg fibre grating as TTD elements in optical phased array systems», Proc. IEEEE Microwave Photonics'97, 205, 1997.

(a) J.E.Roman et al, “Time Steered Array with a Chirped Grating Beamformer”. Electron. Lett., Vol. 33, No.8, pp. 652-653, April 1997.
(b) H. Zmuda et al, "Photonic Bramformer for Phased Array Antennas using a Fiber Grating Prism", IEEE Photonic Technology Letters, Vol. 9, No. 2, pp. 242-243, Feb 1997.

- **2D optical delay lines**

Dolfi et al, « Optically controlled true time delays for phased array antenna », Proc. SPIE1102,152 (1989)
N.A.Riza, « Transmit/Receive time delay beam forming optical architecture for phased array antenna » , Appli.Opt. 30, 4594 (1991)

2.1 Additional references

1. H. Zmuda, E. Toughlian, *Photonic aspects of modern radars,* Artech, Boston (1995)
2. N.A. Riza Ed, *Photonic control systems for phased-array antennas,* SPIE Milestone series, vol. MS136 (1997)
3. D. Dolfi, P. Joffre, J. Antoine, J.P. Huignard, D. Philippet, D. Granger, *Experimental demonstration of a phased-array antenna optically controlled with phase and time delays*, Appl. Opt., **35**, pp.5293-5300 (1996)
4. M. Y. Frankel and R. D. Esman, *True time-delay fiber optic control of an ultrawideband array transmitter/receiver with multibeam capability,* IEEE MTT/JLT Special Joint Issue, MTT-43, pp.2387-2394 (1995)
5. R.R. Stephens, J.J. Lee, G.L. Tangonan, I.L. Newberg, H.T. Wang, *Photonic RF mixing feed for multibeam arrays*, IEEE/LEOS International topical meeting on Microwave Photonics MWP’97, D. Jaeger, Ed., Duisburg, Germany, 1997, WE 1-6
6. D. Dolfi, J.P. Huignard, J. Chazelas, O. Maas, *Photonics for microwave processing in radar systems,* IEEE/LEOS International topical meeting on Microwave Photonics MWP’97, D. Jaeger, Ed., Duisburg, Germany , 1997, WE 1-5
7. M.J. Wale, *Component technology for microwave photonic systems,* IEEE/LEOS International topical meeting on Microwave Photonics MWP’97, D. Jaeger, Ed., Duisburg, Germany , 1997, TH 1-2
8. J.J. Lee, R.Y. Loo, S. Livingstone, V.I. Jones, J.B. Lewis, H.W. Yen, G.L. Tangonan, M. Wechsberg, *Photonic wideband array antennas*, IEEE Trans. Antennas Propag., **43**, pp.966-982 (1995)
9. A.P. Goutzoulis, J.M. Zomp, *Development and field demonstration of an eight-element receive wavelength-multiplexed true-time-delay steering system*, Appl. Opt., **36**, pp.7315-7326 (1997)

REPORT DOCUMENTATION PAGE

1. Recipient's Reference	2. Originator's References	3. Further Reference	4. Security Classification of Document
	RTO-EN-028 AC/323(SET-058)TP/42	ISBN 92-837-1094-0	UNCLASSIFIED/ UNLIMITED

5. Originator

Research and Technology Organisation
North Atlantic Treaty Organisation
BP 25, F-92201 Neuilly-sur-Seine Cedex, France

6. Title

Optics Microwave Interactions

7. Presented at/sponsored by

the Sensors and Electronics Technology Panel (SET) and the Consultant and Exchange Programme of RTO presented on 2-3 September 2002 in Jouy en Josas, France, on 5-6 September 2002 in Duisburg, Germany and on 9-10 September 2002 in Budapest, Hungary.

8. Author(s)/Editor(s)	9. Date
Multiple	April 2003
10. Author's/Editor's Address	**11. Pages**
Multiple	170 (text) 60 (slides)

12. Distribution Statement

There are no restrictions on the distribution of this document. Information about the availability of this and other RTO unclassified publications is given on the back cover.

13. Keywords/Descriptors

Analog to digital converters
Design
Fiber optics
Free space optical networks
Integrated systems
Microwave equipment
Microwave frequencies
Microwave photonics
Millimeter waves
Optical beamforming
Optical control equipment
Optical data links
Optical equipment
Optical networks
Optical processing
Optical properties
Optical switches
Optoelectronics
Phased arrays
Signal processing

14. Abstract

The field of optics-microwave covered by this 2 day lecture series can generally be defined as the study of high speed devices and systems operating at microwave, millimeterwave and even THz frequencies. The benefits drawn by the introduction of optics in microwave techniques are illustrated through numerous examples.

This two-day lecture series covers the main applications of optomicrowaves to the defence area through a broad approach going from devices to systems.

This page has been deliberately left blank

Page intentionnellement blanche

NORTH ATLANTIC TREATY ORGANISATION

RESEARCH AND TECHNOLOGY ORGANISATION
BP 25 • 7 RUE ANCELLE
F-92201 NEUILLY-SUR-SEINE CEDEX • FRANCE
Télécopie 0(1)55.61.22.99 • E-mail mailbox@rta.nato.int

DIFFUSION DES PUBLICATIONS
RTO NON CLASSIFIEES

L'Organisation pour la recherche et la technologie de l'OTAN (RTO), détient un stock limité de certaines de ses publications récentes, ainsi que de celles de l'ancien AGARD (Groupe consultatif pour la recherche et les réalisations aérospatiales de l'OTAN). Celles-ci pourront éventuellement être obtenues sous forme de copie papier. Pour de plus amples renseignements concernant l'achat de ces ouvrages, adressez-vous par lettre ou par télécopie à l'adresse indiquée ci-dessus. Veuillez ne pas téléphoner.

Des exemplaires supplémentaires peuvent parfois être obtenus auprès des centres nationaux de distribution indiqués ci-dessous. Si vous souhaitez recevoir toutes les publications de la RTO, ou simplement celles qui concernent certains Panels, vous pouvez demander d'être inclus sur la liste d'envoi de l'un de ces centres.

Les publications de la RTO et de l'AGARD sont en vente auprès des agences de vente indiquées ci-dessous, sous forme de photocopie ou de microfiche. Certains originaux peuvent également être obtenus auprès de CASI.

CENTRES DE DIFFUSION NATIONAUX

ALLEMAGNE
Streitkräfteamt / Abteilung III
Fachinformationszentrum der Bundeswehr, (FIZBw)
Friedrich-Ebert-Allee 34
D-53113 Bonn

BELGIQUE
Etat-Major de la Défense
Département d'Etat-Major Stratégie
ACOS-STRAT-STE – Coord. RTO
Quartier Reine Elisabeth
Rue d'Evère, B-1140 Bruxelles

CANADA
DSIGRD2
Bibliothécaire des ressources du savoir
R et D pour la défense Canada
Ministère de la Défense nationale
305, rue Rideau, 9e étage
Ottawa, Ontario K1A 0K2

DANEMARK
Danish Defence Research Establishment
Ryvangs Allé 1, P.O. Box 2715
DK-2100 Copenhagen Ø

ESPAGNE
INTA (RTO/AGARD Publications)
Carretera de Torrejón a Ajalvir, Pk.4
28850 Torrejón de Ardoz - Madrid

ETATS-UNIS
NASA Center for AeroSpace Information (CASI)
Parkway Center
7121 Standard Drive
Hanover, MD 21076-1320

FRANCE
O.N.E.R.A. (ISP)
29, Avenue de la Division Leclerc
BP 72, 92322 Châtillon Cedex

GRECE (Correspondant)
Defence Industry & Research General Directorate
Research Directorate
Fakinos Base Camp
S.T.G. 1020
Holargos, Athens

HONGRIE
Department for Scientific Analysis
Institute of Military Technology
Ministry of Defence
H-1525 Budapest P O Box 26

ISLANDE
Director of Aviation
c/o Flugrad
Reykjavik

ITALIE
Centro di Documentazione Tecnico-Scientifica della Difesa
Via XX Settembre 123a
00187 Roma

LUXEMBOURG
Voir Belgique

NORVEGE
Norwegian Defence Research Establishment
Attn: Biblioteket
P.O. Box 25, NO-2007 Kjeller

PAYS-BAS
Royal Netherlands Military Academy Library
P.O. Box 90.002
4800 PA Breda

POLOGNE
Armament Policy Department
218 Niepodleglosci Av.
00-911 Warsaw

PORTUGAL
Estado Maior da Força Aérea
SDFA - Centro de Documentação
Alfragide
P-2720 Amadora

REPUBLIQUE TCHEQUE
DIC Czech Republic-NATO RTO
VTÚL a PVO Praha
Mladoboleslavská ul.
Praha 9, 197 06, Česká republika

ROYAUME-UNI
Dstl Knowledge Services
Kentigern House, Room 2246
65 Brown Street
Glasgow G2 8EX

TURQUIE
Millî Savunma Başkanliği (MSB)
ARGE Dairesi Başkanliği (MSB)
06650 Bakanliklar - Ankara

AGENCES DE VENTE

NASA Center for AeroSpace Information (CASI)
Parkway Center
7121 Standard Drive
Hanover, MD 21076-1320
Etats-Unis

The British Library Document Supply Centre
Boston Spa, Wetherby
West Yorkshire LS23 7BQ
Royaume-Uni

Canada Institute for Scientific and Technical Information (CISTI)
National Research Council
Acquisitions
Montreal Road, Building M-55
Ottawa K1A 0S2, Canada

Les demandes de documents RTO ou AGARD doivent comporter la dénomination "RTO" ou "AGARD" selon le cas, suivie du numéro de série (par exemple AGARD-AG-315). Des informations analogues, telles que le titre et la date de publication sont souhaitables. Des références bibliographiques complètes ainsi que des résumés des publications RTO et AGARD figurent dans les journaux suivants:

Scientific and Technical Aerospace Reports (STAR)
STAR peut être consulté en ligne au localisateur de ressources uniformes (URL) suivant:
http://www.sti.nasa.gov/Pubs/star/Star.html
STAR est édité par CASI dans le cadre du programme NASA d'information scientifique et technique (STI)
STI Program Office, MS 157A
NASA Langley Research Center
Hampton, Virginia 23681-0001
Etats-Unis

Government Reports Announcements & Index (GRA&I)
publié par le National Technical Information Service
Springfield
Virginia 2216
Etats-Unis
(accessible également en mode interactif dans la base de données bibliographiques en ligne du NTIS, et sur CD-ROM)

Imprimé par Groupe d'imprimerie St-Joseph inc.
(Membre de la Corporation St-Joseph)
1165, rue Kenaston, Ottawa (Ontario), Canada K1G 6S1

NORTH ATLANTIC TREATY ORGANISATION

RESEARCH AND TECHNOLOGY ORGANISATION
BP 25 • 7 RUE ANCELLE
F-92201 NEUILLY-SUR-SEINE CEDEX • FRANCE
Telefax 0(1)55.61.22.99 • E-mail mailbox@rta.nato.int

DISTRIBUTION OF UNCLASSIFIED RTO PUBLICATIONS

NATO's Research and Technology Organisation (RTO) holds limited quantities of some of its recent publications and those of the former AGARD (Advisory Group for Aerospace Research & Development of NATO), and these may be available for purchase in hard copy form. For more information, write or send a telefax to the address given above. **Please do not telephone**.

Further copies are sometimes available from the National Distribution Centres listed below. If you wish to receive all RTO publications, or just those relating to one or more specific RTO Panels, they may be willing to include you (or your organisation) in their distribution.

RTO and AGARD publications may be purchased from the Sales Agencies listed below, in photocopy or microfiche form. Original copies of some publications may be available from CASI.

NATIONAL DISTRIBUTION CENTRES

BELGIUM
Etat-Major de la Défense
Département d'Etat-Major Stratégie
ACOS-STRAT-STE – Coord. RTO
Quartier Reine Elisabeth
Rue d'Evère, B-1140 Bruxelles

CANADA
DRDKIM2
Knowledge Resources Librarian
Defence R&D Canada
Department of National Defence
305 Rideau Street, 9th Floor
Ottawa, Ontario K1A 0K2

CZECH REPUBLIC
DIC Czech Republic-NATO RTO
VTÚL a PVO Praha
Mladoboleslavská ul.
Praha 9, 197 06, Česká republika

DENMARK
Danish Defence Research Establishment
Ryvangs Allé 1, P.O. Box 2715
DK-2100 Copenhagen Ø

FRANCE
O.N.E.R.A. (ISP)
29 Avenue de la Division Leclerc
BP 72, 92322 Châtillon Cedex

GERMANY
Streitkräfteamt / Abteilung III
Fachinformationszentrum der Bundeswehr, (FIZBw)
Friedrich-Ebert-Allee 34
D-53113 Bonn

GREECE (Point of Contact)
Defence Industry & Research General Directorate
Research Directorate
Fakinos Base Camp
S.T.G. 1020
Holargos, Athens

HUNGARY
Department for Scientific Analysis
Institute of Military Technology
Ministry of Defence
H-1525 Budapest P O Box 26

ICELAND
Director of Aviation
c/o Flugrad
Reykjavik

ITALY
Centro di Documentazione Tecnico-Scientifica della Difesa
Via XX Settembre 123a
00187 Roma

LUXEMBOURG
See Belgium

NETHERLANDS
Royal Netherlands Military Academy Library
P.O. Box 90.002
4800 PA Breda

NORWAY
Norwegian Defence Research Establishment
Attn: Biblioteket
P.O. Box 25, NO-2007 Kjeller

POLAND
Armament Policy Department
218 Niepodleglosci Av.
00-911 Warsaw

PORTUGAL
Estado Maior da Força Aérea
SDFA - Centro de Documentação
Alfragide
P-2720 Amadora

SPAIN
INTA (RTO/AGARD Publications)
Carretera de Torrejón a Ajalvir, Pk.4
28850 Torrejón de Ardoz - Madrid

TURKEY
Millî Savunma Başkanliği (MSB)
ARGE Dairesi Başkanliği (MSB)
06650 Bakanliklar - Ankara

UNITED KINGDOM
Dstl Knowledge Services
Kentigern House, Room 2246
65 Brown Street
Glasgow G2 8EX

UNITED STATES
NASA Center for AeroSpace Information (CASI)
Parkway Center
7121 Standard Drive
Hanover, MD 21076-1320

SALES AGENCIES

NASA Center for AeroSpace Information (CASI)
Parkway Center
7121 Standard Drive
Hanover, MD 21076-1320
United States

The British Library Document Supply Centre
Boston Spa, Wetherby
West Yorkshire LS23 7BQ
United Kingdom

Canada Institute for Scientific and Technical Information (CISTI)
National Research Council
Acquisitions
Montreal Road, Building M-55
Ottawa K1A 0S2, Canada

Requests for RTO or AGARD documents should include the word 'RTO' or 'AGARD', as appropriate, followed by the serial number (for example AGARD-AG-315). Collateral information such as title and publication date is desirable. Full bibliographical references and abstracts of RTO and AGARD publications are given in the following journals:

Scientific and Technical Aerospace Reports (STAR)
STAR is available on-line at the following uniform resource locator:
http://www.sti.nasa.gov/Pubs/star/Star.html
STAR is published by CASI for the NASA Scientific and Technical Information (STI) Program
STI Program Office, MS 157A
NASA Langley Research Center
Hampton, Virginia 23681-0001
United States

Government Reports Announcements & Index (GRA&I)
published by the National Technical Information Service
Springfield
Virginia 22161
United States
(also available online in the NTIS Bibliographic Database or on CD-ROM)

Printed by St. Joseph Print Group Inc.
(A St. Joseph Corporation Company)
1165 Kenaston Street, Ottawa, Ontario, Canada K1G 6S1

ISBN 92-837-1094-0